Caprock integrity evaluation for geosequestration of CO2 in depleted petroleum reservoirs.

AMINAHO, E.N.

2024

CAPROCK INTEGRITY EVALUATION FOR GEOSEQUESTRATION OF CO_2 IN DEPLETED PETROLEUM RESERVOIRS

BY

EFENWENGBE NICHOLAS AMINAHO

A thesis submitted in partial fulfilment of the requirements of Robert Gordon University for the degree of Doctor of Philosophy in Engineering

May 2024

ACKNOWLEDGEMENT

It was a great time and a wonderful opportunity to learn and conduct research at Robert Gordon University (Aberdeen). I want to use this opportunity to thank Robert Gordon University (RGU) for providing the full tuition fee funding to engage in this doctoral research. This research would not have been possible without the funding and support provided by the institution. I would also like to appreciate the support provided by the UK Carbon Capture and Storage Research Centre (UKCCSRC) through their flexible funding of £8000. This research was also supported by the Aberdeen Formation Evaluation Society (AFES) with £1000 – this funding obtained at the beginning of the doctoral programme was very helpful for this research.

I would like to thank my principal supervisor, Professor Mamdud Hossain for his commitment to supervising my doctoral research and the constructive criticism provided upon reviewing my thesis, to improve the content. My secondary supervisor, Professor Nadimul Haque Faisal, has also been very supportive in co-supervising this research and critiquing the thesis. I would like to thank Dr. Reza Sanaee for selecting me to engage in this doctoral research, he started as the principal supervisor before handing over to Professor Mamdud Hossain due to some professional engagements he needed to attend to. The RGU IT team has been very supportive in installing suitable software and programs to enable me to perform numerical simulations and analyses. The entire administrative team of the School of Engineering at RGU has also been very supportive, by providing adequate information and advice to access necessary resources.

I would like to thank the love of my life, Mrs. Faith Aminaho, for her support and encouragement throughout the doctoral programme. I can move mountains having her around me. My parents and siblings have been very supportive in my career, from my Bachelor of Engineering degree to the completion of this doctoral (PhD) degree. My parents, Mr. Aminaho Godwin Arihen and Mrs. Gladys Arihen are devout Christians who have paid a great sacrifice in giving me good home training and leading me to Christ. My parents regularly pray for me and have financially supported me up to this PhD programme. I am proud to have them and celebrate them as my heroes. The prayers and encouragements I received from my siblings during the PhD programme played a major role in strengthening me to complete the programme. Mr. Ehianu Maynard Aminaho, Dr. (Mrs.) Mariam-Aminaho Osakwe, Mr. Konyengwaehie Augustus Aminaho, Ms. Faith Kikachukwu Aminaho, and Mr. Ndukaegho Sabastine Aminaho are my siblings and great fans of my career.

I cannot forget the love and care from the body of Christ. Ambassadors Word International has been a good environment to grow my Christian faith in God. I would like to thank the President of Ambassadors Word International, Pastor David Okoye, for his commitment to serving the people of God. I would also like to thank different ministers of the gospel around the world playing similar roles and leading the world in God's purpose. Pastor David Okoye and Pastor David Ibiyeomie (founder of the Salvation Ministries Church), great teachers of the gospel of Christ, have played an invaluable role in preparing me for success through their teachings. I am very proud of them for their commitment to building a nation that would fulfil God's purpose.

Finally, I would like to thank everyone committed to combating global climate change through research, funding, and environmental sustainability practices.

ABSTRACT

The geological storage of carbon dioxide (CO_2), also referred to as CO_2 geosequestration, represents one of the most promising options for reducing greenhouse gases in the atmosphere. However, sometimes, CO_2 is captured with small amounts of other industrial gases such as sulphur dioxide (SO_2) and hydrogen sulphide (H_2S), incurring extra costs to separate these other acid gases before CO_2 storage in depleted petroleum reservoirs or aquifers. So, it might be necessary to inject CO_2 with a small amount of these gas impurities to save cost. Moreover, during CO_2 geosequestration in reservoirs, pressure variations during injection and storage could force some amount of CO_2 into the caprock; thereby, altering the petrophysical and geochemical properties of the caprock. Also, CO_2-brine-rock interactions during CO_2 geosequestration can impact the brittleness of the formations due to changes in their mineralogical compositions during the geochemical reactions. Therefore, studies on the co-injection of CO_2 with other acid gases from industrial emissions and their impact on caprock integrity are paramount. In this study, numerical simulations were performed using TOUGHREACT codes, to investigate the injection of pure CO_2 and CO_2 co-injection with SO_2 or H_2S into carbonate and sandstone formations, and their migration to shale caprock. Mineralogical brittleness models were derived from existing models, and one of the models that accounts for the relative level of brittleness of brittleness minerals was applied to evaluate the mineralogical brittleness index of the rocks. In addition, a machine learning approach to predicting the brittleness index of rocks was adopted and an artificial neural network (ANN) model was developed to evaluate the brittleness index of rocks using data from the numerical simulations of CO_2 geosequestration in sandstone and carbonate reservoirs, overlain by shale caprock. The ANN model was developed using Python programming language. The findings of the study revealed that SO_2 gas dissolves faster in brine compared to H_2S gas when co-injected with CO_2 gas in reservoir rocks. Thus, the region in the reservoir contacted by SO_2 gas is smaller compared to H_2S gas. SO_2 gas dissolves more in sandstone reservoirs compared to carbonate reservoirs, due to the availability of more Fe-bearing minerals in the sandstone formation. The findings of the study also indicate that porosity and permeability increase for the CO_2 alone and CO_2-H_2S injection cases, in both the carbonate and shale rocks; while for the CO_2-SO_2 injection case, porosity and permeability increase in the shale rock and carbonate rock (initially composed of calcite and dolomite) and decrease in the carbonate (pure and impure limestone) and sandstone rocks, due to anhydrite precipitation from the injection zone to the reservoir-caprock interface. During cyclic injection and withdrawal of CO_2, for all the injection cases, the porosity and permeability of the sandstone reservoir decreased in a few layers directly below the perforation interval of the production zone. In all the sequestration cases and techniques, the brittleness of the shale and sandstone rocks decreases, while the change in the brittleness of the carbonate rocks varies depending on calcite precipitation or dissolution. The brittleness of the carbonate rock (initially made up of calcite and dolomite minerals) decreased only in a small region in the lower part of the reservoir. Therefore, carbonate reservoirs with similar mineralogy may be suitable for SO_2 gas co-injection with CO_2. Based on the mineralogical composition of the formations in this study, the injection of pure CO_2 or CO_2 co-injection with H_2S or SO_2 decreased the brittleness index of the clay-rich shale caprock slightly. The brittleness index of carbonate-rich shale caprock might increase during pure CO_2 geosequestration. Therefore, a proper understanding of the mineralogical composition of formations before CO_2 geosequestration is vital. The ANN model developed in this study predicted the brittleness index of rocks with R^2 value greater than 99% and mean absolute percentage error (MAPE) of less than 0.7%. Hence, the ANN model predicts the brittleness index of the formations accurately.

Keywords: Carbon dioxide, Geosequestration, Depleted petroleum reservoirs, Caprock, Integrity, Porosity, Permeability, Brittleness index, Numerical simulations, Machine learning

TABLE OF CONTENTS

List of Tables **Page**

List of Figures **Page**

CHAPTER ONE

INTRODUCTION

1.1 Background to the Study

Carbon dioxide (CO_2) geosequestration represents one of the most promising options for reducing atmospheric emissions of CO_2 (Bachu, 2002). It has been proposed as one solution to global climate change caused by heat-trapping of anthropogenic gases in the atmosphere (Wei et al., 2015; Klokov et al., 2017; Liu et al., 2020). What is fascinating about geosequestration is that CO_2 can be stored underground in caverns (salt caverns or engineered caverns) or porous media (aquifer and depleted oil or gas reservoirs). For long-term storage of gases, underground storage in aquifers or depleted oil (or gas) reservoirs is preferable due to the large storage capacity of gases in aquifers and depleted oil or gas reservoirs (Panfilov, 2016). Nonetheless, caprock integrity ascertained based on its petrophysical, geochemical, and geomechanical properties is vital to ensure safe and sustainable storage of CO_2 (Pearce et al., 2016; Liu et al., 2020).

Caprock is any impermeable or low permeability formation that may trap gas, oil, or water, preventing it from migrating to the surface (Klokov et al., 2017). Originally, most cap rocks have high mechanical strength, high stiffness, high capillary entry pressure, low compressibility, and very low permeability (Smith et al., 2009; Edlmann et al., 2013). However, during petroleum depletion as well as CO_2 injection and storage, caprock undergoes stresses and strains that impact its integrity. Hence, for long-term CO_2 storage, it is paramount to understand whether stress and strain changes caused by the gas injection or storage would lead to irreversible mechanical damage of the reservoir and impact the caprock integrity which could lead to CO_2 leakage, through previously sealing structures (Li, 2016). Thus, to properly evaluate caprock integrity, certain criteria based on rock theories of failure and rock mineral alterations must be set to reflect changes in the brittleness of reservoir and cap rocks.

During CO_2 injection and storage, the CO_2-brine-rock interaction results in dissolution and/or precipitation of minerals which impacts the petrophysical and geomechanical properties of the rock. Due to the mineral alterations, the resulting change in mechanical properties of the minerals impact the brittleness of the rock. Thus, different concepts including fraction of reversible strain to total strain at rock failure (Hucka and Das, 1974; Hou et al., 2018; Li, 2022), brittleness based on rock strength parameters (Hucka and Das, 1974; Meng et al., 2015; Li, 2022), brittleness based

on rock elastic parameters (Luan et al., 2014; Rickman et al., 2008), and brittleness based on mineralogical composition of the rock (Guo et al., 2016; Kang et al., 2020; Li, 2022) have been adopted to determine the brittleness of rocks. So, different studies have been conducted to investigate the impact of CO_2 geosequestration on the petrophysical, geochemical, and geomechanical properties of rocks.

Dissolution of primary minerals in reservoir and cap rocks during pure CO_2 geosequestration increases their porosity and permeability (Wang et al., 2022, Fatima et al., 2021). The maximum impurity level of H_2S and SO_2 in captured CO_2 can be as high as 3.2 mol% and 2.5 mol%, respectively (Murugan et al., 2019). An increase in permeability of reservoir and caprock has been observed in the case of co-injection of CO_2 and 100 ppm of H_2S in an experimental study conducted by Bolourinejad and Herber (2014) on Permian Rotliegend sandstone reservoir (no initial calcite content) and Zechstein caprock (anhydrite and carbonate component) core samples at in situ conditions of 300 bar and 100 ^{0}C for 30 days. In the case of co-injection of CO_2 and 100 ppm of SO_2, the permeability of the sandstone reservoir rock samples increased by a factor of 1.18 to 2.2, while the permeability of the caprock samples changed by a factor of 0.8 to 23 (permeability increased in caprock samples with a higher ratio of initial carbonate mineral concentration to anhydrite content, due to the carbonate dissolution). The increase in the permeability of the sandstone reservoir for the CO_2-SO_2 co-injection case could be attributed to the lack of calcite content in the initial composition of the rock. Thus, the release of Ca^{2+} from dolomite dissolution was not enough to precipitate a significant amount of anhydrite (which could have decreased the permeability of the reservoir rock in the CO_2-SO_2 case) as the duration of the experiment is short (Hedayati et al., 2018).

A similar experimental study was conducted by Aminu et al. (2018) to evaluate the effect of impurities on the permeability of sandstone reservoirs at 70^{0}C and 140 bar for 9 months. They found that the effect of H_2S on the permeability of the reservoir is relatively small. CO_2 increased the reservoir rock permeability by 5.83%, while CO_2-H_2S increased it by 6.25%. CO_2 co-injection with SO_2 slightly decreased permeability by 6.25%; while CO_2 co-injection with NO_2 significantly decreased permeability by 41.67%. The changes in the rock permeability are significantly influenced by the existing rock minerals dissolution and precipitation, as well as the precipitation of secondary minerals. These changes in permeability and porosity result from the dissolution of these gases in formation water, thus reducing pH which enhances chemical reactions in the rock and results in the dissolution and precipitation of minerals (Li et al., 2016; Pearce et al., 2016; Pearce et al., 2019).

Changes in the porosity of reservoir and cap rocks during CO_2 geosequestration are also impacted by the formation temperature and pressure. Davila et al. (2017) found that porosity of the caprock increases more under any partial pressure of CO_2 at lower temperature, while porosity reduced as temperature increased. Moreover, as partial pressure of CO_2 rises (increase in proportion of dissolved CO_2 in the formation water up to supercritical condition), porosity of the caprock enlarges over greater distances. Thus, the temperature of the system could have selective impact on dissolution and precipitation of minerals, and temperature is inversely related to porosity of the rock at the conditions considered. Therefore, dissolution or precipitation of minerals, and changes in porosity and permeability of a rock depend on the amount of impurities in the injected CO_2 stream, brine composition, lithology of the rock, formation temperature and pressure, and duration of CO_2 geosequestration.

AL-Ameri et al. (2014) and Tariq et al. (2018) studied the time-dependent effect of CO_2 geosequestration on the mechanical properties of rocks. Mechanical weakening of the rock increases with the duration of CO_2 geosequestration. Alam et al. (2014) found that the impact of supercritical CO_2 injection on the geomechanical properties of chalk depends on the carbonate mineral content as rocks with high carbonate content experience significant mechanical weakening due to CO_2 injection, while rocks with low carbonate content experience a negligible amount of mechanical weakening. In sandstone and shale rocks, Young's modulus, uniaxial compressive strength, and Brazilian tensile strength decrease with co-injection of supercritical CO_2 ($scCO_2$) and brine (Huang et al., 2018; Lyu et al., 2018). But, the tensile fracturing behaviour of sandstone is not significantly affected by gaseous CO_2 in the presence or absence of water (Liu et al., 2014). Masoudi et al. (2011) found that at low injection pressure (below 4200 psi), carbonate reservoir and shale caprock remained elastic even though the strength and elastic properties of the materials degraded as CO_2 saturation increased, and the local permeability of the carbonate reservoir increased up to 70% due to injection. Compactions induced in the reservoir rock during CO_2 production were completely recovered during the injection phase to their pre-production values when the reservoir pressures were restored. However, at high injection pressure, the rocks experience plastic deformation. Thus the rocks could fail over a certain amount of plastic deformation depending on the level of brittleness of the rocks.

Lyu et al. (2018) conducted an experimental study and developed a damage constitutive model to investigate the effects of CO_2-brine-rock interactions on the brittleness index of a low-clay shale (with a carbonate or calcite content of only 4.4 wt.%, cristobalite content of 2.88 wt.%, quartz content of 55.50 wt.%, feldspar content of 14.57 wt.%, clay content of 5.85 wt.%, and other

minerals). They found that the CO_2-brine-shale interactions in the soaked shale sample decreased the brittleness values. A similar experimental study was conducted by Elwegaa et al. (2019) to investigate the impact of cyclic cold carbon dioxide injection on the brittleness of shale rock samples. The shale rock samples used in the study were carbonate-rich with 81.6 wt.% calcite, 14.2 wt.% calcite, 3.0 wt.% kaolinite, and 1.3 wt.% basanite. The rock samples were subjected to the same cyclic injection temperature conditions (74^0F, 32^0F, 0^0F, and -15^0F), but different injection pressure conditions (1000 psi, 2000 psi, 3000 psi, or 4000 psi). They observed an increase in the brittleness index (or brittleness ratio) of the three shale core samples, while the brittleness index of the fourth shale core sample subjected to cyclic injection temperature conditions at 3000 psi decreased. Elwegaa et al. (2019) evaluated the brittleness index of the rock samples mainly by the ratio of the sum of the volume of quartz and dolomite to the sum of the volume of all the minerals in the rock sample; and the brittleness ratio was evaluated based on dynamic elastic modulus and Poisson's ratio, which do not accurately reflect the brittleness of rocks.

However, the decrease in the brittleness index of the low-clay shale samples in the study conducted by Lyu et al. (2018) might be related to the low initial carbonate content, while the increase in the brittleness index of the shale rock samples in the study conducted by Elwegaa et al. (2019) might be related to the high initial carbonate content of the shale rock samples. Therefore, it is important to evaluate the brittleness index of different formations (with different initial mineralogical compositions) subjected to CO_2 sequestration conditions using a similar and more robust mathematical model for a better comparison. Other studies on the brittleness of rocks have not considered the impact of CO_2 injection on the brittleness of rock but developed models to determine the brittleness of rocks based on the weight fraction of the minerals (Kang et al., 2020), tensile brittleness index (Hou et al., 2018), and post-peak stress-strain curves under different confining pressure conditions (Meng et al., 2015).

Meanwhile, CO_2 geosequestration could involve a non-cyclic or cyclic process. On the one hand, a non-cyclic process entails the injection of CO_2 over a period, then the injection is stopped, and the injected CO_2 is trapped in the reservoir. On the other hand, the cyclic process of geosequestration involves the injection of CO_2 for some period (in some cases, withdrawing some of the injected CO_2 and leaving behind some amount of CO_2 in the reservoir), and repeating the process over the geosequestration period. Cyclic injection and withdrawal of CO_2 in reservoirs might be an effective technology to promote CO_2 utilization, as this technology would enable seasonal injection and withdrawal of CO_2. Following this approach, CO_2 can be produced from

the reservoir when needed for electrochemical hydrogen production (Koomson et al., 2023), to produce renewable methanol (Sollai et al., 2023; Wang et al., 2023) or other forms of energy. Thus, the utilization of CO_2 for energy creation will reduce the world's reliance on fossil fuels (Wang et al., 2023).

CO_2 storage is possible by its different trapping mechanisms including residual trapping, solubility trapping, mineral trapping, and structural/stratigraphic trapping mechanisms (Sun et al., 2016). Residual trapping occurs as injected CO_2, which initially displaced the existing water (or brine) in the reservoir, gets displaced as the formation water imbibes back to the trailing edge of the CO_2 plume and traps the gas in the form of isolated blobs. This trapping mechanism occurs relatively fast during CO_2 injection. As the injected CO_2 comes in contact with brine in the reservoir, some of it will dissolve into the formation water (solubility trapping). Thus, the fluid phase can no longer exist separately and the buoyant force that drives it upwards is eliminated. After some time, the dissolved CO_2 in water lowers the initial brine pH (acidification of the groundwater) resulting in fluid-rock interactions (chemical reactions) and leading to mineral trapping as the rock is made up of different minerals. This mineralization reaction begins after some time during CO_2 injection and continues during the storage life of the porous rock leading to dissolution and precipitation of minerals or aqueous complexes. During the period of CO_2 geosequestration, it is important to have a physical (or structural) trapping which impedes the migration of CO_2 plume to the earth's surface. It is a region or layer of porous media with a low-permeability seal and high capillary entry pressure, and caprock serves this purpose (Saraji et al., 2013; Edlmann et al., 2013; Sun et al., 2016).

Residual trapping of CO_2 increases during cyclic CO_2 injection (Herring et al., 2016; Edlmann et al., 2019). During cyclic CO_2 injection, about 40-50% of CO_2 can be stored mainly through residual and solubility trapping mechanisms in the porous medium (Abedini and Torabi, 2014). Water alternating gas (CO_2) and CO_2 cyclic injection strategies provide significantly higher effective CO_2 storage capacities compared to the continuous CO_2 injection strategy (Li et al., 2021). However, residually trapped CO_2 might reconnect with injected CO_2 in subsequent injection cycles mainly close to the large pore clusters, like the cyclic hydrogen (H_2) injections (Lysyy et al., 2023). Moreover, increased residual trapping of CO_2 during cyclic injection, could result in reduction in effective permeability, thereby limiting flow and injectivity (Edlmann et al., 2019).

The exposure of supercritical CO_2 in certain geologic materials may induce surface chemical reactions which are time-dependent (Herring et al., 2016). Thus, the surface chemical reactions

can influence the pore structure of the rock (especially over longer periods of cyclic CO_2 injection), as dissolution-dominant reactions of rock minerals would result in increased porosity and permeability, while precipitation-dominant reactions would result in decreased porosity and permeability of the rock (Xu et al., 2014; Ma et al., 2019). Elwegaa et al. (2019) conducted a study on cyclic cold carbon dioxide injection for improved oil recovery from shale oil reservoirs. They found that injection of cold CO_2 increased both porosities and permeabilities of the core samples by up to 3.5% and 8.8%, respectively. The porosity and proportion of macropores of coal (a porous medium for CO_2 storage) increase after treatment on cyclical injection of supercritical CO_2, as new pores were formed and some small pores possibly converted into macropores (Su et al., 2021). Moreover, the microporosity of sandstone increases during cyclic wetting-drying process, similar to cyclic CO_2 injection, as the microstructure of the rock changes. The driving forces of the changes in the microstructure of the sandstone is water-rock interaction including physical, mechanical, and chemical interactions (Ke et al., 2023). The chemical interaction that causes the dissolution and precipitation of some minerals in the rock can increase or decrease the porosity of the rock. For instance, in a study conducted by Badrouchi et al. (2022), after four CO_2 injection cycles, the effective porosity of the rock samples decreased, as the dissolved CO_2 could react with rock minerals and form precipitates that block some pores. These changes in the microstructure impact the petrophysical (porosity and permeability) and mechanical (elastic and strength parameters) properties of the rock.

Experiments conducted on coal samples (a porous medium that has similar minerals found in other rocks, although in different proportions) show that the uniaxial compressive strength (or peak strength) of coal samples decreases more in the case of cyclic CO_2 saturation and as the cycles get larger (increased number of cycles), compared to continuous (sustained) saturation (Su et al., 2020; Xu et al., 2021). Rocks' strength and deformation (or elastic) parameters are strongly dependent on the mineral compositions of the rock samples (Li et al., 2023). Li et al. (2023) conducted an experimental study to evaluate the mechanical properties of different shale-layered samples with different mineral compositions under cyclic loading. They found that Young's (elastic) modulus of the clay-rich shale was highest, followed by calcareous and siliceous shale; while the Poisson's ratio of calcareous shale was observed to be highest, followed by clay-rich and siliceous shale samples. In addition, the compressive strengths under cyclic loading and unloading were lower compared to the compressive strengths under uniaxial quasi-static loading. Due to the variations in the mineral compositions of the shale samples, the average decline in the compressive strength of calcareous shale was the largest, followed by the siliceous and clay-rich

shale. The relatively higher average decline in the compressive strength of the calcareous shale might be related to the increase in the brittleness index of the carbonate-rich shale rock samples in the study conducted by Elwegaa et al. (2019). Furthermore, Xu et al. (2022) found that the compressive strength and elastic modulus of coal samples correlate negatively with the increasing cyclical parameters, while the Poisson's ratio and damage variable positively correlate with the increasing affecting parameters. This non-uniform variation in Young's modulus and Poisson's ratio might be related to the brittleness of rocks, as these parameters are used in brittleness index evaluations. Thus, it is possible that the brittleness of rocks varies during cyclic CO_2 injection.

The studies reviewed have considered the impact of CO_2 and impurities (H_2S, SO_2, or NO_2) on porosity, permeability, and mineralogical changes in different rock lithologies, as well as the impact of pure CO_2-brine interaction on geomechanical properties and brittleness of rocks. Furthermore, several researchers have studied cyclic CO_2 injection as a drainage-imbibition process in which case CO_2 is injected followed by water, from the same end of the rock sample and similar to water alternating gas approach of enhanced oil recovery: or periodic injection of CO_2 and producing from the other end of the reservoir (in cartesian coordinate system) or observing the impact of the injected CO_2 in the reservoir. To the best knowledge of the researcher, no study has been conducted to investigate the impact of CO_2 impurities (H_2S or SO_2) on the brittleness of reservoir or cap rocks during cyclic or non-cyclic CO_2 injection technique of CO_2 geosequestration. In addition to the non-cyclic approach of CO_2 geosequestration, the present study adopts a novel approach of cyclic CO_2 geosequestration (with or without H_2S/SO_2 impurity) to promote CO_2 utilization and storage by injecting CO_2 at the bottom of the reservoir and producing CO_2 at the top part of the reservoir using the same well for both operations, to save cost and produce a purer form of CO_2 (with little or no formation water production). Thus, the utilization of CO_2 for energy creation will reduce the world's reliance on fossil fuels (Wang et al., 2023). However, the cyclic injection-withdrawal of CO_2 (with or without impurities), will induce cyclic stress in the reservoir and cap rocks (as bottomhole pressure is higher during injection, and lower during fluid withdrawal from the reservoir), thereby altering the petrophysical, geochemical, and geomechanical properties of the rocks. During CO_2 geosequestration (cyclic or non-cyclic), as the mineralogical compositions and petrophysical properties of the rocks are altered, the brittleness of the rocks might be impacted. It is important for the caprock to be less brittle relative to the reservoir rock during CO_2 geosequestration to minimize the chance of fracturing the caprock and creating pathways for CO_2 leakage to the earth's surface. A highly brittle rock can be easily fractured by an increase in pressure in the formation. Therefore, a decrease in the brittleness

index of caprock and an increase in the brittleness index of reservoir rocks are favourable during CO_2 geosequestration. Hence, this study evaluates the impact of impurities in CO_2 on the petrophysical properties and brittleness index of reservoir and cap rocks during CO_2 geosequestration.

1.2 Statement of the Problem

There has been significant climate change over the past few decades compared to a century ago, as CO_2 emissions from industrial activities have increased. Reduction and possibly elimination of industry-based greenhouse gas emissions have become almost a daily discussion among scientists and environmental protection advocates in every part of the world. In fact, in Paris Agreement of 2015, all the parties to the United Nations Framework Convention on Climate Change agreed on putting more effort and investments into combating climate change and creating a net-zero carbon future for the world. A key strategy to achieving this goal is the geosequestration of CO_2 in depleted hydrocarbon reservoirs, to remove anthropogenic CO_2 emissions from the atmosphere. It is true that such reservoirs originally contained pressurized gases over long geological times as their natural caprock integrity was sufficient. However, there is no guarantee that after depletion of the hydrocarbon that the caprock is still capable of containing injected CO_2. In fact, some impurities can be found in association with CO_2 and it is necessary to investigate if some of the impurities could possibly enhance the self-sealing of caprock. Nonetheless, cap rocks have different mineralogical compositions (clay-rich, calcareous, or siliceous shale), and their properties are influenced by their environment of deposition and the tectonic activities such rocks have undergone. Therefore, their grain size distribution and pore networks are different and could impact their potential to maintain caprock integrity during CO_2 geosequestration.

Furthermore, complex pressure variation exists in reservoirs during CO_2 injection. During CO_2 injection, a slight increase in reservoir pressure or CO_2 injection pressure could result in reservoir fluid invasion into the caprock as soon as its capillary entry pressure is exceeded. CO_2 could also migrate into the caprock through diffusion, over a long period. Moreover, CO_2 streams contain some fraction of gas impurities such as H_2S or SO_2. Thus, as CO_2 penetrates the caprock, these gas impurities might continue to invade some of the caprock layers with the CO_2 by convective reactive transport. Hence these invaded reservoir fluids become trapped in the caprock layers penetrated. The CO_2 mixture could alter the mineral composition of the rock, and consequently change the brittleness of the caprock. If the brittleness of the caprock layers contacted by the CO_2

mixtures increases, with a slight increase in the reservoir pressure during the period of CO_2 injection or storage, it will become easier for the reservoir fluid to induce tensile fracture in the caprock layers. Otherwise, the caprock layers are able to handle a higher amount of developed pressure during the period of CO_2 geosequestration. Therefore, investigating the impact of CO_2 mixtures on the brittleness of caprock is paramount.

To properly evaluate the brittleness of cap rocks, the rock mineralogical and mechanical changes are required, as the changes in brittleness are controlled by alteration of the rock minerals and geomechanical properties. During CO_2 geosequestration in depleted petroleum reservoirs or aquifers, the rock experiences induced stresses as the fluid flows through interconnected pore spaces and contacts the surrounding rock grains, especially during the cyclic injection process. The induced stresses developed lead to deformation and reduction in the strength (weakening) of the cement in rocks during CO_2 sequestration (Liu and Dai, 2021). Moreover, most times, CO_2 is captured with some other acid gases (such as H_2S and SO_2) and injected in petroleum reservoirs or aquifers. These acid gases might impact the reservoir and caprock integrity. Hence, the problem of this study is to find out whether the co-injection of CO_2 with some gas impurities impacts the petrophysical properties and brittleness of reservoir and cap rocks.

1.3 Aim and Objectives of the Study

The aim of this study is to evaluate caprock integrity for geosequestration of CO_2 in depleted petroleum reservoirs.

In specific terms, the objective of this study is to:

1. investigate the impact of impurities in CO_2 on the porosity, permeability, and geochemical composition of reservoir and cap rocks during injection, withdrawal, and storage of CO_2 gas stream;
2. derive mathematical models to calculate the brittleness index of reservoir and cap rocks based on their mineral volume fraction;
3. evaluate the impact of impurities in CO_2 on the brittleness index of reservoir and cap rocks during the non-cyclic and cyclic process of CO_2 geosequestration;
4. determine best depleted reservoirs and suitable caprock lithology for CO_2 geosequestration, based on changes in their porosity, permeability, and brittleness index;

5. develop a machine learning model to predict the brittleness index of rocks before and during CO_2 geosequestration.

1.4 Significance of the Study

The outcome of this study will impact the Carbon Capture, Utilization, and Storage (CCUS) industry. The findings on the selection of best-depleted oil and gas reservoirs or aquifers for CO_2 storage will help the CCUS industry in taking proactive measures in identifying such reservoirs (and cap rocks) even during oil and gas production (or depletion) as this study adopts the same approach of evaluating caprock integrity before and during CO_2 geosequestration. Furthermore, based on the properties of the caprock, better operational conditions for CO_2 injection and storage will be developed to maintain caprock integrity and save the industrial cost of pollution as CO_2 leakage to the surface will be prevented. Also, cost of decommissioning will be saved, by adopting proactive measures which this study provides, as suitable reservoirs for CO_2 injection or storage will be identified even during oil or gas production life of the reservoir. Thus, only wells around reservoirs that are not useful for CO_2 injection, withdrawal, or storage are decommissioned. In addition, this study will provide more insight into the feasibility of seasonal energy storage and CO_2 utilization, by adopting the technology of cyclic injection-withdrawal of CO_2 during the geosequestration period. Overall, this study provides the carbon capture, utilization, and storage (CCUS) industry with valuable tools to evaluate the integrity of reservoir and cap rocks for injection, withdrawal, and storage of CO_2.

1.5 Contribution to Existing Body of Knowledge

This study evaluates caprock integrity during the non-cyclic and cyclic process of CO_2 geosequestration. To achieve the cyclic process of CO_2 geosequestration, a dual-tubing string system of well completion was designed in this study for cyclic injection and withdrawal of CO_2 gas streams. Hence, cyclic stress was created in the formations as CO_2 (with or without impurities) is injected at a higher bottom hole pressure to enable the displacement of existing fluids in the reservoir, and withdrawn at a lower bottom hole pressure to enable flow from the reservoir to the wellbore. This study further evaluates the impact of co-injecting SO_2 or H_2S impurities with CO_2 on the petrophysical properties and brittleness index of reservoir and cap rocks.

The impact of injecting pure CO_2 or co-injecting SO_2 or H_2S impurity with CO_2 on the porosity and permeability of reservoir rock (sandstone or carbonate) and shale caprock were evaluated in the non-cyclic and cyclic approach of CO_2 geosequestration. Thus, providing a detailed comparison

of porosity and permeability changes during CO_2 geosequestration. The changes in the porosity and permeability of the rocks can be used to evaluate the self-sealing potential of rocks, as well as their injectivity and productivity, during CO_2 geosequestration.

Furthermore, mathematical models were derived in the present study to evaluate the mineralogical brittleness index of reservoirs and caprocks based on the volume fraction, molecular weight, and molar volume of the rock minerals. Thus, making it possible to evaluate the mineralogical brittleness index of rocks from numerical simulation results, as volume fractions (not weight fractions) of minerals are outputted from reactive transport modelling of CO_2-brine-rock interactions (after mineral dissolution or precipitation). In addition, previous studies have only evaluated the impact of pure CO_2 (without other gas impurities) on the brittleness index of shale rocks. But the present study evaluates the impact of CO_2, with or without gas (SO_2 or H_2S) impurities, on the brittleness index of shale rocks (clay-rich and carbonate-rich shale) as well as carbonate and sandstone rocks using the derived mathematical model.

Finally, machine learning models were developed in this study, to establish that the brittleness index of a formation can be predicted from the ionic composition of the formation fluid and the formation temperature. Thus, this study contributes to the existing body of knowledge by providing a combination of methods and parameters to determine the best depleted petroleum reservoirs for CO_2 geosequestration and to evaluate the integrity of the caprock.

1.6 Scope of the Study

This study is based on numerical simulations to evaluate the impact of sulphur dioxide (SO_2) or H_2S impurities during CO_2 geosequestration in depleted petroleum reservoirs. However, the depleted petroleum reservoir considered in this study was assumed to be under a strong aquifer, such that a very large fraction of the hydrocarbon in the reservoir has been produced and the reservoir pore spaces were replaced by water. Therefore, the reservoir simulation is similar to CO_2 geosequestration in aquifers. Thus, the effect of hydrocarbon reactions with the injected gases and formation water were not considered in this study.

Coupled thermal, hydrological, and chemical (THC) numerical simulations were performed to investigate petrophysical and geochemical changes of the rocks (carbonate, sandstone, and shale rocks) during CO_2 injection and storage, and determine mineralogical brittleness index of the rocks at constant reservoir and caprock temperature. Thus, the selection of best depleted petroleum reservoirs for CO_2 storage was based on changes in petrophysical properties of the

reservoir and cap rocks as well as changes in their brittleness index. Changes in the properties of sandstone and carbonate reservoirs, and shale caprock were evaluated during the non-cyclic approach of CO_2 geosequestration; while only changes in the properties of sandstone reservoir and shale caprock were evaluated during the cyclic approach of CO_2 geosequestration.

1.7 Structural Outline of the Study

This study is organised into five chapters (Chapter One to Chapter Five), namely, Introduction, Literature Review, Research Methodology, Results and Discussions, and Conclusions and Recommendations.

In Chapter One, the background to the study and the problem this study intends to address have been explored. The research aim and objectives have been identified. The significance of the study to the CCUS industry and the contribution of the research to the existing body of knowledge have been discussed. The scope of the study has also been discussed.

In Chapter Two, existing literature relevant to this study will be reviewed, and theories upon which the brittleness index of rocks is evaluated will be laid out. The rock types that will be discussed in the literature review as reservoirs are sandstone, carbonate, carbonate-rich shale, coal, and unconventional shale reservoir rock; while the rock types that will be discussed as a caprock are mainly anhydrite (with a small fraction of carbonate minerals), carbonate, marl, calcareous shale (calcite-rich), siliceous shale (rich in silica mineral or silicon dioxide), clay-rich shale, and siltstone. So, some formations considered as reservoir rocks may also be suitable as cap rocks, depending on their permeability. Reservoir rocks have a higher permeability, while cap rocks have relatively low permeability.

In Chapter Three, the research methodology will be explored. This chapter will include the derivation of mathematical models for the calculation brittleness index of rocks, the design of the well and reservoir-caprock system for the non-cyclic and cyclic approach of CO_2 (with or without impurities) geosequestration, reactive transport numerical modelling approach using TOUGHREACT codes, the equations for calculating the porosity and permeability of rocks from reactive transport modelling, the analytical approach of applying the brittleness index models, the development of machine learning models for the prediction of brittleness index of rocks, and the limitations of the study.

In Chapter Four, the results from the data analysis will be presented and discussed based on the objectives of the study.

In Chapter Five, Conclusions will be made based on the research findings, and recommendations for future studies will be made. Also, the contributions of the research to practice will be discussed.

CHAPTER TWO

LITERATURE REVIEW

2.1 Conceptual Review

CO_2 geosequestration represents one of the most promising options for reducing atmospheric emissions of CO_2 (Bachu, 2002). It involves the injection and storage of captured CO_2 in geological structures. These geological structures are mainly aquifers or depleted oil or gas reservoirs. CO_2 geosequestration has been proposed by different scholars as one solution to world climate change resulting from heat-trapping (Wei et al., 2015; Klokov et al., 2017; Liu et al., 2020). CO_2 storage is possible by its different trapping mechanisms including residual trapping, solubility trapping, mineral trapping, and structural/stratigraphic trapping mechanisms (Sun et al., 2016). During the period of CO_2 geosequestration, it is important to have a good seal or caprock overlying the reservoir rock which impedes the migration of CO_2 plume to the earth's surface.

2.1.1 Caprock

Caprock, is a low permeability or impermeable formation (Figure 2.1), that is capable of trapping gas, oil, or water; ensuring those fluids do not migrate to the surface (Klokov et al., 2017). Originally, most cap rocks have high mechanical strength, high stiffness, low compressibility, and very low permeability (Smith et al., 2009). However, during petroleum depletion as well as CO_2 injection and storage, caprock undergoes stress and strain which impact its integrity. For long-term CO_2 storage, it is paramount to understand whether stress and strain changes caused by CO_2 injection would lead to irreversible mechanical damage of the reservoir and impact the caprock integrity, in which case CO_2 leakage could be experienced through previously sealing structures (Li, 2016).

Deformation of caprock results from several factors including the impact of fluid properties in the reservoir-caprock system and impurities in association with CO_2, variation in temperature and pressure of the reservoir-caprock system, and the rock properties in general (Pearce et al., 2016; Li et al., 2018; Liu et al., 2020). These factors can result in change in the petrophysical, geochemical, and geomechanical properties of the rock. The caprock should be such that can withstand the short-term excess injection pressure as well as the long-term buoyancy pressure (Espinoza and Santamarina, 2017). Thus, caprock integrity ascertained based on the

petrophysical, geochemical, and geomechanical properties of caprock is paramount to ensure sustainable storage of CO_2 (Liu et al., 2020).

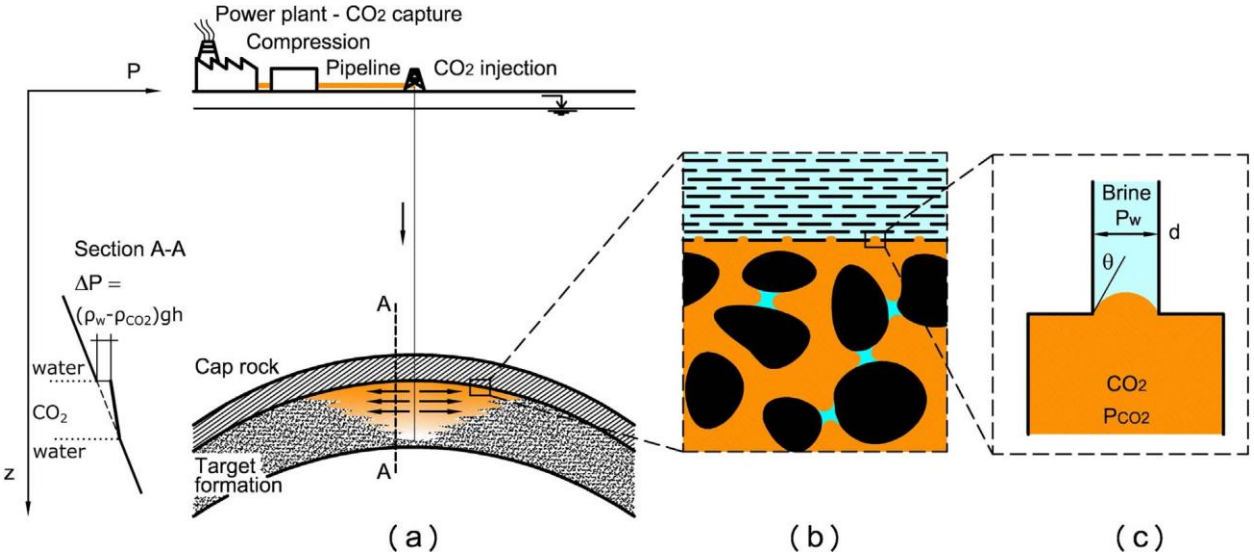

Figure 2.1: Carbon dioxide geosequestration beneath a caprock (a) injection and storage of captured CO_2 (b) CO_2-water menisci at the interface between the reservoir and the caprock (c) Capillary-tube analogy for water-wet minerals (Espinoza and Santamarina, 2017).

During CO_2 injection, rock pore pressure increases and could lead to changes in stress and strain in the reservoir and cap rocks. However, changes in the rock porosity caused by the variation of pressure and total mean stress could be small and limited. In fact, with a certain CO_2 injection rate as high as 200,000 t/yr, the geomechanical effect can be very small (Li, 2016). In such a case, both the reservoir and cap rocks might behave elastically with no noticeable plastic deformations under the conditions considered. A stress path analysis could indicate that the caprock still retains the primary stress state and the caprock integrity is not significantly affected (Gou et al., 2016). Although supercritical CO_2 is known to extract organic matter from rocks (Okamoto et al., 2005), specimens reacting with only supercritical CO_2 can induce a self-sealing effect as secondary sediments precipitate, creating a more intact rock with increased elastic modulus and strength. But, when brine is found in association with supercritical CO_2, which is common in aquifers and depleted oil and gas reservoirs, dissolution dominates precipitation which consequently leads to the weakening of the rock mechanical properties (Choi et al., 2021). So, impurities in CO_2 storage systems, especially in aquifers and depleted oil and gas fields, impact reservoir and caprock integrity.

Carbon dioxide streams stored geologically from industrial sources, for example, coal oxy-fuel firing sources (or coal combustion sources), steel or cement processing contain gas impurities that might have higher or lower reactivity to rock than pure CO_2 (Pearce et al., 2016; Pearce et al., 2019). Reactive impurities co-injected with CO_2 might have detrimental effects on seal performance (Lu et al., 2014) or enhance caprock integrity through a self-sealing mechanism (Pearce et al., 2016). However, the sealing capacity of caprock is highly controlled by the anisotropy and heterogeneity of macropores (Wu et al., 2019). Shale and carbonate rocks are typical cap rocks for CO_2 geosequestration, but their failure mechanisms have not been properly understood due to their severe anisotropy and heterogeneity (Wu et al., 2019; Liu et al., 2020). Anisotropy refers to the variation in properties of materials with direction (the value of the property of the material at the same location changes depending on the direction in which the measurement is made), while a material is heterogeneous if its properties (for example, porosity) when measured in the same direction change with location in 3D space (Liu and Martinez, 2014). The pore throat structures of different carbonate cap rocks (e.g. dolomite, limestone, etc.) are affected by lithology. In other words, even different carbonate cap rocks in the same field have different pore throat structures (Wu et al., 2019). It is believed that the more poorly sorted the grains in a rock are, the more efficient packing, lower porosity, and higher velocity it produces due to framework stiffening (Nooraiepour et al., 2017).

However, in a study conducted by Du and Radonjic (2019) on the mechanism of fracture initiation in shale rocks (Pottsville shale caprock and Marcellus unconventional reservoir-shale), Pottsville shale (with a smaller range of grain size compared to Marcellus shale) exhibited higher rigid grain content and higher bulk mechanical properties (including Young's modulus, which is a measure of the stiffness of a material). It is worth noting that Pottsville shale has about 46% clay minerals (no carbonate content), while Marcellus shale is carbonate-rich (about 27%) and has about 22% clay minerals. Both shale rocks have homogeneous grain distribution. However, Pottsville shale has more uniform grain size (smaller range of grain size) compared to the Marcellus shale (wider range of grain size). Du and Radonjic (2019) concluded that Pottsville shale has better sealing properties than Marcellus shale, even though one would have expected Marcellus shale to exhibit higher mechanical properties due to its wider range of grain size. So, there is a limit to the extent of heterogeneity in rock grain distribution to maintain its sealing capacity. It is possible that the range of grain size and the high clay content of the Pottsville shale were enough to create an effective framework stiffening that resulted in the rock having higher bulk mechanical properties than the Marcellus shale.

Caprock sealing capacity can be evaluated from capillary pressure. Capillary entry and breakthrough pressures can give an insight into the early stage of deformation and the extent of deformation. The capillary entry pressure represents the highest amount of pressure difference that might be experienced across the interface between two immiscible fluids before the penetration of the non-wetting fluid into the pore space (Minardi et al., 2021). Capillary entry pressure (P_{cE}) is simply the pressure difference between non-wetting fluid phase and wetting fluid phase. For CO_2 injection, it signifies when CO_2 phase pressure (P_{CO2}) is high enough to displace water (or brine) in the caprock formation (Zhou et al., 2017). This threshold capillary pressure (P_{cE}) for the CO_2 phase, based on the Laplace law, is given as

$$P_{cE} = P_{CO_2} - P_w \approx \frac{2\sigma cos\theta}{r} \qquad 2.1$$

Where P_w is the water (or brine) pressure, r is the radius of the largest connected pore throats in the caprock, σ is the water (or brine)/CO_2 interfacial tension, and θ is the contact angle of the rock/water/CO_2 system measured through the water phase (Edlmann et al., 2013, Zhou et al., 2017). Small pores in clay-rich rocks result in high capillary entry pressures and high viscous drag that limit the migration of buoyant carbon dioxide (Espinoza and Santamarina, 2017). In fact, gas phase CO_2 has a larger capillary pressure than the supercritical CO_2 phase (Edlmann et al., 2013). The breakthrough pressure, which represents the pressure difference when water (or brine) is produced downstream due to CO_2 invasion in the caprock, increases as the sediment specific surface increases and the porosity (or pore throat size) decreases (Espinoza and Santamarina, 2017). Capillary breakthrough pressure is higher than the capillary entry pressure. In other words, once the CO_2 starts to penetrate the rock sample (on a laboratory scale), the pore fluid has to be displaced under the influence of the capillary forces, and the time of migration across the sample before reaching the downstream side should be noted (Minardi et al., 2021).

Generally, leakage of CO_2 during geosequestration could occur through diffusion of CO_2 through the water-saturated caprock; when the capillary entry pressure is exceeded, leading to the leakage of CO_2 through the interconnected flow paths in the pore system of the caprock; or natural or induced fracture flows in the caprock (Edlmann et al., 2013; Minardi et al., 2021). Diffusive and advective CO_2 leaks through a caprock that has not been fractured will be minor and might not compromise the storage capacity of CO_2 in the underlying reservoir (Espinoza and Santamarina, 2017). However, rapid leakage in the caprock may result from capillary failure, which is controlled by the CO_2/brine interfacial tension and CO_2/brine/caprock mineral contact angle (Saraji et al.,

2013). Therefore, CO_2 streams composed of different impurities would result in different interfacial tensions and contact angle, leading to variation in capillary entry pressure for the different fluid mixtures. For instance, if the wettability (contact angle) of the caprock changes during CO_2 geosequestration from strongly to weakly water-wet, the capillary entry or threshold pressure is reduced (Saraji et al., 2013).

Furthermore, mineral dissolution or precipitation during CO_2 geosequestration leads to microstructural changes in rocks, resulting in increase or decrease in the porosity and permeability of the reservoir and cap rocks. For dissolution-dominant pore fluid-rock interaction, porosity and permeability increase, while for precipitation-dominant interaction, porosity and permeability decrease. Moreover, caprock formations that exhibit low reactivity to carbonic acid and capable of maintaining their integrity at low pH conditions are preferred for geosequestration of CO_2 (Minardi et al., 2021). Ideally, the ductility of caprock would allow it to deform without developing high permeability pathways that can enable CO_2 leakage (Espinoza and Santamarina, 2017). Therefore, it is paramount to select less brittle cap rocks for CO_2 geosequestration.

2.1.2 Brittleness

Brittleness is defined as a deficiency of plasticity during material failure (Hou et al., 2018). It is an important characteristic to evaluate the ‘drillability’ and ‘fracability’ of rocks (Lyu et al., 2018). Rocks that are very brittle are easier to drill and fracture, as they do not exhibit significant ductile or plastic behaviour before failure. In other words, the rock terminates by fracture only slightly beyond or at the yield stress (that is, little or no plastic deformation occurs at failure) (Hucka and Das, 1974; Meng et al., 2015). In terms of a reservoir-caprock system for CO_2 storage, it is important for the caprock to be less brittle relative to the reservoir rock during CO_2 geosequestration to minimize the chance of fracturing the caprock and creating pathways for CO_2 leakage to the earth's surface. Different methods have been proposed for the evaluation of the brittleness of geomaterials, generally referred to as the brittleness index. Different approaches for the evaluation of the brittleness index of rock include geochemical and geomechanical approaches.

The geochemical approach is mainly the ratio of the sum of the weight of brittle minerals (with or without their respective weighting coefficients) to the total weight of the rock minerals (Kang et al., 2020). Because the brittleness index is calculated using the composition (weight fractions) of minerals in the rock, it can be referred to as the mineralogical brittleness index. The

geomechanical approach evaluates the brittleness index by elastic parameters (elastic modulus and Poisson's ratio), strength parameters (compressive and tensile strength) of the material, and stress-strain curve analysis (Li, 2022). Because the brittleness index is calculated using the mechanical properties of the rock, it can be referred to as the mechanical brittleness index (Kang et al., 2020). The brittleness index evaluated based on the elastic parameters of the material can be determined using static or dynamic elastic modulus and Poisson's ratio. The dynamic elastic parameters are calculated from the acoustic or ultrasonic wave velocities (compressional or P-wave and shear or S-wave) and bulk density of the material, while the static elastic parameters are measured directly in a deformational experiment (AL-Ameri et al., 2014; Tariq et al., 2018). The static tests are destructive tests, while the dynamic tests are non-destructive tests. The ratio of P to S wave velocities at different axial and lateral stresses ranges between 1.25 and 1.40 (Heidari et al., 2020).

It is important to understand the changes that occur in the elastic and strength parameters of reservoir and cap rocks during injection and storage of CO_2 in aquifers or depleted oil or gas reservoirs for long-term stability of CO_2 geosequestration (Huang et al., 2020). Uniaxial compressive strength (UCS), Brazilian tensile strength (BTS), and fracture toughness of brine-saturated sandstone increase with increasing NaCl concentration (in the absence of supercritical CO_2), but decreased after supercritical CO_2 injection; while the elastic moduli of brine-supercritical CO_2 co-saturated sandstone were higher relative to brine-saturation condition, unlike the case of the peak strength (Heidari et al., 2020). In a similar study conducted by Lyu et al. (2018), CO_2-NaCl-shale interactions decrease the brittleness values of the shale rock. They found that CO_2-NaCl-shale interaction has more effect on the rock's strength and Young's modulus than on the brittleness. Therefore, changes in the rock's elastic and strength parameters, as well as the mineralogical composition during CO_2 geosequestration might impact the brittleness index of the rock. It is worth noting that the values obtained from the mechanical brittleness index and mineralogical brittleness index calculations are different, as different parameters (mechanical properties and mineralogical composition, respectively) are used in the calculations (Elwegaa et al., 2019). However, the focus is on the change in the brittleness index (mechanical or mineralogical) to account for an increase or a decrease in the brittleness index of the rock during CO_2 geosequestration.

2.1.3 Cyclic approach of CO_2 geosequestration

CO_2 geosequestration could involve a non-cyclic or cyclic process. The non-cyclic process entails the injection of CO_2 over a period, and allows the injected CO_2 to be trapped in the reservoir; while the cyclic process of geosequestration involves the injection of CO_2 for some period (in some cases, withdrawing some of the injected CO_2 and leaving behind some amount of CO_2 in the reservoir to be stored), and repeating the process over the geosequestration period. The cyclic injection and withdrawal of CO_2 in reservoirs might be an effective approach to promote CO_2 utilization and storage, as it would enable seasonal injection and withdrawal of CO_2. Following this approach, CO_2 can be produced from the reservoir when needed for electrochemical hydrogen production (Kim et al., 2018; Koomson et al., 2023), to produce renewable methanol (Sánchez-Díaz, 2017; Sollai et al., 2023; Wang et al., 2023), in CO_2 plume geothermal (CPG) systems for heat and power production (Schifflechner et al. 2022), or other forms of energy. Thus, the utilization of CO_2 for energy creation will reduce the world's reliance on fossil fuels (Wang et al., 2023). However, cyclic injection and withdrawal of CO_2 would induce cyclic stress in the reservoir and possibly create more stress at the reservoir-caprock interface. Hence, the brittleness of the reservoir and caprock might be impacted by the cyclic stress effect during cyclic injection and withdrawal of CO_2. Therefore, it is vital to evaluate the brittleness index of the rocks, to ascertain the feasibility of adopting the CO_2 cyclic injection and withdrawal technology.

Furthermore, in sandstone formations, sand management challenges might be experienced as CO_2 is injected and withdrawn under high pressure conditions. Sand management involves the control and monitoring process of well pressures and fluid flow rates to avoid or minimize sand influx into the well (Mahmud et al., 2020). When the stress on the formation is beyond the formation strength, rock failure occurs, increasing the chance of sand production (Vincent et al., 2012; Mahmud et al., 2020). During CO_2 withdrawal from a sandstone formation, rock failure could occur due to overburden pressure, pore pressure, and drag force from the producing fluid (Vincent et al., 2012). Based on Stoke's law, the frictional (drag) force acting on the sand particles is proportional to the formation fluid flow velocity (or flow rate) and viscosity (Mahmud et al., 2020). Therefore, as production is initiated in the well at the production interval (or perforations) after CO_2 injection and during storage, the fluid flow rate increases and consequently results in the increase in drag force on the formation particles. This effect of drag force, coupled with chemical reactions between the sandstone rock minerals and the formation fluid, might result in severe erosion (or corrosion) of rock minerals and migration of fines from the reservoir to production facilities.

The dissolution and precipitation of minerals in the rock change the petrophysical properties of the rock (during the non-cyclic or cyclic process of CO_2 geosequestration) as well as the geochemical composition of the formation, thereby altering the ionic composition of the formation fluid. Thus, the integrity of the formation can be linked to the changes in the petrophysical properties of the formation and the geochemical composition of the fluid in the formation. The alteration in the reservoir and caprock integrity can be evaluated using machine learning-based models to save the cost of running multiple experimental or field tests. Yu et al. (2020) conducted a study on the geochemistry of formation water for carbonate reservoirs in the Ordos basin in China. They proposed statistical relationships between the geochemical properties and hydrocarbon storage using the machine learning (Decision tree) method. The findings of the study revealed that the salinity, Na^+/Cl^- ratio, $(Cl^- - Na^+)/Mg^{2+}$ ratio, $(HCO_3^- - CO_3^{2-})/Ca^{2+}$ ratio, and Mg^{2+}/Ca^{2+} ratio correlate highly with the gas preservation. The model accurately predicts where to find gas reservoirs in the Ordos basin, leading to improved exploitation of the hydrocarbon. Thus, this finding can be extended to reservoir-caprock systems exhibiting different levels of brittleness during CO_2 geosequestration.

2.2 Theoretical Framework

During CO_2 injection, stresses are induced in the rock, and the cement that binds the rock grains is impacted. Thus, creating pathways for CO_2-brine-rock interaction in the rock cement and enhancing the dissolution of some of its minerals. Hence, resulting in deformation and a decrease in strength of the rock. The decrease in strength of the rock results in a change in the brittleness of the rock, as the rate of decrease in the tensile and compressive strengths of the rock, as well as changes in the rock minerals are different. Brittleness is the lack of ductility or plasticity of a material, while ductility is the property of a material that allows it to be drawn out by tension to a smaller section (Hucka and Das, 1974; Hou et al., 2018). In other words, brittle materials can hardly be drawn into shapes. Instead, they fracture or break when such amount of stress is applied on them (Figure 2.2). Most rocks exhibit brittle behaviour. However, their degrees of brittleness vary by lithology and conditions subjected to during fluid-rock interactions.

Brittleness is a relative term as there are no accepted values of strength and elastic parameters ratios or brittle minerals ratio below which a material is considered brittle or ductile (Hucka and Das, 1974). The brittleness of a material is compared by its brittleness index at one time or condition to another to ascertain whether the material has become more or less brittle. The factors that influence the brittleness of rocks include the type and composition of brittle minerals, the

content and maturity of organic matter, and the formation temperature and confining pressure (Elwegaa et al., 2019; Li, 2022).

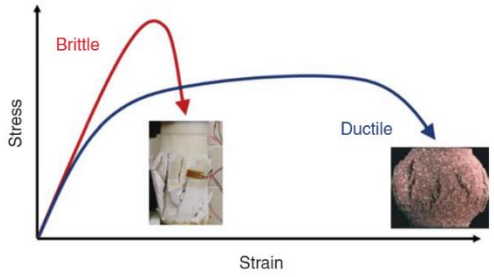

Figure 2.2: Stress-strain representation of brittle and ductile rocks (Jin et al., 2015).

During CO_2 injection, if the injection pressure or pore pressure slightly exceeds the capillary entry pressure of the caprock, CO_2 migrates into the caprock layers closer to the reservoir-caprock interface over a short time until the injection pressure is reduced. Therefore, it is important to investigate whether the CO_2 stream that penetrates the caprock impacts the rock's brittleness. If the caprock layer penetrated becomes more brittle, during CO_2 storage a slight increase in the reservoir pore pressure will enhance convective CO_2 transport into the caprock or induce fracture. Otherwise, the caprock is able to contain the CO_2 and brine in the reservoir such that CO_2 can only penetrate the caprock layer by diffusion, which could take hundreds to thousands of years. To evaluate the brittleness of caprock penetrated by some amount of CO_2 during injection, in this section different methods for the evaluation of brittleness of a material are reviewed. Examples of such methods or concepts are based on material deformation, strength and elastic parameters, and mineralogical composition of the rock.

2.2.1 Determination of brittleness from material deformation

The deformation-based brittleness index is evaluated from the point of failure of the material. In this case, the brittleness index is the ratio of reversible strain to total strain at the point of failure (Hucka and Das, 1974; Meng et al., 2015). The irreversible axial strain can be determined by conducting loading-unloading tests, as shown in Figure 2.3.

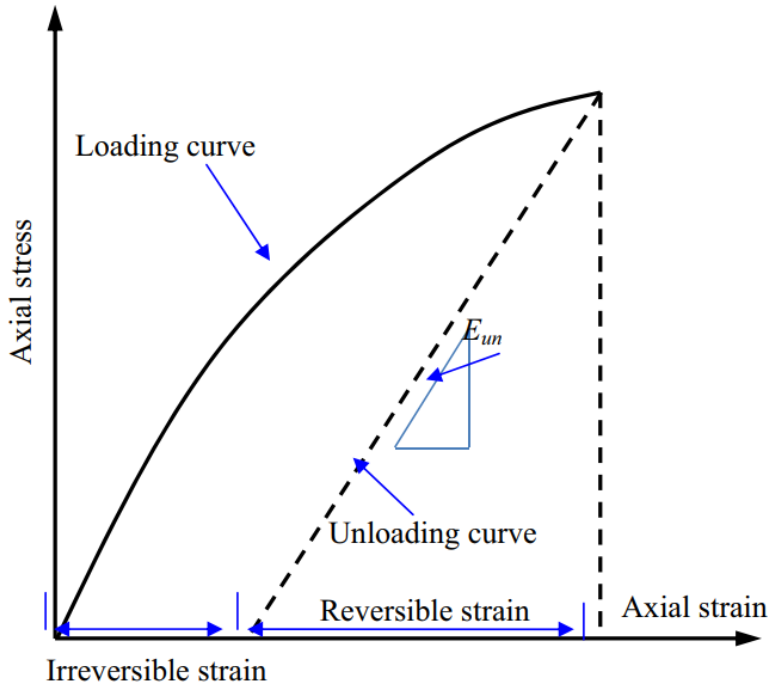

Figure 2.3: Stress-strain relationship to evaluate brittleness index (Meng et al., 2015).

Based on this concept, ductile materials have a lower brittleness index compared to brittle materials. Thus, the brittleness index (BI) is expressed as follows:

$$BI_1 = \frac{reversible\ strain}{total\ strain} \qquad 2.2$$

However, due to the variability or inconsistency (discreteness) in the peak strength of rocks during mechanical tests, the unloading point on the stress-strain curve might be difficult to determine (Meng et al., 2015). Thus, the discreteness in the peak strength will affect the measured irreversible strain.

2.2.2 Determination of brittleness from strength parameters

It has been proposed that the brittleness index of a material depends on its compressive and tensile strengths. The unconfined compressive strength reflects the compressibility of the rock mass, while the Brazilian tensile strength reflects the cohesion of the bonds between the material grains (Hucka and Das, 1974). It has been found that the ratio of compressive strength to tensile strength of a material increases with its brittleness (Meng et al., 2015; Li, 2022). Similarly, some scholars have proposed that the difference in the tensile and compressive strength of a material increases with increase in brittleness index (Hucka and Das, 1974; Meng et al., 2015; Li, 2022). In other words, a rock mass with low [Brazilian] tensile strength is easily subjected to tensile

fracture initiation and a high unconfined compressive strength assists in resisting the closure of natural and induced fractures (Gong and Zhao, 2007). Thus, the brittleness index can be expressed as follows:

$$BI_2 = \frac{\sigma_c}{\sigma_t} \quad 2.3$$

$$BI_3 = \frac{(\sigma_c - \sigma_t)}{(\sigma_c + \sigma_t)} \quad 2.4$$

where σ_c represents the uniaxial compressive strength and σ_t represents the uniaxial tensile strength of the material.

The calculation of brittleness index from strength parameters may not be accurate in a complex stress condition, as rock brittleness is impacted by the stress state. Thus, a rock subjected to a high confining pressure may become less brittle and more ductile (Meng et al., 2015).

2.2.3 Determination of brittleness from elastic parameters

Elastic parameters commonly used for brittleness index evaluation are Young's (or Elastic) modulus (E) and Poisson's ratio (ν). They can be obtained from destructive (static) or non-destructive (dynamic) testing of materials. The brittleness of a material increases with increase in the ratio of elastic modulus to Poisson's ratio (Luan et al., 2014). Although this estimation of brittleness has been criticized by some scholars, claiming that the brittleness of a material depends on several parameters such as bulk modulus and pore pressure (Zhang et al., 2016), it takes the lateral strain of the material into consideration such that under the same amount of axial strain, axial stress is proportion to lateral strain. Thus, when different materials are evaluated under the same amount of axial stress, the material that is able to strain more laterally without failure may be less brittle. Also, the brittleness of a material increases with an increase in the average of normalized dynamic elastic modulus (E_n) and normalized dynamic Poisson's ratio (v_n) for the formation investigated (Rickman et al., 2008; Kang et al., 2020). Therefore, the brittleness index can be expressed as follows:

$$BI_4 = \frac{E}{v} \quad 2.5$$

$$BI_5 = \frac{(E_n + v_n)}{2} = \frac{1}{2}\left[\frac{(E - E_{min})}{(E_{max} - E_{min})} + \frac{(v_{max} - v)}{(v_{max} - v_{min})}\right] \quad 2.6$$

where E_{min} and E_{max} represent minimum and maximum dynamic Young's modulus of the formation; while v_{min} and v_{max} represent minimum and maximum dynamic Poisson's ratio of the formation, respectively.

2.2.4 Determination of brittleness from rock mineralogical composition

During the injection and storage of fluid in a porous rock, the pore fluid-rock interactions result in the dissolution and precipitation of minerals (Edlmann et al., 2013; Sun et al., 2016). The brittleness of the rock depends on its lithology. For instance, clay-rich shale is made up of mainly clay minerals and quartz with little amount of feldspar, calcite, pyrite, and other minerals (Guo et al., 2016); while carbonate rocks are made up of mainly calcite and little amount of other minerals (Wang et al., 2022). Brittle minerals are calcite, dolomite, feldspar (feldspar group of minerals), pyrite, mica (mica group of minerals, for example, muscovite), and quartz (Jin et al., 2015; Guo et al., 2016; Li, 2022). So, the brittleness of a geomaterial or rock is the sum of the mass fraction of its brittle minerals (Jin et al., 2015; Guo et al., 2016; Li, 2022). Therefore, the brittleness index can be expressed as follows:

$$BI_6 = \frac{W_{quartz}+W_{feldspar}+W_{calcite}+W_{dolomite}+W_{pyrite}+W_{mica}}{W_T} \quad 2.7$$

$$BI_7 = \frac{W_{quartz}+0.49W_{feldspar}+0.51W_{calcite}+0.44W_{dolomite}}{W_T} \quad 2.8$$

where W_{quartz}, $W_{feldspar}$, $W_{calcite}$, $W_{dolomite}$, W_{pyrite}, and W_{mica} represent the weights of quartz, feldspar, calcite, dolomite, pyrite, and mica, respectively. W_T is the total weight of minerals in the solid part of the rock, and BI_7 is the mineralogical brittleness index model developed by Kang et al. (2020).

During CO_2 geosequestration, CO_2-brine-rock interaction results in the dissolution and precipitation of minerals; thus, the brittleness of the rock would vary over the geosequestration period as the volume fraction of the brittle minerals per rock solid volume changes. The mineralogical brittleness index correlates with the mechanical brittleness index to some extent (Kang et al., 2020). Therefore, it is possible that precipitation of more brittle minerals relative to their initial state before CO_2 geosequestration inhibits lateral strain on the rock when the same amount of axial stress is applied to the material, thus leading to a higher brittleness index of the rock. Dissolution of brittle minerals during CO_2 geosequestration in some cases can result in the formation of non-brittle minerals. For instance, dissolution or corrosion of feldspar (potassium feldspar [$KAlSi_3O_8$], albite [$NaAlSi_3O_8$], etc.) as CO_2 dissolves in water (brine) might result in the precipitation of kaolinite [$Al_2Si_2O_5(OH)_4$] and quartz (based on increased SiO_2 concentration in the

aqueous phase), and the release of metallic ions (such as Na^+ and K^+) into the aqueous phase, as shown below (Li et al., 2016):

$$2KAlSi_3O_8 + 3H_2O + 2CO_2 \leftrightarrow Al_2Si_2O_5(OH)_4 + 2K^+ + 4SiO_2 + 2HCO_3^- \quad 2.9$$

$$2NaAlSi_3O_8 + 3H_2O + 2CO_2 \leftrightarrow Al_2Si_2O_5(OH)_4 + 2Na^+ + 4SiO_2 + 2HCO_3^- \quad 2.10$$

Kaolinite is a clay mineral, while quartz is a brittle mineral. According to Li et al. (2016), with the co-injection of H_2S and CO_2 in a sandstone formation, the concentrations of K^+ and Na^+ increase, greater than those in the pure CO_2 case. Thus, CO_2-H_2S co-injection enhances the corrosion or dissolution of feldspar, leading to the precipitation of a larger amount of kaolinite compared to the case of pure CO_2. Also, pyrite (FeS_2) precipitates on the surface of the sandstone (Li et al., 2016). Studies have shown that residual or small amount of O_2 in the porous medium or the presence of small minerals containing redox-sensitive species (for example, Fe_2O_3) that has the tendency to dissolve and release oxidants to the formation water or brine, could enhance SO_2 oxidation rate (Turšič et al., 2003; Hedayati et al., 2018). So, in the presence of residual O_2 in the porous medium, SO_2 (g) dissolves almost completely into the water (brine) quickly as SO_2 (aq), and oxidizes to sulphate under conditions controlled kinetically (Hedayati et al., 2017) giving rise to the following reaction:

$$SO_2\,(aq) + 0.5\,O_2\,(aq) + H_2O \rightarrow SO_4^{2-} + 2\,H^+ \quad 2.11$$

Thus, in a porous medium where SO_2 is co-injected with CO_2, as the CO_2 plume rises vertically from the point of injection or perforation, SO_2 (g) might begin to dissolve quickly as SO_2 (aq) and oxidize to sulphate locally, limiting its ability to rise through different layers of the porous medium as SO_2 (g). The upward transport of the SO_2 (g) from the point of injection in the reservoir might be through very few metres in the porous medium. In the CO_2-SO_2 mixture, it is possible that supercritical CO_2 plume will rise relatively higher [or migrate laterally over a larger radial distance] in the porous medium as SO_2 oxidizes rapidly to sulphate. Also, the difference in their relative vertical rise in the porous medium might be attributed to their density or molecular mass difference (as SO_2 is heavier than CO_2) due to gravity segregation (Khan and Mandal, 2020). Zhang et al. (2011) found the mass fraction of CO_2 at the advancing gas front to be higher (vertically) than that of the gas impurity. Thus, the front of the gas impurity behind that of CO_2 gas was attributed to the preferential solubility of the gas impurity in formation water compared to that of CO_2. This leads to a delayed breakthrough of the gas impurity as the impurity separates from the CO_2 gas and [the impurity] becomes suppressed in formation water at the advancing gas front.

Furthermore, as dolomite dissolution in brine elevates Ca concentration, the increased Ca^{2+} reacts with the increased H_2SO_4 (due to enhanced sulphate concentration in the layers contacted by SO_2) to form anhydrite (Hedayati et al., 2018):

$$Ca^{2+} + H_2SO_4 \rightarrow CaSO_4 + 2H^+ \quad 2.12$$

It is possible that as the molecular mass (and density) of CO_2 and H_2S is close, H_2S would correspondingly rise with the CO_2 plume in the porous medium. Thus, the injection of H_2S in the presence of oxygen and increased iron (Fe) concentration (due to the dissolution of siderite and/or ankerite) results in the precipitation of pyrite (Hedayati et al., 2018):

$$Fe^{2+} + 2H_2S + 0.5O_2 \rightarrow FeS_2 + H_2O + 2H^+ \quad 2.13$$

Similarly, dissolved SO_2 (that oxidizes to sulphate) could result in the precipitation of pyrite as follows:

$$2Fe^{2+} + 4H^+ + 4SO_4^{2-} \rightarrow 2FeS_2 + 7O_2 + 2H_2O \quad 2.14$$

Thus, it is possible that co-injection of gases (H_2S, SO_2, etc.) during CO_2 geosequestration impacts the brittleness of porous rocks as brittle and non-brittle minerals are precipitated during the co-injection of CO_2 with different impurities. Therefore, it is vital to evaluate the impact of impurities co-injected with CO_2 on the brittleness of rock during geosequestration.

2.2.5 Determination of brittleness from machine learning model

Fluid-rock chemical interaction during CO_2 geosequestration result in variation in the geomechanical, geochemical, and petrophysical properties of the rock. The changes in the properties of the rock could result in variation in the integrity (mainly brittleness, in this study) of the rock. During CO_2 geosequestration, the fluid-rock chemical interaction results in changes in the ionic composition (including H^+ concentration) of the formation fluid, fluid density, fluid saturations, and porosity and permeability of the formation. Moreover, initially, the rock minerals are in quasi-stable (or nearly steady-state) condition (Zhang et al., 2011). Thus, the ionic composition of the fluid reflects the initial mineral composition of the formation. For instance, a carbonate rock with siderite ($FeCO_3$) mineral may contain higher Fe^{2+} concentration compared to carbonate rock without siderite mineral, due to siderite dissolution as the formation water approaches quasi-stable condition. Also, dolomite dissolution could result in calcite precipitation (due to abundant Ca^{2+} in the formation fluid), while Mg^{2+} in the formation fluid would increase,

resulting in precipitation of magnesium-based minerals during CO_2 geosequestration (Zhang et al., 2011). Therefore, the ionic composition of the formation fluid reflects the mineralogical composition of the formation and consequently influences the mineralogical brittleness index of the formation.

Hence, the brittleness of the formation at different times during CO_2 geosequestration can be predicted using the fluid and rock properties, and other operational conditions; without necessarily using the composition (volume or weight fractions) of the minerals. This can be achieved using machine learning-based models for real-time prediction of the brittleness of formations before or during CO_2 geosequestration. Different machine learning regression algorithms can be used to develop predictive machine learning models, some of them are artificial neural network (ANN), random forest, support vector regression, and decision tree algorithms (Cao et al., 2020; Yu et al., 2020; Ibrahim, 2022; Nyakilla et al., 2022; Thanh et al., 2022; Kolawole et al., 2023). The ANN is very effective for problems with highly non-linear and complex datasets with a large number of variables or features (Kannaiah and Maurya, 2023), and could be useful for the evaluation of the brittleness index of rocks before and during CO_2 geosequestration.

2.3 Artificial Neural Network (ANN)

A simple ANN can be referred to as a linear model based on brain architecture made up of neurons like that of the human brain, which receive and transmit information to all adjacent neurons after processing (He et al., 2022). The connections between these neurons are defined by weights. ANN model is structured in layers (input, hidden, and output layers) having nodes in one layer connected to nodes in the following layer. The input layer contains the input parameters, while the output layer contain the output parameters. A hidden layer has multiple neurons. There can be multiple hidden layers in an ANN model. The nodes (or neurons) utilize the weights of the connections to learn the dataset and adopt an activation function to pass their signal to the output layer (Kannaiah and Maurya, 2023). In other words, the learning process of the ANN model is to adjust the weights (iteratively) between neurons and the bias of each neuron in the way of repeated input and output (a process referred to as model training); thus, making it possess excellent non-linear fitting abilities (He et al., 2022; Yao et al., 2023). So, the weights of a network are initialized and then updated while training the network. The weights can be updated as follows:

$$w_i = w_{i-1} - \alpha\left(\frac{dLoss}{dw_{i-1}}\right) \quad 2.15$$

where w_{i-1} and w_i represent the old weight and updated weights, respectively; α is the learning rate, while $dLoss/dw_{i-1}$ represents the derivative of error (or loss function) with respect to weight.

Some parameters that control the performance of the neural network are optimizers, batch size, and epochs. Optimizers are algorithms used to minimize loss function or error during model training. This is achieved by modifying or changing the weights and learning rate during training. Some common optimizers are root mean square propagation (RMSprop), stochastic gradient descent (SGD), and adaptive moment estimation (Adam). Furthermore, the fitness of the model to the data can be improved by choosing an optimum number of batch size and epochs. Batch size controls how many observations in the training data that pass through the algorithm at a time, until the entire training data pass through the algorithm in an epoch. Epochs control how many times the entire training data pass through the algorithm during the training process. The model parameters of the network are updated with each epoch (Kannaiah and Maurya, 2023).

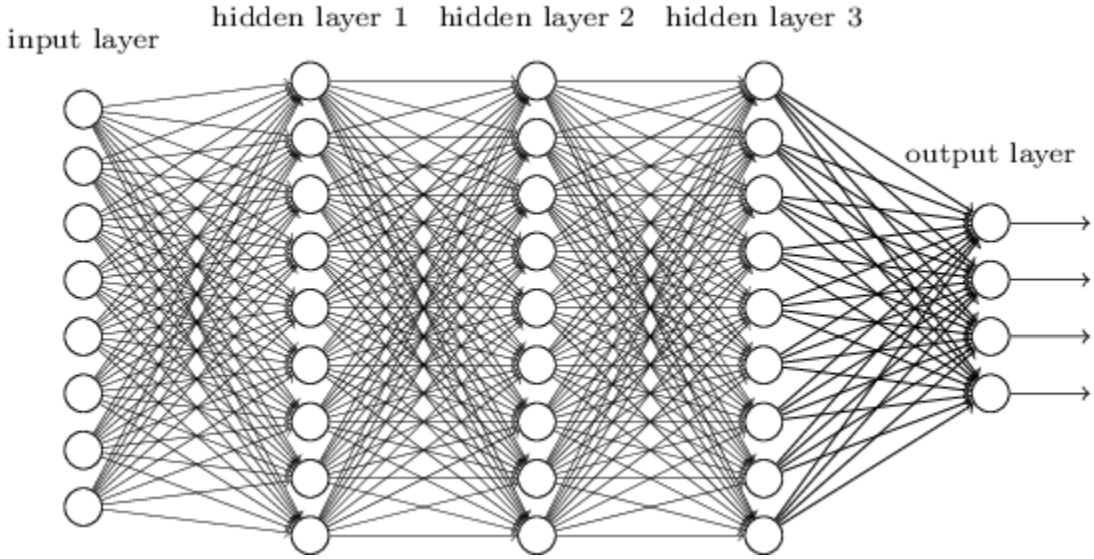

Figure 2.4: Fully connected artificial neural network (McNaughton, 2019).

Fully connected neural network can be referred to as multi-layer perceptron (MLP). The input layer takes the input data (x_i). Each node acts like an artificial neuron. Each node in every layer (except the output layer) is connected to each node in the subsequent layer. The procedure of the mathematical solution is illustrated in Figure 2.5. The input data layer is 'Layer 1', $w^{(1)}$ is the matrix of weights from layer 1 to layer 2, and $a_i^{(2)}$ is the activation on unit i in layer 2. These weights and activations on nodes (or units) also apply when there are multiple hidden layers. In addition, each layer (except the output layer) has a bias unit which is equal to 1. Mathematically, the activations can be expressed as

$$a_1^{(2)} = h\left(w_{10}^{(1)}x_0 + w_{11}^{(1)}x_1 + w_{12}^{(1)}x_2 + w_{13}^{(1)}x_3\right) \quad 2.16$$

Similarly, $a_2^{(2)}$ and $a_3^{(2)}$ can be generated. The activation function is represented by h, which in this study is a rectified linear unit (ReLU), expressed as

$$h(x) = \max(0, x) \quad 2.17$$

The output layer (in this case, layer 3) is mathematically expressed as

$$\hat{y}\,(w, x) = \; a_1^3 = h^*(w_{10}^{(2)}a_0^{(2)} + w_{11}^{(2)}a_1^{(2)} + w_{12}^{(2)}a_2^{(2)} + w_{13}^{(2)}a_3^{(2)}) \quad 2.18$$

where $h^*(x)$ is the activation function on the output unit.

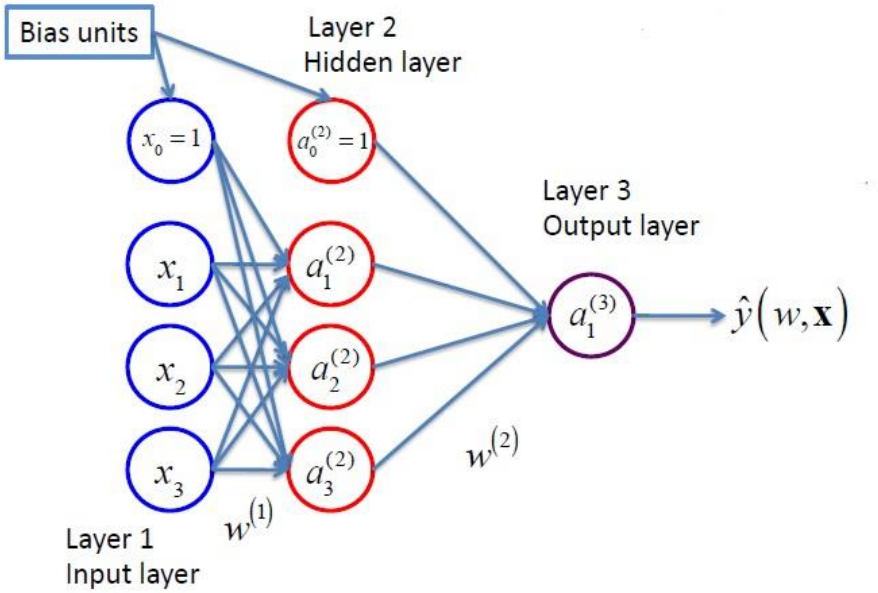

Figure 2.5: Demonstration of solution procedure of a fully connected neural network (McNaughton, 2019).

2.4 Review of Literature Based on Objectives of the Study

CO_2 geosequestration in reservoirs is one major solution to reduce anthropogenic gases from the earth's surface, as aquifers or depleted oil and gas reservoirs are available in many parts of the world for this purpose. During CO_2 injection in reservoirs, as the pore fluid pressure or injection pressure increases slightly and exceeds the caprock capillary entry pressure, CO_2 penetrates some layers of the caprock before the injection pressure is reduced. Thus, CO_2 becomes trapped in the caprock and possibly impacts the properties of the caprock layers invaded. Several studies have been conducted on the impact of CO_2 and formation conditions on porosity, permeability,

mineralogical composition, and geomechanical properties of rocks. Hence, findings from those studies are reviewed in this section.

2.4.1 Impact of CO_2 geosequestration on porosity, permeability, and mineralogical composition of reservoir and cap rocks

Pressure and temperature variations in a CO_2 storage reservoir impact the overlying caprock properties. In fact, some CO_2 injection wells are exposed to low temperatures and strong temperature variations, which threaten well integrity (Torsaeter et al., 2017). A similar condition is possible in a reservoir-caprock system. Davila et al. (2017) conducted an experimental and modelling study on the interaction between a crushed marl caprock (carbonate - weight fraction of calcite in the caprock is greater than 67%) and CO_2-rich solutions under different temperature and pressure conditions. They found that the porosity of the caprock increased more under any partial pressure of CO_2 at lower temperatures, while porosity reduced as temperature increased. Moreover, as the partial pressure of CO_2 rises (increase in the proportion of dissolved CO_2 in the formation water), the porosity of the caprock enlarges over greater distances. The findings revealed that the temperature of the system could have a selective impact on the dissolution and precipitation of minerals, and temperature is inversely related to the porosity of the rock at the conditions considered.

Similarly, Torsæter et al. (2017) conducted a study on avoiding damage of CO_2 injection wells caused by temperature variations. They found that low temperature in CO_2 injection wells could impact well integrity. Moreover, freezing of pore water in the well is strongly detrimental to well integrity, as it has the potential to crack both cement and surrounding rock formations; which implies that to mitigate cracks in well barriers (including cement) surrounding the reservoir and caprock, all sections in the system should always have temperatures above the freezing point of the brine at that particular depth. However, heating can result in radial fracturing, while cooling may result in cement debonding; but the extent of damage is small (about tens of microns). Thus, Torsæter et al. (2017) believe that such defects are likely to be sealed by chemical interactions between carbonated brine and cement. Formation pressure can change during CO_2 geosequestration. According to a study on stress path evolution during fluid injection into geological formations, conducted by Gheibi et al. (2016), CO_2 injection causes pressure changes inside the reservoir and changes the effective and total stresses inside and outside of the reservoir (which is also possible in a caprock). In fact, due to CO_2 injection, faults can deform elastically and the difference in pore pressure between the reservoir and caprock and/or underlying layer

result in different stress changes compared (or relative) to the reservoir centre (Gheibi et al., 2016). In other words, the stress experienced at different sections of the reservoir and caprock is different due to variation in pore pressure in the system. The in situ temperature and pressure conditions in a reservoir or caprock impact CO_2-brine-rock interactions.

Furthermore, brine-rock interactions are influenced by the purity of the injected fluid into a reservoir during CO_2 geosequestration. To save the cost of carbon capture and storage, small amount of some acid gases (such as SO_2 and H_2S) may be co-injected with CO_2. When the gas mixture comes into contact with water, each gas in the mixture exhibits different level of solubility in water due to differences in their polarity and net dipole moment (López-Rendón and Alejandre, 2008; Miri et al., 2014; Wang et al., 2020). Theoretically, water (H_2O), SO_2, and H_2S are polar molecules (electrons are not shared equally between the atoms and there is an electronegativity difference between the bonded atoms), while CO_2 is a linear non-polar molecule and the electrons are shared equally between the atoms (López-Rendón and Alejandre, 2008; Wang et al., 2020). Thus, CO_2 has no net dipole moment (as the two C-O bond dipoles are equal in magnitude and cancel out each other); while the dipole moments of H_2S, SO_2, and H_2O are 0.97 Debye, 1.63 Debye, and 1.83 Debye, respectively (López-Rendón and Alejandre, 2008; Shen et al., 2015; Wang et al., 2020). Also, substances whose polarities (or net dipole moment) are similar tend to be more soluble in each other, and a polar substance is more soluble in a polar solvent than in a non-polar solvent (López-Rendón and Alejandre, 2008, Wang et al., 2020). Thus, at the same temperature and pressure conditions, the solubility of H_2S or SO_2 in water is higher than that of CO_2 (López-Rendón and Alejandre, 2008; Miri et al., 2014; Wang et al., 2020).

Moreover, it is expected that the solubility of SO_2 in water should be higher than that of H_2S at the same temperature and pressure conditions, as the dipole moment of SO_2 is closer to that of water (Wang et al., 2020). Also, the solubility of gases in water is dependent on temperature; as temperature increases, the solubility of CO_2, H_2S, or SO_2 in water may increase (López-Rendón and Alejandre, 2008; Miri et al., 2014). It is worth noting that a gas can separate from a mixture with non-polar gases, due to their difference in property. This concept drives the industrial separation of SO_2/CO_2 in ionic liquid or aqueous phase (Wang et al., 2020). However, the level of solubility of CO_2 or impurities in a brine-rock system or the separation of impurities from CO_2 might be different when gas mixtures are injected in a rock composed of different minerals, thereby resulting in the trapping of the dissolved gases in the aqueous phase for mineral precipitation. More or less fraction of each gas in the mixture might dissolve in the aqueous phase

at different temperature and pressure conditions. So, the CO_2-brine-rock interactions would depend on the initial mineralogical composition of the formation.

Wang et al. (2022) conducted an experimental and geochemical modelling study to investigate CO_2-brine-rock interactions in a carbonate rock containing calcite (91 wt.%), dolomite (8 wt.%), and clay (<1 wt.%) minerals. The geochemical modelling of reactions in the porous media was performed using PHREEQC geochemical package. Results of the study revealed that brine-rock interaction increases the dissolution of CO_2 gas in the aqueous phase. Carbonate ion (CO_3^{2-}) reduced in the solid phase and was released into the aqueous phase. They concluded that the precipitation-dissolution mechanism does not contribute to the carbon dioxide storage in the case studied, as there were many more carbonate ions in the aqueous phase compared to the surface of the minerals. This is possible as calcite and dolomite dissolution in the aqueous phase (as the pH of the solution is reduced as a result of CO_2 dissolution) might not have resulted in the precipitation of secondary minerals over the period of the experiment considered. So, during CO_2 geosequestration, the decrease in pH of the aqueous phase due to CO_2 dissolution in the formation water results in mineral dissolution and/or precipitation.

During CO_2 geosequestration a small fraction of other gas impurities might be co-injected with CO_2 into the reservoir. Thus, pH of the aqueous phase during geosequestration of pure CO_2 will be different when CO_2 is co-injected with impurities into the brine-rock system. The pH of the aqueous phase in sandstone and siltstone formations during CO_2 sequestration experiments is shown in Table 2.1. The pH of the bulk solution or aqueous phase is different even for the same rock type, depending on the ionic composition of the formation water before CO_2 injection. The dissolution of CO_2 in the surrounding formation water (brine) yields carbonic acid (H_2CO_3) or hydrogen ion (H^+) and bicarbonate (HCO_3^-), thereby resulting in a decrease in pH (increased acidity). The dissolution of nitrogen dioxide (NO_2) in formation water results in the formation of HNO_2 (nitrous acid, a weak acid) and HNO_3 (nitric acid, a strong acid) or HNO_3 and NO (nitrogen oxide), thereby decreasing the pH further for CO_2-NO_2 co-injection case. The reaction of SO_2 with formation water produces H_2SO_3 (sulphurous acid, a weak acid) or H_2SO_4 (sulphuric acid, a strong acid) and H_2S. So, the pH of the solution would decrease for CO_2-SO_2 co-injection case (the extent of decrease would depend on whether a strong or weak acid is formed) compared to the injection of pure CO_2 in the formation water. The reaction of SO_2 with O_2 and H_2O produces a strong acid (H_2SO_4), thereby decreasing the pH of the aqueous phase significantly for the CO_2-SO_2-O_2 co-injection in formation water. The dissolution of H_2S in formation water produces HS^- (bisulphide, a weak base) and hydronium ion (H_3O^+). The formation of a weak base results in a

slight increase in pH for the CO_2-H_2S co-injection case compared to the injection of pure CO_2 in the formation water. The chemical equations are presented as follows (Aminu et al., 2018):

$$CO_2 + H_2O \leftrightarrow H_2CO_3 \quad 2.19$$

$$CO_2 + H_2O \leftrightarrow H^+ + HCO_3^- \quad 2.20$$

$$2NO_2 + H_2O \leftrightarrow HNO_2 + HNO_3 \quad 2.21$$

$$3NO_2 + H_2O \leftrightarrow 2HNO_3 + NO \quad 2.22$$

$$SO_2 + H_2O \leftrightarrow H_2SO_3 \quad 2.23$$

$$4SO_2 + 4H_2O \leftrightarrow 3H_2SO_4 + H_2S \quad 2.24$$

$$2SO_2 + 2H_2O + O_2 \leftrightarrow 2H_2SO_4 \quad 2.25$$

$$H_2S + H_2O \rightarrow HS^- + H_3O^+ \quad 2.26$$

$$HS^- + H_2O \rightarrow S^- + H_3O^+ \quad 2.27$$

Based on these reactions, the pH of the bulk solution in a formation decreases significantly during CO_2 co-injection with SO_2 (with or without the addition of a small volume of O_2) or NO_2. The pH of the aqueous phase decreases slightly during the injection of pure CO_2 or CO_2 co-injection with H_2S. Thus, the rate of reaction in a CO_2-brine-rock system with SO_2 or NO_2 might be higher due to the relatively low pH of the bulk solution compared to the rate of reaction in a brine-rock system where pure CO_2 or CO-H_2S mixture is injected. The decrease in pH impacts the brine-rock interactions during CO_2 geosequestration. Also, the chemical reaction between the rock minerals and the aqueous phase further impacts the pH of the bulk solution.

Table 2.1: Impact of impurities in CO_2 on pH of formation fluid.

Rock description	Fluid composition	Sequestration time	Operating conditions	pH before sequestration	pH after sequestration	References
Sandstone	100% CO_2 + brine	62 days	T=60^{0}C P=14.5 MPa	6.3	5.5	Hedayati et al. (2018)
	98.5% CO_2 + 1.5% SO_2 + brine	36 days			1-2	
Sandstone	100% CO_2 + brine	9 months	T=70^{0}C P=140 bar	7.65	5.97	Aminu et al. (2018)
	95% CO_2 + 5% NO_2 + brine				5.23	
	95% CO_2 + 5% SO_2 + brine				5.86	
	95% CO_2 + 5% H_2S + brine				6.55	
Sandstone	97.84% CO_2 + 0.16% SO_2 + 2% O_2 + brine	16 days	T=60^{0}C P=12 MPa	4.55	1.13	Pearce et al. (2019)
Siltstone (caprock)	97.84% CO_2 + 0.16% SO_2 + 2% O_2 + brine			5.60	1.62	

Pearce et al. (2019) performed a geochemical modelling of experimental O_2-SO_2-CO_2 reactions of reservoir (Precipice Sandstone), caprock (Evergreen Formation - siltstone), and overlying aquifer (Hutton Sandstone). The geochemical modelling and experiments were performed using supercritical CO_2 with O_2 and SO_2 impurities (0.16% and 2% respectively) at reservoir in-situ conditions of 60 ^{0}C and 12 MPa. As the O_2-SO_2-CO_2-water-rock reactions in bulk solution proceed, the measured pH solution was low (about 1-2) due to the relatively high concentrations of the gas impurities used. Dissolution of plagioclase, siderite, ankerite, and Fe-chlorite from the core was observed. A 30-year numerical simulation of the reactivity of the reservoir rock revealed that the lowered pH was influenced by mineral dissolution. Compared to SO_2-CO_2-water reactions, as O_2 is present, dissolved Fe subsequently reduced as Fe-oxide, sulphate, and led to the precipitation of clay minerals. Corrosion of minerals including Fe-chlorite and ankerite, as well as precipitation of oxide, silicate, and sulphate minerals was observed on the rock surfaces as the caprock reacted with wet supercritical O_2-SO_2-CO_2 fluid. SO_2 (g) dissolves rapidly in water (brine) as SO_2 (aq) and oxidizes to sulphate as O_2 is present (Hedayati et al., 2018).

Li et al. (2016) conducted an experimental study to investigate the influences of H_2S co-injection with CO_2 on the capacity of solubility trapping and mineral trapping of CO_2 in a sandstone formation at in situ conditions of 21 MPa and 70^{0}C. They found that the decrease in pH in the reservoir is due to the preferential dissolution of H_2S gas into brine (compared with pure CO_2), thereby inhibiting the solubility trapping of CO_2 to some extent. Furthermore, the lower pH resulted in more severe corrosion of primary minerals, favouring the precipitation of secondary minerals (for example, pyrite). The secondary minerals precipitated in the pure CO_2-brine-sandstone interaction are ankerite and dawsonite. Ankerite precipitation was not observed in the CO_2-H_2S-brine-sandstone interaction during the period of experiments (short-term), which implied that the injection of H_2S might have partially inhibited the precipitation of Fe-bearing carbonate minerals. Thus, it is important to understand the behaviour of carbonate minerals during CO_2 injection.

Zhang et al. (2011) conducted a geochemical modelling study to investigate the fate and transport of co-injection of H_2S with CO_2 in deep saline formations. The formations considered in the study are sandstone and carbonate. They found that, compared with CO_2 gas, H_2S gas preferentially dissolves into formation water and results in delayed breakthrough of H_2S gas, and separation between CO_2 and H_2S gases at the moving front. Moreover, co-injection of H_2S reduces CO_2 solubility compared to CO_2 only case. However, the preferential dissolution of H_2S enhances CO_2 dissolution at the gas moving front. They also found that co-injection of H_2S with CO_2 causes the precipitation of pyrite in the sandstone formation as dissolved Fe^{2+} from Fe-bearing minerals

interact with the dissolved H_2S. However, the precipitation of pyrite inhibits ankerite precipitation as H_2S is co-injected with CO_2. The presence of Fe-bearing minerals in geological formations enhances H_2S dissolution through precipitation of sulphide minerals, thereby increasing H_2S mineral trapping. They concluded that sandstone formations are more suitable for geosequestration of CO_2 as they promote mineral trapping, while the dominant trapping mechanisms in carbonate formations are solubility and hydrodynamic trapping.

Li et al. (2022) conducted an experimental study to investigate the mineralogical changes in carbonate-rich shale oil reservoirs during CO_2-brine-rock interactions. The carbonate-rich rock samples tested include limestone, dolomitic shale, and silty dolomite (Table 2.2). The soaking fluid is brine (fully saturated with CO_2), and the CO_2-brine soaking experiment was conducted at 90^0C and 35 MPa for 168 hours. The main mineral in the limestone rock sample is calcite (84.4 wt.%). The calcite content of the limestone reduced to 80.2 wt.% after the soaking treatment, due to a severe chemical reaction between calcite and the low pH (acidic) brine. The content of the other primary minerals (quartz, K-feldspar, albite, siderite, and clay) in the limestone sample increased slightly after the soaking treatment. The main minerals in the dolomitic shale were quartz (35.5 wt.%) and dolomite (24.1 wt.%). The dissolution of calcite, dolomite, and K-feldspar was observed after the soaking treatment, while other minerals (quartz, albite, siderite, and clay) precipitated in the dolomitic shale. The major mineral in the silty dolomite is dolomite (65.3 wt.%). Dolomite and calcite dissolved during the soaking treatment, which resulted in a decrease in their content; while the content of the other minerals (quartz, K-feldspar, albite, siderite, and clay) in the silty dolomite increased. The findings of the study revealed that quartz, albite, siderite, and clay precipitate, while calcite and dolomite dissolve in carbonate-rich shale rocks during CO_2 sequestration at the condition and period of time considered in the experiment. Over a longer period of CO_2 sequestration, some minerals that precipitate over a short time might begin to dissolve as the pH of the aqueous phase continues to change (Bolourinejad and Herber, 2014).

Lu et al. (2014) conducted an experimental study to investigate the geochemical impact of O_2 on sandstone carbon storage reservoirs. The sandstone rock samples tested were obtained from the Miocene sandstone (Texas offshore, USA), lower Tuscaloosa sandstone (Cranfield field, Mississippi, USA), and Cardium sandstone (Pembina field, Alberta, Canada). Samples from the sandstone rocks were treated with 1.88 M NaCl solution and CO_2 (with or without the addition of a small volume of O_2) at 200 bar and 70^0C or 100^0C (to further evaluate the impact of temperature on the geochemical reactions) for approximately 2 weeks (Table 2.3). The findings of the study revealed that for rock samples that do not have reducing minerals (such as pyrite), the co-injection

of a supercritical CO_2 with a small volume of O_2 showed very limited geochemical impact on the sandstone rock samples compared to the reactions with pure CO_2. The presence of O_2 in the mixture did not alter the reaction pathways, and did not accelerate the dissolution of carbonate and feldspar minerals. The Cardium sandstone rock sample, with an initial amount of pyrite up to about 0.7 wt.%, was impacted remarkably by the co-injection of supercritical CO_2 with O_2. As pyrite was oxidized, the pH of the solution was further lowered (more acidic solution), enhancing the dissolution of carbonate and feldspar minerals in the Cardium sandstone. Furthermore, the injection of pure CO_2 (without the addition of a small volume of O_2) at 100^0C and 200 bar into the Miocene sandstone resulted in the precipitation of quartz and the dissolution of the other minerals (albite, K-feldspar, calcite, kaolinite, and illite); while the dissolution of quartz and the precipitation of chlorite was observed in the lower Tuscaloosa sandstone under the same condition (except their initial mineral composition). In fact, more quartz dissolved and more chlorite precipitated in the lower Tuscaloosa sandstone at 100^0C compared to what was observed at 70^0C for the pure CO_2 injection. So, CO_2-brine-rock interaction is impacted by impurities, temperature, and initial mineralogical composition of the rock.

Table 2.2: Mineralogical composition (wt.%) of carbonate-rich shale reservoir rock samples based on XRD analyses (Li et al., 2022).

Rock type	Mineral	Before soaking	After soaking (168 hours)
Limestone	Quartz	5.0	6.9
	K-feldspar	0.2	0.4
	Albite	4.9	5.7
	Calcite	84.4	80.2
	Siderite	1.1	1.6
	Clay	4.4	5.2
Dolomitic shale	Quartz	35.5	38.6
	K-feldspar	3.7	3.3
	Albite	13.0	15.3
	Calcite	12.8	7.1
	Dolomite	24.1	21.7
	Siderite	5.4	7.2
	Clay	5.5	6.8
Silty dolomite	Quartz	14.5	17.6
	K-feldspar	1.8	2.1
	Albite	6.1	7.6
	Calcite	5.1	3.0
	Dolomite	65.3	60.2
	Siderite	1.7	2.6
	Clay	5.5	6.9

Table 2.3: Mineralogical composition (wt.%) of sandstone rock samples based on XRD analyses (Lu et al., 2014).

Sample	Depth (m)	Experiment	Quartz (%)	Albite (%)	K-feldspar (%)	Calcite (%)	Kaolinite (%)	Illite (%)	Chlorite (%)	Pyrite (%)
Miocene Sandstone	2806.60	Unreacted	45.61	11.49	10.96	20.02	3.74	8.18		Trace
	2806.60	7% O_2, 70^{0}C	53.12	11.52	9.4	16.35	1.31	8.29		Trace
	2805.68	Unreacted	45.36	12.16	9.25	15.27	3.45	14.5		Trace
	2805.68	0% O_2, 100^{0}C	50.77	12.04	7.32	13.08	2.41	14.37		Trace
	2805.07	Unreacted	43.04	12.32	10.02	14.53	4.91	15.17		Trace
	2805.07	3.5% O_2, 100^{0}C	48.04	11.48	10.99	12.62	1.16	15.72		Trace
Lower Tuscaloosa Sandstone	3193.28	Unreacted	75.52	Trace	Trace	Trace	1.95	2.37	20.16	Trace
	3193.28	0% O_2, 70^{0}C	75.28	Trace	Trace	Trace	1.73	2.05	20.94	Trace
	3193.28	3.5% O_2, 70^{0}C	75.75	Trace	Trace	Trace	2.18	2.1	19.98	Trace
	3193.28	0% O_2, 100^{0}C	74.83	Trace	Trace	Trace	1.73	2.27	21.17	Trace
	3193.28	3.5% O_2, 100^{0}C	74.94	Trace	Trace	Trace	1.5	2.04	21.51	Trace
Cardium Sandstone	1458.00	Unreacted	55.35	1.5	2.53	Trace	6.64	33.3		0.68
	1458.00	3.5% O_2, 70^{0}C	57.05	1.34	2.54	Trace	4	34.26		0.81

Furthermore, the concentration or fraction of injected fluid in a brine-rock system impacts the geochemical reactions (Parmentier et al., 2013; Bolourinejad and Herber, 2014). Parmentier et al. (2013) conducted experiments to investigate SO_2 reactivity on calcite at 150^{0}C and 100 bar for one month. Two experimental conditions were considered: the injection of low initial content of SO_2 gas (30 mg) and the injection of high initial content of SO_2 gas (535 mg) in a gold capsule containing a monocrystal of calcite and brine (25 g/L NaCl). In both cases, no CO_2 gas was injected during the experiments. In the case of the low SO_2 content, about a quarter of the initial calcite had dissolved after a month of treatment (or incubation); while in the case of the high SO_2 content, all calcite dissolved, and almost all calcium reprecipitated as anhydrite and the remaining sulphate accumulated in the aqueous phase. The analysis of the outlet gas indicates the presence of CO_2 gas in both cases. Thus, the presence of CO_2 gas must have resulted from the dissolution of calcite. Also, SO_2 gas was not detected after the experiment in the first case, while a final molar mixture of 28.4% CO_2 and 71.6% SO_2 was detected in the case of the high SO_2 content experiment. So, it is possible that all the SO_2 gas in the case of the low initial content of SO_2 experiment dissolved rapidly and completely in the aqueous phase as sulphate due to the high temperature condition, as high temperature increases kinetic rate constant and rate of reaction (Miri et al., 2014; Ma et al., 2019). Therefore, it is important to evaluate the impact of SO_2 gas impurity on CO_2-brine-rock interactions.

Hedayati et al. (2018) conducted experiments to evaluate the impacts of SO_2 gas impurity within a CO_2 stream on Heletz sandstone reservoir. The sandstone rock samples were exposed to pure CO_2 gas and CO_2 gas with 1.5 mol% SO_2 gas at 60^{0}C and 14.5 MPa. The rapid dissolution of SO_2 gas decreased the pH of the brine (more acidic solution) more compared to pure CO_2 gas. Hence, increase in mineral dissolution and the precipitation of sulphide minerals (pyrite) were observed

for the CO_2-SO_2 case (Table 2.4). Ankerite and dolomite, which are the most abundant carbonate minerals in the sandstone rock sample dissolved more quickly in the presence of the SO_2 gas. More quartz (feldspar dissolution) and halite (possible increase in Na^+ concentration in the aqueous phase) precipitated for the CO_2-SO_2 case, compared to the pure CO_2 case. In fact, clinochlore (chlorite mineral) precipitated, possibly resulting from the dissolution of dolomite and K-feldspar. For both cases, the dissolution of K-feldspar, ankerite, anatase/brookite, and plagioclase feldspar was observed. Pyrite dissolved for the pure CO_2 case, due to a lack of adequate sulphate ion in the brine to enable its precipitation. The dissolution of pyrite and ankerite enhanced the precipitation of siderite and magnetite, and the dissolution of feldspar minerals enhanced the precipitation of muscovite and kaolinite. The dissolution of dolomite released enough calcium into the aqueous phase and enhanced the precipitation of calcite. More K-feldspar and plagioclase dissolution was observed for the pure CO_2 case and used in the precipitation of quartz and secondary minerals (Aminu et al., 2018), whereas the dissolution of K-feldspar and plagioclase enhanced the precipitation of quartz for the CO_2-SO_2 case. Thus, a higher amount of quartz was precipitated for the CO_2-SO_2 case. The precipitation of halite might have resulted from the plagioclase mineral dissolution together with the initial sodium chloride (NaCl) concentration in the synthetic brine. The sandstone rock samples do not contain calcite as one of their initial minerals, therefore, anhydrite precipitation was not observed. The Ca^{2+} released from dolomite dissolution was not enough to precipitate anhydrite, as most of the sulphate content of the aqueous phase was used in the precipitation of pyrite. So, the initial mineralogical composition of the rock impacts the precipitation of secondary minerals.

Table 2.4: Mineralogical composition (vol.%) of sandstone rock samples before and after treatment in CO_2-brine and CO_2-SO_2-brine (Hedayati et al., 2018).

Mineral	Before treatment	Pure CO_2 (62 days)	CO_2+1.5 mol% SO_2 (36 days)
Quartz	75.05	77.78	81.86
K-feldspar	12.94	7.66	8.90
Ankerite	6.08	4.08	2.86
Anatase/brookite	0.52	0.451	0.32
Pyrite	0.26	0.21	0.63
Plagioclase	3.34	1.21	2.43
Dolomite	1.49	-	-
Halite	-	0.74	2.08
Clinochlore	-	-	1.40
Calcite	-	1.37	-
Siderite	-	0.40	-
Muscovite	-	2.54	-
Magnetite	-	0.10	-
Phlogopite	-	1.28	-
Kaolinite	-	1.84	-

Studies have been conducted on the impact of SO_2 gas or other gas impurities co-injected with CO_2 on the geochemical and petrophysical properties (porosity and permeability) of rocks. Bolourinejad and Herber (2014) conducted an experimental study on the storage of CO_2 and impurities in a depleted gas field in the northeast Netherlands. Experiments were conducted on Permian Rotliegend sandstone reservoir (no initial calcite content) and Zechstein caprock (anhydrite and carbonate component) core samples at in situ conditions of 300 bar and 100 ^{0}C for 30 days. Anhydrite precipitation was observed in H_2S or SO_2 co-injection case with CO_2, as the geochemical reaction with the formation water provided additional sulphur; while anhydrite dissolved in the pure CO_2 injection case. Pyrite and halite precipitated for the CO_2-H_2S co-injection case. In the CO_2-SO_2 co-injection case, enhanced levels of dissolution of carbonate and feldspar minerals were observed due to the formation of sulphuric acid from the geochemical reaction. Furthermore, after CO_2 injection, the permeability of the reservoir samples increased by 10-30%; while the permeability of caprock samples increased by a factor of 3-10, which indicates a significantly higher increase in the permeability of the caprock samples compared to the sandstone reservoir rock samples. CO_2 co-injection with 5000 ppm H_2S (higher concentration of the gas impurity, different from the other cases with 100 ppm gas impurity) reduced the permeability of the reservoir and caprock samples significantly (due to significant halite precipitation and little amount of pyrite and anhydrite precipitation), while only minimal change in permeability (less than 3% increase in permeability of the sandstone reservoir sample, and an increase in permeability up to 30% in the caprock sample) was observed when the concentration of H_2S was reduced to 100 ppm as the dissolution of minerals resulted in corresponding precipitation of secondary minerals. It is worth noting that after 17 days of CO_2 co-injection with 100 ppm H_2S, the permeability of the reservoir and caprock samples decreased as the precipitation of halite dominated the dissolution of feldspar and carbonate minerals. However, over time the mineral dissolution process dominated, resulting in increase in the permeability of the rock samples after 30 days. In the case of CO_2 co-injection with 100 ppm SO_2, the permeability of reservoir samples increased by a factor of 1.18 to 2.2, while the permeability of the caprock samples changed by a factor of 0.8 to 23 (permeability increased in caprock samples with a higher ratio of initial carbonate mineral concentration to anhydrite content, due to the carbonate dissolution). The increase in the permeability of the sandstone reservoir could be attributed to the lack of calcite mineral in the initial composition of the rock. Thus, the release of Ca^{2+} from dolomite dissolution was not enough to precipitate a significant amount of anhydrite (which could have decreased the permeability of the reservoir rock in the CO_2-SO_2 case). So, it appears that the initial mineralogical composition of the rock, duration of the geochemical reaction, and

concentration of impurities in a CO_2 gas stream in reservoir and caprock samples impact the amount of change in their permeability.

A similar experimental study was conducted by Aminu et al. (2018) to evaluate the effect of impurities on the permeability of sandstone reservoir rock samples. The impurities considered are NO_2, H_2S, and SO_2. The experiment was conducted at 70^0C and 140 bar for 9 months. They found that the effect of H_2S on the permeability of the rock samples is relatively small. CO_2 increased the reservoir rock permeability by 5.83%, while CO_2-H_2S increased it by 6.25%. CO_2 co-injection with SO_2 slightly decreased permeability by 6.25%; while CO_2 co-injection with NO_2 significantly decreased permeability by 41.67%. The changes in the rock permeability are significantly influenced by the existing rock minerals' dissolution and precipitation, as well as some secondary minerals precipitation. A similar study was conducted by Fatima et al. (2021) to evaluate the impact of pure CO_2 on the porosity of carbonate and shale rocks.

Fatima et al. (2021) conducted experimental and simulation studies on CO_2 geosequestration to investigate its impact on the geomechanical and petrophysical properties of rocks. The rock samples used in the experiment are carbonate and sandstone at in situ conditions of 200 psi and 120^0C. CO_2 was stored in the samples for different times (10, 20, and 120 days). The rocks' compressive and tensile strength tests as well as petrophysical properties tests were performed before and after CO_2 sequestration. Furthermore, numerical simulations, using CMG-GEM software, were performed to cover CO_2 geosequestration period of 250 years (25 years of injection and 225 years of storage). Results of the study showed that the solubility of CO_2 decreased with the increase in salinity and injection pressure. So, CO_2 solubility trapping is influenced by salinity, injection pressure, and presence of impurities such as H_2S (Li et al., 2016; Fatima et al., 2021). Fatima et al. (2021) also found that the storage of CO_2 increased the porosity and permeability of the formation when the storage period is more than 20 days as CO_2 dissolves in water (brine). In the study, a CO_2 storage period of less than 20 days did not show any significant change in the porosity and permeability of carbonate reservoir rock. In the experimental study conducted by Fatima et al. (2021) to evaluate the impact of CO_2 geosequestration in carbonate (Ordinary limestone and Khuff limestone) and Berea sandstone reservoirs at 120^0C and 1200 psi for 120 days, the percentage increase in the porosity and permeability of the sandstone reservoir is negligible compared to the carbonate reservoir rocks.

Al-Yaseri et al. (2022) conducted an experimental study to evaluate the impact of rock-wettability (water-wet and oil-wet scenarios) on CO_2-carbonate rock interaction. The impact of CO_2 flooding on the porosity and permeability of water-wet (to represent a saline aquifer) and oil-wet (to

represent a depleted carbonate reservoir) Indiana limestone core samples (98% calcite + 2% montmorillonite initial mineralogical composition) were evaluated at 50^0C and 10.23 MPa. The porosity of the water-wet and oil-wet core samples increased relative to the initial values by 82.50% and 50%, respectively; while the permeability of the water-wet and oil-wet core samples increased relative to the initial values by 1073.91% (over a factor of 10) and 236.26% (over a factor of 2), respectively. Findings of the study suggests that the reactivity of the CO_2-brine-carbonate rock is more pronounced in the water-wet rock compared to the oil-wet rock. So, the increase in porosity and permeability of carbonate aquifers might be higher compared to depleted petroleum carbonate reservoir rocks during CO_2 geosequestration, as aqueous solutions enhance mineral reactions.

Lu et al. (2016) conducted an experimental study to investigate the geochemical impact of O_2 impurity in CO_2 gas stream in carbonate (limestone and dolostone) reservoirs. The experiments were performed at 70^0C (or 100^0C) and 200 bar for about 3 weeks to investigate the effect of O_2 impurity on CO_2-brine-rock interactions. The increase in porosity and permeability of the limestone reservoir for CO_2 co-injection with 3.5 % O_2 was higher compared to that of pure CO_2 at the same temperature. The increase in permeability in the limestone reservoir at 70^0C is higher compared to the increase in permeability at 100^0C for the CO_2 co-injection with 3.5 % O_2 case. Porosity and permeability of dolostone increased significantly when CO_2 was added, but the addition of 3.5% O_2 did not result in notable changes in the porosity and permeability of the dolostone rock samples. Also the impact of temperature on the porosity and permeability of the dolostone rock samples was not significant. Findings of the study revealed that the CO_2 co-injection with O_2 impurity will not cause significant damage to carbonate formations. Thus, retaining a small amount of O_2 in the CO_2 gas stream will save cost of carbon capture and storage. Therefore, it is important to understand the impact of impurities co-injected with CO_2 on the porosity and permeability of different formations (Table 2.5).

Table 2.5: Impact of CO_2 (with or without the addition of impurities) on the porosity (ϕ) and permeability (K) of rocks.

Rock description	Fluid composition	Operating conditions	Before sequestration		After sequestration		Percentage change in ϕ	Percentage change in K	References
			ϕ (%)	K (mD)	ϕ (%)	K (mD)			
Ordinary limestone	CO_2 + brine	$T=120^0C$ P=1200 psi t=120 days	10.235	19.6425	10.495	25.455	2.54	29.59	Fatima et al. (2021)
Khuff limestone			6.56	4.56	6.89	5.451	5.03	19.54	
Berea sandstone			17.3	201.6	17.4	202.4	0.58	0.40	
Sandstone	100% CO_2 + brine	$T=70^0C$ P=140 bar t=9 months	-	240	-	254	-	5.83	Aminu et al. (2018)
	95% CO_2 + 5% NO_2 + brine					140		-41.67	
	95% CO_2 + 5% SO_2 + brine					225		-6.25	
	95% CO_2 + 5% H_2S + brine					255		6.25	
Indiana limestone (water-wet)	CO_2 + brine	$T=50^0C$ P=10.23 MPa	3.9	9.2	7.1	108	82.50	1073.91	Al-Yaseri et al. (2022)
Indiana limestone (oil-wet)			3.2	9.1	4.8	30.6	50.00	236.26	
Limestone (98.8% calcite + 0.5% dolomite + 0.4% quartz + 0.3% illite)	100% CO_2 + brine	$T=100^0C$ P=200 bar t= 18 days	1.6	0.0022	1.9	0.0168	18.75	663.64	Lu et al. (2016)
	96.5% CO_2 + 3.5% O_2 + brine	$T=70^0C$ P=200 bar t= 18 days	1.6	0.0022	2.3	0.0855	43.75	3786.36	
	96.5% CO_2 + 3.5% O_2 + brine	$T=100^0C$ P=200 bar t= 20.9 days	1.6	0.0022	2.3	0.0376	43.75	1609.09	
Dolostone (64.5% dolomite + 28.1% Ankerite + 5.8% illite + 0.6% siderite + 0.6% K-feldspar + 0.5% chlorite)	100% CO_2 + brine	$T=70^0C$ P=200 bar t= 18 days	0.4	0.0003	2.0	0.0034	400	1033.33	
	96.5% CO_2 + 3.5% O_2 + brine	$T=70^0C$ P=200 bar t= 19 days	0.4	0.0003	1.5	0.0132	275	4300.00	
	96.5% CO_2 + 3.5% O_2 + brine	$T=100^0C$ P=200 bar t= 19 days	0.4	0.0003	1.2	0.0158	200	5166.67	

While the impact of CO_2 on the petrophysical properties of sandstone and carbonate formations have been widely studied, only a few studies have investigated the impact of CO_2 on the petrophysical properties of shale formations (Elwegaa et al., 2019; Ma et al., 2019). Ma et al. (2019) conducted a geochemical modelling study on the impact of CO_2-brine-rock interaction on the permeability of a mudstone (referred to as shale in the present study for simplicity, due to its high clay content) caprock. A vertical one-dimensional (1D) model of a sandstone reservoir overlain by the mudstone (shale) caprock was developed, and the geochemical modelling of the CO_2-brine-rock interaction was performed using TOUGHREACT. The initial CO_2 saturation in the reservoir (at 47^0C and 10.1 MPa) was set as 0.5, while the initial CO_2 saturation in the caprock was set as zero (0). Findings of the study revealed that after 5000 years of CO_2 geosequestration, CO_2 diffused up to about 2.3 m (from the reservoir-caprock interface) into the caprock. Thus, the

permeability of the caprock increased from $3.0x10^{-17}$ to $4.8x10^{-17}$ (60% increase relative to the initial permeability) due to significant dissolution of K-feldspar and albite, and the dissolution of some amount of calcite and chlorite in the caprock (while very little amount of quartz precipitated). Furthermore, they evaluated the impact of salinity on the CO_2-brine interaction with the caprock by increasing the salinity from 0.10 to 0.20, and found that the dissolution depth of the mudstone caprock was slightly larger at the lower salinity (0.10). This result indicates that an increase in the salinity to 0.20 attenuated the CO_2 dissolution in the caprock, thereby enhancing the sealing ability of the caprock. An experimental study conducted by Elwegaa et al. (2019) also showed that the porosity and permeability of shale formations increases during pure CO_2 sequestration at low temperature conditions. It would be important to investigate the impact of impurities in CO_2 on the porosity and permeability of shale formations.

2.4.2 Impact of CO_2 geosequestration on brittleness of reservoir and cap rocks

Alam et al. (2014) carried out a study on petrophysical and rock-mechanics effects of CO_2 injection for enhanced oil recovery. The experimental study was conducted over a period of 8 days on chalk from South Arne field, North Sea. Two types of chalk from the field were studied: Ekofisk Formation containing more than 12% non-carbonate (silica and clay) minerals, and Tor Formation made up of less than 5% non-carbonate (silica and clay) minerals. They found that porosity of the rock samples increased by 2-3% and a small increase in permeability. A reduction in elastic stiffness of the rock was indirectly determined based on an increase in Biot's effective stress coefficient by 1-2%. Nuclear Magnetic Resonance (NMR) data showed that there was no change in wettability (or contact angle) and the rock samples remained water-wet throughout the period of the experiment. Furthermore, they found that the effect of supercritical CO_2 injection on petrophysical and geomechanical properties of chalk depend on the carbonate mineral content. Tor Formation (pure chalk) with high carbonate content encountered significant mechanical weakening due to CO_2 injection, while no significant mechanical effect was found in the Ekofisk Formation (impure chalk).

A similar study was carried out on a sandstone rock by Huang et al. (2018). The study was based on the influence of supercritical CO_2 on the strength and fracture behaviour of brine-saturated sandstone specimens. Uniaxial compression, Brazilian splitting, and fracture tests were conducted on sandstone specimens with brine saturation or supercritical CO_2 ($scCO_2$)-brine co-saturation to investigate the impact of $scCO_2$ injection and brine salinity on the fracture toughness, Brazilian tensile strength (BTS), and uniaxial compressive strength (UCS) of sandstone reservoir.

Findings of the study revealed that the fracture toughness, BTS, and UCS of sandstone saturated with only brine increased as sodium chloride (NaCl) concentration increased, but decreased as $scCO_2$-brine was co-injected in the rock samples. However, increase in the elastic modulus and average stiffness of $scCO_2$-brine co-saturated sandstone was observed compared to the brine-saturated sandstone. Mineral composition changes and dissolution of quartz was not observed. However, many micro pores were created in the sandstone after $scCO_2$ injection, thereby reducing strength and fracture toughness while porosity increased. They attributed the strength reduction and porosity increase in the tested sandstone to the dissolution of clay-cementation (kaolinite) in the acidic solution. However, both the salinity and $scCO_2$ injection showed no significant impact on the fracture behaviour of the tested sandstone specimens.

Moreover, Liu et al. (2014) conducted an experimental study on the short-term effect of CO_2 on the tensile failure of sandstone. The sandstone samples were fractured under different pore fluid conditions: dry, dry with CO_2, water-wet, and CO_2-water-wet. Results of the study revealed that the effective fracturing pressure of samples varied linearly with the effective confining pressure in the range of 1-6 MPa under the same pore fluid condition. The water-saturated rock experienced tensile strength weakening up to 5.638%, but the tensile fracturing behaviour of the sandstone was not significantly affected by gaseous CO_2 in the presence or absence of water. However, laboratory experiments are conducted over a short period (less than a year), whereas CO_2 geosequestration in the field can take 100 years or more. So, the time-dependent effect of CO_2 on the geomechanical properties of rock is vital.

AL-Ameri et al. (2014) conducted a study to investigate the impact of CO_2 storage on the mechanical properties of carbonate aquifer rocks. CO_2 was stored in carbonate rock core samples at a pressure and temperature of 2000 psi and 100^0C, respectively. CO_2-brine-rock contact time or solubility time ranged between two weeks to three months before the core samples were analysed for changes in mechanical properties using acoustics, unconfined compression, and indirect tensile strength testing machines. Results of the experiments revealed that CO_2 storage for longer times significantly altered the mechanical properties of the rock samples. The longer the storage time the greater the change in the mechanical properties of the rock samples studied. The unconfined compressive strength, Young's Modulus, and Poisson's ratio of the rock samples decreased after 90 days of CO_2 sequestration. Therefore, the geochemical interaction between the CO_2-brine and rock samples, which altered the mechanical properties of the rock is time-dependent. Similarly, Tariq et al. (2018) carried out a geomechanical study on CO_2 sequestrated rocks in an aqueous saline environment. The study was conducted on limestone and sandstone

rocks, to investigate the degradation of the petrophysical and mechanical properties of rocks due to supercritical CO_2 storage. The carbonate and sandstone rock samples were exposed to a CO_2-brine solution at reservoir condition of 1200 psi pressure and 120 ^{0}C temperature over a period of 10 to 120 days. The mechanical properties of the rocks were examined by static and dynamic mechanical tests, while the petrophysical properties of the rock were determined by routine core analysis. The findings of the study revealed that the duration of solubility of CO_2 in brine has a significant impact on the mechanical and petrophysical properties of the rock samples considered, especially when CO_2 is stored for a longer period of time in the rock. Thus, CO_2-brine-rock interaction resulting in a change in mechanical and petrophysical properties of the rock is time-dependent. Based on the study, they concluded that the potential candidate for CO_2 geosequestration is limestone (carbonate rock) as it exhibits minimal change in rock properties.

Masoudi et al. (2011) performed an integrated reservoir simulation to evaluate the impact of CO_2 storage on the geomechanical properties of a depleted carbonate gas reservoir. They conducted petrophysical measurements and laboratory rock mechanics tests on core samples before and after injection of CO_2-saturated brine solution. The laboratory results were used to develop petrophysical property, elastic, and material strength degradation models due to CO_2-brine-carbonate rock interaction. A coupled hydrological-mechanical modeling was performed, which incorporates CO_2 saturation and reservoir pressure from dynamic simulation, and the resulting changes in porosity, permeability, and effective stress were calculated by a Geomechanical modeler and passed back to the dynamic reservoir simulation. The simulation was performed to investigate time-dependent effect of rock petrophysical and geomechanical properties during CO_2 sequestration. Findings of the study revealed that the reservoir and cap rocks remained elastic even though the elastic and strength properties of the formations degraded with increase in CO_2 saturation and an increase in local permeability of the formations up to 70% due to injection. Compactions induced in the reservoir during production were fully recovered during the injection phase when the reservoir pressures were restored to their pre-production values. However, large injection pressures gave rise to large amounts of plasticity of up to 3% after over 35 years of CO_2 geosequestration. In fact, the reservoir volume substantially increases with volumetric strain up to 5%. The computed shear strains indicated that vertical fracture would be initiated at an injection pressure of 4200 psi. The capacity of caprock sealing and integrity can be limited by the presence of any sub-seismic faults and/or fractures. Therefore, a critical field pressure limit up to 4200 psi, based on the injection rate of 50 MMSCF/day at each of the injection wells was recommended. So, at high CO_2 injection pressure, the reservoir and caprock can experience plastic deformation. Thus, it is important to investigate whether CO_2 streams injected in a storage reservoir influence

the brittleness of the reservoir or cap rocks; as the more brittle rocks become, the higher the chance of induced fracture in the rocks.

Lyu et al. (2018) developed a damage constitutive model to evaluate the effects of CO_2-brine-rock interactions on the brittleness of a low-clay shale. They conducted a series of strength tests to determine the stress-strain characteristics of shale rock samples soaked in different CO_2 phases, including subcritical or supercritical CO_2 with formation water at different time intervals or solubility time (10, 20, and 30 days). They established two damage constitutive equations based on the Weibull distribution and power function distribution, to predict the threshold stress for both soaked and intact shale samples. Results of the study revealed that physical and chemical reactions of CO_2-brine-rock during injection and storage cause significant reductions in the peak axial strength and Young's modulus of shale rocks. Furthermore, they applied the energy balance method together with the Weibull distribution-based constitutive model to calculate the brittleness values of samples with or without CO_2-brine soaking. They found that the intact shale sample had the highest brittleness index of 0.9961, which corresponds with the high percentage of brittle minerals in the shale samples; while the CO_2-brine-shale interactions in the soaked shale sample decreased the brittleness values. In addition, among the three soaking durations considered, the minimum brittleness values occurred on samples with 20 days of soaking in CO_2-brine solution in both subcritical and supercritical CO_2 phases. However, shale rock sample soaking in subcritical or supercritical CO_2-brine solutions has higher effect on the strength and Young's modulus of shale rocks than on the brittleness. In fact the low-clay shale still keeps good fracture performance after the period of soaking in brine-subcritical/supercritical CO_2.

Lyu et al. (2018) subdivided the minerals in the intact rock as brittleness component (72.95 wt.%), clay component (5.85 wt.%), and others (20.97 wt.%). Quartz (55.50 wt.%), feldspar (14.57 wt.%), and cristobalite (2.88 wt.%) were classified as the brittleness component; kaolinite (1.00 wt.%), illite (1.42 wt.%), and smectite (3.43 wt.%) were classified as the clay component; while calcite (4.44 wt.%), pyrite (4.08 wt.%), muscovite (5.57 wt.%), annite (1.41 wt.%), marble (5.10 wt.%), and braunite (0.37 wt.%) were classified as the other minerals. The mineralogical composition of the low-clay shale is similar to mineralogical composition of some sandstone reservoirs. The change in rock strength and brittleness during CO_2-brine-rock interaction (Table 2.6) could be attributed to the alteration in rock mineralogy, as some brittle minerals dissolve and/or some non-brittle minerals precipitate in the rock.

Table 2.6: Impact of CO_2 sequestration on the brittleness index and uniaxial compressive strength of shale rock (Lyu et al., 2018).

Rock description	Soaking condition	Operating conditions	Soaking time (days)	Brittleness index	Percentage change in brittleness index	Average UCS (MPa)	Percentage change in UCS
Low-clay shale	Intact	T=22^{0}C		0.9961		53.30	
	Subcritical CO_2 + NaCl	T=40^{0}C P=7 MPa	10	0.9843	-1.18	42.22	-20.79
			20	0.9754	-2.08	34.15	-35.93
			30	0.9851	-1.10	23.03	-56.79
	Supercritical CO_2 + NaCl	T=40^{0}C P=9 MPa	10	0.9757	-2.05	37.75	-29.17
			20	0.9713	-2.49	25.28	-52.57
			30	0.9835	-1.26	20.51	-61.52

Thus, Kang et al. (2020) conducted a study on mineralogical brittleness index as a function of weighting brittle minerals. They found that the simple sum of brittle minerals model does not significantly correlate to the mechanical brittleness index model. Thus, considering the bulk modulus of the brittle minerals, the researchers proposed a new model of mineralogical brittleness index as a function of brittle minerals with their corresponding weighting coefficients. The new brittleness index is significantly correlated to the mechanical brittleness index. However, for a single mineral rock (for instant calcite only), regardless of the weighting coefficient assigned to it with respect to other minerals, the mass fraction will remain the same regardless of its mass over the period of CO_2 geosequestration as long as no other mineral precipitates in the rock under the geosequestration condition. So, both the simple sum of brittle minerals and the new mineralogical brittleness index, suggest that the brittleness of a single mineral rock remains the same unless another mineral precipitates during the period of geosequestration.

Some studies on brittleness of rock have been conducted without considering CO_2 injection or storage. For instance, Hou et al. (2018) conducted a study to evaluate brittleness of shale based on the Brazilian splitting test. The shale cores are from the Longmaxi Formation, Silurian system, Sichuan basin. They evaluated brittleness using a comprehensive brittleness model developed by regression analysis (based on experiments) on the rock elastic parameters (using normalized Poisson's ratio and Young's modulus), curve peak characteristics (ratio of tensile strength to deformation at peak point), and energy dissipation (ratio of intrinsic cohesion of rocks to total fracture propagation resistance exerted by the frontal zone when the peak stress value is reached). They found that the tensile brittleness index (evaluated by the comprehensive brittleness index model) is more accurate and sensitive to changes in different conditions than the compressive brittleness index.

Furthermore, Meng et al. (2015) developed an evaluation methodology of brittleness of rock based on post-peak-stress-strain curves. They believe that the evaluation of brittleness index of

rock based on strength ratio or product cannot properly describe rock brittleness, as most of those indices neglect how brittleness is impacted by stress state of the rock. The new brittleness evaluation method developed in the study includes two brittleness indices: the degree of brittleness and brittle failure intensity, based on the magnitude and velocity of the post-peak stress drop. This post-peak stress drop is easily obtained from the conventional triaxial and uniaxial compression tests. The two indices account for the impact of confining pressure on the brittleness of rocks. A high degree of brittleness of rock implies that the ratio of the stress drop (positive difference between peak stress and residual stress) to the peak stress is large and the peak stress decreases rapidly to the residual stress. So, the relative stress drop and stress drop velocity (which involves the stress path) is considered in the degree of brittleness of the rock. Thus, while the brittleness index of rocks are related to their mineralogical compositions, it is important to compare brittleness of different rocks at similar confining pressure conditions.

2.4.3 Impact of cyclic injection of CO_2 on the properties of reservoir and cap rocks

CO_2 geosequestration could involve non-cyclic or cyclic process. On the one hand, non-cyclic process entails injection of CO_2 over a period, then stop the injection and allow the injected CO_2 to be trapped in the reservoir. On the other hand, cyclic process of geosequestration involves injection of CO_2 for some period (in some cases, withdrawing some of the injected CO_2 leaving behind some amount of CO_2 in the reservoir), and repeating the process over the geosequestration period. Rock tests based on cyclic injection and withdrawal of fluid could be classified as environmental cyclic tests on rocks, as it relates to cyclic wetting-drying or cyclic freezing-thawing tests on rocks. For instance, for cyclic wetting-drying tests, the effective pressure in the reservoir decreases during the wetting process, while the rock's cement weakens during the drying process. Thus, the rock strength decreases during wetting-drying tests due to the water-rock interaction. (Liu and Dai, 2021). Hence, during the cyclic injection-withdrawal of CO_2, the process induces cyclic stress on the rock, leading to the rock's deformation and decrease in strength. Several studies have been conducted on cyclic injection of CO_2, to investigate the multiphase flow behaviour, and its impact on pore structure and mechanical properties of rocks.

Residual trapping of immiscible fluids such as hexane during cyclic injection exhibit similar characteristics as supercritical CO_2. Ahn et al. (2020) conducted a study on migration and residual trapping of immiscible fluids during cyclic injection. They performed five sets of drainage-imbibition cycles. Findings of the study revealed that as cyclic injection of hexane and water progressed, saturation of the hexane repeatedly increased in the drainage cycles and dropped

during imbibition cycles, but the differences in the saturation gradually diminished at later cycles. Furthermore, the mobile fractions in hexane saturation decreased rapidly, while the immobile fractions increased consistently at the drainage cycles (but the immobile fractions or residual saturation of hexane increased slightly but consistently at imbibition cycles). The increase in the immobile fractions of hexane occurs as newly invading water causes the previously flooded hexane (as continuous and interconnected streams) to be dispersed and isolated into several small-scale blobs. Thus, a conglomerate of blobs and clusters of immiscible fluids, dispersed in the same manner builds up during the repetitive (cyclic) injection processes until the immobile region comes in contact with the main flow channels. In fact, as the residually trapped CO_2 increases, the upward mobility of stored CO_2 in the reservoir is limited due to decreased buoyancy, thereby promoting effective and secured CO_2 geosequestration. Thus, the application of cyclic CO_2-brine injection may be useful for long-term storage of CO_2 streams as small-scale dispersed blobs and clusters of CO_2 by hydrodynamic and mineral trapping (Ahn et al., 2020). During cyclic CO_2 injection, about 40-50% of CO_2 can be stored mainly through residual and solubility trappings in the porous medium (Abedini and Torabi, 2014). Therefore, residual and hydrodynamic trapping mechanisms play key roles in CO_2 storage during cyclic injection. This finding is supported by a study conducted by Li et al. (2021) on strategies of CO_2 injection for enhanced oil recovery. They found that water alternating gas (CO_2) and CO_2 cyclic injection strategies provide significantly higher effective CO_2 storage capacities compared to the continuous CO_2 injection strategy. However, residually trapped CO_2 might reconnect with injected CO_2 in subsequent injection cycles mainly close to the large pore clusters, as observed during cyclic hydrogen (H_2) injections (Lysyy et al., 2023).

Furthermore, Saeedi et al. (2011) conducted a study on multiphase flow behaviour during cyclic CO_2-brine flooding in sandstone rock samples. They found that for rock samples with low permeability or susceptible to formation damage (including migration of fines, dissolution or precipitation of minerals, etc.), injectivity may reduce during cyclic CO_2-brine injection, even though the level of damage would stabilise after several cycles of injection. Moreover, during several CO_2-brine flooding cycles, the porous rock could experience some level of plastic deformations due to the dissolution of some host minerals in the cement which initially binds grains of the rock together. Edlmann et al. (2019) conducted a study on cyclic CO_2-H_2O injection and residual trapping. They found that differential pressure increases continuously over several injection cycles due to reduction in effective permeability as residual trapping of CO_2 increased, therefore limiting flow and injectivity. The increase in residual trapping of CO_2 results in increase

in the storage security of CO_2 as the buoyant [free] gas phase is reduced. However, the more residually trapped CO_2 close to the well results in more tortuous flow paths for the CO_2 injected, thereby posing as a barrier to fluid flow and resulting in reduction in injectivity. Herring et al. (2016) conducted a similar study on residual trapping of supercritical CO_2 through cyclic injections in a sandstone system. Findings of the study revealed that residual supercritical CO_2 trapping increases with several drainage-imbibition cycles. They suggest that exposure of supercritical CO_2 in certain geologic materials may induce surface chemical reactions which are time-dependent. Thus, the surface chemical reactions can influence the pore structure of the rock (especially over longer period of cyclic CO_2 injection), as dissolution-dominant reactions of rock minerals would result in increased porosity and permeability, while precipitation-dominant reactions would result in decreased porosity and permeability of the rock.

Elwegaa et al. (2019) conducted a study on cyclic cold carbon dioxide injection for improved oil recovery from shale oil reservoirs. They found that injection of cold CO_2 increased both porosities and permeabilities of the core samples by up to 3.5% and 8.8%, respectively. In a similar study conducted by Su et al. (2021) on cyclical supercritical CO_2 treatment, to investigate the fractal characteristics and structures of pores in long-flame coal. They observed significant increase in the porosity and proportion of macropores after treatment, as new pores were formed and some small pores possibly converted into macropores. Moreover, as duration of treatment increased, the trend of the daily average porosity rate increased, possibly caused by the effects of fatigue of the coal matrix. Ke et al. (2023) conducted a comparative study to characterize sandstone microstructure affected by cyclic wetting-drying process. Findings of the study revealed that the microporosity of the sandstone increases during the cyclic wetting-drying process, as a result of progressive changes in micro grains and micropore structure as micropores expand gradually and merge. This results in loose mineral particles and blocks, cracks developing into interconnected networks, enabling smooth mineral surfaces. During the following cycles, the average pore throat diameters increase gradually. As the cyclic wetting-drying process continues, the structures and mechanical properties of the sandstone changes due to cumulative changes in microstructure. The driving forces of the changes in the microstructure of the sandstone is water-rock interaction including physical, mechanical, and chemical interactions. Badrouchi et al. (2022) carried out a study on CO_2 injection side effects on reservoir properties in ultra-tight formations. They found that carbonic acid dissolve some amount of the calcite, dolomite, and feldspar minerals in the rock and create new micro- and nano-pores, thereby increasing the microporosity of the rock samples after one cycle of CO_2 injection. However, after four CO_2

injection cycles, the effective porosity of the rock samples decreased, as the dissolved CO_2 could react with rock minerals and form precipitates that block some pores. Therefore, due to changes in the rock's microstructure, the porosity of the rock changes (increases or decreases) at different cycles during the injection process. These changes in the microstructure impacts the petrophysical (porosity and permeability) and mechanical (elastic and strength parameters) properties of the rock.

Su et al. (2020) conducted a study on the effects of cyclic saturation of supercritical CO_2 on the pore structures and mechanical properties of bituminous coal. They found that porosity of continuously saturated coal samples increased by 3.76-11.57% as saturation progressed, while that of cyclic-saturated coal samples increased by 2.85-16.03%. Cyclic saturation of the coal samples has a higher significant effect on the pore structures, compared to the continuous saturation. After 13 days of saturation, the uniaxial compressive strength of the coal samples decreased by 47.17% and 61.05% in the case of continuous (sustained) saturation and cyclic saturation, respectively. Moreover, as the number of saturation cycles increased, the tensile stress required to create new cracks in the coal decreased as the dissolved and extracted materials by supercritical CO_2 are probably removed from the pores as the gas flows. Thus leading to rapid propagation and connection of cracks in the coal, eventually resulting in a significant decrease in strength. Xu et al. (2021) conducted a study on non-isothermal effect of cyclic carbon dioxide on the petrography of coals for coal mine methane recovery. They found that the peak strength of coals decreased as the liquid CO_2 affecting cycles increased, and greater decrease in strength of the coal was observed as the cycles get larger. In addition, the pore volume of the coal increased during the cyclic process, creating some flow channels for the seepage of methane by destroying the matrix structure and weakening the structure. The pore structure and mechanical properties of rocks are linked to their mineralogical composition. Therefore, investigating dissolution and precipitation of minerals in the rock is paramount.

Li et al. (2023) conducted an experimental study on mechanical properties and fracture characteristics of shale layered samples under cyclic loading. Shale layered samples with different mineral compositions were classified as clay-rich, calcareous, and siliceous black shales based on their x-ray diffraction (XRD) analysis. Findings of the study revealed that strength and deformation (or elastic) parameters are strongly dependent on the mineral compositions of the rock samples. The Young's (elastic) modulus of the clay-rich shale was highest, followed by calcareous and siliceous shale; while the Poisson's ratio of calcareous shale was observed to be highest, followed by clay-rich and siliceous shale samples. In addition, the compressive strengths

under cyclic loading and loading were lower compared to the compressive strengths under uniaxial quasi-static loading. Due to the variations in the mineral compositions of the shale samples, the average decline in the compressive strength of calcareous shale was the largest, followed by the siliceous and clay-rich shale. Similarly, Xu et al. (2022) conducted a study to investigate the mechanical responses of coals under the effects of cyclical liquid CO_2 during coalbed methane recovery process. They found that the compressive strength and elastic modulus exhibit negative correlations with the increasing cyclical parameters, while Poisson's ratio and damage variable correlate positively with the increasing affecting parameters. This shows that the corresponding cyclical temperature shock could promote the crack growth and CO_2 adsorption, aggravating the strength reduction and eventually destroying coals with the lower yield strength. These non-uniform variation in the Young's modulus and Poisson's ratio might impact the brittleness of rocks, as these parameters are useful in brittleness index evaluations. Thus, it is possible that the brittleness of rocks vary during cyclic CO_2 injection.

Elwegaa et al. (2019) conducted a study on cyclic cold carbon dioxide injection for improved oil recovery from shale oil reservoirs. The shale rock samples used in the study was carbonate-rich with 81.6 wt.% calcite, 14.2 wt.% calcite, 3.0 wt.% kaolinite, and 1.3 wt.% basanite. The rock samples were subjected to the same cyclic injection temperature conditions (74^0F, 32^0F, 0^0F, and -15^0F), but different injection pressure condition (1000 psi, 2000 psi, 3000 psi, or 4000 psi). They observed an increase in the brittleness index (or brittleness ratio) of the three shale core samples, while the brittleness index of the fourth shale core sample subjected to cyclic injection temperature conditions at 3000 psi decreased. In their study, CO_2 was injected in the shale rock and brittleness index was calculated mainly by the ratio of sum of the volume of quartz and dolomite to the sum of the volume of all the minerals in the rock sample; and the brittleness ratio was evaluated based on dynamic elastic modulus and Poisson's ratio, which do not accurately reflect the brittleness of rocks. Also, the impact of impurities in CO_2 during the cyclic injection was not considered in the study. Moreover, Lyu et al. (2018) developed a damage constitutive model for the effects of CO_2-brine-rock interactions on the brittleness of a low-clay shale (but with a carbonate or calcite content of only 4.4 wt.%, cristobalite content of 2.88 wt.%, quartz content of 55.50 wt.%, feldspar content of 14.57 wt.%, clay content of 5.85 wt.%, and other minerals). They found that the CO_2-brine-shale interactions in the soaked shale sample decreased the brittleness values. The decrease in the brittleness index might be related to the low initial carbonate content, while the increase in the brittleness index of the shale rock samples in the study conducted by Elwegaa et al. (2019) might be related to the high initial carbonate content of the shale rock samples. Therefore, it is important to evaluate the brittleness index of different rock samples (with different

initial mineralogical compositions) subjected to CO_2 sequestration conditions using similar and more robust mathematical model for a better comparison.

2.4.4 Application of machine learning in evaluating the integrity of materials and in CO_2 geosequestration

Several researchers have adopted machine learning approaches which provides a substantial way to solve rock engineering problems (Wang et al., 2021). Bérubé et al. (2018) applied support vector machines (SVMs) to predict the types of rock sample based only on their grain density and magnetic susceptibility. Similarly, Cao et al. (2020) utilized the support vector regression (SVR) surrogate model to predict pressure change and formation deformation with reliable accuracy. They used reservoir permeability and fluid injection rate to determine pressure change, and reservoir Young's Modulus for formation deformation including vertical displacement. In fact, machine learning algorithms have been coupled with optimizers (hybrid models), and calibrated with a few mechanical rock test measurements to predict geomechanical characteristics along an entire wellbore. Rashidi et al. (2020) adopted this approach to identify zones at risk of casing collapse by predicting shear modulus with high accuracy. They used compressional velocity, shear velocity, bulk density, and Poisson's ratio as inputs in the hybrid models, and found that shear stresses tend to build up along the interfaces between two dissimilar formations such as ductile low-density salts and rigid, brittle and more difficult to displace layers like anhydrite. Similarly, Nyakilla et al. (2022) conducted a study on machine learning application in the prediction of compressive and shear bond strengths, based on experimental data in oil well cement at 80^0C, using gradient boosting regression tree (GBRT) ensemble techniques. The experimental data were obtained from compressive strength (CS) and shear bond strength (SBS) studies using supplementary cementitious materials (class F fly ash) in different proportions. The results indicated that GBRT model performed better than support vector machine (SVM), Gaussian process regression (GPR), and artificial neural network (ANN) models. The GBRT model gave the greatest accuracy (higher R^2 values: R^2 = 0.995 for CS and R^2=0.989 for SBS, and least loss functions (mean square error = 0.160 and mean absolute error = 0.174 for CS, and mean square error = 0.0005 and mean absolute error = 0.0031 for SBS). These results suggest that for the long life of oil and gas wells, GBRT can be implemented for cement hydration prediction.

Furthermore, Singh (2019) proposed a machine learning method for fluid leakage surveillance using deconvolution response function (time varying bottomhole pressure and injection rates non-

linear function) from injection and monitoring wells. Detection of leakage is based on comparison between expected (base case without leaks) deconvolution response of all monitoring wells and their observed deconvolution response. In a similar study, Kolawole et al. (2023) conducted a study to investigate the mechanical integrity of microbial-induced calcite precipitation (MICP) and oilwell cement (OWC), which are cementitious materials, to assess their leakage-plugging potential around the wellbore. They applied Artificial Neural Network (ANN) and Random Forest (RF) machine learning algorithms to predict near-wellbore mechanical integrity at macro-scale. The results indicate that the degree of correlation between the mechanical integrity obtained from experimental tests and the machine learning predictions is high. The RF model predicted the macro-scale mechanical integrity of MICP and OWC-cemented specimens with higher accuracy (higher R^2 value and lower mean absolute error) for uniaxial compressive strength (R^2 = 0.9738 and MAE=1.04 MPa) and fracture toughness (R^2 = 0.9988 and MAE=0.02 MPa.√m) predictions compared to the ANN model. However, the performance of machine learning models depend on the model parameters or hyperparameters selected. In other words, a machine learning algorithm adopted might perform better by tuning the hyperparameters of the model. Therefore, ANN model could perform relatively better, if the hyperparameters were different.

The application of machine learning can be extended to CO_2 geosequestration in reservoirs. Ibrahim (2022) conducted a study on the application of machine learning for prediction of coal wettability during CO_2 geosequestration. Artificial neural network (ANN) and adaptive neuro-fuzzy inference system (ANFIS) were adopted to predict the contact angle in coal-water-CO_2 system. The input parameters were the coal properties, operating pressure, and temperature. The correlation coefficient (R) and the mean absolute percent error (MAPE) were used to measure the model performance. The results indicated that ANN and ANFIS models predicted the contact angle in the coal-water-CO_2 system accurately. Both models predicted the contact angle with R values higher than 0.96 and MAPE less than 7%. Thus, these models can be useful to screen coal formation targets for CO_2 storage. Furthermore, Thanh et al. (2022) adopted knowledge-based machine learning techniques for predicting CO_2 storage performance in saline aquifers. They developed three machine learning-based models: random forest (RF), extreme gradient boosting (XGBoost), and support vector regression (SVR) in the study. The XGBoost-based model predicted more accurately (based on higher R^2 and extremely low root mean square error) for both residual and solubility trapping efficiency. Therefore, the proposed model might be viable for predicting the CO_2 trapping index in other saline formations around the world. However, the CO_2 trapping index or CO_2 storage potential might be influenced by the geochemistry of the

formation. Geochemical composition of formation fluids in reservoirs could be useful in predicting properties of the formation, as the ionic composition of the fluid is based on fluid-rock chemical interactions. Yu et al. (2020) conducted a study on formation water geochemistry for carbonate reservoirs in Ordos basin China. They proposed statistical relationships between the geochemical properties and hydrocarbon storage using machine learning (Decision tree) method. Findings of the study revealed that the salinity, Na^+/Cl^- ratio, $(Cl^- - Na^+)/Mg^{2+}$ ratio, $(HCO_3^- - CO_3^{2-})/Ca^{2+}$ ratio and Mg^{2+}/Ca^{2+} ratio correlate highly with the gas preservation. The model accurately predicts where to find gas reservoirs in the Ordos basin, leading to improved exploitation of the hydrocarbon. Thus, this finding can be possibly extended to reservoir-caprock system exhibiting different level of brittleness during CO_2 geosequestration.

2.5 Summary of Literature Review

The studies reviewed have considered the impact of CO_2 and impurities (H_2S, SO_2, NO_2, and O_2) on porosity, permeability, and mineralogical composition of different rock lithologies, as well as the impact of pure CO_2-brine interaction on geomechanical properties and brittleness of rocks. The pH of aqueous phase in reservoir and caprock decreases during CO_2 (with or without the addition of impurities) geosequestration and enhances the dissolution and precipitation of minerals. The changes in the porosity and permeability of the rocks during CO_2 geosequestration depend on their initial mineralogical compositions, fluid composition and properties (ionic composition and salinity of the aqueous phase, and the type of gas impurity co-injected with CO_2), in situ temperature and pressure conditions, and duration of the CO_2 geosequestration. In many sandstone, carbonate (or carbonate-rich), and shale formations, CO_2-brine-rock interaction results in increase in porosity and permeability. In fact, CO_2-O_2-brine-rock interaction result in increase in porosity and permeability of carbonate rocks. However, the change in porosity and permeability when CO_2 is co-injected with impurities (such as SO_2 or H_2S) varies depending on the initial mineralogical composition of the rocks and the duration of sequestration. For instance, in the studies conducted by Bolourinejad and Herber (2014) and Hedayati et al. (2018), CO_2-SO_2 co-injection into a sandstone reservoir (with no initial calcite mineral) resulted in increase in porosity and permeability of the rock, as Ca^{2+} released (from severe dolomite dissolution) into the aqueous phase was not enough to precipitate significant amount of anhydrite; while in the study conducted by Aminu et al. (2018), CO_2-SO_2 co-injection into a sandstone reservoir (with initial calcite content < 0.5 wt.%) resulted in a decrease in the permeability of the rock. Also, comparing the impact of CO_2-SO_2 on different caprock samples (anhydrite-rich and carbonate-rich), permeability increased in caprock samples with higher ratio of initial carbonate mineral

concentration to anhydrite content, due to the carbonate dissolution. According to the study conducted by Bolourinejad and Herber (2014), in the case of CO_2 co-injection with H_2S, permeability decreased in the sandstone reservoir and caprock (anhydrite-rich and carbonate-rich) after 17 days of sequestration, and increased after 30 days of sequestration. The decrease in permeability after 17 days was attributed to the significant precipitation of halite which dominated the dissolution of feldspar and carbonate minerals, while the increase in permeability after 30 days was attributed to the severe dissolution of feldspar and carbonate minerals which dominated the precipitation of halite in the rock samples.

So far, previous studies have evaluated the impact of impurities on rock core samples experimentally, and numerical simulations performed in previous studies did not consider the diffusion and convective reactive transport of impurities from a reservoir to a caprock. CO_2 (with or without the addition of impurities) does not only accumulate in the reservoir, but some amount of the CO_2 (with some fraction of the impurities) migrate into and reach some layers of the caprock. So, some fraction of the gas impurities might be distributed in varying amounts in the reservoir and caprock, while some fraction of the impurities dissolve in the formation water. A study that attempted to implement the reactive transport mechanism described, was conducted by Ma et al. (2019). They developed a vertical one-dimensional (1D) model of a sandstone reservoir overlain by the mudstone (shale) caprock to investigate the impact of CO_2-brine-rock interaction on the permeability of a mudstone. However, they did not consider the impact of impurities co-injected with CO_2 on the properties of the formations, as their study was based on the injection of pure CO_2. Also, the complex mechanism of reactive fluid transport from the reservoir to caprock cannot be visualised in a 1D model, as reactions in different part of the reservoir and caprock are different, depending on the ionic composition of the aqueous phase in that region, as CO_2 and/or co-injected impurities dissolve in the formation water. Nevertheless, another study was conducted by Wang et al. (2021) to simulate the potential for uranium release under geologic CO_2 storage condition based on a three-dimensional (3-D) flow model in a cartesian coordinate. In their study, the CO_2 storage reservoir is overlain by a caprock, and the caprock is overlain by a shallow ground water formation. Co-injection of CO_2 with an impurity or impurities was not considered in the study; the uranium release was expected from geochemical reactions between the rock minerals (mainly uranite) and aqueous species in the formations. Also, the impact of CO_2 geosequestration on the porosity and permeability of the formations were not evaluated by Wang et al. (2021).

Therefore, in the present study, two-dimensional radial flow model will be developed for proper visualisation of the changes in porosity, permeability, and mineralogical compositions of the

formations (sandstone and carbonate reservoirs, and a shale caprock) during CO_2 geosequestration (with or without the addition of SO_2 or H_2S impurity). Also, the impact of temperature on a shale caprock and a calcite-dominant carbonate reservoir properties during CO_2 (with or without the addition of SO_2) geosequestration will be investigated in the present study. SO_2 gas impurity has been selected to evaluate the impact of temperature on the calcite-dominant carbonate reservoir as mineral trapping of SO_2 is expected to be high in such reservoir, possibly leading to the formation of anhydrite, whereas mineral trapping of H_2S in the reservoir is expected to be very little due to little or no Fe-bearing mineral in the reservoir (Zhang et al., 2011).

The impact of CO_2-brine-rock interaction on porosity, permeability, and mineralogical composition of rocks during cyclic approach of CO_2 geosequestration is similar to the non-cyclic approach. However, during cyclic CO_2-brine injection, reduced injectivity might be experienced in a reservoir with low permeability or susceptible to formation damage, although the level of damage could stabilise after several cycles of injection (Saeedi et al., 2011). Also during cyclic CO_2-brine injection, residual trapping of CO_2 increases, and could result in reduction in effective permeability (or effective porosity) of the reservoir, thereby limiting flow and injectivity (Edlmann et al., 2019). However, the increase in residual trapping results in increase in the storage security of CO_2 as the buoyant gas phase is reduced (Edlmann et al., 2019; Ahn et al., 2020). Although some studies have found an increase in porosity of rocks during cyclic CO_2 injection (Elwegaa et al., 2019; Su et al., 2020); after several cycles of CO_2 injection the effective porosity of the rock sample could decrease, as dissolved CO_2 reacts with rock minerals and form precipitates that block some pores (Badrouchi et al., 2022). So, the change in effective porosity and permeability during cyclic CO_2 injection might be different in different regions in the same reservoir. Therefore, it is better to visualise the changes in the rock properties during cyclic CO_2 geosequestration by developing a 2D radial flow model (applied in the present study) instead of relying on a 1D vertical flow model, and evaluate the impact of impurities in a CO_2 gas stream on the rock properties.

Several studies on the cyclic approach of CO_2 geosequestration have been based on CO_2 injection as drainage-imbibition process in which case CO_2 is injected followed by water, from the same end of the rock sample and similar to water alternating gas approach of enhanced oil recovery; or periodic injection of CO_2, and observing its impact in the reservoir. The cyclic injection-withdrawal of CO_2 during the geosequestration period in this study is different from the common drainage-imbibition technique adopted in other studies. In the present study, a novel approach of cyclic CO_2 geosequestration (with or without the addition of H_2S or SO_2 impurity) was developed to promote CO_2 utilization and storage by injecting CO_2 at the bottom of the well in a

reservoir and producing CO_2 from the top part of the reservoir using the same well for both operations, to save cost and produce a purer form of CO_2. The proposed technology could be replicated on a laboratory scale by injecting CO_2 from one end of a water-saturated rock sample, followed by the injection of water from the other end of the rock sample [after the CO_2 injection period], making a cycle. This cycle can be repeated and therefore referred to as cyclic injection-withdrawal of CO_2 in the present study. This technology can be applied to several wells in the same reservoir, enabling the production of purer form of CO_2 (with minimal chance of producing large amount of brine together with the gas) as larger amount of gas is few meters away (laterally) from the injection zone and at the top part of the reservoir; while multiphase mixture of CO_2-brine is found farther away from the injection well with a thin layer at the top of the reservoir having relatively low amount of CO_2 gas. Therefore, producing CO_2 gas from the same well used for injection, would save cost and enhance the production of a purer form of CO_2 for the development of renewable resources or energy (CO_2 utilization for hydrogen and methanol production, as well as for heat and power generation).

Furthermore, previous studies have performed experiments and applied mathematical models to evaluate the impact of CO_2 on the brittleness of only shale rock samples (without any consideration for a sandstone or carbonate reservoir rock) during non-cyclic and cyclic CO_2 injection (Lyu et al., 2018, Elwegaa et al., 2019). Also, no study has been conducted to evaluate the impact of impurities in a CO_2 gas stream on the brittleness index of rocks (sandstone, carbonate, and shale). Moreover, previous studies have evaluated the brittleness index of a rock based on mechanical properties of the rock. A few studies that evaluated the brittleness index of rocks based on the mineralogical composition of rocks were based on weight fraction of the rock minerals (Kang et al., 2020), thereby limiting the evaluation of the brittleness index of rocks from numerical simulations, as some reactive transport geochemical modelling software (such as TOUGHREACT) output volume fraction (not weight fraction) of rock minerals. Lyu et al. (2018) conducted experiments and applied a damage constitutive model using the mechanical properties of shale rock samples before and after CO_2-brine-shale interactions. They found that the brittleness index of the shale rock samples decreased after CO_2 sequestration. Also, Elwegaa et al. (2019) evaluated the brittleness index of shale rock samples based on mechanical properties and mineralogical composition of the samples. They found that the brittleness index of one out of the four shale core samples (with similar mineralogical composition) tested decreased after cyclic (cyclic stress created by thermal shock) cold CO_2 injection, while the brittleness index of the remaining three shale core samples increased. The inconsistency in the brittleness index (of the shale rock samples, although the rock samples were subjected to different pressure conditions)

calculated by Elwegaa et al. (2019) and the need to determine brittleness index of rocks based on the volume fraction output from geochemical modelling software call for the derivation of a more robust mathematical model to determine the brittleness index of a shale caprock during CO_2 sequestration. The new mathematical model derived in the present study will be applied to determine the brittleness index of sandstone and carbonate reservoirs as well as shale caprocks during CO_2 (with or without the addition of impurities) geosequestration.

Previous studies have developed machine learning models to evaluate brine-rock interactions. Machine learning models have been applied in the prediction of coal wettability during CO_2 geosequestration (Ibrahim, 2022), prediction of CO_2 trapping index in saline formations (Thanh et al., 2022), and to establish statistical relationships between the geochemical properties of formation water and hydrocarbon storage in carbonate reservoirs (Yu et al., 2020). These studies have shown that water-rock interactions lead to mineral transformation, and the ionic composition of the formation fluid indicates the type of water-rock interactions (dolomitization, illitization, or dissolution) that have taken place (Yu et al., 2020). Therefore, the ionic composition of formation fluid depends on the mineralogical composition of the rock, as the rock minerals are in equilibrium with the formation fluid. Also, the geochemical composition of the formation fluid depends on the in situ temperature and pressure conditions of the formation (Ibrahim, 2022). As the brittleness index of rocks depend on the mineralogical compositions of the rocks, these parameters (formation fluid ionic composition and in situ temperature and pressure) might be related to the brittleness index of the rocks. Therefore, in the present study, machine learning models will be developed to predict the brittleness index of rocks based on their geochemical composition and in situ temperature and pressure conditions.

The gaps identified in the previous studies reviewed will be filled in the present study for the selection of best depleted petroleum reservoirs or aquifers and a suitable caprock lithology for CO_2 geosequestration, based on the changes in the porosity, permeability, and mineralogical composition of the rocks, as well as the brittleness index of the rocks. Thus, the present study will evaluate the impact of impurities in CO_2 gas streams on the porosity, permeability, mineralogical compositions, and brittleness index of reservoir and cap rocks during non-cyclic and cyclic CO_2 geosequestration, and further explore the application of machine learning in the evaluation of the brittleness index of reservoir and cap rocks during CO_2 geosequestration.

CHAPTER THREE

RESEARCH METHODOLOGY

3.1 Research Design

The research design involves mathematical modelling and numerical simulations. The present study developed mathematical models for evaluation of brittleness index of rocks. Numerical simulations were performed by adopting three strategies: Strategy 1, Strategy 2, and Strategy 3. Strategies 1 and 2 are non-cyclic approach of CO_2 geosequestration, while Strategy 3 is a model of cyclic injection-withdrawal technology during CO_2 geosequestration. Strategy 1 was designed to evaluate the migration of fluid (with or without the addition of a small amount of H_2S or SO_2) injected in a pure limestone reservoir (100% calcite) to an intermediate formation (impure limestone, vertically above the pure limestone reservoir) and shale caprock (vertically above the impure limestone formation). In addition, the impact of temperature on the petrophysical and geochemical properties, as well as the brittleness index of the formations were evaluated in Strategy 1. Strategy 2 was designed to compare the injected fluid flow from a sandstone reservoir to a shale caprock and the fluid flow from a carbonate reservoir to a shale caprock, due to their different mineralogical compositions. In addition, the impact of CO_2 or an impurity (H_2S or SO_2) co-injected with CO_2 on the petrophysical and geochemical properties, as well as the brittleness index of the formations were evaluated in Strategy 2. Strategy 3 was designed to implement cyclic injection and withdrawal of CO_2 (with or without some amount of H_2S or SO_2) in a sandstone formation overlain by a shale caprock. In addition, the impact of CO_2 or an impurity (H_2S or SO_2) co-injected with CO_2 on the petrophysical and geochemical properties, as well as the brittleness index of the formations were also evaluated in Strategy 3. A sandstone reservoir was selected in Strategy 3 to evaluate the potential of sand migration to production facilities during cyclic withdrawal of CO_2 from the reservoir. Finally, machine learning models were developed to evaluate the brittleness of reservoir and cap rocks using the geochemical composition of the formation fluid, and in-situ and operating conditions of the formations.

3.2 Governing Equations

Reactive transport in a porous medium result in the dissolution and/or precipitation of minerals under kinetic conditions or local equilibrium. Kinetic reactions of the minerals are based on rate law. Thus, the rate law relation is presented in this section. Also, new brittleness index models following the ratio of simple sum of brittle minerals to total minerals in rocks as well as brittleness

index with respect to their relative level of brittleness based on their bulk modulus, using the concept of weight (or mass) fraction of minerals, is presented in this section.

3.2.1 Kinetic rate law for mineral dissolution and precipitation

Generally, the rate expression applied in TOUGHREACT is taken from Lasaga et al. (1994) and expressed as:

$$r_n = \pm k_n A_n \left[1 - \left(\frac{Q_n}{K_n}\right)^{\theta}\right]^{\eta} \qquad 3.1$$

where k_n is the rate constant (in moles per unit mineral surface area and unit time) which is temperature-dependent, A_n denotes the specific reactive surface area per kilogram H_2O, Q_n is the reaction quotient, K_n is the equilibrium constant for the mineral-water written for the destruction of one mole of mineral n, and η represents kinetic mineral index. The parameters θ and η which are determined by experiments, are more often assumed to equal to one. Positive values of r_n indicate dissolution, while negative values indicate precipitation.

The kinetic rate constant (k) can be integrated or summed from three mechanisms for many minerals (Palandri and Kharaka, 2004) and expressed as:

$$k = k_{25}^{nu} exp\left[\frac{-E_a^{nu}}{R}\left(\frac{1}{T} - \frac{1}{298.15}\right)\right] + k_{25}^{H} exp\left[\frac{-E_a^{H}}{R}\left(\frac{1}{T} - \frac{1}{298.15}\right)\right] a_H^{n_H} + k_{25}^{OH} exp\left[\frac{-E_a^{OH}}{R}\left(\frac{1}{T} - \frac{1}{298.15}\right)\right] a_{OH}^{n_{OH}} \qquad 3.2$$

where superscripts or subscripts nu, H, and OH indicate neutral (neutral pH - pure H_2O), acid (H^+ catalysed), and base (OH^- catalysed) mechanisms, respectively; k_{25} is the rate constant at 25^0C, E_a is the activation energy, R is the gas constant, T is the absolute temperature, a is the activity of the species, and n is an exponent (constant).

The rate constant (k) can also be dependent on other species such as Al^{3+} and Fe^{3+}. In fact, two or more species might be involved in one mechanism. Thus, a general form species-dependent rate constants implemented in TOUGHREACT is expressed as:

$$k = k_{25}^{nu} exp\left[\frac{-E_a^{nu}}{R}\left(\frac{1}{T} - \frac{1}{298.15}\right)\right] + \sum_i k_{25}^{i} exp\left[\frac{-E_a^{i}}{R}\left(\frac{1}{T} - \frac{1}{298.15}\right)\right] \prod_j a_{ij}^{n_{ij}} \qquad 3.3$$

where superscripts or subscripts i represents the additional mechanism index, and j represents the species index involved in one mechanism that could be primary or secondary species.

3.2.2 Petrophysical properties and derived mineralogical brittleness index equations

Change in porosity of the rock is calculated based on mineral precipitation and/or dissolution, while change in permeability is calculated from Carman-Kozeny relation, using the following equations (Xu et al., 2006; Xu et al., 2014):

$$\emptyset = 1 - \sum_{m=1}^{nm} fr_m - fr_u \quad 3.4$$

$$k = k_0 \left(\frac{1-\emptyset_0}{1-\emptyset}\right)^2 \left(\frac{\emptyset}{\emptyset_0}\right)^3 \quad 3.5$$

where, ϕ and k represent current porosity and permeability, ϕ_0 and k_0 represent initial porosity and permeability, parameters fr_m and fr_u represent volume fraction of mineral m in the rock (volume of mineral to volume of the medium including porosity) and volume fraction of non-reactive mineral, respectively. So, the output volume fraction of each mineral is the volume of mineral divided by volume of medium including porosity (V_{frac}). Thus, the volume of each mineral divided by total volume of solid [part of the rock] is calculated as follows (Xu et al., 2014):

$$f_m = \frac{V_{frac}}{1-\emptyset_{med}} \quad 3.6$$

where ϕ_{med} represents [current] porosity of the medium, and f_m represents the volume of mineral per volume of [the solid part of] the rock.

Mass fraction of composite materials has been calculated to determine their mechanical properties (Ezema et al., 2015) using their densities and volume fractions. Therefore, it is possible to determine the mass fraction of minerals in a rock using similar approach. Mass fraction of each material that forms a composite structure is the mass of that material to the total mass of materials that form the structure. Similarly, mass fraction of each mineral that forms a rock is the mass of each [individual] mineral to the total mass of minerals that form the rock and can be expressed as follows:

$$Mass\ fraction\ of\ a\ mineral, x_i = \frac{mass\ of\ the\ mineral,}{total\ mass\ of\ minerals\ in\ the\ rock,} = \frac{m_i}{\sum_{i=1}^{nm} m_i} \quad 3.7$$

$$m = V\rho \quad 3.8$$

$$x_i = \frac{v_i \rho_i}{\sum_{i=1}^{nm} v_i \rho_i} \quad 3.9$$

where V and ρ represent volume and density of solid, respectively; v_i represents volume fraction of each mineral in the solid part of the rock (same as f_m in Equation 3.6). Density can be expressed as molecular weight divided by molar volume.

$$\rho = \frac{\bar{M}}{\bar{V}} \tag{3.10}$$

Thus, the mass fraction becomes:

$$x_i = \frac{\frac{v_i \bar{M}_i}{\bar{V}_i}}{\sum_{i=1}^{nm} \frac{v_i \bar{M}_i}{\bar{V}_i}} \tag{3.11}$$

where $\bar{M}$ and $\bar{V}$ represent molecular weight (g/mol) and molar volume (m^3/mol) of mineral. Hence, mineralogical brittleness index by simple sum of brittle minerals becomes:

$$BI = \frac{\sum_{j=1}^{nB} \frac{v_j \bar{M}_j}{\bar{V}_j}}{\sum_{i=1}^{nm} \frac{v_i \bar{M}_i}{\bar{V}_i}} \tag{3.12}$$

where j represents each brittle mineral in the rock, i represents any mineral in the rock, and nB represents the number of brittle minerals in the rock.

To simplify the derived brittleness index equation, the same molar volume can be assumed for all minerals, depending on the mineralogical composition of the rock. However, some clay minerals such as smectite-Ca, smectite-Na, illite, and kaolinite may have larger mineral surface areas (Fatah et al., 2022) and significantly different molar volumes. Assuming equal molar volume of minerals, the brittleness index in terms of the simple sum of brittle minerals in a rock can be expressed as:

$$BI_8 = \frac{\sum_{j=1}^{nB} v_j \bar{M}_j}{\sum_{i=1}^{nm} v_i \bar{M}_i} \tag{3.13}$$

Brittle minerals considered in this study are quartz, feldspar (as albite, k-feldspar, oligoclase, orthoclase, and anorthite), calcite, dolomite, pyrite, and mica (as muscovite). Their relative level of brittleness among themselves (brittle minerals) is not considered in the simple sum of brittle minerals approach given above. Thus, to consider their relative level of brittleness, the bulk modulus (Table 3.1) of the brittle minerals was incorporated into the equation using weighting coefficients (Table 3.2) following the mineralogical brittleness index developed by Kang et al. (2020). The bulk modulus of a mineral is associated to the relative fractional change in the volume of the mineral with increase in pressure (Kang et al., 2020). In other words, bulk modulus

represents the ratio of increase in pressure to the relative fractional change in the volume of a material. Therefore, the bulk modulus of minerals can be assessed under the same amount of pressure, by noting the corresponding fractional change in the volume of each mineral. The higher the absolute bulk modulus, the less brittle (and more ductile) the material, and vice versa.

Table 3.1: Bulk modulus of different brittle minerals (Fjaer et al., 2008).

Brittle mineral	Quartz	Feldspar	Calcite	Dolomite
Bulk modulus (GPa)	37.5	76	74	76-95

Table 3.2: Weighting coefficients of different brittle minerals (Kang et al., 2020).

Brittle mineral	Quartz	Feldspar	Calcite	Dolomite
Weighting coefficient	1	0.49	0.51	0.39-0.49/0.44

The mineralogical brittleness index, considering the bulk modulus of minerals, developed by Kang et al. (2020) is given as:

$$BI_{BMod} = \frac{W_Q + 0.49W_F + 0.51W_C + 0.44W_D}{W_T} \quad 3.14$$

where W_Q, W_F, W_C, and W_D represent the weights of quartz, feldspar, calcite, and dolomite, respectively; W_T represents the total mineral weight. The brittleness index in this case considers only quartz (Q), feldspar (F), calcite (C), and dolomite (D) as brittle minerals, assuming the level of brittleness of pyrite and mica is negligible compared to other brittle minerals. Equation 3.14 suggests that quartz is more brittle (lower bulk modulus) than the other brittle minerals. Thus, in the present study, the brittleness index becomes:

$$BI_{bm} = \frac{\frac{v_Q\bar{M}_Q}{\bar{V}_Q} + \frac{0.49v_F\bar{M}_F}{\bar{V}_F} + \frac{0.51v_C\bar{M}_C}{\bar{V}_C} + \frac{0.44v_D\bar{M}_D}{\bar{V}_D}}{\sum_{i=1}^{nm}\frac{v_i\bar{M}_i}{\bar{V}_i}} \quad 3.15$$

So, assuming the same molar volume of minerals in this present study, the brittleness index can be expressed as:

$$BI_9 = \frac{v_Q\bar{M}_Q + 0.49v_F\bar{M}_F + 0.51v_C\bar{M}_C + 0.44v_D\bar{M}_D}{\sum_{i=1}^{nm} v_i\bar{M}_i} \quad 3.16$$

The models developed in the present study extend the application of the brittleness index model based on the simple sum of the fraction of brittle minerals in a rock and the brittleness index model based on the brittleness level of the brittle minerals developed by Kang et al. (2020). Unlike the previous models which are based on the weight or weight fraction of the rock minerals, the models

derived in the present study, for the first time, would enable the determination of the brittleness index of rocks based on their volume fraction, molecular weight, and molar volume. So, in the present study, the derived brittleness index model (BI_{bm}, based on the relative level of brittleness of the brittle minerals) was applied to evaluate the mineralogical brittleness index of the formations before and after CO_2 geosequestration.

3.3 Numerical Approach

3.3.1 Numerical tool

This study employed the non-isothermal multiphase reactive geochemical transport code, TOUGHREACT (Xu et al., 2006). TOUGHREACT (ECO2N module) was developed by incorporating reactive chemistry into the heat and multiphase fluid flow code, TOUGH2 (Pruess, 2004). TOUGHREACT (ECO2N module) can be utilized in modelling the injection of CO_2 in saline formations (including aquifers or depleted petroleum reservoirs) and can take into consideration the presence of additional gaseous species that could be co-injected with CO_2, such as H_2S and SO_2.

The numerical solution of chemical transport and fluid flow is based on an integral finite difference (IFD) method of space discretization (Narasimhan and Whiterspoon, 1976). The IFD method is flexible for the discretization of geologic media, as it can be adapted for irregular and regular grids. Thus, it is possible to simulate flow, transport, and fluid-rock interaction in homogeneous or heterogeneous rock systems with similar or varying petrology (Zhang et al., 2011). TOUGHREACT provides an implicit time-weighing scheme used for the flow, transport, and kinetic geochemical equations, and uses a sequential iteration approach similar to the model demonstration by Yeh and Tripathi (1991). Thus, after solving the flow equations, the velocities and saturations of the aqueous phase are utilized for aqueous chemical transport simulation. Then, on a component basis, the chemical transport is solved (Zhang et al., 2011). The concentration obtained from the transport as well as CO_2 and/or H_2S/SO_2 gas pressures in the multiphase flow calculation is substituted into the chemical reaction model. On a grid-block basis, the system of chemical reaction equations is solved by Newton-Raphson iteration. During mineral dissolution and/or precipitation, the porosity and permeability of the porous medium change, thereby modifying the fluid flow. Thus, feedback between flow and chemistry is considered in this model. The changes in porosity are calculated from rock volume changes due to mineral dissolution and/or precipitation. Then permeability changes are then evaluated using a selected

model that describes the porosity-permeability relationship. In the present study, the Kozeny-Carman porosity-permeability model was used.

3.3.2 Model setup

In this study, a simple two-dimensional (2-D) radial well model was adopted. The 2-D model is a vertically heterogeneous formation of 40 m thickness and a cylindrical geometrical configuration (Figure 3.1). In the vertical direction, the model domain is discretized into 20 layers with a 2 m constant spacing (Δz). TOUGHREACT is able to handle such thick spacing effectively (Zhang et al., 2011; Ma et al., 2019; Wang et al., 2021). The top and bottom model boundaries are closed to flow (no-flow boundaries). The top model layers represent a shale caprock, while the remaining model layers at the bottom represent reservoir rock(s). The model layers for each strategy (Strategies 1, 2, and 3) are shown in Tables 3.3 and 3.4, respectively.

Table 3.3: Mesh generation of the model (Strategy 1).

Rock formation	Vertical mesh number	Mesh thickness (m)
Shale caprock	3	2.0
Impure limestone (potential caprock)	3	2.0
Pure limestone (carbonate reservoir)	14	2.0

Table 3.4: Mesh generation of the model (Strategies 2 and 3).

Rock formation	Vertical mesh number	Mesh thickness (m)
Shale caprock	6	2.0
Carbonate or sandstone reservoir	14	2.0

In Strategy 1, three different formations with different properties were evaluated, and the reservoir where CO_2 was injected into is the pure limestone. Hence, the number of reservoir vertical layers in the pure limestone (Strategy 1) and the reservoirs in Strategy 2 and Strategy 3 are the same. The higher number of vertical layers in the reservoir compared to the caprock, would help delay the migration of the injected fluid to the caprock and to properly visualise the fluid distributions from the point of injection to the caprock. In Strategy 1, shale and impure limestone (carbonate) were examined as cap rocks, while pure limestone (carbonate) was examined as a reservoir formation. The evaluation of the shale and impure limestone as cap rocks would help identify a better lithology for a caprock based on their initial properties and changes in their properties during CO_2 geosequestration. In Strategy 2, carbonate (initially made up of calcite and dolomite minerals only) and sandstone formations are examined as reservoirs, and shale formation as caprock. In other words, in Strategy 2, some of the numerical simulations were performed having the

carbonate reservoir overlain by the shale caprock, while other simulations were performed having the sandstone reservoir overlain by the shale caprock. So, the carbonate reservoir-shale caprock simulations and the sandstone reservoir-shale caprock simulations were performed separately in Strategy 2. The carbonate and sandstone formations were not placed next to each in the same numerical simulations. In Strategy 3, the sandstone formation was examined as a reservoir, while the shale formation was examine as the caprock. In the horizontal direction, a 100 km radial distance was modelled with a radial grid spacing increasing logarithmically from the injection well. A total of 56 radial grid elements were generated. A large volume of 10^{30} m^3 is assigned to the outer grid element to represent an infinitive lateral boundary (a constant hydrostatic pressure boundary). CO_2 only (also referred to as CO_2 alone, in this study) or impure CO_2 (containing H_2S or SO_2) injection was applied at the bottom portion of the well in the reservoir. The thickness of the injection portion is 8 m, as shown in Figures 3.1 and 3.2.

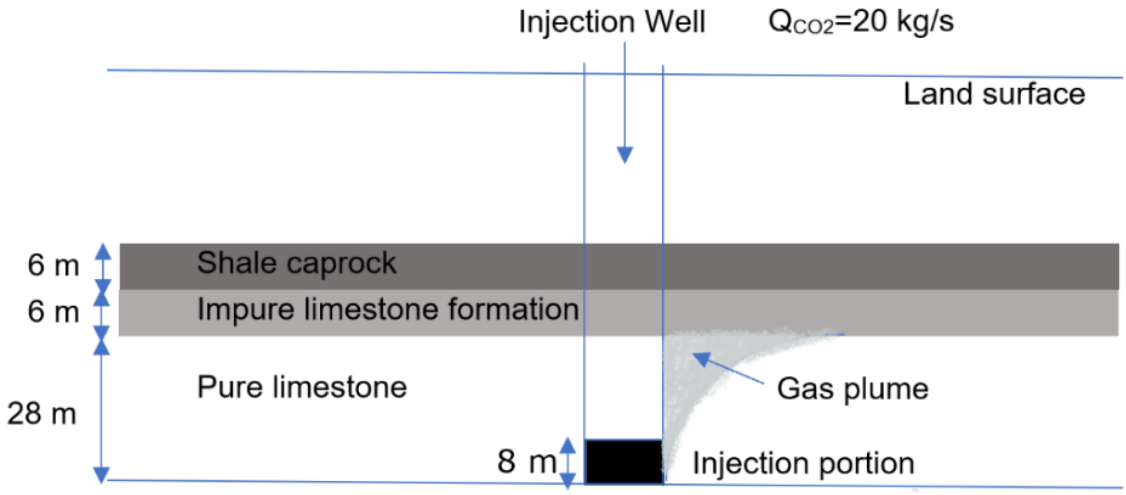

Figure 3.1: Strategy 1 - Schematic representation of the 2-D radial flow model for the geosequestration of CO_2 in a carbonate formation (Modified from Zhang et al., 2011).

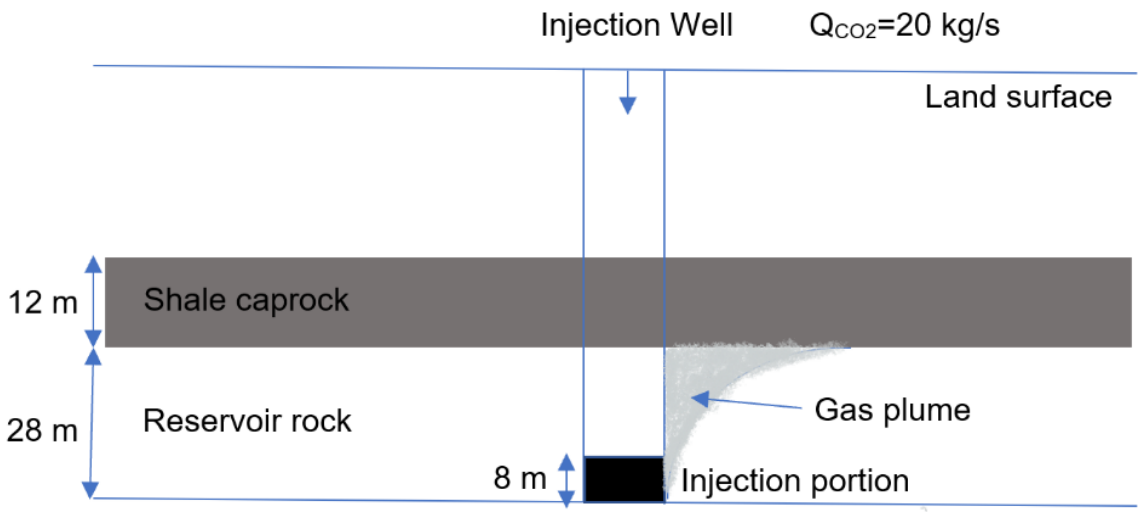

Figure 3.2: Strategy 2 – Schematic representation of the 2-D radial flow model for the geosequestration of CO_2 in a reservoir (Modified from Zhang et al., 2011).

Similarly, the cyclic injection of CO_2 in reservoirs (Strategy 3) is illustrated in Figure 3.3. CO_2 is injected at the bottom of the well, and produced (or withdrawn) at the upper part of the well in the same reservoir (close to the caprock zone), to produce relatively pure CO_2 gas and limit the production of aqueous-phase fluid. The thickness of the injection portion is 8 m, while the thickness of the production portion is 6 m as shown in Figure 3.3.

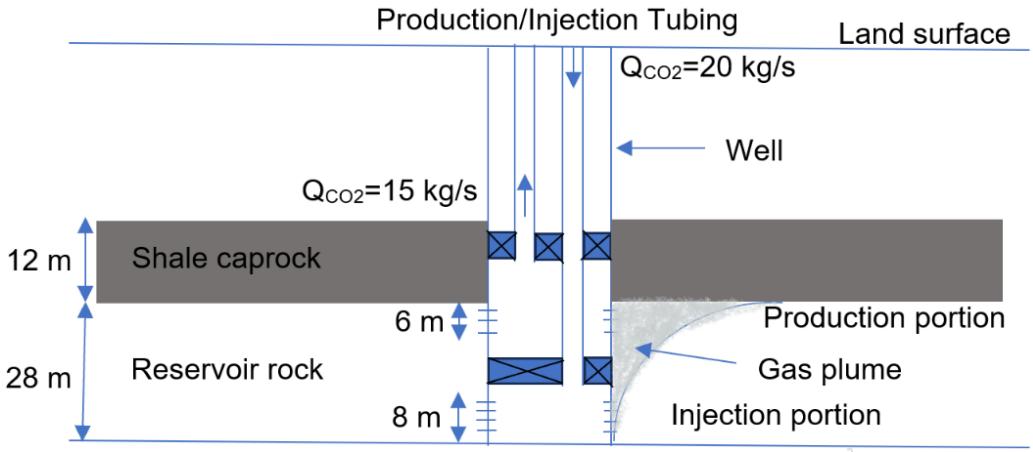

Figure 3.3: Strategy 3 – Schematic representation of the 2-D radial flow model for cyclic injection-withdrawal of CO_2.

In Strategy 1, two simulation conditions were considered: injection into a high saline (salinity up to 0.21) formation at a pressure and temperature of 13.7 MPa (137 bar) and 100^{0}C, respectively; and injection into a low saline (salinity up to 0.06) formation at a pressure and temperature of 10 MPa (100 bar) and 40^{0}C (low-temperature condition), respectively. Injection of acid gases into the high saline reservoir was carried out for a period of 90 days [in order to compare with an

experiment conducted by AL-Ameri et al. (2016) over that same period], using a CO_2 injection rate of 20 kg/s (with or without a gas impurity) and with 0.025-mole fraction of H_2S or SO_2 (for the co-injection cases); while injection of acid gases into the low saline reservoir was applied for a period of 10 years, using a CO_2 injection rate of 20 kg/s (with or without a gas impurity) and with 0.025-mole fraction of H_2S or SO_2 (for the co-injection cases). The mole fraction of 0.025 for H_2S and SO_2 was selected as it is within the range of CO_2 co-capture from Pet Coke (SNC-Lavalin Inc., 2004). Similarly, in Strategy 2, CO_2 is injected into the low salinity reservoir for a period of 10 years, at an injection rate of 20 kg/s (with or without a gas impurity) and with 0.025-mole fraction of H_2S or SO_2 (for the co-injection cases). The simulation of fluid flow and geochemical transport was run for a period of 100 years (Strategies 1 and 2), which is a reasonable time scale for geosequestration of CO_2 (Spycher et al., 2019; Wang et al., 2021). It is worth noting that in the case of CO_2 co-injection with H_2S in the high saline formation, simulation was run only over the injection period (90 days) only, as the simulation did not progress beyond that period, possibly the high salinity and the reservoir temperature and pressure conditions were unfavourable for H_2S co-injection. Meanwhile, the injection profile of CO_2 in Strategy 3 is quite different.

The CO_2 injection-withdrawal profile (Strategy 3) is shown in Figure 3.4 and Appendix A1. The injection-withdrawal process was completed over seven (7) cycles. For each cycle, CO_2 gas (with or without H_2S/SO_2 gas) is injected into the reservoir at the rate of 20 kg/s (at the 8 m injection portion/zone) over a period of 10 years, and injection is stopped for 3 months (0.25 year), then CO_2 is withdrawn from the reservoir at the rate of 15 kg/s (at the 6 m production portion/zone) over a period of 2 years and withdrawal is stopped for 3 months before the next cycle commences. The longer period of production compared to the shut-in time is based on field applications of cyclic gas injection in reservoirs (Reeves, 2001). Figure 3.4 shows that during injection, fluid is added to the reservoir (injection rate is positive); during the shut-in period, no fluid is added to or removed from the reservoir from the well (injection rate is zero); while during production fluid is removed from the reservoir and withdrawn through the well (injection rate is negative). The hydrogeological parameters used in this study are shown in Tables 3.5, 3.6, and 3.7.

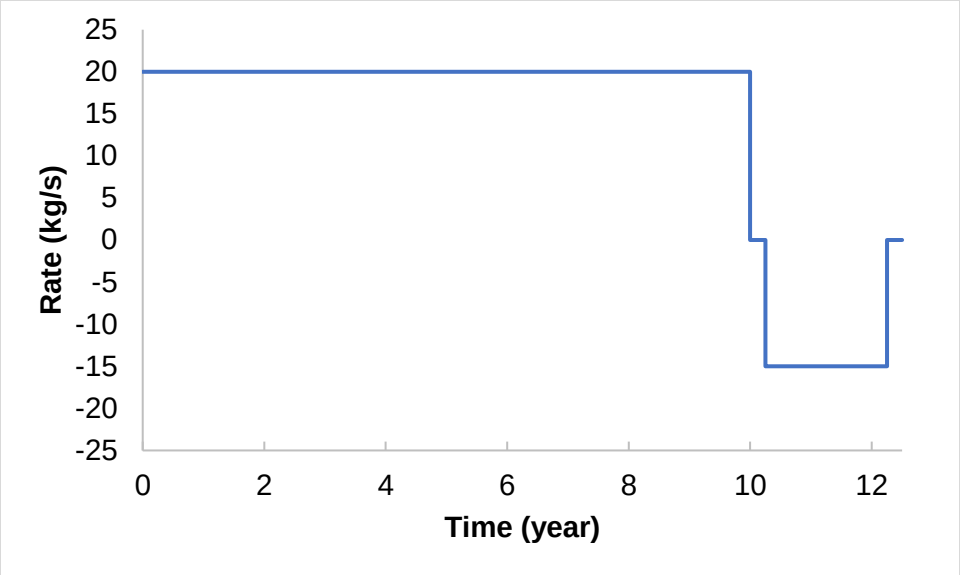

Figure 3.4: Strategy 3 – CO_2 injection-withdrawal profile.

Table 3.5: Hydrogeological parameters used in the simulation at formation temperature and pressure of 100^{0}C and 137 bar (Strategy 1), respectively (Modified from Zhang et al., 2011, AL-Ameri et al., 2016, and Ma et al., 2019).

Parameters	**Formation**		
	Pure limestone	**Impure limestone**	**Shale caprock**
Porosity	0.26	0.26	0.07
Horizontal permeability (m^2)	$2.264x10^{-12}$	$2.264x10^{-12}$	$2.264x10^{-17}$
Vertical permeability (m^2)	$2.264x10^{-13}$	$2.264x10^{-13}$	$2.264x10^{-18}$
Pore compressibility (Pa^{-1})	$2.10x10^{-9}$	$2.10x10^{-9}$	$2.10x10^{-9}$
Rock grain density (kg/m^3)	2600	2600	2600
Formation heat conductivity (W/m ^{0}C)	2.51	2.51	2.51
Rock grain specific heat (J/kg ^{0}C)	920.0	920.0	920.0
Temperature (^{0}C)	100.0	100.0	100.0
Salinity (mass fraction)	0.21	0.21	0.21
Pressure (bar)	137	137	137
Molecular diffusion coefficient of gas species (m^2/s)	$1.1x10^{-5}$	$1.1x10^{-5}$	$1.1x10^{-5}$
Gas saturation	0.00	0.00	0.00
CO_2 injection rate (kg/s)	20.0	-	-
Relative permeability Liquid: Van Genuchten function $k_{rl} = \sqrt{S^*}\left\{1-\left(1-[S^*]^{1/m}\right)^m\right\}^2$ S_{lr}: residual water saturation m: exponent Gas: Corey $k_{rg} = (1-\hat{S})^2(1-\hat{S}^2)$ S_{gr}: residual gas saturation	$S^* = (S_l - S_{lr})/(1-S_{lr})$ $S_{lr} = 0.30$ $m = 0.457$ $\hat{S} = (S_l - S_{lr})/(1-S_{lr}-S_{gr})$ $S_{gr} = 0.05$		
Capillary pressure Van Genuchten function $P_{cap} = -P_0\left([S^*]^{-1/m}-1\right)^{1-m}$ S_{lr}: residual water saturation m: exponent	$S^* = (S_l - S_{lr})/(1-S_{lr})$ $S_{lr} = 0.03$ $m = 0.457$		
P_0: strength coefficient	19.61 kPa	19.61 kPa	19.61 kPa

In Strategy 1, the initial porosity and permeability of the impure limestone were higher for the high salinity condition compared to the low salinity condition, to enable the injected fluid reach the shale caprock as self-sealing potential of rocks might be higher at high salinity conditions. This is because salt minerals might precipitate during the CO_2 geosequestration and block some pores in the formations. Also, in Strategy 1, the higher initial porosity and permeability of the impure limestone (potential caprock) compared to the shale caprock was to enable the injected fluid reach the shale caprock. A similar technique has been applied by Wang et al. (2021), where they increased initial porosity and permeability in some regions of a caprock to enhance the migration of CO_2 from the reservoir into the layer above the caprock. Overall, the goal of using the different porosities and permeabilities of the pure limestone reservoir, impure limestone, and shale caprock during the numerical simulations was to ensure that the injected fluid reached the shale caprock.

Table 3.6: Hydrogeological parameters used in the simulation at formation temperature and pressure of 40^0C and 100 bar (Strategy 1), respectively (Modified from Zhang et al., 2011, AL-Ameri et al., 2016, and Ma et al., 2019).

Parameters	**Formation**		
	Pure limestone	**Impure limestone**	**Shale caprock**
Porosity	0.34	0.20	0.07
Horizontal permeability (m^2)	$2.264x10^{-12}$	$2.264x10^{-13}$	$2.264x10^{-16}$
Vertical permeability (m^2)	$2.264x10^{-13}$	$2.264x10^{-14}$	$2.264x10^{-17}$
Pore compressibility (Pa^{-1})	$2.10x10^{-9}$	$2.10x10^{-9}$	$2.10x10^{-9}$
Rock grain density (kg/m^3)	2600	2600	2600
Formation heat conductivity (W/m ^{0}C)	2.51	2.51	2.51
Rock grain specific heat (J/kg ^{0}C)	920.0	920.0	920.0
Temperature (^{0}C)	40.0	40.0	40.0
Salinity (mass fraction)	0.06	0.06	0.06
Pressure (bar)	100	100	100
Molecular diffusion coefficient of gas species (m^2/s)	$1.1x10^{-5}$	$1.1x10^{-5}$	$1.1x10^{-5}$
Gas saturation	0.00	0.00	0.00
CO_2 injection rate (kg/s)	20.0	-	-
Relative permeability Liquid: Van Genuchten function $k_{rl} = \sqrt{S^*}\left\{1-\left(1-[S^*]^{1/m}\right)^m\right\}^2$ S_{lr}: residual water saturation m: exponent Gas: Corey $k_{rg} = (1-\hat{S})^2(1-\hat{S}^2)$ S_{gr}: residual gas saturation	$S^* = (S_l - S_{lr})/(1-S_{lr})$ $S_{lr} = 0.30$ $m = 0.457$ $\hat{S} = (S_l - S_{lr})/(1-S_{lr}-S_{gr})$ $S_{gr} = 0.05$		
Capillary pressure Van Genuchten function $P_{cap} = -P_0\left([S^*]^{-1/m}-1\right)^{1-m}$ S_{lr}: residual water saturation m: exponent	$S^* = (S_l - S_{lr})/(1-S_{lr})$ $S_{lr} = 0.03$ $m = 0.457$		
P_0: strength coefficient	19.61 kPa	19.61 kPa	19.61 kPa

Table 3.7: Hydrogeological parameters used in the simulation at formation temperature and pressure of 40^0C and 100 bar (Strategies 2 and 3), respectively (Modified from Zhang et al., 2011 and Ma et al., 2019).

Parameters	**Formation**		
	Carbonate	**Sandstone**	**Shale caprock**
Porosity	0.34	0.34	0.07
Horizontal permeability (m^2)	$2.264x10^{-12}$	$2.264x10^{-12}$	$2.264x10^{-16}$
Vertical permeability (m^2)	$2.264x10^{-13}$	$2.264x10^{-13}$	$2.264x10^{-17}$
Pore compressibility (Pa^{-1})	$2.10x10^{-9}$	$2.10x10^{-9}$	$2.10x10^{-9}$
Rock grain density (kg/m^3)	2600	2600	2600
Formation heat conductivity (W/m ^{0}C)	2.51	2.51	2.51
Rock grain specific heat (J/kg ^{0}C)	920.0	920.0	920.0
Temperature (^{0}C)	40.0	40.0	40.0
Salinity (mass fraction)	0.06	0.06	0.06
Pressure (bar)	100	100	100
Molecular diffusion coefficient of gas species (m^2/s)	$1.1x10^{-9}$	$1.1x10^{-9}$	$1.1x10^{-9}$
Gas saturation	0.00	0.00	0.00
CO_2 injection rate (kg/s)	20.0	20.0	-
CO_2 withdrawal rate (kg/s) – Strategy 3 only	-	15.0	-
Relative permeability Liquid: Van Genuchten function $k_{rl} = \sqrt{S^*}\left\{1-\left(1-[S^*]^{1/m}\right)^m\right\}^2$ S_{lr}: residual water saturation m: exponent Gas: Corey $k_{rg} = (1-\hat{S})^2(1-\hat{S}^2)$ S_{gr}: residual gas saturation	$S^* = (S_l - S_{lr})/(1-S_{lr})$ $S_{lr} = 0.30$ $m = 0.457$ $\hat{S} = (S_l - S_{lr})/(1-S_{lr}-S_{gr})$ $S_{gr} = 0.05$		
Capillary pressure Van Genuchten function $P_{cap} = -P_0\left([S^*]^{-1/m}-1\right)^{1-m}$ S_{lr}: residual water saturation m: exponent	$S^* = (S_l - S_{lr})/(1-S_{lr})$ $S_{lr} = 0.03$ $m = 0.457$		
P_0: strength coefficient	19.61 kPa	19.61 kPa	19.61 kPa

Different types of initial mineralogical compositions were used. In Strategy 1, the mineralogical composition of the carbonate (pure limestone) formation was from a study conducted by AL-Ameri et al. (2016); the carbonate (impure limestone) formation was modified to account for the impact of minor minerals in carbonate rocks; while the shale formation was modified from a study conducted by Ma et al. (2019). In Strategy 2, the mineralogical compositions of the sandstone and carbonate formations were obtained from a study conducted by Zhang et al. (2011), while the shale formation was modified from the study conducted by Ma et al. (2019). In Strategy 3, the mineralogical compositions of the sandstone reservoir was obtained by Zhang et al. (2011), while the shale formation was modified from the study conducted by Ma et al. (2019). The molar volumes of the minerals were obtained from Robie et al. (1967) and Wang et al. (2021), except the molar volumes of dawsonite, smectite-Ca and ankerite that were assumed. The molar volume of dawsonite was obtained from Marini (2007); the molar volume of smectite-Ca was estimated within the range of density of Smectites (2.6 g/cm^3) (Deer et al., 1966; Totten et al., 2002), while the molar volume of ankerite was estimated using a density of 2.97 g/cm^3 (Shafiq et al., 2022).

The mineralogical compositions used in Strategies 1, 2 and 3 are shown in Tables 3.8 and 3.9, respectively.

Table 3.8: Initial mineral volume fractions and possible secondary minerals used in the simulations (Strategy 1).

Mineral name	Chemical formula	Molecular weight (g/mol)	Molar volume (cm^3/mol)	Pure Limestone (volume percent of solid)	Impure Limestone (volume percent of solid)	Shale Caprock (volume percent of solid)
Illite	$K_{0.6}Mg_{0.25}Al_{1.8}(Al_{0.5}Si_{3.5}O_{10})(OH)_2$	383.899	138.900	0	0.01	65.30
Kaolinite	$Al_2Si_2O_5(OH)_4$	258.159	99.520	0	0.01	1.11
Smectite-Ca	$Ca_{0.145}Mg_{0.26}Al_{1.77}Si_{3.97}O_{10}(OH)_2$	365.394	140.536	0	0.01	6.90
Chlorite	$Mg_{2.5}Fe_{2.5}Al_2Si_3O_{10}(OH)_8$	634.648	210.260	0	0.01	6.40
Quartz	SiO_2	60.084	22.688	0	0.01	8.00
K-feldspar	$KAlSi_3O_8$	278.33	108.900	0	0.01	2.80
Albite	$NaAlSi_3O_8$	262.222	100.070	0	0.01	3.20
Calcite	$CaCO_3$	100.087	36.934	100.00	99.91	0.83
Pyrite	FeS_2	119.98	23.940	0	0.01	0.40
Dolomite	$CaMg(CO_3)_2$	184.401	64.341	0	0.01	5.00
Anhydrite	$CaSO_4$	136.142	45.940	0	0	0
Alunite	$KAl_3(OH)_6(SO_4)_2$	414.214	146.800	0	0	0
Ankerite	$CaMg_{0.3}Fe_{0.7}(CO_3)_2$	206.48	69.522	0	0	0
Dawsonite	$NaAlCO_3(OH)_2$	143.995	58.520	0	0	0
Magnesite	$MgCO_3$	84.314	28.018	0	0	0
Siderite	$FeCO_3$	115.856	29.378	0	0	0
Smectite-Na	$Na_{0.290}Mg_{0.26}Al_{1.77}Si_{3.97}O_{10}(OH)_2$	366.25	132.510	0	0	0
Hematite	Fe_2O_3	159.692	30.274	0	0	0
Anorthite	$CaAl_2Si_2O_8$	278.206	100.790	0	0	0
Muscovite	$KAl_2(AlSi_3O_{10})(F,OH)_2$	398.306	140.710	0	0	0
Oligoclase	$CaNa_4Al_6Si_{14}O_{40}$	1327.094	502.480	0	0	0

Table 3.9: Initial mineral volume fractions and possible secondary minerals used in the simulations (Strategies 2 and 3).

Mineral name	Chemical formula	Molecular weight (g/mol)	Molar volume (cm^3/mol)	Carbonate formation (volume percent of solid)	Sandstone formation (volume percent of solid)	Shale Caprock (volume percent of solid)
Illite	$K_{0.6}Mg_{0.25}Al_{1.8}(Al_{0.5}Si_{3.5}O_{10})(OH)_2$	383.899	138.900	0	2.80	65.30
Kaolinite	$Al_2Si_2O_5(OH)_4$	258.159	99.520	0	0.90	1.11
Smectite-Ca	$Ca_{0.145}Mg_{0.26}Al_{1.77}Si_{3.97}O_{10}(OH)_2$	365.394	140.536	0	0	6.96
Chlorite	$Mg_{2.5}Fe_{2.5}Al_2Si_3O_{10}(OH)_8$	634.648	210.260	0	2.70	6.40
Quartz	SiO_2	60.084	22.688	0	25.80	8.00
K-feldspar	$KAlSi_3O_8$	278.33	108.900	0	23.30	2.80
Albite	$NaAlSi_3O_8$	262.222	100.070	0	41.50	3.20
Calcite	$CaCO_3$	100.087	36.934	40.00	3.00	0.80
Pyrite	FeS_2	119.98	23.940	0	0	1.43
Dolomite	$CaMg(CO_3)_2$	184.401	64.341	60.00	0	0
Anhydrite	$CaSO_4$	136.142	45.940	0	0	4.00
Siderite	$FeCO_3$	115.856	146.800	0	0	0
Alunite	$KAl_3(OH)_6(SO_4)_2$	414.214	69.522	0	0	0
Ankerite	$CaMg_{0.3}Fe_{0.7}(CO_3)_2$	206.48	58.520	0	0	0
Dawsonite	$NaAlCO_3(OH)_2$	143.995	28.018	0	0	0
Magnesite	$MgCO_3$	84.314	29.378	0	0	0
Smectite-Na	$Na_{0.290}Mg_{0.26}Al_{1.77}Si_{3.97}O_{10}(OH)_2$	366.25	132.510	0	0	0
Hematite	Fe_2O_3	159.692	30.274	0	0	0
Anorthite	$CaAl_2Si_2O_8$	278.206	100.790	0	0	0
Muscovite	$KAl_2(AlSi_3O_{10})(F,OH)_2$	398.306	140.710	0	0	0
Oligoclase	$CaNa_4Al_6Si_{14}O_{40}$	1327.094	502.480	0	0	0

Before the simulation of reactive transport, a batch geochemical modelling of water-rock interaction was performed to obtain an aqueous-phase chemical composition similar to the composition of a typical formation brine. So, synthetic brine formulated by AL-Ameri et al. (2016) with very little amount of other necessary ions based on the mineral compositions considered in the simulations was used. The synthetic brine was equilibrated separately for the different formations and injection conditions considered, in the presence of the primary minerals listed in Table 3.8 (Strategy 1) and Table 3.9 (Strategies 2 and 3). The batch geochemical modelling was conducted for 100 years to obtain a quasi-stable (or nearly steady-state) aqueous solution composition as shown in Tables 3.10 and 3.11 (Strategy 1), and Table 3.12 (Strategies 2 and 3).

Table 3.10: Initial composition of the formation water at formation conditions of 100^{0}C and 137 bar (Strategy 1).

Component	Concentration (mol/kg H_2O)		
	Pure limestone formation	**Impure limestone formation**	**Shale caprock**
Ca^{2+}	4.7289E-01	4.6644E-01	3.4482E-01
Mg^{2+}	1.0034E-01	1.0489E-01	2.2812E-01
Na^{+}	2.5885E+00	2.5890E+00	2.5628E+00
K^{+}	1.9832E-10	2.6301E-03	1.1096E-02
Fe^{2+}	1.9861E-10	3.5599E-05	1.0361E-10
SiO_2 (aq)	1.9829E-10	3.7782E-03	2.6134E-03
HCO_3^-	3.6143E-03	2.3516E-03	6.5321E-05
SO_4^{2-}	3.6425E-03	3.6432E-03	3.6316E-03
AlO_2^-	1.9847E-10	2.4826E-09	1.0141E-08
Cl^-	3.7257E+00	3.7255E+00	3.7115E+00
pH	5.65	5.78	7.25

Table 3.11: Initial composition of the formation water at formation conditions of 40^{0}C and 100 bar (Strategy 1).

Component	Concentration (mol/kg H_2O)		
	Pure limestone formation	**Impure limestone formation**	**Shale caprock**
Ca^{2+}	4.7399E-01	4.6568E-01	9.0216E-03
Mg^{2+}	1.0036E-01	1.0693E-01	5.6313E-01
Na^{+}	2.5878E+00	2.5876E+00	2.5807E+00
K^{+}	1.9830E-10	4.9708E-04	2.6561E-03
Fe^{2+}	1.9835E-10	4.4246E-04	3.7561E-09
SiO_2 (aq)	1.9829E-10	1.3134E-03	1.7668E-03
HCO_3^-	4.6875E-03	2.9917E-03	5.8033E-03
SO_4^{2-}	3.6439E-03	3.6416E-03	3.6336E-03
AlO_2^-	1.9834E-10	1.7750E-10	4.0858E-11
Cl^-	3.7251E+00	3.7240E+00	3.7151E+00
pH	5.91	6.08	7.44

Table 3.12: Initial composition of the formation water at formation conditions of 40^{0}C and 100 bar (Strategies 2 and 3).

Component	Concentration (mol/kg H_2O)		
	Carbonate formation	**Sandstone formation**	**Shale caprock**
Ca^{2+}	9.0400E-03	4.7137E-01	4.8163E-01
Mg^{2+}	5.6496E-01	1.0038E-01	9.7547E-02
Na^{+}	2.5814E+00	2.5868E+00	2.6006E+00
K^{+}	1.9781E-10	2.8166E-03	3.3113E-03
Fe^{2+}	1.9785E-10	4.9784E-04	2.7904E-08
SiO_2 (aq)	1.9782E-10	2.9555E-03	1.3991E-03
HCO_3^-	5.7553E-03	2.1733E-03	1.2688E-04
SO_4^{2-}	3.6350E-03	3.6425E-03	1.7486E-02
AlO_2^-	1.9782E-10	1.3611E-11	6.1835E-11
Cl^-	3.7158E+00	3.7245E+00	3.7264E+00
pH	7.4418	6.1989	7.3919

Dissolution and precipitation of minerals are considered under kinetic conditions based on the rate law, except calcite and anhydrite which are assumed to react with aqueous species at local equilibrium. This is because the reaction rates of calcite and anhydrite are typically quite rapid (Zheng et al., 2009). The kinetic parameters were taken from Xu et al. (2006) and Zhang et al. (2011) and shown in Table 3.13.

Table 3.13: List of parameters for calculating the kinetic rate of minerals (Xu et al., 2006; Zhang et al., 2011).

Mineral name	Initial reactive surface area (cm^2/g)	Neutral mechanism		Acid mechanism			Base mechanism		
		K_{25} (mol/m^2s)	E_a (kJ/mol)	K_{25} (mol/m^2s)	E_a (kJ/mol)	n(H^+)	K_{25} (mol/m^2s)	E_a (kJ/mol)	n(H^+)
Calcite	Assumed in equilibrium								
Anhydrite	Assumed in equilibrium								
Quartz	9.8	1.0233E-14	87.7						
Kaolinite	151.63	6.9183E-14	22.2	4.8978E-12	65.90	0.777	8.9125E-18	17.90	-0.472
Illite	151.63	1.6596E-13	35.00	1.0471E-11	23.6	0.34	3.02E-17	58.9	-0.40
Pyrite	12.87	2.8184E-05	56.90 $n_{O2(aq)}$=0.5	3.02E-08	56.9	n_{H+}=-0.5 n_{Fe3+}=0.5			
K-feldspar	9.8	3.8905E-13	38.0	8.7096E-11	51.7	0.5	6.3096E-22	94.1	-0.823
Dolomite	9.8	2.9512E-08	52.20	6.4565E-04	36.1	0.5			
Siderite	9.8	1.2598E-09	62.76	6.4565E-04	36.1	0.5			
Ankerite	9.8	1.2598E-09	62.76	6.4565E-04	36.1	0.5			
Albite	9.8	2.7542E-13	69.80	6.9183E-11	65.0	0.457	2.5119E-16	71.0	-0.572
Muscovite	9.8	3.160E-13	58.6						
Hematite	12.87	2.5119E-15	66.2	4.0738E-10	66.2	1.0			
Chlorite	9.8	3.020E-13	88.0	7.7624E-12	88.0	0.5			
Oligoclase	9.8	1.4454E-13	69.8	2.1380E-11	65.0	0.457			
Magnesite	9.8	4.5709E-10	23.5	4.1687E-07	14.4	1.0			
Dawsonite	9.8	1.2598E-09	62.76	6.4565E-04	36.1	0.5			
Smectite-Na	151.63	1.6596E-13	35.0	1.0471E-11	23.6	0.34	3.0200E-17	58.9	-0.40
Smectite-Ca	151.63	1.6596E-13	35.0	1.0471E-11	23.6	0.34	3.0200E-17	58.9	-0.40
Alunite	9.8	1.0000E-12	57.78				1.0000E-12	7.5	-1.00
Anorthite	9.8	1.5000E-14	18.4						

A temperature of 100^0C was used in the high saline reservoir which may represent the temperature at a depth of about 2800 m, given a land surface temperature of 16^0C and a geothermal gradient of 30^0C/km; while a temperature of 40^0C was used in the low saline reservoir which may represent shallow formation temperature at a depth of about 800 m, given a land surface temperature of 16^0C and a geothermal gradient of 30^0C/km. The temperature in the reservoir and cap rocks are assumed to be initially the same as the rock thickness considered in the simulation is only 40 m. Also, the numerical simulations are conducted under isothermal condition.

3.3.3 Simulations

Six (6) groups of numerical simulations were performed in Strategies 1 and 2, and three (3) groups of numerical simulations in Strategy 3; with different combinations of injection and formation conditions as shown in Tables 3.14, 3.15, and 3.16. The objective is to investigate the effect of CO_2 injection or CO_2 co-injection with other gases (H_2S or SO_2) on the petrophysical (porosity and permeability) and geochemical (aqueous composition and mineral dissolution/precipitation)

changes of the rocks, and evaluate the brittleness of the rocks during non-cyclic and cyclic technique of CO_2 geosequestration.

Table 3.14: Six groups of simulations in this study (Strategy 1).

Simulation groups	Injection scenarios	Formation	Formation salinity
1	CO_2 only	Carbonate and shale	0.21
2	CO_2 and H_2S	Carbonate and shale	0.21
3	CO_2 and SO_2	Carbonate and shale	0.21
4	CO_2 only	Carbonate and shale	0.06
5	CO_2 and H_2S	Carbonate and shale	0.06
6	CO_2 and SO_2	Carbonate and shale	0.06

Table 3.15: Six groups of simulations in this study (Strategy 2).

Simulation groups	Injection scenarios	Formation	Formation salinity
1	CO_2 only	Carbonate and shale	0.06
2	CO_2 and H_2S	Carbonate and shale	0.06
3	CO_2 and SO_2	Carbonate and shale	0.06
4	CO_2 only	Sandstone and shale	0.06
5	CO_2 and H_2S	Sandstone and shale	0.06
6	CO_2 and SO_2	Sandstone and shale	0.06

Table 3.16: Six groups of simulations in this study (Strategy 3).

Simulation groups	Injection scenarios	Formation	Formation salinity
1	CO_2 only	Sandstone and shale	0.06
2	CO_2 and H_2S	Sandstone and shale	0.06
3	CO_2 and SO_2	Sandstone and shale	0.06

3.4 Analytical Approach

Numerical simulations were performed in this study to investigate the formation fluid and rock interactions during CO_2 geosequestration. The model derived in the present study, was based on the brittleness index model developed by Kang et al. (2020). The model derived in the present study (based on molecular weight, molar volume, and volume fraction of the minerals, which replace the weight of the minerals mathematically) that takes the bulk modulus of the brittle minerals into consideration, like that of Kang et al. (2020) which is based on the weight or weight fraction of the minerals should give the same result for the same rock at the same condition. The mineralogical brittleness index model developed by Kang et al. (2020) was validated using field data in their study. Therefore, the model was proven to be reliable. Hence, from the numerical simulations performed in the present study, the mineralogical compositions of the formations before and during the CO_2 geosequestration (with or without the addition of some amount of SO_2 or H_2S impurity) were applied to the mineralogical brittleness index model derived in the present study to calculate the brittleness index of the rocks.

The brittleness index calculations based on data from the numerical simulations performed in this study cannot be validated using rock core samples, as some portion of the fluids injected into the reservoir migrated to the caprock. Therefore, field data would be more suitable to validate such numerical simulations. However, experimental or field data on the change in the rock strength properties and fracture behaviour (stress-strain relationship) during CO_2 co-injection with an impurity such as SO_2 or H_2S are not available. Hence, the trends in the brittleness index using data from the numerical simulations in the present study, were compared with the trends in the brittleness index calculated using rock samples geochemical experimental data. The geochemical experimental data from studies conducted by Hedayati et al. (2018), Li et al. (2020), and Mavhengere et al. (2022) were used to calculate the mineralogical brittleness index of rocks during CO_2 sequestration. The experiments conducted by Hedayati et al. (2018) and Li et al. (2020) have been discussed in the literature review of the present study. The mechanical test data available was obtained from a study conducted by AL-Ameri et al. (2016) on the impact of pure CO_2 on the mechanical properties of Pink Desert limestone (PL). Hence, the data were applied to calculate the mechanical brittleness index of the pure limestone reservoir.

AL-Ameri et al. (2016) conducted a study to determine the long-term effects of CO_2 sequestration on rock mechanical properties. The porosity of the rock samples are shown in Table 3.17, indicating an average porosity of 26% for the carbonate rocks in Strategy 1 under the experimental condition of 100^0C and 137 bar. X-ray diffraction (XRD) was used to determine the mineral composition of the carbonate samples, which is shown in Table 3.18.

Table 3.17: Basic core properties (AL-Ameri et al., 2016).

Sample ID	Brine porosity (%)
PL-S-1-A	26.067
PL-S-2-A	27.792
PL-S-3-B	28.745
PL-U-1-A	26.022
PL-U-2-A	25.680
PL-U-3-B	26.652
PL-T-1-A	26.740
PL-T-1-B	26.332
PL-T-2-A	26.634
PL-T-3-C	26.005

Table 3.18: Quantitative analysis of the core samples using XRD (AL-Ameri et al., 2016).

Sample name	Phase name	Content (%)
Pink Desert limestone (PL)	Calcite Quartz	100 0

The purity of CO_2 used in the study was 99%, to minimize the chance of introducing contaminants in the rock samples. The composition of the brine used in the study is shown in Table 3.19. The total dissolved solids (TDS) of the brine was 213,734 ppm (this can be assumed to be 0.21 salinity). The system temperature and pressure during the CO_2 sequestration experiments were 100^0C and 2000 psi (~ 137 bar), respectively. Destructive tests including unconfined compressive tests and Brazilian tensile tests were conducted to determine Young's modulus, Poisson's ratio, and peak strengths (uniaxial compressive strength [UCS] and indirect tensile strength [ITS]) of the rock samples before and after CO_2 storage. Results of the experiments are shown in Table 3.20.

Table 3.19: Ionic composition of the brine (AL-Ameri et al., 2016).

Ions	Composition (ppm)
Sodium	59,491
Calcium	19,040
Magnesium	2439
Sulphate	350
Chloride	132060
Carbonate	0
Bicarbonate	354
TDS	213734

Table 3.20: Mechanical properties of the PL core samples before and after CO_2 sequestration (AL-Ameri et al., 2016).

Rock mechanical properties	Before CO_2 sequestration	After CO_2 sequestration (90 days)
Indirect tensile strength (psi) (MPa)	199.137 1.3730	142.800 0.9846
Uniaxial compressive strength (MPa)	17.0000	12.4000
Static Young's modulus (GPa)	16.1800	14.0000
Static Poisson's ratio	0.3530	0.2330

The impact of SO_2 impurity on the brittleness of rocks was evaluated using experimental data obtained from a study conducted by Mavhengere et al. (2022) on the influences of SO_2 contamination in long term supercritical CO_2 treatment on the physical and structural characteristics of sandstone rock. They conducted two types of storage experiments on sandstone core samples (Cenomanian Sandstone, ZG and Siltstone lateral seal Aptian

Sandstone, ZC) from Zululand Basin in South Africa, using pure CO_2 gas (purity of 99.9% by weight); and another case using a mixture of 99% (weight) CO_2 and 1% (weight) SO_2 gas. Non-stirred Teflon lined N4766 Parr reactors were used to simulate geosequestration conditions of 17.5 MPa and 346 K for the ZC core samples, and 10 MPa and 316K for the ZG core samples for 2 months. XRD analyses were conducted on the samples before and after treatment with CO_2 or CO_2-SO_2 mixture to investigate any mineral phase alterations. The ZC core sample exhibited mineral phase alteration after treatment (fluid-rock interaction) similar to the sandstone rock in the present study. The brittleness index model developed by Kang et al. (2020) was applied to evaluate the impact of contaminant (SO_2) in CO_2 on brittleness index of sandstone, using the weight fraction of the minerals in the ZC and ZG core samples (shown in Table 3.21). In this case, the brittle minerals are quartz, plagioclase (feldspar), calcite, pyrite, and orthoclase (feldspar).

Table 3.21: Mineralogical compositions of ZC and ZG core samples before and after $ScCO_2$-water and $ScCO_2$-SO_2-water treatment.

Sample	Quartz (wt. %)	Plagioclase (wt. %)	Smectite (wt. %)	Calcite (wt. %)	Pyrite (wt. %)	Stilbite (wt. %)	Diopside (wt. %)	Gypsum (wt. %)	Orthoclase (wt. %)
ZC untreated	44.1	44.7	1.0	3.5	0.4	3.6	2.7	0.0	0.0
ZC CO_2 treated	47.5	42.5	2.5	1.7	0.4	2.7	2.8	0.0	0.0
ZC CO_2-SO_2 treated	49.1	28.6	11.8	0.0	0.8	4.9	2.3	2.5	0.0
ZG untreated	21.5	46.0	22.2	0.0	0.0	2.0	0.0	0.0	8.3
ZG CO_2 treated	22.3	50.5	16.3	2.9	0.0	4.8	0.0	0.0	3.2
ZG CO_2-SO_2 treated	26.1	53.4	12.1	2.3	0.0	0.0	0.0	0.0	6.2

3.5 Machine Learning Approach

Machine Learning (ML) is a subset of artificial intelligence which integrates statistics and computer science to build algorithms that become more efficient when they are subject to relevant data instead of giving a specific instruction. Machine learning helps produce predictions or decisions without being specifically produced for the task (Jijo and Abdulazeez, 2021). Machine learning algorithm creates a model population based on a sample called training data, such that test data can be used to test the efficiency or accuracy of the developed model. Among several applications of machine learning, it can be used for classification and regression purpose. In this study, a regression model was developed using artificial neural network (ANN) algorithm, to predict brittleness index of rocks.

3.5.1 Data preparation

Data from numerical simulations in Strategies 1 and 2 are used in developing the machine learning model. The concentration and mineral data from the TOUGHREACT numerical simulation were merged, and data of all the modelled cases (in comma-separated values file

format) were concatenated to cover a wide range of data for the model development, making a total of 38,080 observations. Mineralogical brittleness index was calculated for each of the observations using the brittleness index model (the model that considers the bulk modulus of brittle minerals) derived in this study using the volume fraction and molecular weight of the minerals. Thus, a new column for brittleness index was created, making a total of 51 features in the dataset.

In order to create a dataset for the machine learning model development, to predict brittleness index, all the mineral volume fraction columns were deleted (or dropped) to ensure the prediction of the brittleness index is not influenced by the mineral volume fractions from which the brittleness index was calculated from. This is because, the goal of developing the machine learning model in this study, is to demonstrate how other features can be used to predict the brittleness index of the rocks.

The correlation coefficients between each of the variables with another were determined using Pearson correlation coefficient (r), expressed as

$$r = \frac{n\sum xy - (\sum x)(\sum y)}{\sqrt{[n\sum x^2 - (\sum x)^2][n\sum y^2 - (\sum y)^2]}} \quad 3.17$$

where, n is the number of observations, and x and y represent the features correlated.

It is good and acceptable to have a strong correlation between dependent and independent variables. However, it is undesirable to have a strong correlation between two independent variables. When two independent variables strongly correlate with each other, it suggests that excluding one of them from the training data would be beneficial to prevent redundancy and helps to improve the model performance (Kannaiah and Maurya, 2023). Hence, for two independent variables in the dataset perfectly correlating (r=1.0) with each other, one of the features is removed. For instance, temperature and pressure, liquid saturation and gas saturation, permeability in the x and z directions, and permeability ratio in the x and z directions, are correlating perfectly with each pairs. Therefore, one of each feature was removed. In this case, pressure, liquid saturation, permeability in the x-direction, and permeability ratio in the x-direction were removed in the dataset. In addition, features whose values never changed during the numerical simulations were removed as well. Although the correlation coefficient between some independent variables are high, those features were not removed as their individual correlation with some other independent variables are relatively different. The correlation coefficient matrix of the remaining features (independent and dependent variables) is shown in Figure 3.5.

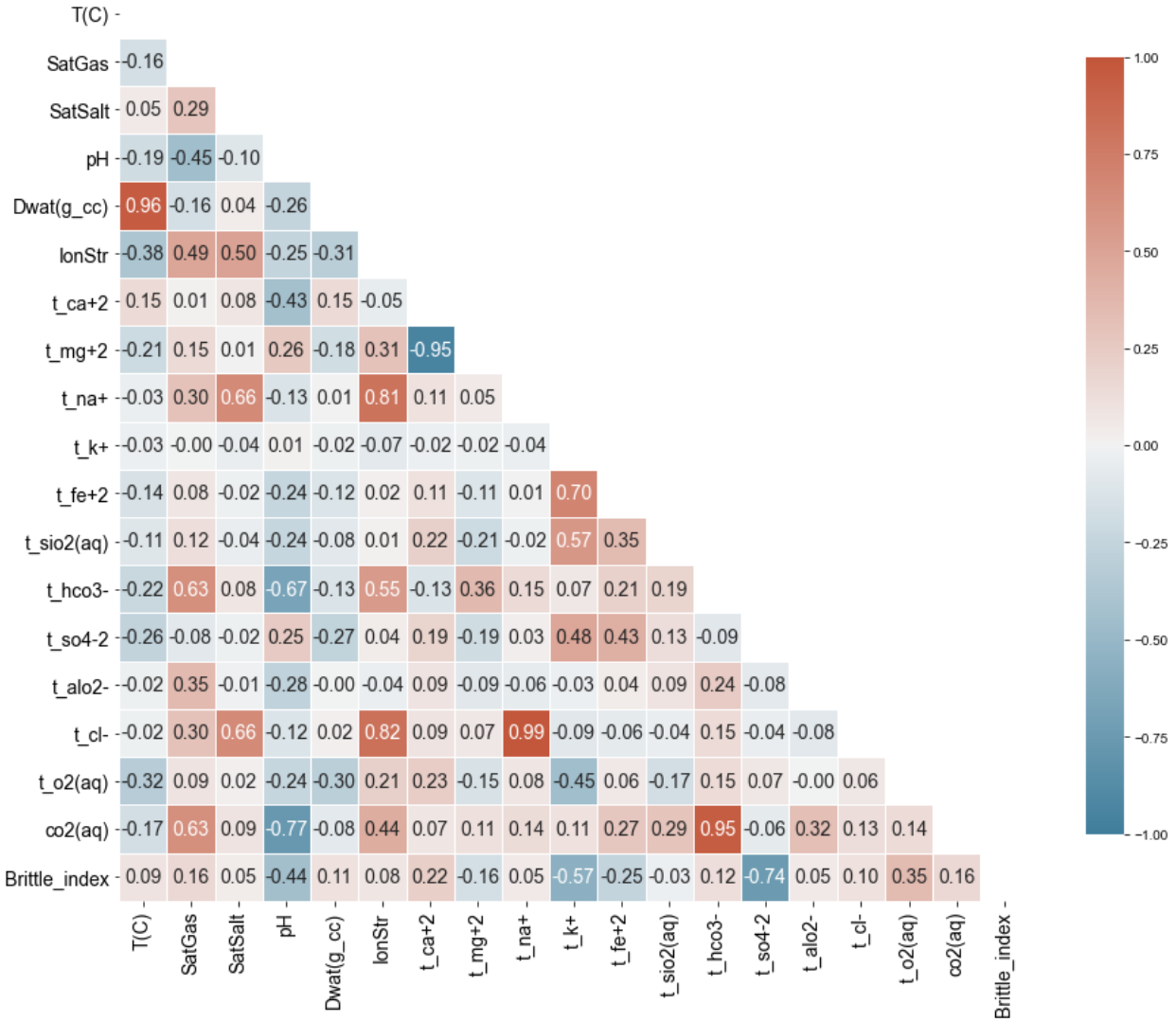

Figure 3.5: Correlation coefficient matrix of features.

The concentrations of K^+ and SO_4^{2-} are negatively correlated to the brittleness index of rocks. The correlations suggest that the higher the concentrations of K^+ and SO_4^{2-}, the lower the brittleness index of the rocks. The distribution of the features is presented in Table 3.22.

Table 3.22: Statistical parameters of the dataset.

Variables	Mean	Standard deviation	Minimum	50th percentile	Maximum
T(C)	5.764706e+01	2.733906e+01	4.000000e+01	4.000000e+01	1.000000e+02
SatGas	7.473813e-02	1.608901e-01	0.000000e+00	0.000000e+00	9.818800e-01
SatSalt	5.958950e-04	6.460365e-03	0.000000e+00	0.000000e+00	1.686400e-01
pH	5.740421e+00	1.045728e+00	4.362300e+00	5.649200e+00	7.491000e+00
Dwat(g_cc)	1.062711e+00	3.759167e-02	9.645000e-01	1.043300e+00	1.196900e+00
IonStr	3.281328e+00	1.159284e-01	2.967200e+00	3.271800e+00	4.352500e+00
t_ca+2	3.717171e-01	2.005988e-01	8.954700e-03	4.729800e-01	7.513800e-01
t_mg+2	2.392790e-01	2.509667e-01	9.398500e-02	1.003900e-01	1.004300e+00
t_na+	2.601796e+00	1.076680e-01	2.444800e+00	2.586800e+00	4.051600e+00
t_k+	2.255553e-03	3.771088e-03	1.947900e-10	1.307150e-04	4.134900e-02
t_fe+2	6.208039e-04	2.483182e-03	1.677900e-11	4.252600e-08	2.484400e-02
t_sio2(aq)	1.573913e-03	2.133439e-03	1.948500e-10	2.882450e-04	9.197300e-03
t_hco3-	3.213137e-01	4.268074e-01	6.532200e-05	5.757000e-03	1.346900e+00
t_so4-2	5.747741e-03	5.151247e-03	3.440300e-03	3.642400e-03	4.379000e-02
t_alo2-	1.165757e-08	4.530096e-08	1.288900e-11	1.984900e-10	7.362100e-07
t_cl-	3.740544e+00	1.551220e-01	3.518800e+00	3.723000e+00	5.831600e+00
t_o2(aq)	-2.038282e-07	8.303031e-07	-1.445500e-05	-2.482550e-11	3.260200e-16
co2(aq)	2.465815e-01	3.198288e-01	1.221500e-06	1.974400e-03	8.939000e-01
Brittle_index	3.897865e-01	1.706044e-01	1.070956e-01	5.100000e-01	5.893410e-01

The input features include formation temperature (T in degrees Celsius), gas saturation (SatGas), salt saturation (SatSalt), formation fluid pH, formation water density (Dwat in g/cm^3), ionic strength (IonStr), and the primary aqueous species/ions concentrations (including the amount of dissolved CO_2, in mol/kg H_2O). The unit of concentrations in the table is mol/kg H_2O. The input features (18 variables) are believed to be related to the brittleness index (the output feature). This assumption was made, as the geochemical properties of formation fluid depends on the mineralogical composition of the rock, as the rock minerals are in equilibrium with the formation fluid (Yu et al., 2020; Thanh et al., 2022). Also, the geochemical composition of the formation fluid depends on the in situ temperature conditions of the formation (Ibrahim, 2022). Therefore, the geochemical properties of the formation fluid and the formation temperature might be related to the brittleness index of the formation. The statistical distribution of the dataset shows that the mean and median (50th percentile) are different for most of the features. Therefore, the features were scaled. The dependent and independent variables were scaled using a standard scaler, to prevent any input feature with high values from overfitting the model as other equally important features might be neglected if not scaled. Thus, scaling the features improves the training accuracy (Kannaiah and Maurya, 2023). Standard scaler standardizes the features as follows:

$$z = \frac{x-\mu}{\sigma} \qquad 3.18$$

where, x represents the input variable, μ and σ are the mean and standard deviation of the variable dataset, respectively.

3.5.2 Model architecture

This study applied the prepared data in developing the machine learning model. The structure of the ANN model is made up of 18 nodes (representing the input parameters) in the input layer, 1-3 hidden layers (each layer has 64 neurons), and a node in the output layer (representing the output parameter – brittleness index). The neural network is fully connected. In each layer (except the output layer), a rectified linear unit (ReLU) was used as an activation function, while a linear activation function was used in the output layer. The 'He_normal' weight initializer was applied (He et al., 2015), as it samples the weights following a normal distribution and a modified standard deviation, taking the number of input neurons for each layer into consideration (Wolfgang et al., 2020).

3.5.3 Model evaluation

To gauge the accuracy of the numerical simulation and machine learning models, some evaluation criteria including mean absolute error (MAE), mean square error (MSE), mean absolute percentage error (MAPE), and coefficient of determination (R^2 or R-squared score). In the model evaluation, N is the total number of observations (or total number of data values), $\hat{y}_i$ is the predicted ith value, y_i is the actual ith value, and $\bar{y}$ is mean of actual value.

Mean absolute error (MAE), can be expressed as

$$MAE = \frac{1}{N}\sum_{i=1}^{N}|y_i - \hat{y}_i| \qquad 3.19$$

Similarly, mean square error, can be expressed as

$$MSE = \frac{1}{N}\sum_{i=1}^{N}(y_i - \hat{y}_i)^2 \qquad 3.20$$

While root-mean-square error (RMSE) is obtained by taking the square root of MSE, and can be expressed as

$$RMSE = \sqrt{\frac{1}{N}\sum_{i=1}^{N}(y_i - \hat{y}_i)^2} \qquad 3.21$$

The magnitude of relative error (MRE) for each observation i, and mean magnitude of relative error (MMRE) can be expressed as:

$$MRE_i = \frac{|y_i - \hat{y}_i|}{y_i} \quad 3.22$$

$$MMRE = \frac{1}{N}\sum_{i=1}^{N} MRE_i \quad 3.23$$

Mean absolute percentage error (MAPE) is another form of MMRE, but it is expressed in percentage as

$$MAPE = \frac{1}{N}\sum_{i=1}^{N} MRE_i * 100 \quad 3.24$$

Coefficient of determination, also called R-squared (R^2) score represents the proportion of the variance in the dependent variable that is predictable from the independent variables (Chicco et al., 2021). It can be expressed as:

$$R^2 = 1 - \frac{\sum_{i=1}^{N}(y_i - \hat{y}_i)^2}{\sum_{i=1}^{N}(y_i - \bar{y}_i)^2} \quad 3.25$$

To test the statistical significance of differences in tests or observations at different stages or conditions, the concept of reliable change index (RCI) with 95% confidence (Blampied, 2016) can be adopted as follows:

$$RCI = 1.96(\sigma)\sqrt{2}\sqrt{(1-r)} \quad 3.26$$

3.5.4 Model development

To build the artificial neural network model, the prepared dataset made up of 38,080 observations (or rows) and 19 features (18 input features and an output feature) was used in this study. The optimal ANN model was achieved by dividing the data into three sets: 63% of the dataset was selected as the training set, 27% as validation set, and 10% as testing set. The training set was used to build the model, while the validation set was employed to ensure the model was not overfitting or underfitting. The testing set was reserved to test the developed and validated model, to ensure there was no form of data leakage during the model development stage and to reveal the accuracy of the ANN model in estimating brittleness index. Three options were considered for the model building. The first option has a hidden layer, the second option has 2 hidden layers, while the third option has 3 hidden layers. Satisfactory tuning of optimizer hyperparameters (the batch size and epochs) of training was performed, using the grid search approach, to obtain better predictions of brittleness index. The batch sizes considered are 32, 64, and 128; while the number

of epochs considered are 10, 20, 50, and 100. The loss function and optimizer employed in this study are ‘mean square error’ and ‘Adam’, respectively. During the hyperparameter tuning, the third option (Option 3) together with a combination of batch size of 64 and 100 epochs, gave the lowest mean absolute percentage error of 0.18% and 0.19% for the training and validation datasets, respectively (Figure 3.6). Hence, in this study, the optimum batch size and number of epochs used in the final model (Option 3) building are 64 and 100, respectively.

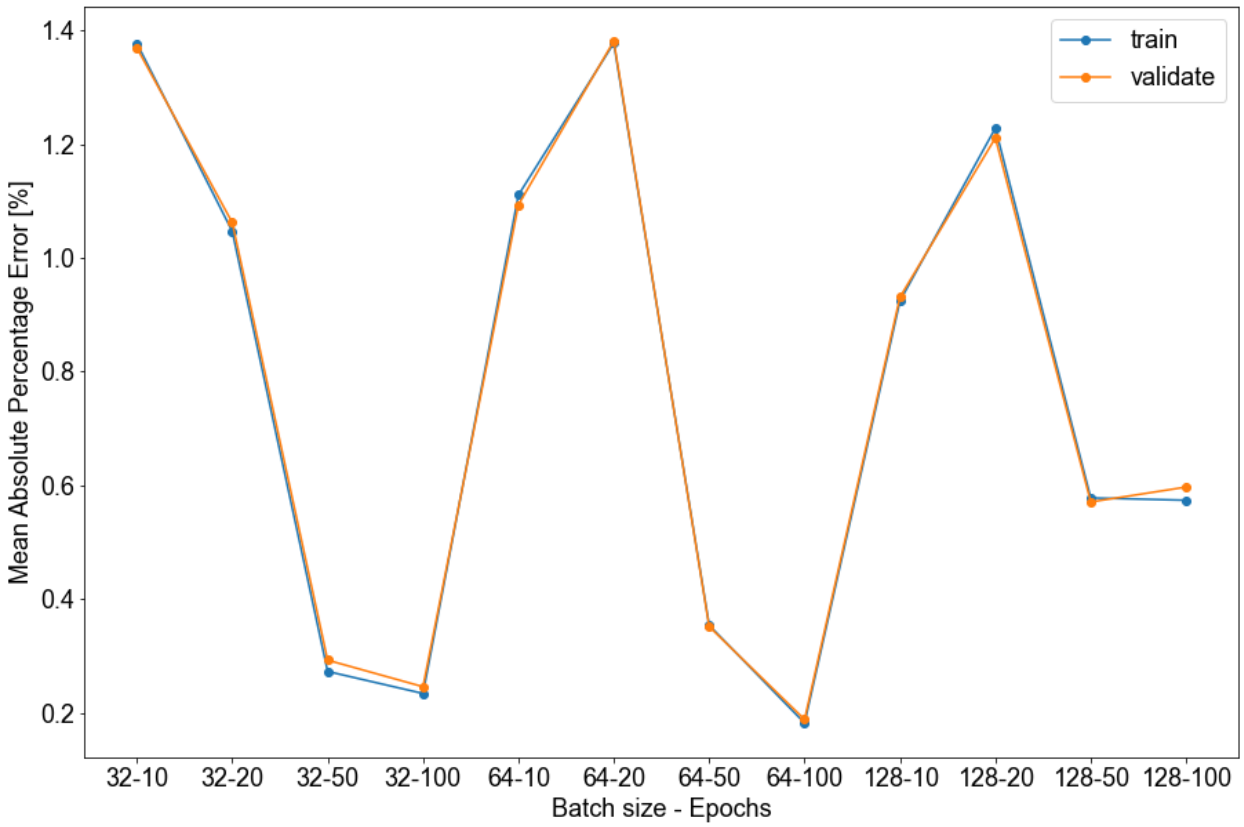

Figure 3.6: Hyperparameter tuning of batch size and epochs.

The final ANN model was developed using the predefined architecture and the selected optimal hyperparameters, as shown in Table 3.23. The feature importance of the input parameters were determined by comparing the sum of the absolute weights (in the first hidden layer) of each parameter that predicted brittleness index and ranked in order. This technique helps to understand the relative importance of different input features in predicting brittleness index.

Table 3.23: Model structure and parameters.

Model Parameters	Option 1	Option 2	Option 3
Number of hidden layers	1	2	3
Number of neurons in each hidden layer	64	64	64
Number of neurons in the output layer	1	1	1
Number of output feature(s)	1	1	1
Number of input features	18	18	18
Activation function in the hidden layers	ReLU	ReLU	ReLU
Kernel initializer	He_normal	He_normal	He_normal
Seed value	42	42	42
Loss function	MSE	MSE	MSE
Optimizer	Adam	Adam	Adam
Learning rate	Default	Default	Default
Best batch size	64	32	64
Best number of epochs	100	100	100
Model Performance			
MAPE on the train dataset (%)	0.55	0.24	0.19
MAPE on the validation dataset (%)	0.56	0.25	0.18

3.6 Data Analysis Techniques

Numerical simulations were analysed for changes in petrophysical and geochemical properties of reservoir and cap rocks, to investigate the impact of CO_2 mixtures on those properties. In addition, data from the experiment conducted by AL-Ameri et al. (2016) were analysed to determine the mechanical brittleness index of the rock, using equations of elastic and strength parameters; while the mineralogical brittleness index was calculated from the models developed in the present study. The calculated mechanical brittleness indices were compared with the mineralogical brittleness indices for the high saline formations injected with CO_2 only. Furthermore, the mineralogical brittleness index of the formations was calculated for simulation groups of CO_2 co-injection with another gas (H_2S or SO_2) into the reservoir and advective [and diffusive] transport into the caprock layers, to determine the impact of CO_2 mixtures on the brittleness of reservoir and cap rocks in high or low salinity conditions. The results from the analyses are presented in tables and graphs for proper visualization and comparison. It is worth noting that while discussing the results of the analyses, the expression "SO_2 (or H_2S) gas co-injection with CO_2" or "SO_2/H_2S gas co-injection with CO_2" implies that SO_2 co-injection with CO_2 is one case, and H_2S co-injection with CO_2 is another case in the numerical simulations. Also, CO_2 only case and CO_2 alone case are used interchangeably. Also, for clarity, it is important to identify the interface between the different formations. In Strategy 1, the interface between the shale caprock and the impure limestone is 6 m from the top of the caprock (marked X in Figure 3.7a), while the interface between

the impure limestone and the pure limestone is 12 m from the top of the caprock (marked Y in Figure 3.7a). In Strategy 2 and Strategy 3, the interface between the reservoir (carbonate or sandstone) and caprock is 12 m from the top of the caprock (marked X in Figure 3.7b).

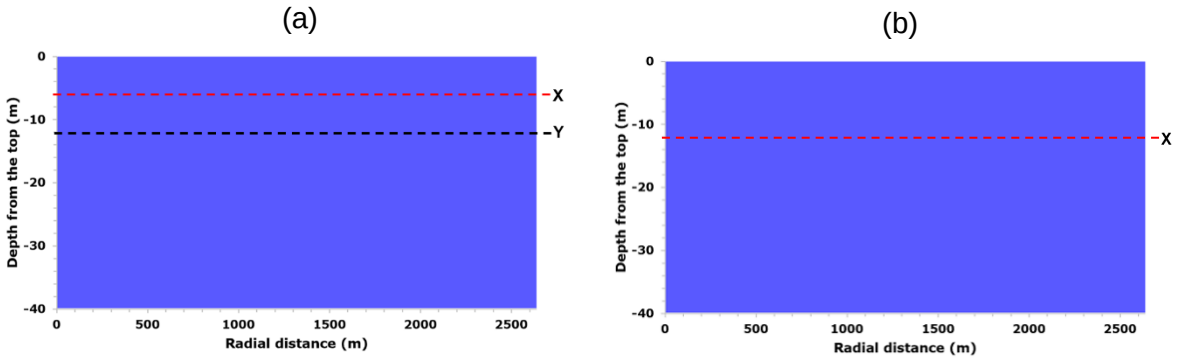

Figure 3.7: Interface between the formations (a) Strategy 1 (b) Strategy 2 and Strategy 3.

3.7 Limitations of the Study

1. The depleted petroleum reservoirs considered in the numerical simulations were assumed to be under a strong aquifer drive during their petroleum production life and the hydrocarbon was completely depleted. Therefore, the reservoirs were assumed to be fully saturated with formation water, like aquifers. Hence, the impact of hydrocarbon on the CO_2-brine-rock interactions was not considered during the numerical simulations.
2. No experimental data available to determine changes in the mechanical strengths (compressive and tensile strengths) and mechanical brittleness index of the rocks during CO_2 co-injection with H_2S or SO_2 gas. Therefore, the impact of impurities in CO_2 on the mechanical brittleness index of the rocks was not determined as mechanical tests are required.
3. This study adopted a numerical simulation and analytical approach to evaluate the brittleness index of rocks during CO_2 geosequestration (with or without SO_2/H_2S impurity). Experiments were not conducted in the present study to investigate the fracture behaviour (stress-strain relationship) of reservoir and caprock samples before and after pure CO_2 injection or CO_2 co-injection with H_2S or SO_2 gas. The fracture behaviour of rock samples for the different cases (CO_2-brine-rock, CO_2-H_2S-brine-rock, and CO_2-SO_2-brine-rock interactions) could have been validated with changes in the mineralogical brittleness index if mechanical tests were performed as well as geochemical experiments and XRD analyses of the rock samples (to determine the changes in the mineralogical compositions of the rock samples).
4. In the present study, the CO_2 geosequestration period considered was 100 years. Therefore, the impact of CO_2 mineral trapping on the rock properties was not considered, as it is expected

to be significant after hundreds to thousands of years. Therefore, residual and solubility trapping were the main CO_2 trapping mechanisms in this study.

CHAPTER FOUR

RESULTS AND DISCUSSION

4.1 Results

4.1.1 Impact of impurities on porosity, permeability, and geochemical composition of reservoir and cap rocks during CO_2 injection and storage (Strategy 1)

The supercritical CO_2 fluid (referred to as 'gas' in this study for simplicity) is injected or co-injected with H_2S (or SO_2) near the bottom of the pure limestone (carbonate reservoir). The injected fluid migrates rapidly upward by buoyant forces, as the density of the supercritical CO_2 phase is less than that of the aqueous phase or formation water (Figure 4.1). After the period of injection, a small fraction of CO_2 gas is trapped in the pure and impure limestone porous rocks as residual gas. The mobile gas continues to migrate into the shale caprock by the action of buoyant forces. At the same time, some amount of the gas continues to dissolve into brine (formation water) and precipitate carbonate minerals. Hence, the residual gas slowly disappears at the bottom of the pure limestone reservoir.

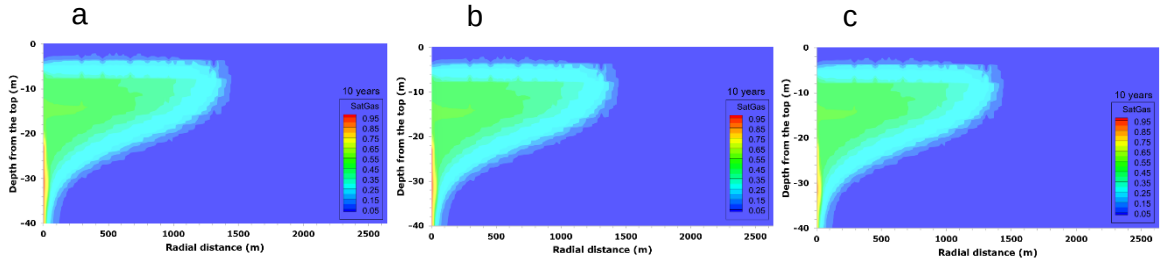

Figure 4.1: Gas saturation after 10 years at 40^0C and 100 bar (a) CO_2 alone case (b) CO_2-H_2S case (c) CO_2-SO_2 case.

After some time, most of the free CO_2 gas accumulates in the shale caprock layers, few metres from the reservoir-caprock interface, and spreads laterally. At 10 years of injection, reservoir rock pores are majorly filled with free CO_2 gas few metres close to the injection well (water nearly drying out in the zone). In fact, the higher gas saturation in the rock pores near the injection well extends over a longer radial distance in the CO_2 and H_2S/SO_2 co-injection cases compared to the CO_2 alone case, as shown in Figure 4.1. However, after injection (10 years), formation water re-invades the zones where water was nearly dried out, enabling chemical reactions (dissolution and precipitation) between the dissolved CO_2 and minerals. The gas saturation in the reservoir and caprock after 100 years of geosequestration is shown in Figure 4.2.

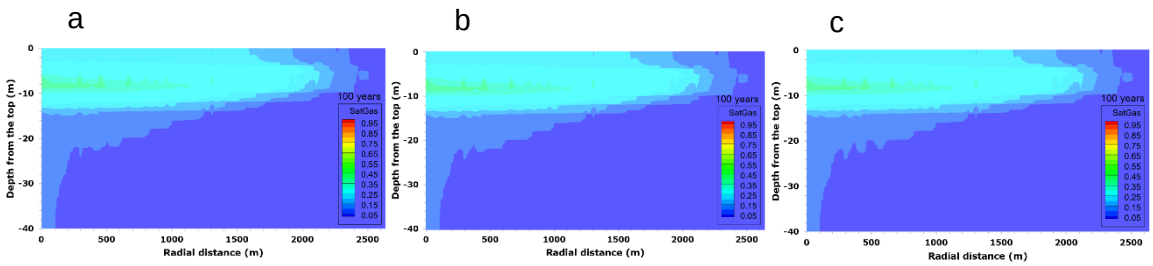

Figure 4.2: Gas saturation after 100 years at 40^0C and 100 bar (a) CO_2 alone case (b) CO_2-H_2S case (c) CO_2-SO_2 case

The front of H_2S (or SO_2) gas are behind that of CO_2 gas (Figure 4.3). This is due to the preferential solubility of H_2S and SO_2 in formation water compared to that of CO_2. Thus, delayed breakthrough of H_2S (or SO_2) gas is experienced, and H_2S (or SO_2) gas begins to separate from the CO_2 gas (in the gas mixture), and H_2S (or SO_2) concentration in the formation water at the advancing gas front gets suppressed. This situation is more severe with SO_2 gas compared to H_2S gas. The front of SO_2 gas is far behind that of CO_2 gas compared to the front of H_2S gas with respect to CO_2 gas at 40^0C and 100 bar (which corresponds to low salinity formation fluid in the present study) as shown in Figure 4.3. Hence, the solubility of SO_2 gas in formation water is higher than that of H_2S and CO_2. The solubility of SO_2 gas in water increases at a higher salinity (0.21), which corresponds to the temperature and pressure conditions of 100^0C and 137 bar, respectively in the present study. Thus, resulting in complete dissolution of SO_2 in formation water after 100 years of CO_2 geosequestration as shown in Figure 4.4.

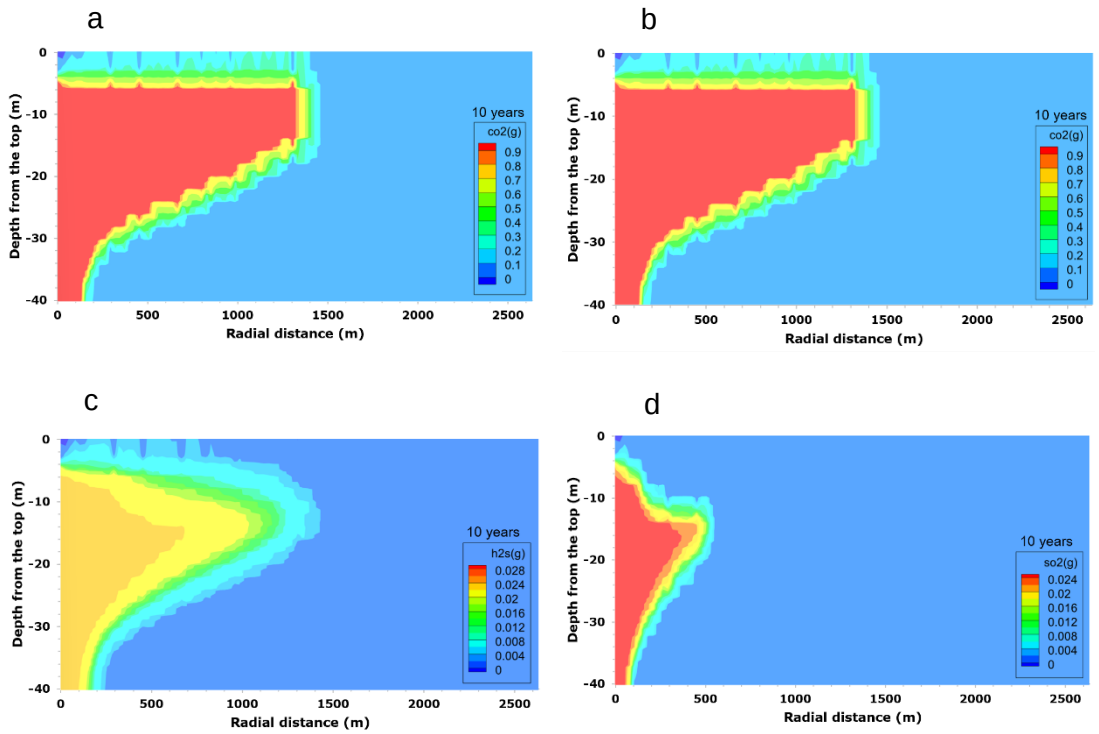

Figure 4.3: Gas front of (a) CO_2 in CO_2-H_2S(b) CO_2 in CO_2-SO_2 (c) H_2S (d) SO_2 at 40^0C and 100 bar.

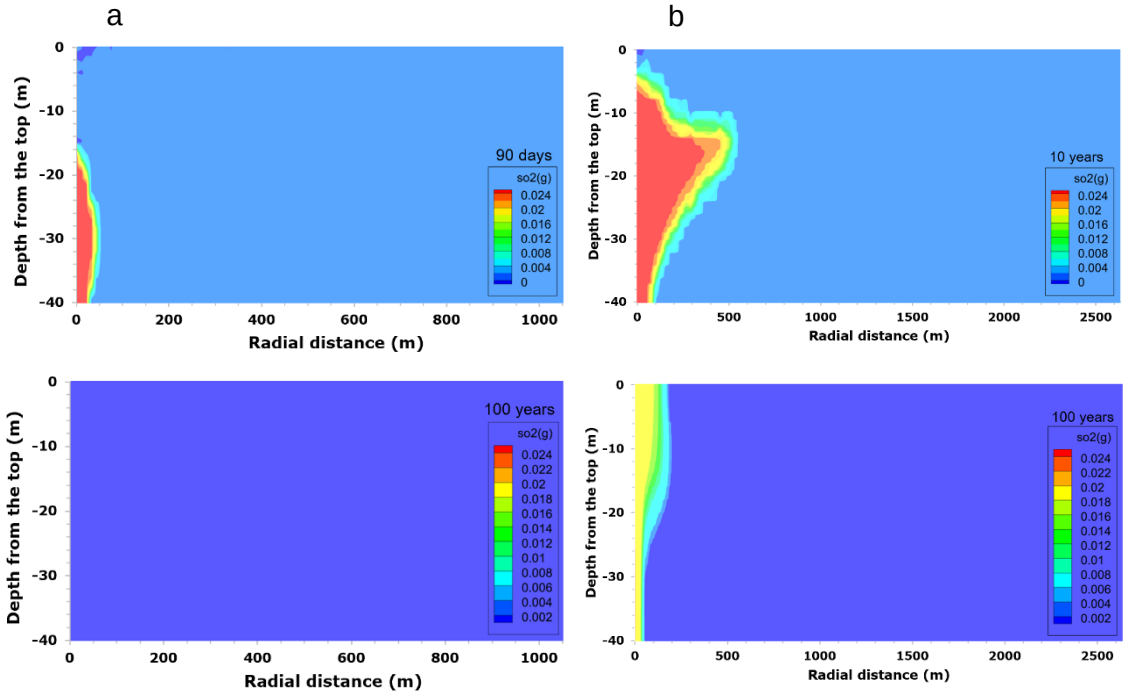

Figure 4.4: SO_2 gas mole fraction after CO_2 co-injection and 100 years of geosequestration (a) at 100^0C and 137 bar (b) at 40^0C and 100 bar.

Figure 4.5 shows the spatial distribution of total dissolved carbon (TDC) in the rocks. CO_2 mobilizes faster than H_2S (or SO_2). This is due to the preferential dissolution of H_2S and SO_2 compared with CO_2. The concentration of total dissolved carbon at the advancing front increases as the concentration of H_2S (or SO_2) gas has been suppressed in the formation water. Moreover, the concentration of TDC in the co-injection cases is lower than that in the CO_2 alone case. This implies that the preferential dissolution of H_2S (or SO_2) gas reduces the potential and capacity for the dissolution of the injected CO_2 gas in formation water (Zhang et al., 2011).

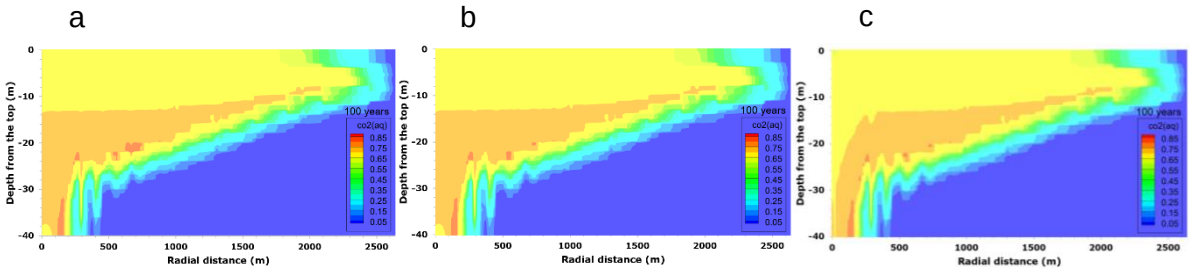

Figure 4.5: Total dissolved carbon at 40^{0}C and 100 bar for (a) CO_2 alone case (b) CO_2-H_2S case (c) CO_2-SO_2 case.

The total dissolved CO_2 concentrations after 100 years of geosequestration are shown in Figure 4.5. The concentration of dissolved CO_2 increases to over 0.6 mol/kg H_2O in the two-phase region due to the CO_2 gas migration. The dissolution of the injected CO_2 (with or without cases of H_2S or SO_2 gas co-injection) in the surrounding formation water yields H_2CO_3, HCO_3^-, and CO_3^{2-}, and decreases pH (increases acidity). The pH profiles of all the injection cases are similar, as shown in Figure 4.6.

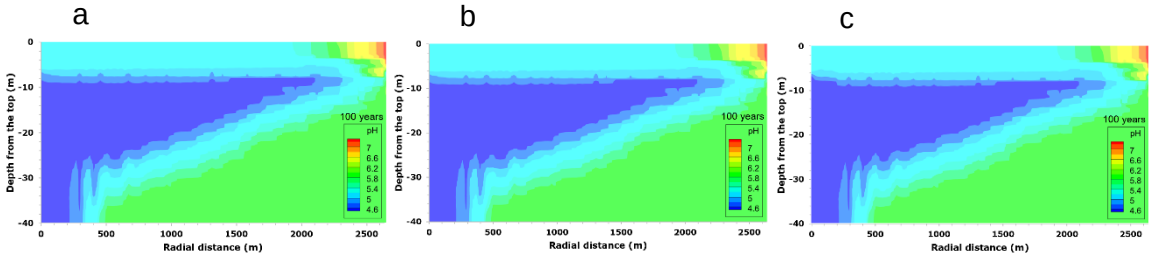

Figure 4.6: Formation fluid pH at 40^{0}C and 100 bar for (a) CO_2 alone case (b) CO_2-H_2S case (c) CO_2-SO_2 case.

The low pH induces the dissolution and precipitation of minerals. As aqueous complexes are formed, more CO_2 goes into solution and enhance solubility trapping. However, mineral trapping of CO_2 was not considered in this study as it is a slow process that occurs over hundreds to thousands of years, while the numerical simulations in the present study were performed up to a maximum of 100 years. So, the CO_2 trapping mechanisms in the present study are structural/stratigraphic trapping (caprock), residual trapping, and solubility trapping. During the

CO_2 injection period (up to 10 years), out of a total of about 6.31 M ton of CO_2 injected, a large amount of injected CO_2 remains as a free supercritical phase. After injection, some amount of CO_2 dissolved in the formation water gradually, while the injected gas plume continued to migrate upward and horizontally. Convective mixing between CO_2-saturated water and unsaturated water also takes place at the same time.

Minerals such as chlorite, albite, dolomite, and K-feldspar in the shale and impure limestone formations dissolve in the two-phase region and near the front of the single aqueous-phase zone. On the other hand, quartz, illite, smectite-Ca, and smectite-Na precipitated in those zones. Other minerals exhibited selective dissolution or precipitation in different formations. It is worth noting that due to fluid-rock interaction between zones with different lithology, minerals such as quartz and smectite-Na precipitated in some layers of the pure limestone formation (which would not have been possible without upward and downward (vertical) flow of fluids from different rock layers). After 100 years of CO_2 only sequestration, minerals such as ankerite, magnesite, pyrite, and calcite (due to higher pH in the region) precipitated in the shale caprock; while kaolinite dissolution was observed in the formation. On the other hand, kaolinite, dawsonite, ankerite and small amount of magnesite and siderite precipitated in the impure limestone formation; while pyrite and calcite dissolution was observed in the impure limestone formation. In the pure limestone reservoir, calcite dissolution was observed throughout the period of sequestration. Changes in the composition (volume fraction of the solid rock) of the minerals in the CO_2 alone sequestration case is shown in Figures 4.7 and 4.8.

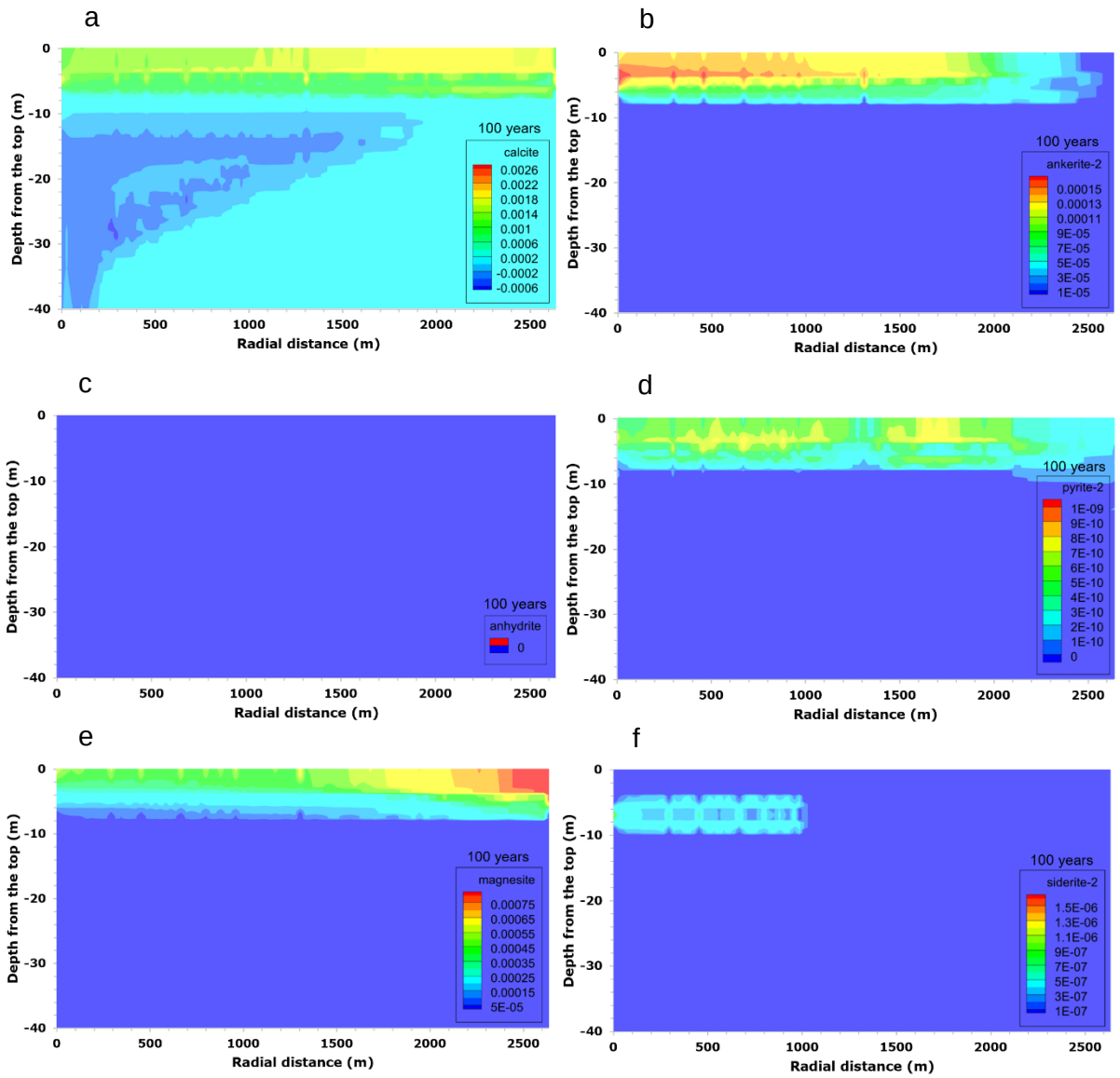

Figure 4.7: CO_2 alone case at 40^0C and 100 bar (a) calcite (b) ankerite (c) anhydrite (d) pyrite (e) magnesite (f) siderite.

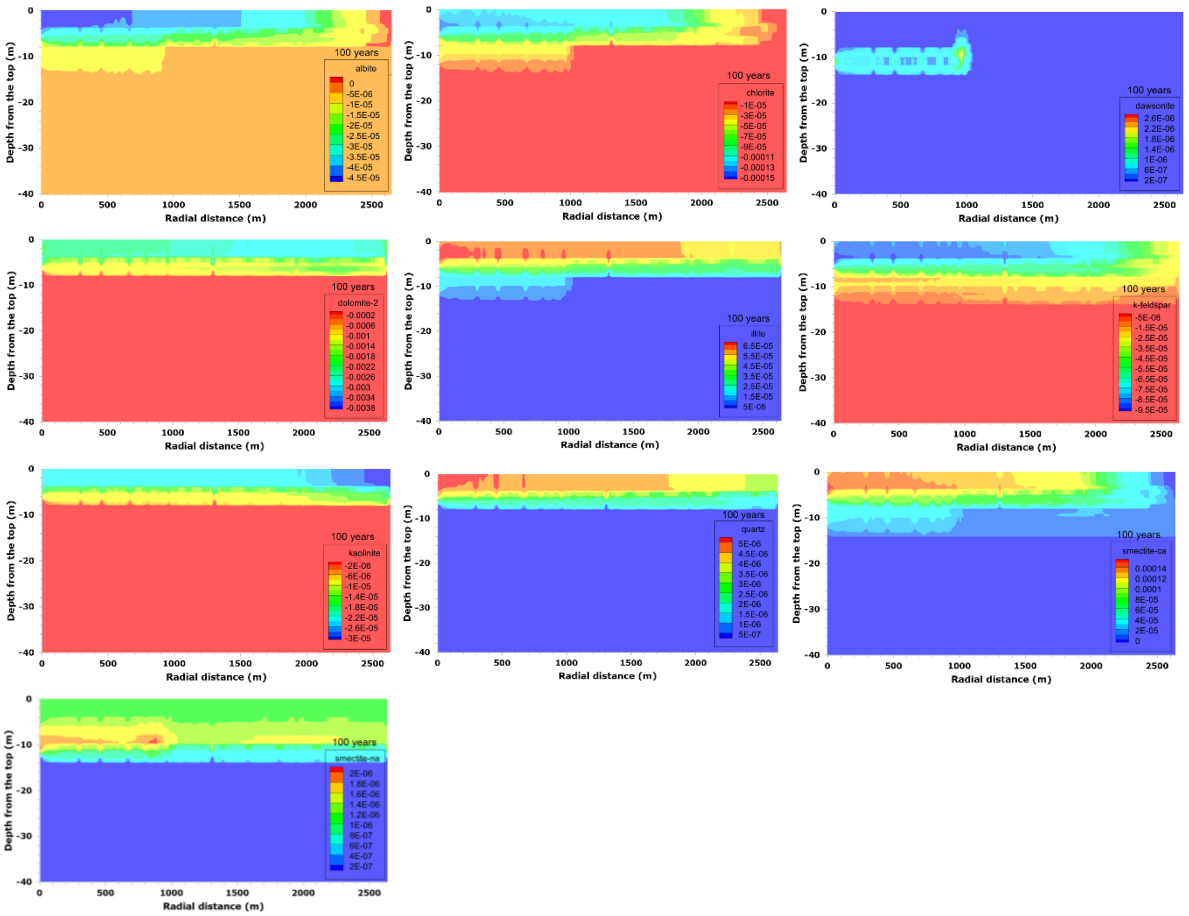

Figure 4.8: Dissolution and precipitation of other minerals (albite, chlorite, dawsonite, dolomite, illite, K-feldspar, kaolinite, quartz, smectite-Ca, and smectite-Na) in the formations for the CO_2 alone case at 40^0C and 100 bar.

The same kind of mineral precipitation and dissolution was observed in the co-injection cases, except that in the case of H_2S co-injection with CO_2, no siderite precipitation (Figures 4.9 and 4.10). Little amount of ankerite was observed in the shale caprock only in the region where dissolved H_2S in formation water is low in concentration. But pyrite precipitation was observed in all the formations considered, in all the regions where H_2S dissolved in the formation water. This is because precipitation of siderite and ankerite requires Fe^{2+} which can be supplied by the dissolution of iron-bearing minerals such as chlorite. Furthermore, in the case of SO_2 co-injection with CO_2, after 100 years of sequestration, ankerite, and magnesite precipitated in the shale caprock, while anhydrite and pyrite precipitated in the carbonate rocks in the region where SO_2 gas has dissolved in formation water (Figures 4.11 and 4.12). Beyond this region, ankerite, siderite, and magnesite precipitation were observed. Precipitation of pyrite reduces ankerite precipitation (Zhang et al., 2011). Overall, the mineral precipitation and dissolution are similar at temperatures of 40^0C (low temperature formation - the focus in the present study) and 100^0C. The

main difference is that calcite precipitated in the shale and impure limestone formations in the case of CO_2 alone sequestration.

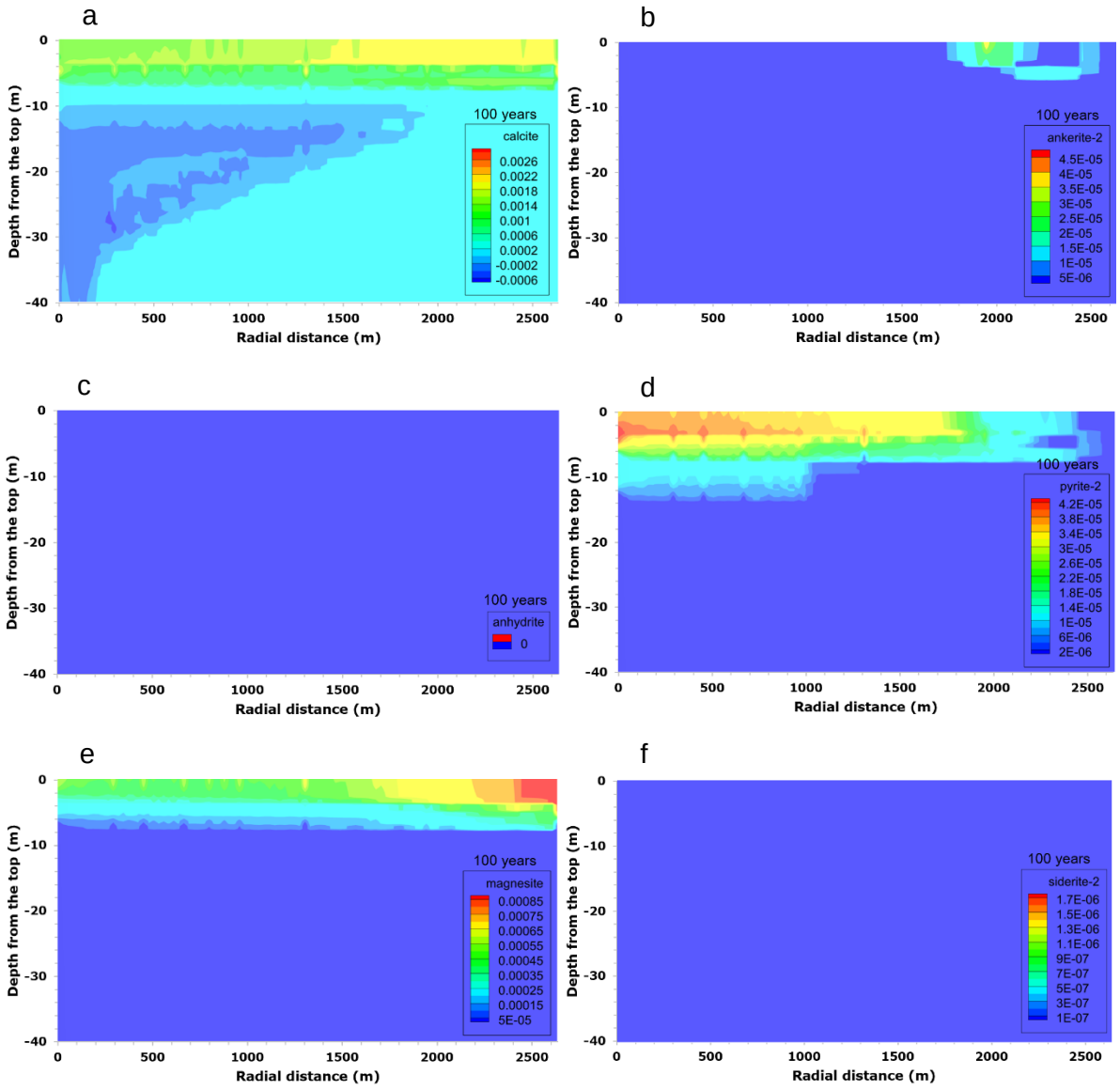

Figure 4.9: CO_2-H_2S co-injection case at 40^0C and 100 bar (a) calcite (b) ankerite (c) anhydrite (d) pyrite (e) magnesite (f) siderite.

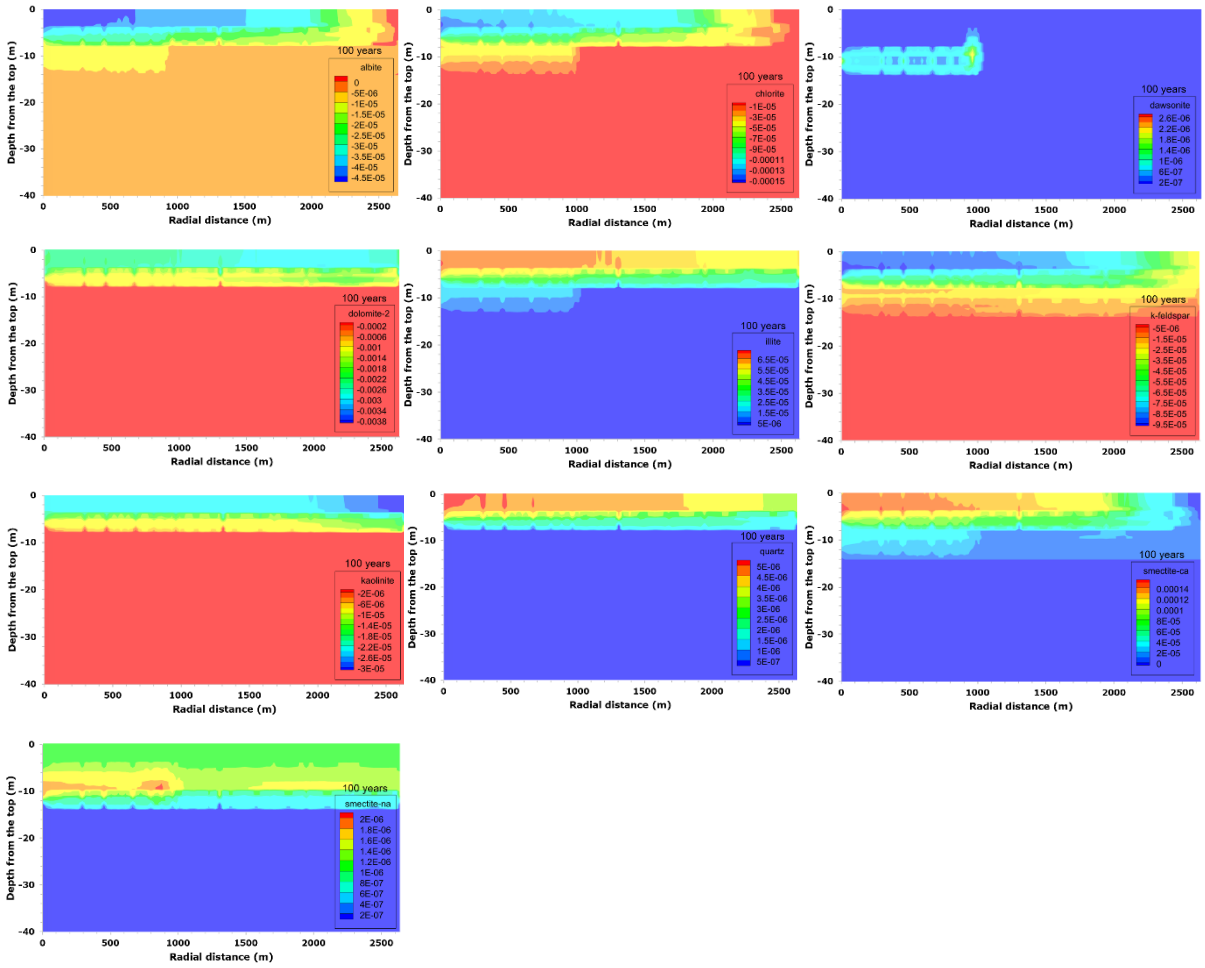

Figure 4.10: Dissolution and precipitation of other minerals (albite, chlorite, dawsonite, dolomite, illite, K-feldspar, kaolinite, quartz, smectite-Ca, and smectite-Na) in the formations for the CO_2-H_2S co-injection case at 40^0C and 100 bar.

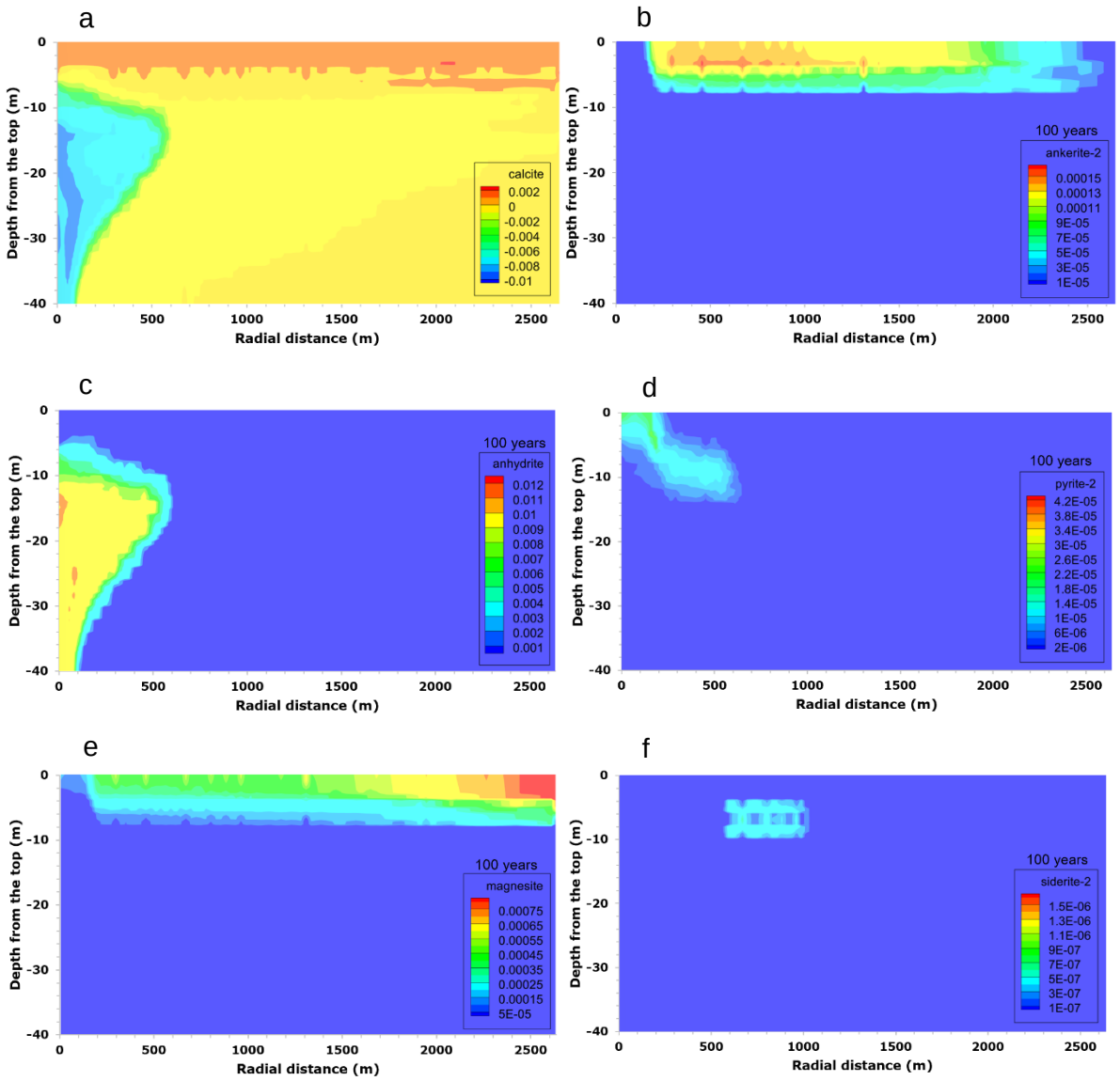

Figure 4.11: CO_2-SO_2 co-injection case at 40^0C and 100 bar (a) calcite (b) ankerite (c) anhydrite (d) pyrite (e) magnesite (f) siderite.

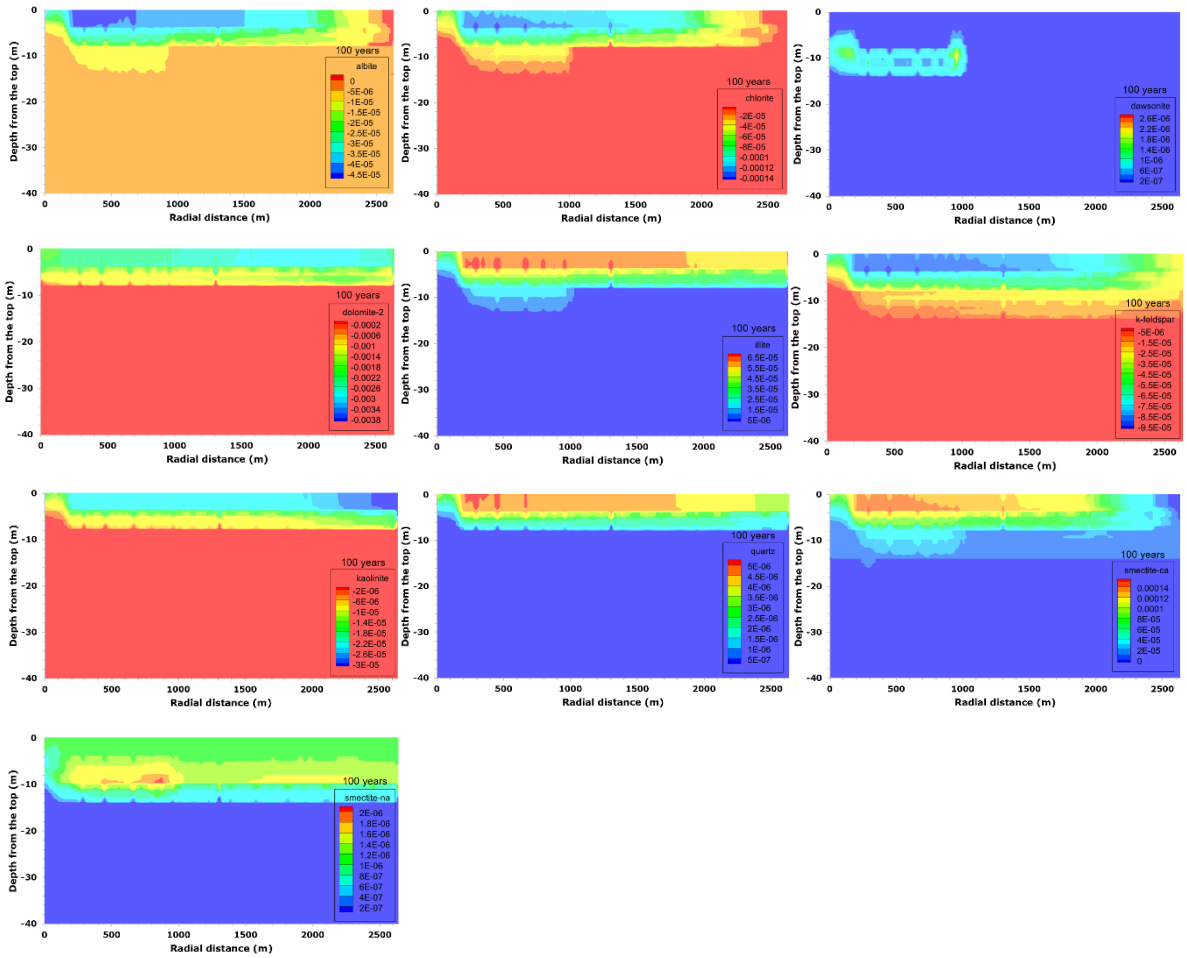

Figure 4.12: Dissolution and precipitation of other minerals (albite, chlorite, dawsonite, dolomite, illite, K-feldspar, kaolinite, quartz, smectite-Ca, and smectite-Na) in the formations for the CO_2-SO_2 co-injection case at 40^0C and 100 bar.

Changes in porosity are calculated from variations in the volume fraction of the minerals and presented in Table 4.1 and Figure 4.13. In the two-phase region, due to dominant mineral dissolution caused by low pH, porosity increases slightly in the shale and carbonate rocks, in the case of CO_2 alone and CO_2-H_2S co-injection, while in the case of CO_2-SO_2 co-injection, porosity increases only in the shale rock, and decreases in the carbonate rocks due to anhydrite precipitation. Outside the regions where SO_2 dissolved in the formation water in the carbonate rocks (pure limestone and impure limestone), an increase in porosity was observed. After 100 years of sequestration, the porosity of the carbonate rocks and shale caprock increased by 0.16% and 0.89% respectively, for the CO_2 alone case; and slightly increased by 0.17% and 0.91% respectively, for the CO_2-H_2S co-injection case. However, in the case of CO_2-SO_2 co-injection, the porosity of the carbonate rocks decreased by 0.58%, while the porosity of the shale caprock increased by 1.21%.

Table 4.1: Change in petrophysical properties of the formation at different times of CO_2 geosequestration at temperature and pressure of 40^0C and 100 bar, respectively.

Formation type	Petrophysics	After sequestration, t=100 years		
		CO_2	CO_2-H_2S	CO_2-SO_2
Shale	Percentage change in porosity (%)	0.63 - 0.89	0.63 - 0.91	0.63 - 1.21
	Percentage change in permeability (%)	1.97 - 2.81	2.01 - 2.93	2.01 - 3.86
Impure limestone	Percentage change in porosity (%)	0.10 - 0.11	0.11 - 0.12	-ve (0.48 - 0.58)
	Percentage change in permeability (%)	0.36 - 0.39	0.36 - 0.40	-ve (1.67 - 2.01)
Pure limestone	Percentage change in porosity (%)	0.12 - 0.16	0.12 - 0.17	-ve (0.35 - 0.50)
	Percentage change in permeability (%)	0.48 - 0.66	0.49 - 0.69	-ve (1.42 – 2.00)

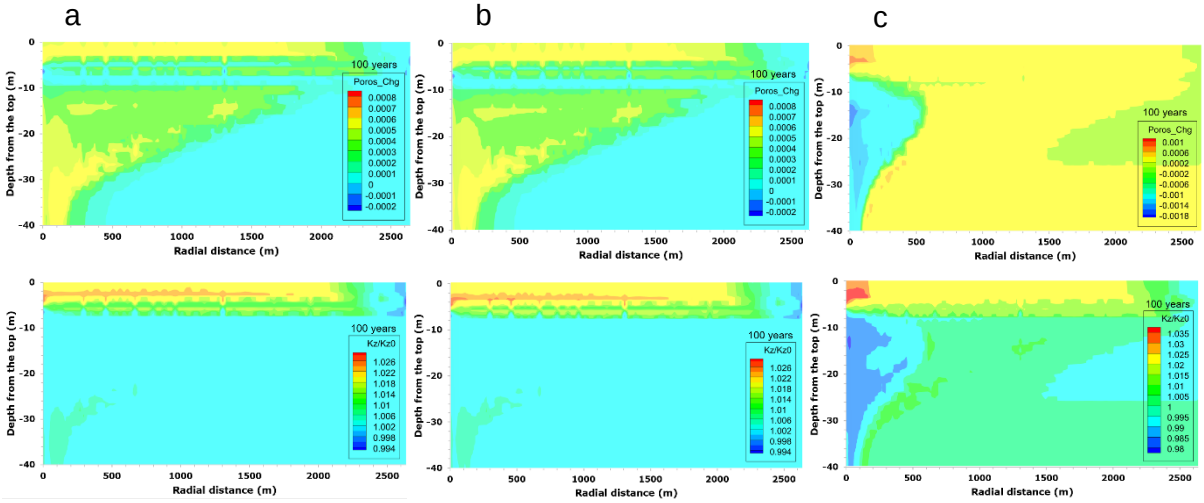

Figure 4.13: Porosity change and permeability ratio (a) CO_2 alone case (b) CO_2-H_2S case (c) CO_2-SO_2 case at 40^0C and 100 bar.

A similar trend in porosity was observed in the CO_2 sequestration cases at higher formation salinity and temperature. The difference is that the porosity of the shale caprock decreased during CO_2 sequestration as shown in Table 4.2 and Figure 4.14. Even though calcite precipitated in the impure limestone in the CO_2 alone case (Appendix A2) at high temperature and pressure conditions (and high formation salinity), porosity increased, since very little amount of calcite precipitated (dominated by dissolution of other minerals). So, at higher temperature (100^0C) and salinity (0.21), the porosity of the carbonate rocks increased by 0.06%, while the porosity of the shale caprock decreased by 7.44% for the CO_2 alone case. In the case of CO_2-SO_2 co-injection case, porosity decreased by 1.27% and 7.44% in the carbonate rocks and shale caprock, respectively. This implies that mainly CO_2 migrated to the caprock zone, SO_2 gas front hardly reached the shale formation as rapid dissolution of SO_2 occurs at high temperature and pressure

conditions. Kozeny-Carman model was used to calculate the corresponding changes in permeability. The trend of permeability variation is similar to that of porosity as shown in Table 4.2.

Table 4.2: Change in petrophysical properties of the formation at different times of CO_2 geosequestration at temperature and pressure of 100^0C and 137 bar, respectively.

Formation type	**Petrophysics**	**After sequestration, t=100 years**	
		CO_2	**CO_2-SO_2**
Shale	Percentage change in porosity (%)	-ve (0.64 - 7.44)	-ve (0.64 - 7.44)
	Percentage change in permeability (%)	-ve (2.02 - 21.58)	-ve (2.02 - 21.60)
Impure limestone	Percentage change in porosity (%)	0.008 – 0.01	-ve (0.04 – 0.33)
	Percentage change in permeability (%)	0.03 – 0.05	-ve (0.14 – 1.21)
Pure limestone	Percentage change in porosity (%)	0.01 – 0.06	-ve (0.63 - 1.27)
	Percentage change in permeability (%)	0.05 – 0.22	-ve (2.33 - 4.60)

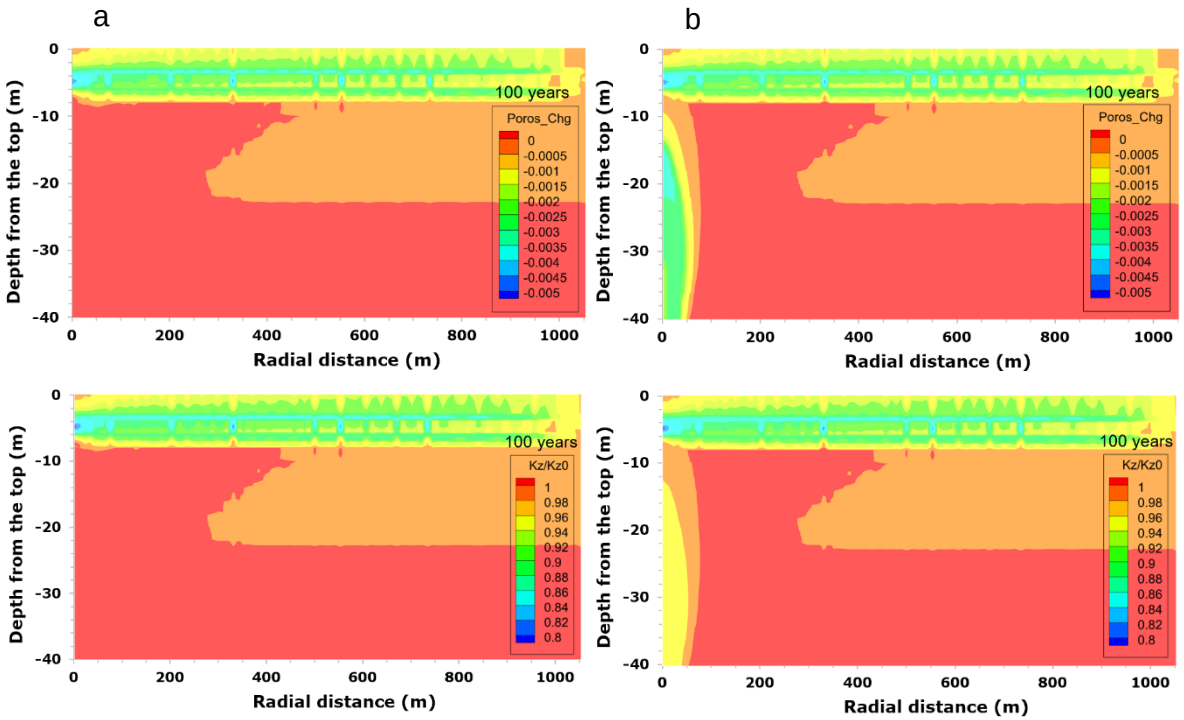

Figure 4.14: Porosity change and permeability ratio (a) CO_2 alone case (b) CO_2-SO_2 case at 100^0C and 137 bar.

Table 4.1 shows the permeability changes in the formations at 40^0C and 100 bar. After 100 years of sequestration, the permeability of the carbonate rocks and shale caprock increased by 0.66% and 2.81% respectively, for the CO_2 alone case; and slightly increased by 0.69% and 2.93% respectively, for the CO_2-H_2S co-injection case. However, in the case of CO_2-SO_2 co-injection,

the permeability of the carbonate rocks decreased by 2.01%, while the permeability of the shale caprock increased by 3.86%. A similar trend in permeability was observed in the CO_2 sequestration cases at higher formation salinity and temperature (Table 4.2). The difference is that the permeability of the shale caprock decreased during CO_2 sequestration. Even though calcite precipitated in the impure limestone in the CO_2 alone case at high temperature and pressure conditions (and high formation salinity), permeability increased, since very little amount of calcite precipitated (dominated by dissolution of other minerals). So, at a higher temperature (100^0C) and salinity (0.21), the permeability of the carbonate rocks increased by 0.22%, while the permeability of the shale caprock decreased by 21.58% for the CO_2 alone case. In the case of CO_2-SO_2 co-injection case, permeability decreased by 4.60% and 21.60% in the carbonate rocks and shale caprock, respectively.

4.1.2 Impact of impurities on porosity, permeability, and geochemical composition of reservoir and cap rocks during CO_2 injection and storage (Strategy 2)

In Strategy 2, carbonate reservoir with shale caprock and sandstone reservoir with shale caprock were considered separately. The fluid distributions and pH are similar to Strategy 1 for the different formation combinations considered. The gas saturations and gas fronts in the formations (reservoir rocks and shale caprock) are shown in Figures 4.15 and 4.16 and Figures 4.17 and 4.18, respectively. H_2S gas front in both the carbonate and sandstone reservoirs are similar. However, SO_2 gas mobilizes a longer lateral distance in the carbonate reservoir compared to the sandstone reservoir (Figures 4.17 and 4.18). It appears that SO_2 dissolves faster in formation brine in the sandstone reservoir, thereby limiting the amount of SO_2 gas that mobilizes laterally in the reservoir.

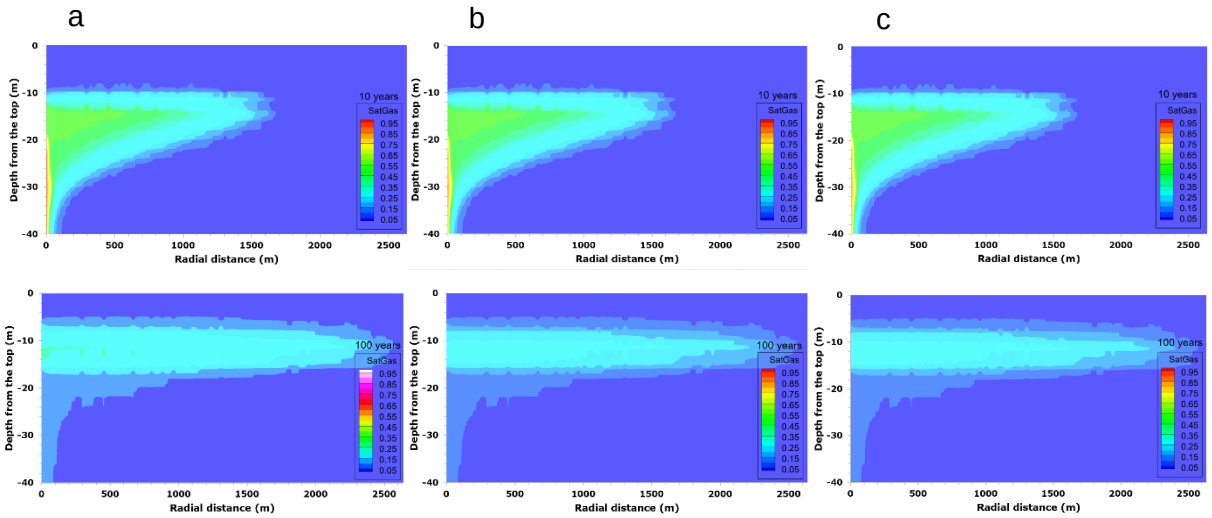

Figure 4.15: Gas saturation (Strategy 2) in the carbonate reservoir and shale caprock (a) CO_2 alone case (b) CO_2-H_2S case (c) CO_2-SO_2 case.

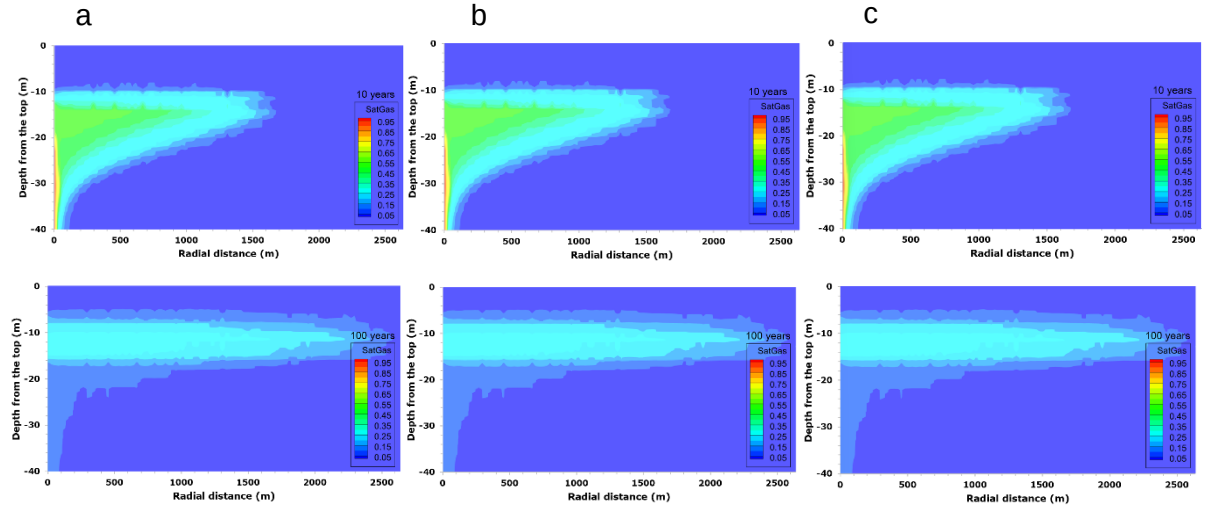

Figure 4.16: Gas saturation (Strategy 2) in the sandstone reservoir and shale caprock (a) CO_2 alone case (b) CO_2-H_2S case (c) CO_2-SO_2 case.

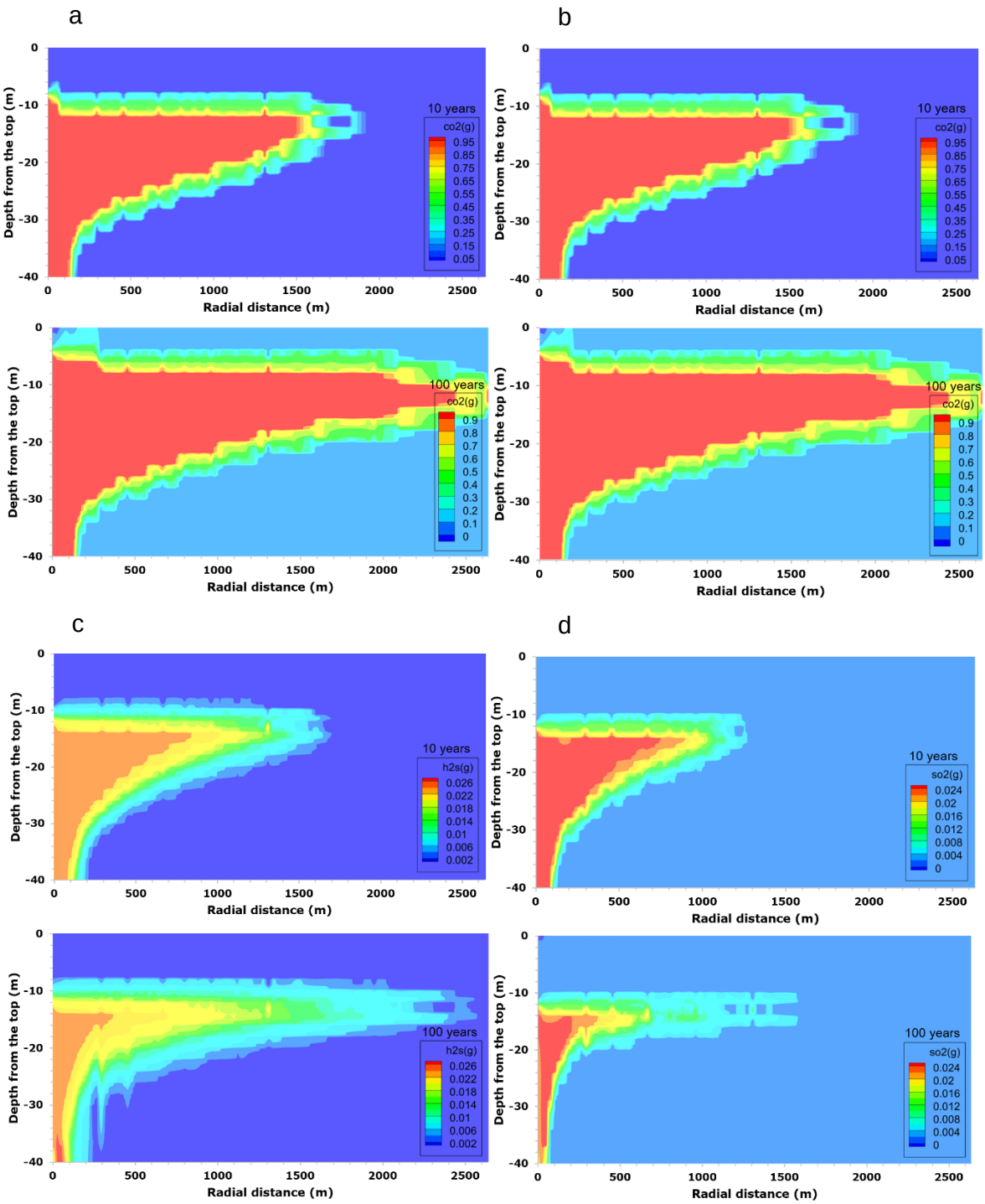

Figure 4.17: Gas front of (a) CO_2 in CO_2-H_2S (b) CO_2 in CO_2-SO_2 (c) H_2S (d) SO_2 in the carbonate reservoir and shale caprock.

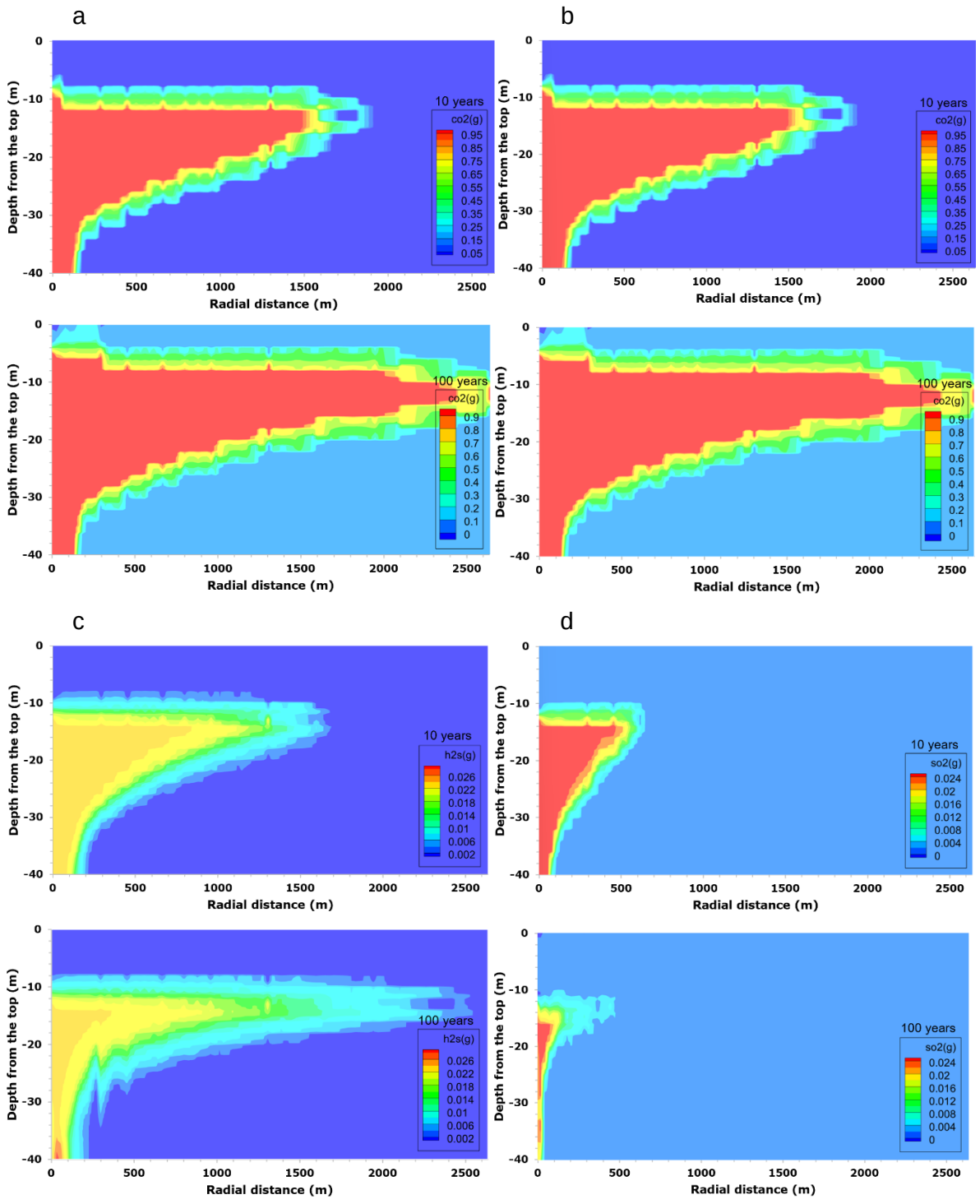

Figure 4.18: Gas front of (a) CO_2 in CO_2-H_2S(b) CO_2 in CO_2-SO_2 (c) H_2S (d) SO_2 in the sandstone reservoir and shale caprock.

The total dissolved carbon (TDC) in the carbonate reservoir (with calcite and dolomite minerals) for all the sequestration cases are similar. No notable delay in the dissolution of CO_2 in the co-injection cases. However, a notable delay in the dissolution of CO_2 in the sandstone formation brine for the CO_2-SO_2 co-injection case was observed a few metres (laterally) from the injection well (Figures 4.19 and 4.20). This can be ascribed to the rapid dissolution of SO_2 gas in the sandstone formation compared to the carbonate reservoir with calcite and dolomite minerals. Also more CO_2 dissolved in the sandstone formation compared to the carbonate reservoir due to the presence of adequate amount of Fe-bearing minerals and carbonate minerals in the sandstone formation.

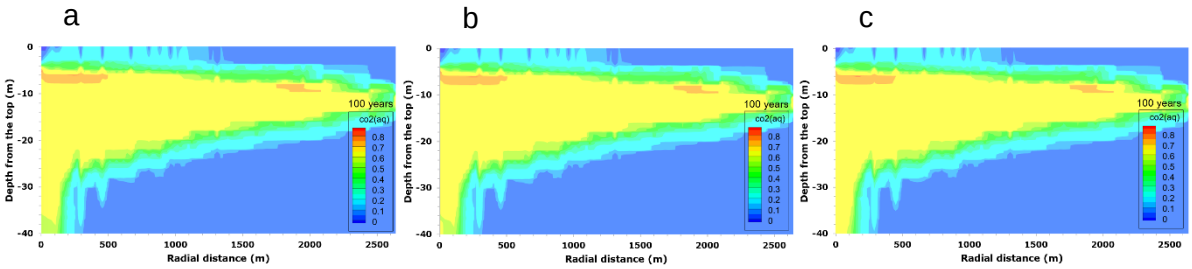

Figure 4.19:Total dissolved carbon in the carbonate reservoir and shale caprock for (a) CO_2 alone case (b) CO_2-H_2S case (c) CO_2-SO_2 case.

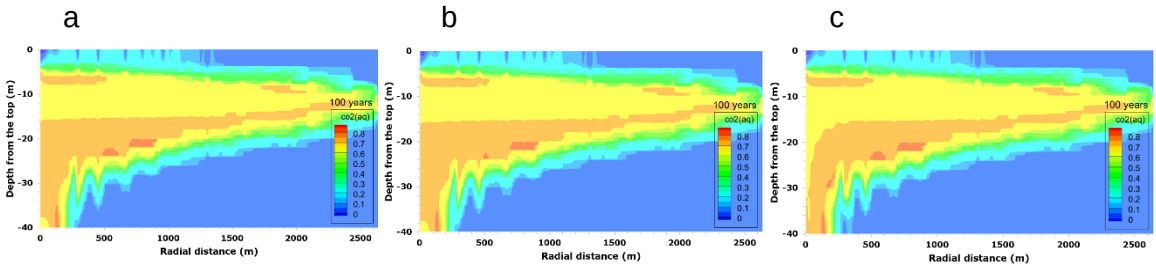

Figure 4.20: Total dissolved carbon in the sandstone reservoir and shale caprock for (a) CO_2 alone case (b) CO_2-H_2S case (c) CO_2-SO_2 case.

The formation fluid pH in the carbonate reservoir is higher than that of the sandstone reservoir after 100 years of CO_2 geosequestration for all the cases (Figures 4.21 and 4.22). Therefore, the reaction of the formation fluid with the rock minerals would be different for the carbonate and sandstone reservoirs.

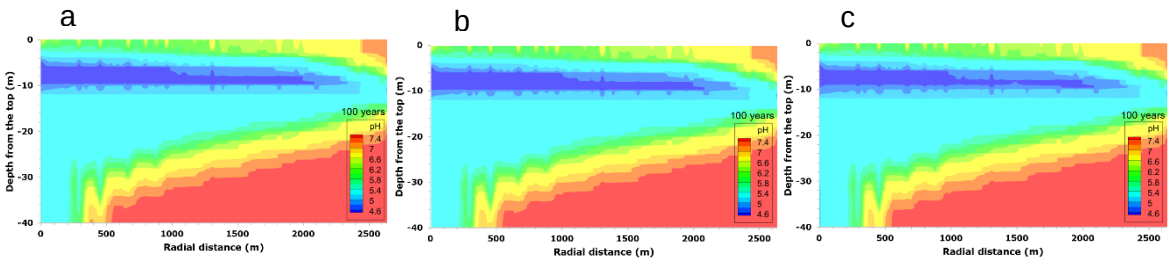

Figure 4.21: Formation fluid pH for (a) CO_2 alone case (b) CO_2-H_2S case (c) CO_2-SO_2 case in the carbonate reservoir and shale caprock.

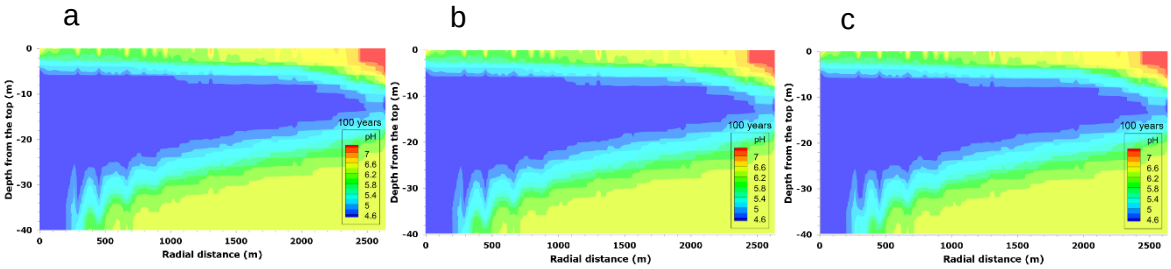

Figure 4.22: Formation fluid pH for (a) CO_2 alone case (b) CO_2-H_2S case (c) CO_2-SO_2 case in the sandstone reservoir and shale caprock.

In Strategy 2, for all the cases considered, dissolution and precipitation of minerals in the shale formation are similar (Figures 4.23 to 4.28). Calcite, anhydrite, albite, chlorite, illite, K-feldspar, and kaolinite dissolved in the shale formation; while ankerite, quartz, siderite, smectite-Ca, smectite-Na, and little amount of pyrite precipitated. In the sandstone formation, dissolution of calcite, albite, chlorite, K-feldspar, and kaolinite was observed; while illite, quartz, smectite-Ca, and smectite-Na precipitated (Figure 4.26). In addition, pyrite precipitated in the CO_2-H_2S and CO_2-SO_2 co-injection cases; while anhydrite precipitated only in the CO_2-SO_2 co-injection case (Figures 4.27 and 4.28). In the carbonate formation, initially composed of calcite and dolomite minerals only, dissolution of dolomite was observed in all the injection cases (Figures 4.23, 4.24, and 4.25). Calcite dissolution was observed near the injection zone for the CO_2-SO_2 case, where the concentration of dissolved SO_2 is higher, resulting in precipitation of anhydrite in that zone; while calcite precipitation was observed in the upper part of the reservoir (few metres above the injection zone). The dissolution of dolomite (increasing Mg^{2+} and Ca^{2+} concentration in the carbonate formation) resulted in precipitation of magnesite and calcite in the formation. Pyrite precipitation was only observed in the CO_2-H_2S and CO_2-SO_2 co-injection cases, although little amount as the Fe^{2+} concentration in the carbonate formation is low.

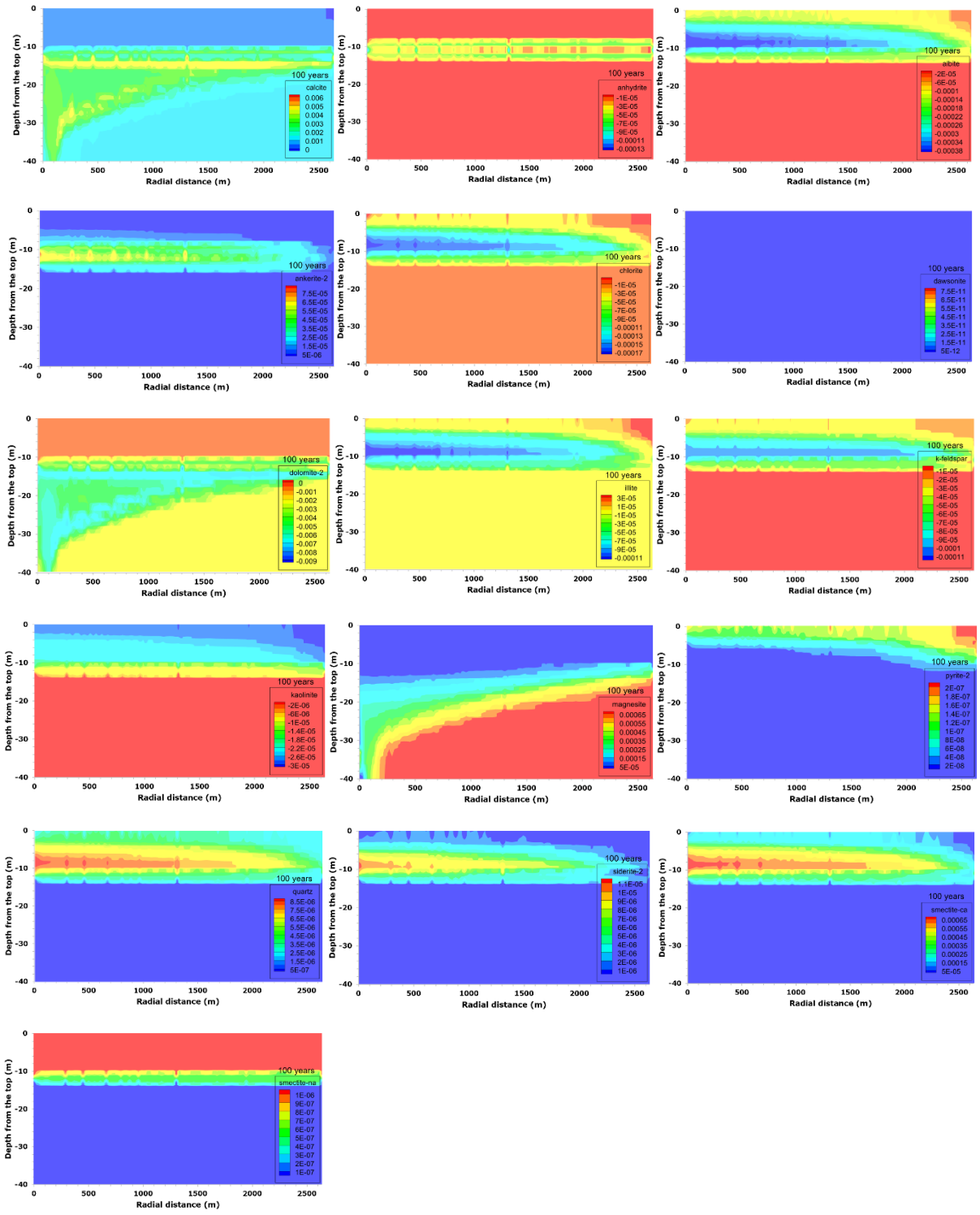

Figure 4.23: Mineral dissolution and precipitation in the carbonate reservoir and shale caprock for the CO_2 alone case.

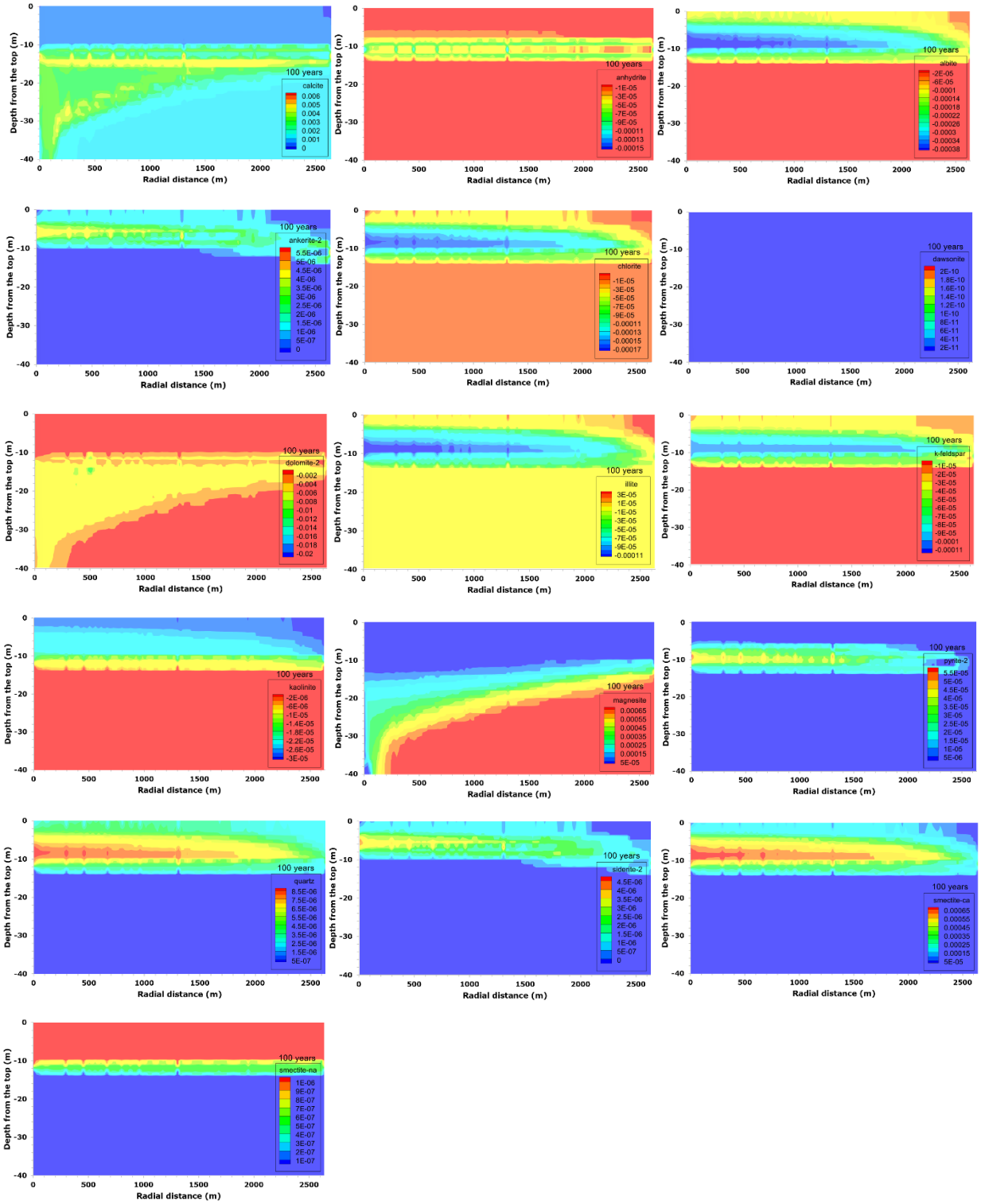

Figure 4.24: Mineral dissolution and precipitation in the carbonate reservoir and shale caprock for the CO_2-H_2S case.

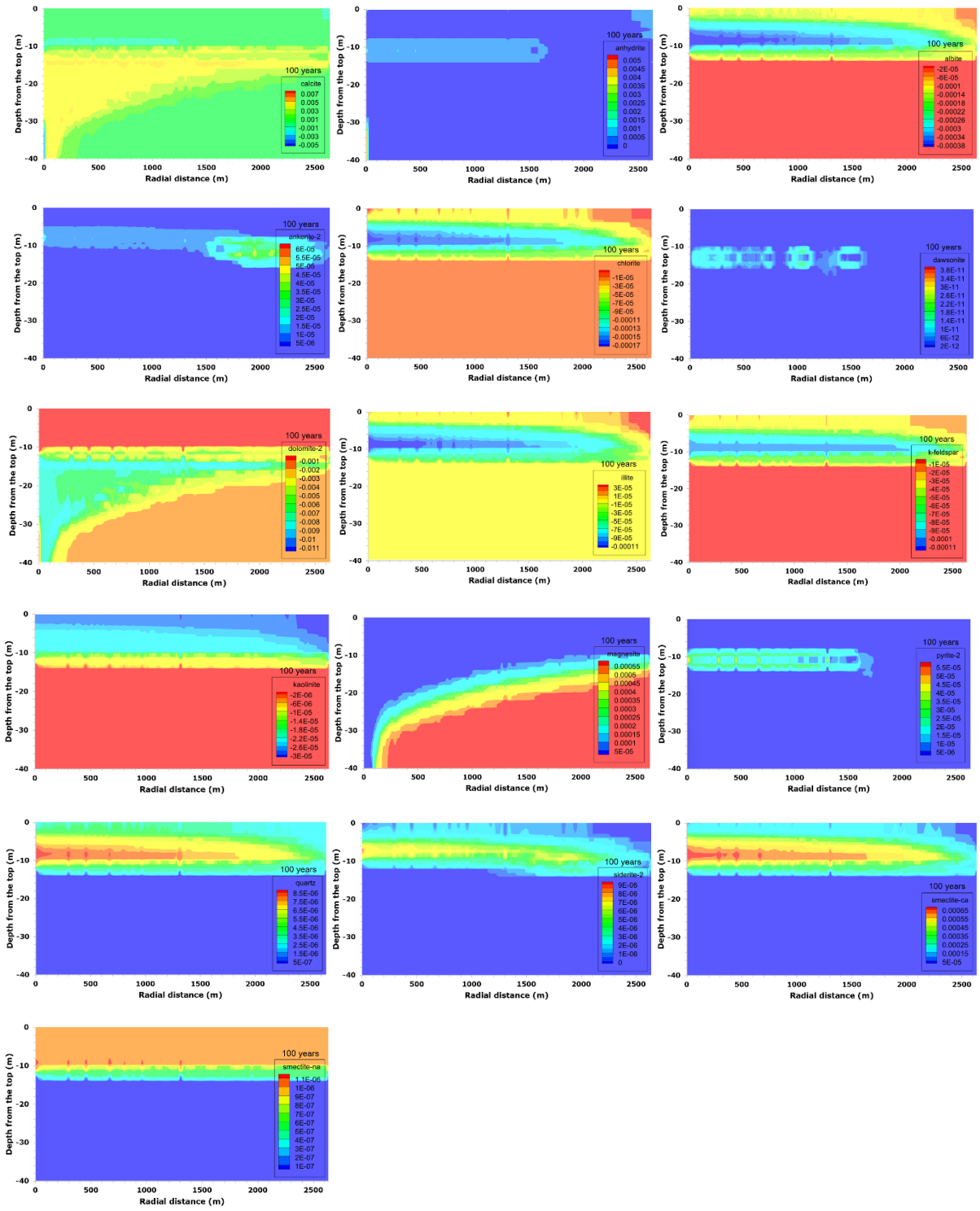

Figure 4.25: Mineral dissolution and precipitation in the carbonate reservoir and shale caprock for the CO_2-SO_2 case.

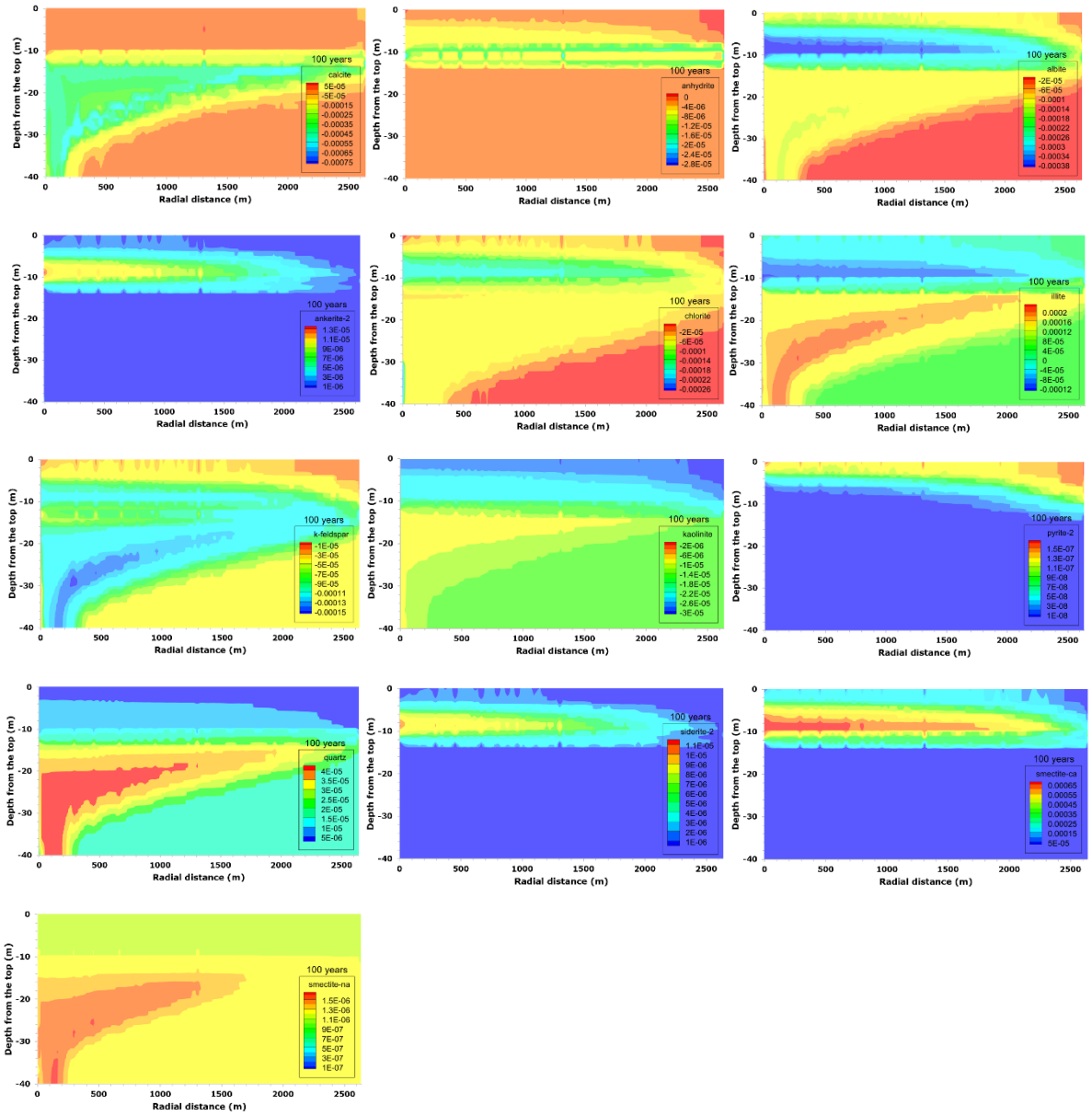

Figure 4.26: Mineral dissolution and precipitation in the sandstone reservoir and shale caprock for the CO_2 alone case.

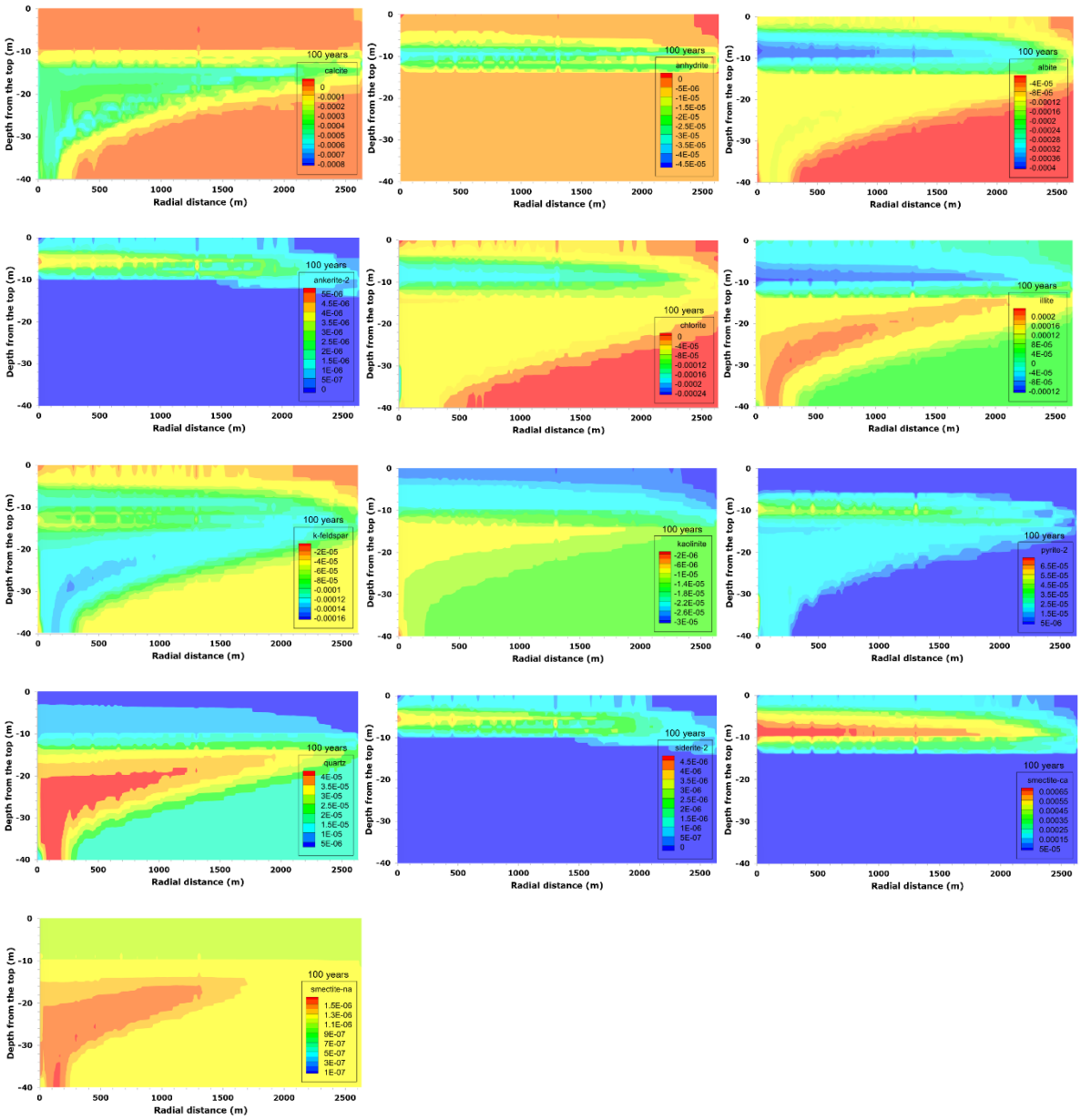

Figure 4.27: Mineral dissolution and precipitation in the sandstone reservoir and shale caprock for the CO_2-H_2S case.

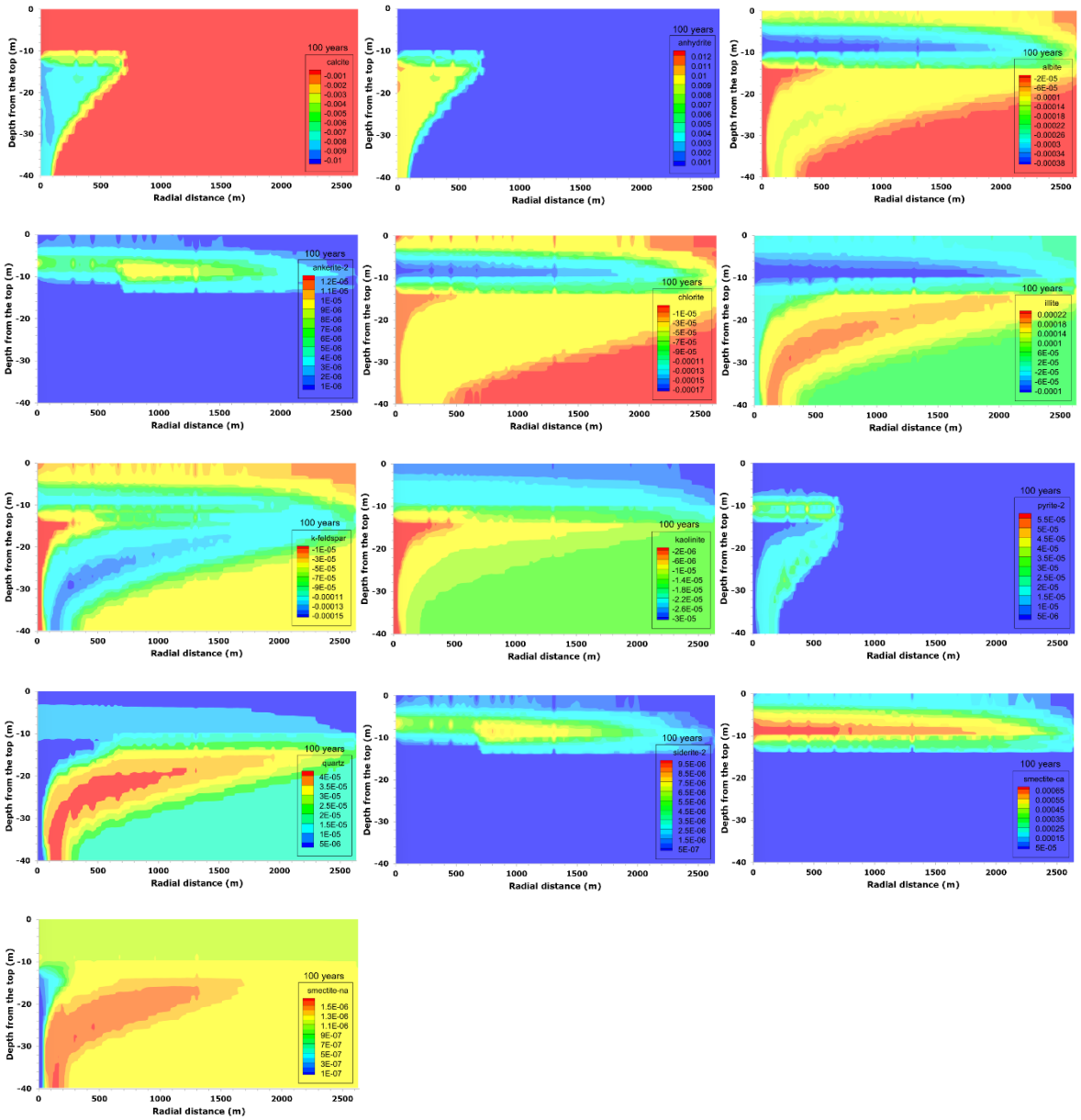

Figure 4.28: Mineral dissolution and precipitation in the sandstone reservoir and shale caprock for the CO_2-SO_2 case.

Changes in porosity of the formations are calculated from variations in the volume fraction of the minerals. Table 4.3 shows that porosity and permeability increased slightly in the shale formation (read from the results of the carbonate reservoir and shale caprock numerical simulation group), but increased significantly in the carbonate formation (due to large amount of dolomite dissolution) for all the cases considered (Figure 4.29) in Strategy 2 (permeability increase between 0.59 – 5.68%). In the sandstone formation (Figure 4.30), porosity and permeability only increased for the CO_2 alone and CO_2-H_2S injection cases (permeability increases between 0.23 – 1.09%). Precipitation of anhydrite (few metres from the injection well over the entire height of the

sandstone formation) for the CO_2-SO_2 co-injection case resulted in decrease in porosity and permeability in the region where SO_2 dissolved in formation water (permeability decreases up to 2.40%). Farther away from the injection well, porosity and permeability of the reservoir increased as more CO_2 dissolved in the formation water (very little or no concentration of SO_2 in the formation water in that region).

Table 4.3: Change in petrophysical properties of the formation after 100 years of CO_2 geosequestration at temperature and pressure of 40^0C and 100 bar, respectively (Strategy 2).

Formation type	**Petrophysics**	**After sequestration, t=100 years**		
		CO_2	**CO_2-H_2S**	**CO_2-SO_2**
Shale	Percentage change in porosity (%)	-0.07 - 0.13	-0.07 – 0.16	-0.49 – 0.11
	Percentage change in permeability (%)	-0.20 - 0.39	-0.20 – 0.47	-1.50 – 0.34
Sandstone	Percentage change in porosity (%)	0.07 – 0.27	0.06 – 0.25	-ve (0.29 - 0.61)
	Percentage change in permeability (%)	0.28 – 1.09	0.23 – 1.02	-ve (1.18 - 2.40)
Carbonate	Percentage change in porosity (%)	0.21 – 0.76	0.15 – 1.00	0.08 – 1.38
	Percentage change in permeability (%)	0.84 -3.11	0.59 – 4.10	0.32 – 5.68

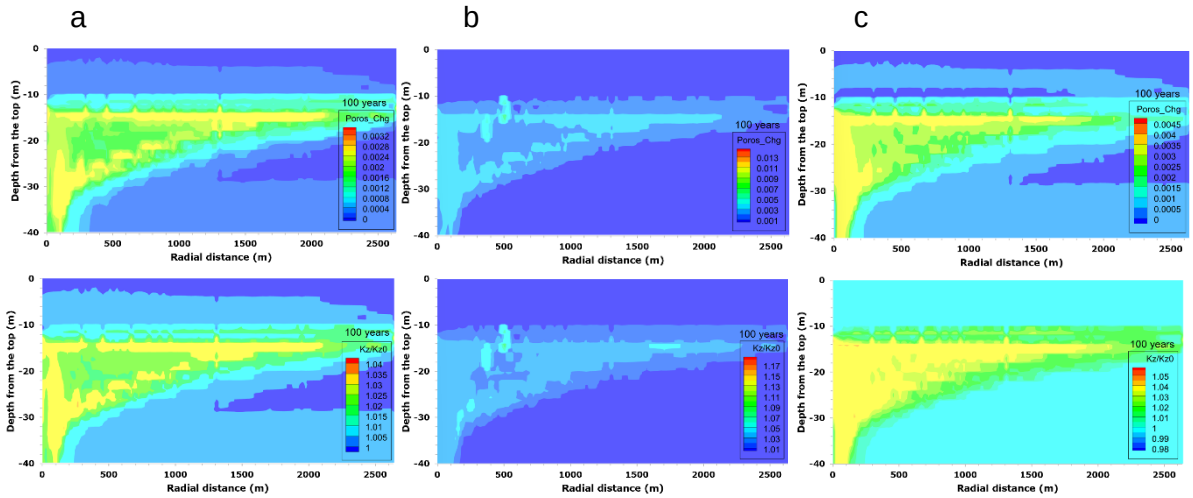

Figure 4.29: Porosity change and permeability ratio (Strategy 2) in the carbonate reservoir and shale caprock (a) CO_2 alone case (b) CO_2-H_2S case (c) CO_2-SO_2 case.

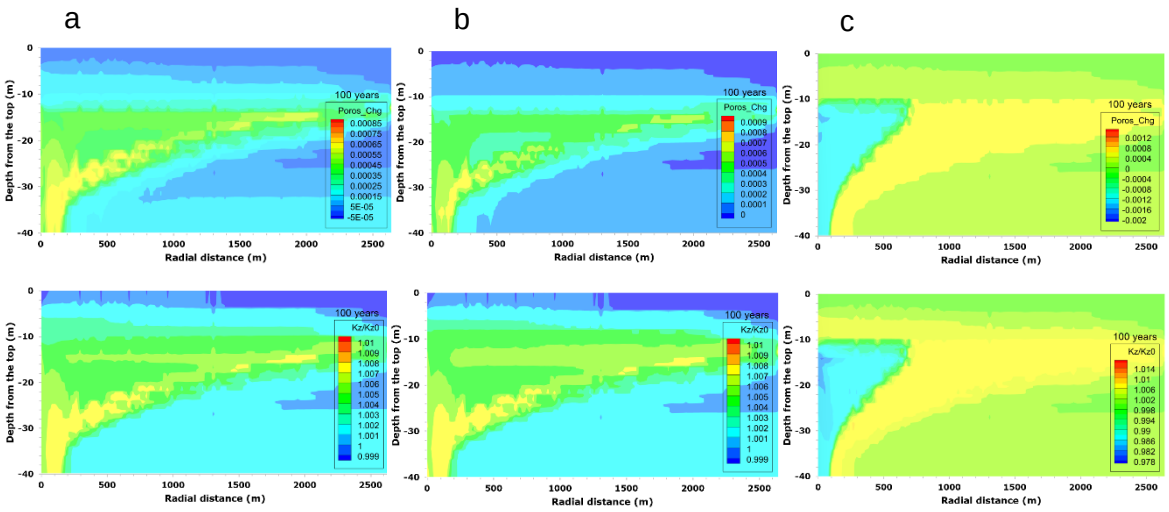

Figure 4.30: Porosity change and permeability ratio (Strategy 2) in the sandstone reservoir and shale caprock (a) CO_2 alone case (b) CO_2-H_2S case (c) CO_2-SO_2 case.

4.1.3 Impact of impurities on porosity, permeability, and geochemical composition of reservoir and cap rocks during CO_2 injection, withdrawal, and storage (Strategy 3)

CO_2 gas is injected or co-injected with H_2S (or SO_2) near the bottom of the sandstone reservoir and withdrawn near the top of the reservoir, in a cyclic process (over a total of seven cycles). The injected fluid migrates rapidly upward by buoyant forces. After every cycle of injection, a small fraction of CO_2 gas is trapped in the reservoir as residual gas; while the mobile gas continues to migrate into the shale caprock by the action of buoyant forces. At the same time, some amount of the gas continues to dissolve into brine (formation water), resulting in precipitation of minerals. Hence, the residual gas slowly disappears at the bottom of the reservoir. After some time, most of the free CO_2 gas accumulates in the shale caprock layers, few metres from the reservoir-caprock interface, and spreads laterally. Similar to the non-cyclic process (Strategies 1 and 2), the front of SO_2 gas is far behind that of CO_2 gas compared to the front of H_2S gas with respect to CO_2 gas as shown in Figure 4.31. Hence, the solubility of SO_2 gas in formation water is higher than that of H_2S and CO_2. However, some amount of H_2S gas and SO_2 gas remain in the reservoir even after the seventh cycle, as they continue to be replenished due to the cyclic injection process (Figure 4.32).

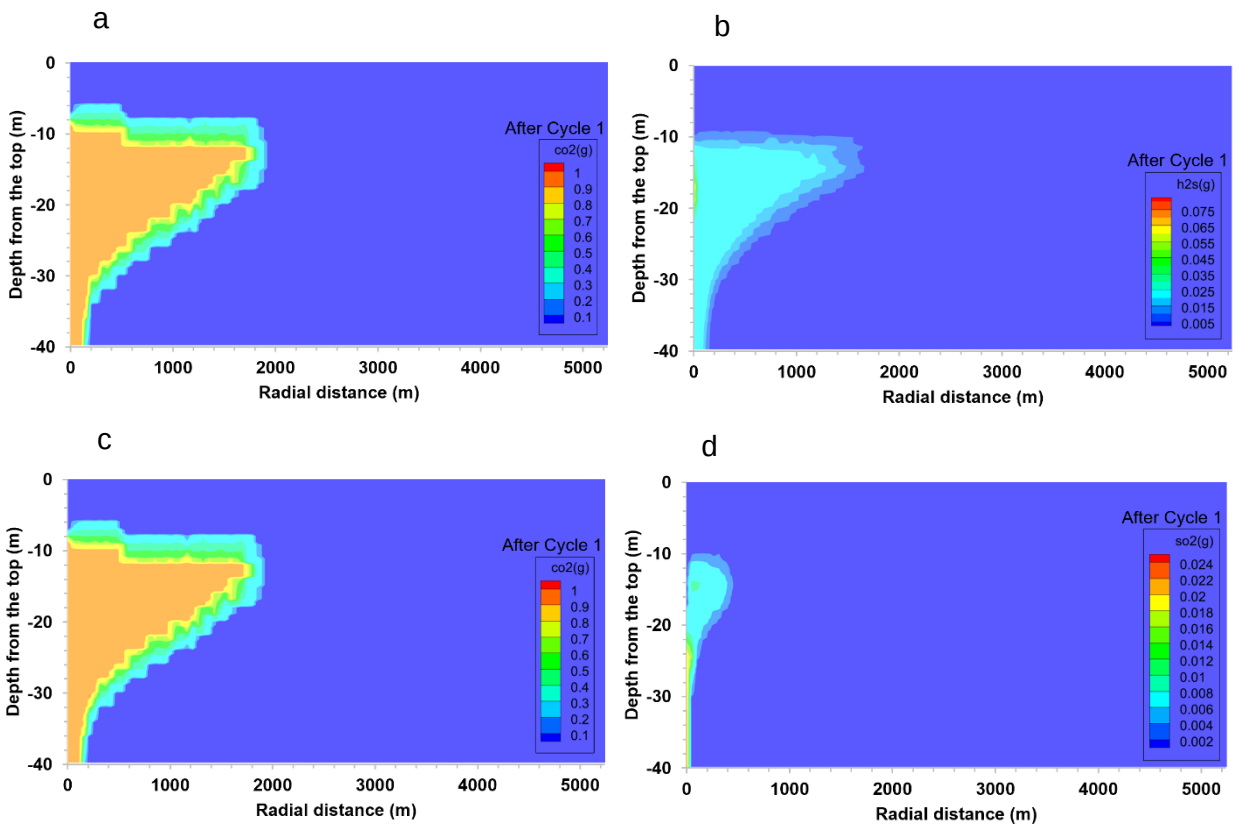

Figure 4.31: Gas front of (a) CO_2 in CO_2-H_2S(b) CO_2 in CO_2-SO_2 (c) H_2S (d) SO_2 in cyclic process.

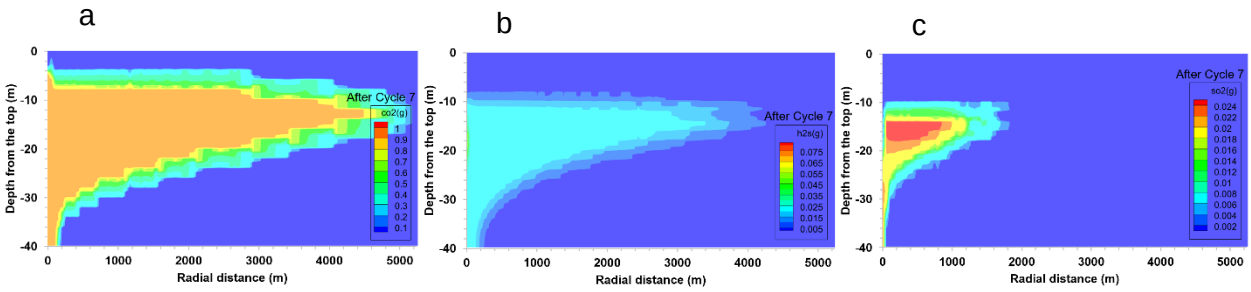

Figure 4.32: (a) CO_2 gas (b) H_2S gas (c) SO_2 gas in the formation after seven cyclic injection-withdrawal process.

Figure 4.32 shows that H_2S gas hardly penetrated up to 4m vertical thickness of the shale caprock, while SO_2 gas only penetrated up to 2m vertical thickness of the caprock after seven (7) cyclic injection-withdrawal of CO_2 stream. Only CO_2 gas penetrated over 8m vertical thickness of the shale caprock during the period of geosequestration.

There is no notable difference in the distribution of total dissolved carbon (TDC) after seven cyclic injection-withdrawal process of fluid, as the initially displaced formation water during supercritical fluid injection flows towards the injection-production well to provide sufficient pressure needed for the gas production. Thus, convective mixing of the CO_2 with formation water during the withdrawal process makes the TDC for all the injection cases similar. The concentration of dissolved CO_2 increases up to 0.9 mol/kg H_2O in the two-phase region due to the CO_2 gas migration (Figure 4.33). The dissolution of the injected CO_2 (with or without cases of H_2S or SO_2 gas co-injection) in the surrounding formation water yields H_2CO_3, HCO_3^-, and CO_3^{2-}, and decreases pH (increases acidity). The pH profiles of all the injection cases are similar, as shown in Figure 4.34. However, for the CO_2-SO_2 co-injection case, the pH of the reservoir at and near the perforations in the production zone is relatively very low compared to the other injection cases. This could be attributed to severe calcite dissolution in those regions resulting in very low pH. In other regions of the formations, the pH values are similar for all the injection cases.

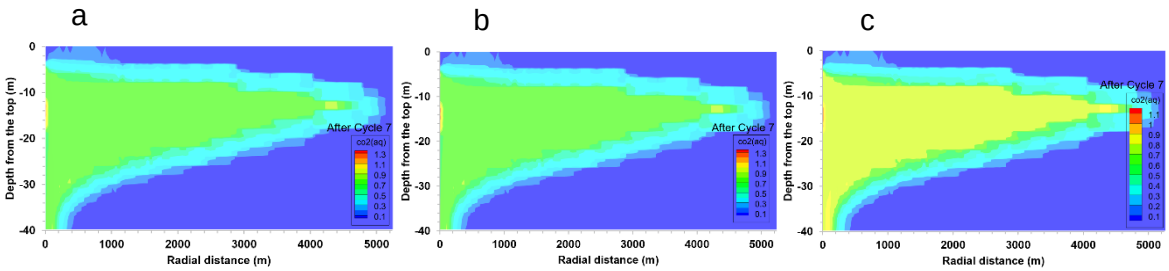

Figure 4.33: TDC for (a) CO_2 alone case (b) CO_2-H_2S case (c) CO_2-SO_2 case in the formation after seven (7) cyclic injection-withdrawal process.

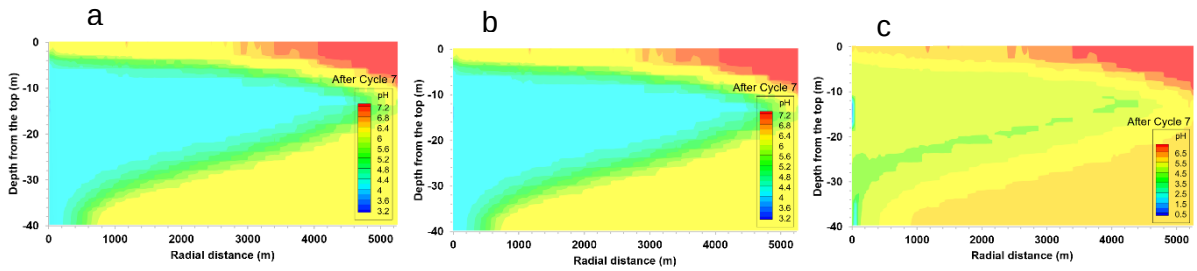

Figure 4.34: pH for (a) CO_2 alone case (b) CO_2-H_2S case (c) CO_2-SO_2 case in the formation after seven (7) cyclic injection-withdrawal process.

The low pH induces the dissolution and precipitation of minerals. Minerals such as anhydrite, albite, chlorite, illite, K-feldspar, and kaolinite in the shale formation dissolve in the two-phase region and near the front of the single aqueous-phase zone; while calcite, albite, chlorite, and K-

feldspar in sandstone reservoir dissolve in the two-phase region and near the front of the single aqueous-phase zone. On the other hand, calcite, ankerite, quartz, siderite, smectite-Ca, smectite-Na, and small amounts of hematite and pyrite precipitated in the shale caprock; while illite, kaolinite, quartz, and smectite-Na precipitated in the sandstone reservoir during the cyclic injection and withdrawal of CO_2 (Figures 4.35 to 4.38). For CO_2-H_2S co-injection case, pyrite precipitated in the sandstone reservoir and shale caprock; while for the CO_2-SO_2 co-injection case, anhydrite, pyrite, and a small amount of dawsonite precipitated in the shale and sandstone formations. A very large amount of calcite dissolved in the CO_2-SO_2 case compared to the other injection cases. In fact, complete to significant dissolution of calcite mineral was observed at and near the perforations in the production zone for all the injection cases. Thus, erosion of the calcite mineral during CO_2 withdrawal resulted in the deposition of some of the calcite mineral in reservoir layers directly below the perforation interval in the production zone. Consequently, the porosity of those few reservoir layers directly below the perforation interval in the production zone decreased during the CO_2 geosequestration. Moreover, the large amount of calcite dissolution at and near the perforation interval of the production zone, resulted in significant precipitation of anhydrite in that region for the CO_2-SO_2 co-injection case. Changes in the composition (volume fraction of the solid rock) of calcite, anhydrite, and pyrite during the cyclic process of the CO_2 geosequestration are shown in Figure 4.35.

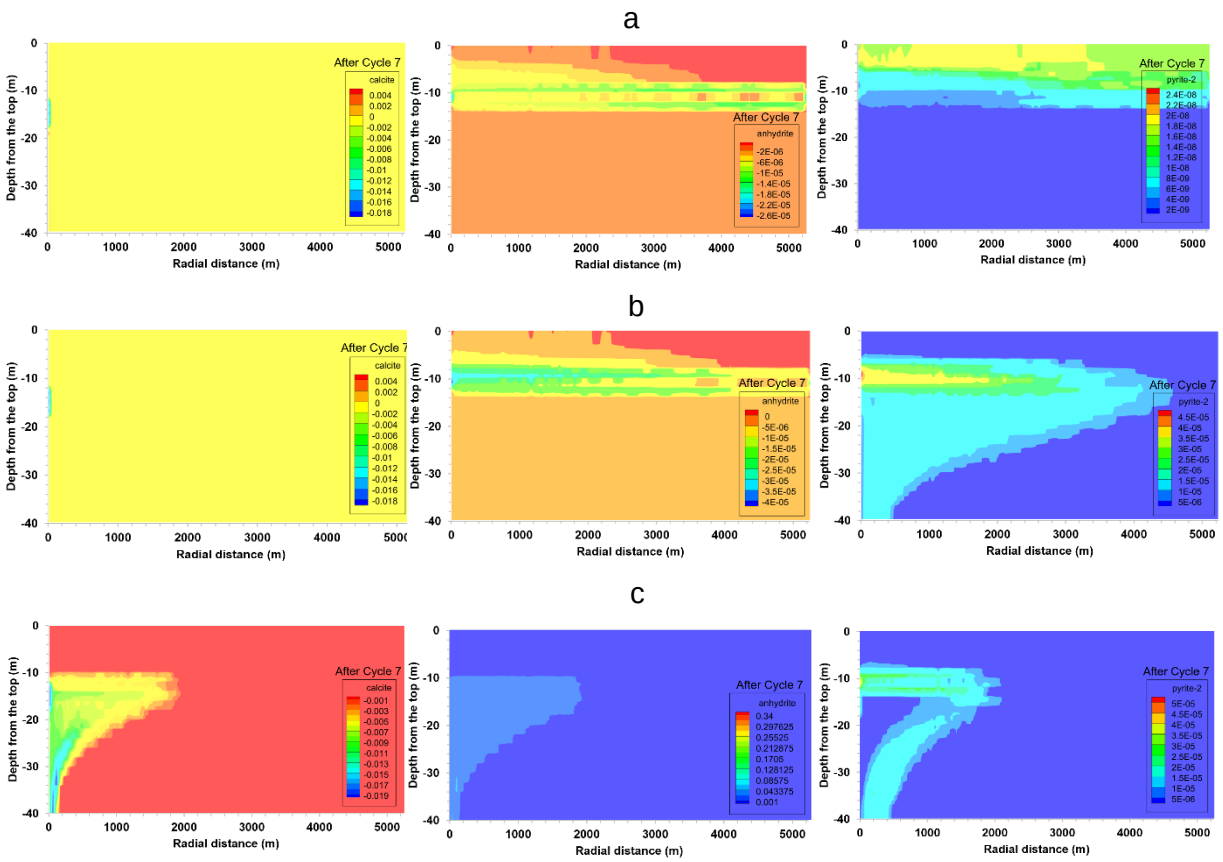

Figure 4.35: Changes in calcite, anhydrite, and pyrite composition for (a) CO_2 alone (b) CO_2-H_2S (c) CO_2-SO_2 injection cases in the formations after seven (7) cyclic injection-withdrawal process.

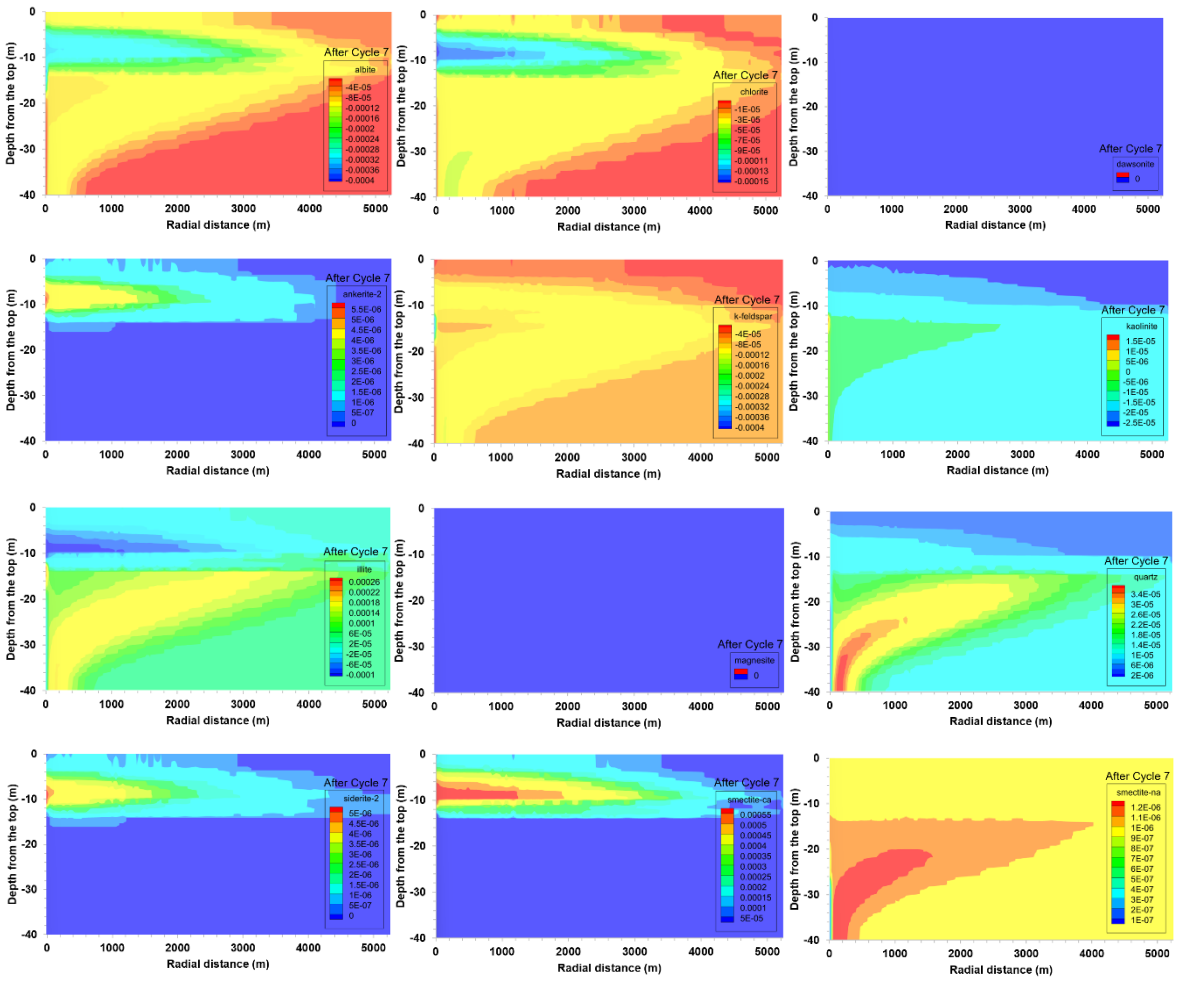

Figure 4.36: Mineral dissolution and precipitation in the sandstone reservoir and shale caprock for the CO_2 alone case after seven (7) cycles of injection and withdrawal.

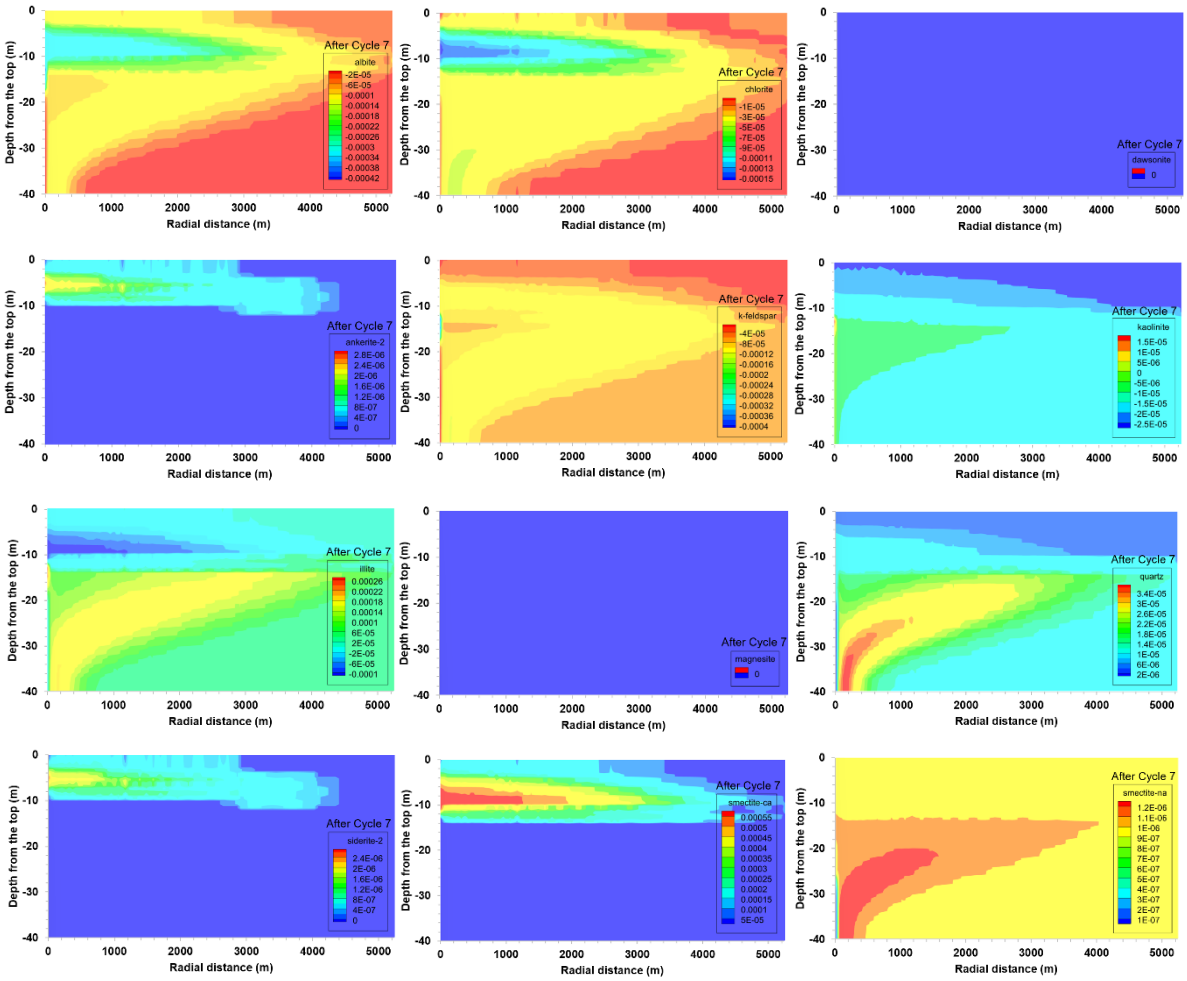

Figure 4.37: Mineral dissolution and precipitation in the sandstone reservoir and shale caprock for the CO_2-H_2S case after seven (7) cycles of injection and withdrawal.

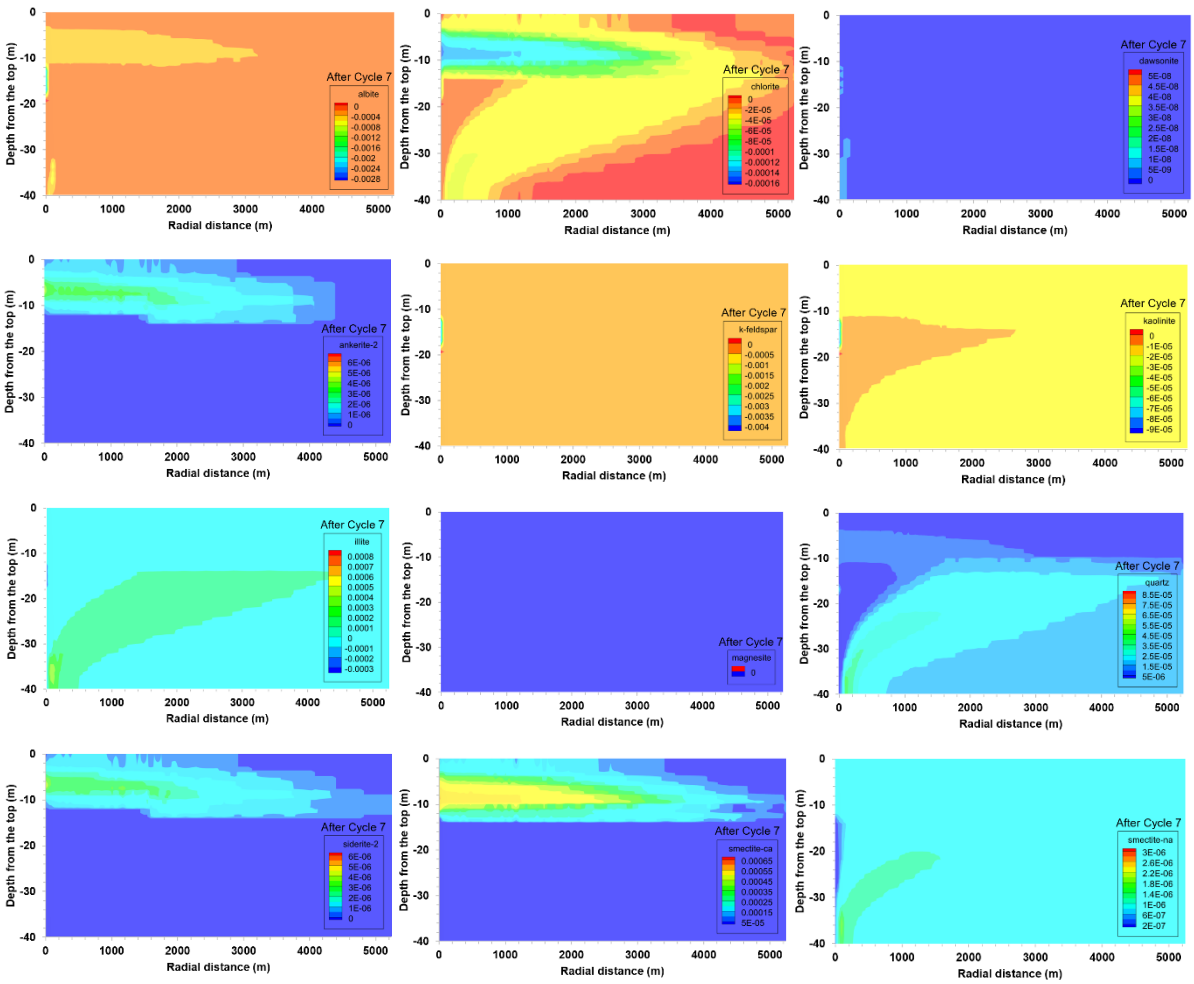

Figure 4.38: Mineral dissolution and precipitation in the sandstone reservoir and shale caprock for the CO_2-SO_2 case after seven (7) cycles of injection and withdrawal.

Changes in porosity are calculated from variations in the volume fraction of the minerals, while the permeability ratios are calculated by the changes in the porosity using the Kozeny-Carman relation. In the two-phase region, due to dominant mineral dissolution caused by low pH, porosity increases slightly in the shale and sandstone rocks, in the cases of CO_2 alone and CO_2-H_2S co-injection, while in the case of CO_2-SO_2 co-injection, porosity increases in most part of the shale rock (except in the layer contacted by SO_2 and where anhydrite precipitated) and decreases in the sandstone reservoir due to anhydrite precipitation.

For the CO_2-SO_2 co-injection case, at the perforations in the production zone, the reservoir porosity increased and it is between 0.3612-0.36672, while in every other regions where SO_2 dissolved in water, porosity decreased (the lowest porosity observed is 0.32496). Beyond the regions contacted by SO_2 (mainly dissolved CO_2), porosity increased up to 0.34891 (the corresponding permeability increase is 11.05%). In the caprock, porosity decreased in the layer

of the shale caprock contacted by SO_2 (about 2 m vertical thickness); in other areas of the caprock contacted mainly by CO_2, porosity increased slightly. For the CO_2-H_2S co-injection case, at the perforations in the production zone, porosity increased (between 0.36018-0.36031). From the lower perforation layer at the perforation zone down to 2-6 m vertical thickness and up to about 7 m lateral distance in the reservoir, porosity decreased. This decrease in porosity can be attributed to the deposition of fines or minerals due to the erosion of some minerals or rock materials in the production zone during CO_2 gas withdrawal from the perforation interval. However, porosity increased in other areas contacted by CO_2. Similarly, for the CO_2 alone case, at the perforations in the production zone, porosity increased (between 0.36019-0.36032). From the lower perforation layer at the perforation zone down to 2-6 m vertical thickness and up to about 9 m lateral distance in the reservoir, porosity decreased, while porosity increased in other areas contacted by CO_2. In all the injection cases, the porosity and permeability of that shale caprock decreased slightly in the regions that were not contacted by any of the gases. The changes in porosity and permeability of the formations are shown in Figure 4.39.

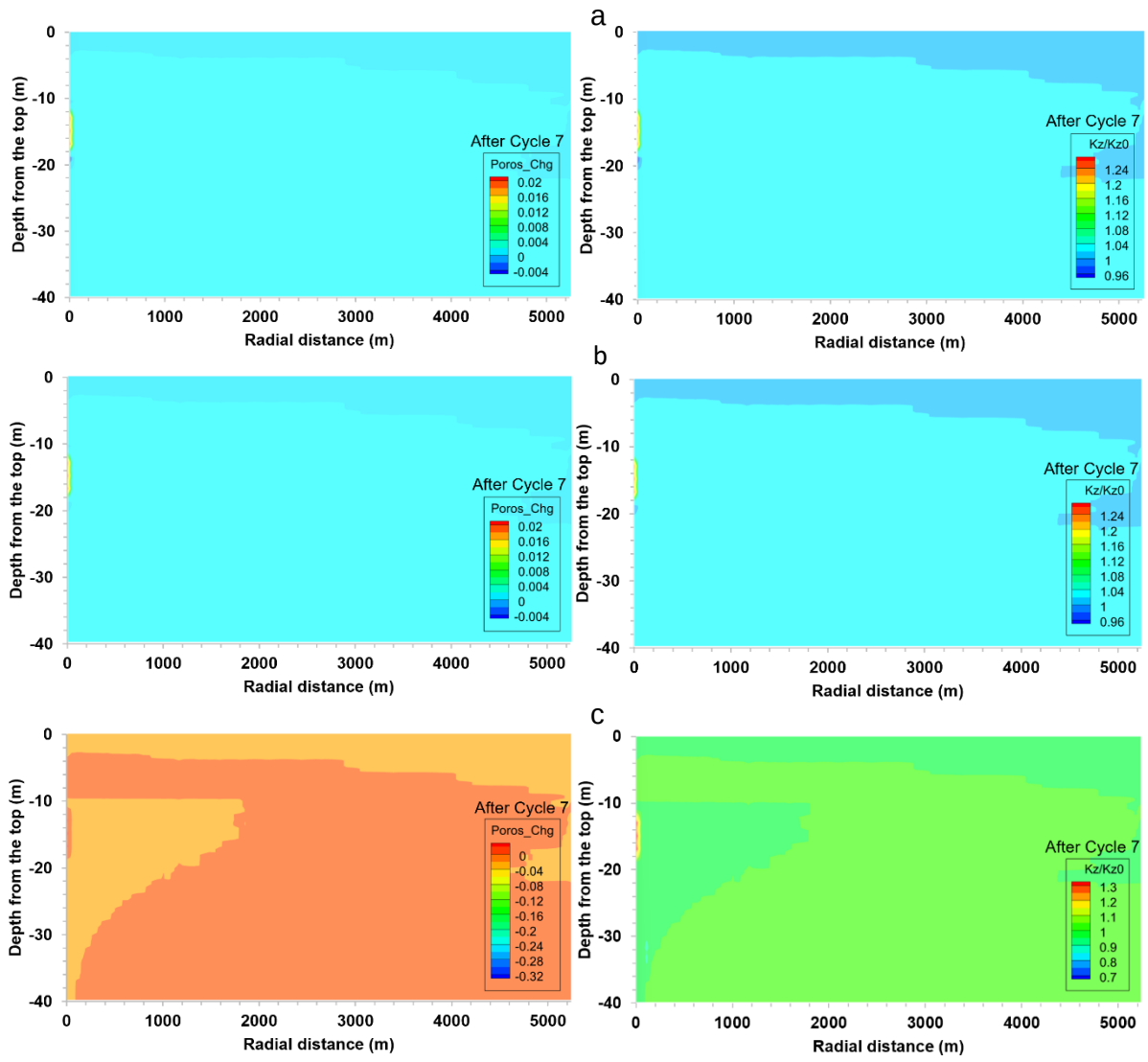

Figure 4.39: Porosity changes and permeability ratios for (a) CO_2 alone (b) CO_2-H_2S (c) CO_2-SO_2 injection cases in the formations after seven (7) cyclic injection-withdrawal process.

After seven (7) cycles of CO_2 injection and withdrawal, for the CO_2 alone case, the maximum increase in porosity is 0.19% and 5.98% (corresponding to permeability increase of 0.59% and 26.70%) in the shale caprock and sandstone reservoir, respectively; while the maximum decrease in porosity is 0.03% and 1.56% (corresponding to permeability decrease of 0.10% and 6.12%) in the caprock and reservoir, respectively (Table 4.4). Similarly, for the CO_2-H_2S co-injection case, the maximum increase in porosity is 0.21% and 5.97% (corresponding to permeability increase of 0.66% and 26.68%) in the shale caprock and sandstone reservoir, respectively; while the maximum decrease in porosity is 0.03% and 1.54% (corresponding to permeability decrease of 0.10% and 6.06%) in the caprock and reservoir, respectively. In the case of CO_2-SO_2 co-injection,

the maximum increase in porosity is 0.13% and 7.86% (corresponding to permeability increase of 0.40% and 36.29%) in the shale caprock and sandstone reservoir, respectively; while the maximum decrease in porosity is 0.3% and 4.42% (corresponding to permeability decrease of 0.92% and 16.54%) in the caprock and reservoir, respectively. The significant decrease in porosity in the CO_2-SO_2 co-injection case can be attributed to the precipitation of anhydrite. Also, the significant increase in porosity at the perforations in the production zone can be attributed to the severe calcite dissolution in the CO_2-SO_2 co-injection case.

Table 4.4: Changes in porosity and permeability of the formations after seven (7) cycles of CO_2 injection and withdrawal (Strategy 3).

Formation type	Petrophysics	After Cycle 7		
		CO_2	CO_2-H_2S	CO_2-SO_2
Shale caprock	Percentage change in porosity (%)	-0.03-0.19	-0.03-0.21	-0.3-0.13
	Percentage change in permeability (%)	-0.10-0.59	-0.10-0.66	-0.92-0.40
Sandstone reservoir	Percentage change in porosity (%)	-1.56-5.98	-1.54-5.97	-4.42-7.86
	Percentage change in permeability (%)	-6.12-26.70	-6.06-26.68	-16.54-36.29

4.1.4 Impact of impurities on brittleness of reservoir and cap rocks during CO_2 geosequestration (Strategy 1)

The mineralogical brittleness index can be evaluated taking into consideration the bulk modulus of the minerals and their relative level of brittleness (BI_{bm}). The mineralogical brittleness index of the pure limestone using volume fraction of minerals obtained from numerical simulations of the experimental condition and molecular weight of the minerals, BI_{bm} remained constant at 0.51, after 90 days of CO_2 sequestration. This is because no mineral precipitated in the pure limestone formation after 90 days of CO_2 sequestration; calcite dissolution continues. The simulation was run further for 100 years, yet no mineral precipitated, except a small amount of quartz that precipitated in the pure limestone reservoir layer closest to the impure limestone. So, the mineralogical brittleness index of the pure limestone remained relatively constant.

The mineralogical brittleness index of the carbonate rocks and shale caprock was evaluated at the same temperature and pressure condition (100^0C and 137 bar) for the co-injection cases, to evaluate the impact of impurities in CO_2 on the brittleness of rocks (Table 4.5).

Table 4.5: Brittleness index of the formation at different times of CO_2 geosequestration at temperature and pressure of 100^0C and 137 bar, respectively.

Formation type	Brittleness index	Before sequestration, t=0		During sequestration, t=90 days		After sequestration, t=100 years	
		CO_2	CO_2-SO_2	CO_2	CO_2-SO_2	CO_2	CO_2-SO_2
Shale	BI_{bm}	0.1313	0.1313	0.1314-0.1315	0.1314-0.1315	0.1105-0.1232	0.1105-0.1231
Impure limestone	BI_{bm}	0.5097	0.5097	0.5097	0.5062-0.5097	0.5097	0.5060-0.5097
Pure limestone	BI_{bm}	0.5100	0.5100	0.5100	0.4771-0.5100	0.5100	0.4966-0.5100

The result shows that the brittleness index of the carbonate (pure and impure limestone) rocks remained relatively constant after 90 days of sequestration for the CO_2 alone case, while the brittleness of the carbonate rocks decreased for the CO_2-SO_2 co-injection case. The brittleness index of the shale formation increased slightly after 90 days of CO_2 sequestration, but decreased significantly after 100 years of sequestration for all the injection cases. The reduction in the brittleness index of the shale caprock was only due to the upward migration of CO_2 by buoyant forces. SO_2 did not migrate to the shale caprock, due to preferential dissolution of SO_2 gas in the carbonate formation water. Even after 100 years, SO_2 never migrated (if it did, a very negligible fraction migrated to the caprock) to the shale formation (Figure 4.40).

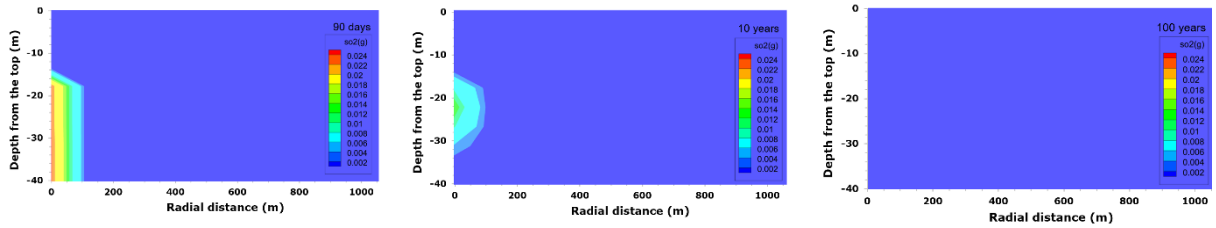

Figure 4.40: SO_2 gas in the formations at 100^0C and 137 bar (salinity=0.21) after 90 days, 10 years, and 100 years of CO_2 sequestration.

It is worth noting that under this condition (100^0C and 137 bar), CO_2 was injected for 90 days only and the sequestration period was 100 years. So, it is possible that SO_2 could have reached the shale caprock if the gas injection period was up to 10 years, which is a realistic CO_2 injection period. Therefore, further numerical simulations were performed to evaluate the brittleness of rocks in low-temperature formations.

The brittleness of carbonate and shale formations was evaluated at temperature and pressure conditions of 40^0C and 100 bar, respectively. The CO_2 gas (with or without impurities) was injected for 10 years. SO_2 (or H_2S) gas reached the shale caprock during the sequestration period for the

co-injection cases. The brittleness index of the rocks at different times of the sequestration are shown in Table 4.6. There is no significant change in the brittleness index of the carbonate and shale rocks for the CO_2 alone and CO_2-H_2S co-injection cases. Furthermore, for the CO_2-SO_2 co-injection case, there is no significant decrease in the brittleness of shale caprock. However, the brittleness of the carbonate rocks decreased significantly in the CO_2-SO_2 co-injection case. The decrease in brittleness in the carbonate rocks is due to precipitation of anhydrite. Anhydrite did not precipitate in the shale caprock, hence the slight decrease in brittleness of the shale formation is similar in all the cases considered.

Table 4.6: Brittleness index of the formation at different times of CO_2 geosequestration at temperature and pressure of 40^0C and 100 bar, respectively (Strategy 1).

Formation type	**Brittleness index**	**Before sequestration, t=0**			**During sequestration, t=90 days**			**After sequestration, t=100 years**		
		CO_2	**CO_2-H_2S**	**CO_2-SO_2**	**CO_2**	**CO_2-H_2S**	**CO_2-SO_2**	**CO_2**	**CO_2-H_2S**	**CO_2-SO_2**
Shale	BI_{bm}	0.1313	0.1313	0.1313	0.1312-0.1313	0.1312-0.1313	0.1312-0.1313	0.1308-0.1311	0.1308-0.1311	0.1308-0.1311
Impure limestone	BI_{bm}	0.5097	0.5097	0.5097	0.5097	0.5097	0.5097	0.5097	0.5097	0.5045-0.5097
Pure limestone	BI_{bm}	0.5100	0.5100	0.5100	0.5100	0.5100	0.5002-0.5100	0.5100	0.5100	0.4997-0.5100

Overall, the brittleness of the shale caprock decreased slightly during CO_2 geosequestration (with or without impurities), while the brittleness of carbonate rocks is relatively constant for CO_2 alone and CO_2-H_2S co-injection cases. However, the brittleness of carbonate rocks decreased significantly for the CO_2-SO_2 co-injection case. These results imply that shale formations considered in the present study are preferable for cap rocks, as their brittleness decreases during CO_2 geosequestration. Carbonate formations can also be suitable as cap rocks during co-injection of CO_2 with SO_2 gas in depleted petroleum reservoirs or aquifers, as the brittleness of the carbonate rocks decreases in this case. During CO_2 geosequestration (with or without H_2S), carbonate formations are suitable reservoir rocks as their brittleness is relatively constant (easier to fracture when needed, for enhanced fluid recovery or production activity), and CO_2 injection and storage capacity of the carbonate reservoirs are maintained as the porosity and permeability of the formation remains constant or increases slightly.

4.1.5 Impact of impurities on brittleness of reservoir and cap rocks during CO_2 geosequestration (Strategy 2)

The brittleness of carbonate, sandstone, and shale formations was evaluated at temperature and pressure conditions of 40^0C and 100 bar, respectively. Table 4.7 shows that the brittleness index

of the sandstone formation (0.5892) is higher than that of the carbonate formation (0.4671) before CO_2 sequestration; while the brittleness of the shale formation is relatively very low (0.1073). The relatively higher brittleness index of sandstone formation before CO_2 sequestration is due to the high amount of the initial quartz and feldspar minerals, and some amount of calcite. The CO_2 gas (with or without impurities) was injected for 10 years. SO_2 (or H_2S) gas hardly contacted the shale caprock (very low mole fraction, as higher concentration of SO_2 or H_2S is in the reservoir due to preferential dissolution of SO_2 (or H_2S) gas in the formation water. Thus, the brittleness of the shale caprock is largely dependent on the reaction of CO_2 with the rock minerals. Hence, the brittleness of the shale caprock for all the injection cases are similar and decreased slightly during the period of CO_2 geosequestration.

Table 4.7: Brittleness index of the formation before and after CO_2 geosequestration at temperature and pressure of 40^0C and 100 bar, respectively (Strategy 2).

Formation type	Brittleness index	Before sequestration, t=0			After sequestration, t=100 years		
		CO_2	CO_2-H_2S	CO_2-SO_2	CO_2	CO_2-H_2S	CO_2-SO_2
Shale	BI_{bm}	0.1073	0.1073	0.1073	0.1071-0.1073	0.1071-0.1073	0.1068-0.1073
Sandstone	BI_{bm}	0.5892	0.5892	0.5892	0.5891-0.5893	0.5891-0.5892	0.5775-0.5892
Carbonate	BI_{bm}	0.4671	0.4671	0.4671	0.4667-0.4678	0.4667-0.4683	0.4625-0.4680

Meanwhile, the change in the brittleness index of the sandstone formation is negligible for the CO_2 only and CO_2-H_2S injection cases, while the brittleness index of the sandstone formation decreased significantly for the CO_2-SO_2 co-injection case, due to the dissolution of most of the brittle minerals (calcite, albite, and K-feldspar) and precipitation of more non-brittle and clay minerals such as illite, smectite-Ca, smectite-Na, and anhydrite (for the CO_2-SO_2 co-injection case). However, the brittleness of the carbonate reservoir increased for the CO_2 only and CO_2-H_2S injection cases as more dolomite dissolved and triggered calcite precipitation. Considering the relative brittleness of different brittle minerals, the weighting coefficient of calcite is higher than that of dolomite (coefficient applied in the developed mineralogical brittleness index model in the present study, to account for the relative brittleness of the minerals) and the amount of magnesite that precipitated is too low (its effect on the brittleness index is negligible), resulting in increased brittleness of the carbonate formation during CO_2 geosequestration (with or without H_2S). Surprisingly, for the CO_2-SO_2 co-injection case, brittleness increased in the upper part of the carbonate reservoir and decreased in its lower part. This is because calcite precipitated in the upper part of the reservoir (no anhydrite), while anhydrite precipitated in the lower part of the

carbonate reservoir in the region where the concentration of dissolved SO_2 is high (as calcite and dolomite dissolved). Therefore, in the regions with very little or no dissolved SO_2 in formation water, the brittleness of the carbonate reservoir increases.

4.1.6 Impact of impurities on brittleness of reservoir and cap rocks during CO_2 geosequestration (Strategy 3)

The brittleness of sandstone and shale formations was evaluated at temperature and pressure conditions of 40^0C and 100 bar, respectively. The brittleness index of the rocks, considering the relative level of the brittleness of brittle minerals is presented in Table 4.8. Table 4.8 shows that the brittleness index of the sandstone formation is significantly higher than that of the shale formation. Applying the brittleness index equation developed in the present study (and incorporating the different molecular weight and molar volume corresponding to each mineral in the rock), the initial brittleness index (BI_{bm}) of the shale caprock is 0.1073, while the initial brittleness index (BI_{bm}) of the sandstone reservoir is 0.5892. The relatively higher brittleness index of the sandstone formation before CO_2 sequestration is due to the high amount of the initial quartz and feldspar minerals, and some amount of calcite.

The CO_2 gas (with or without impurities) was injected and withdrawn in cycles (up to seven cycles) for 87.5 years. SO_2 (or H_2S) gas hardly contacted the shale caprock up to 2-4 m vertical thickness from the reservoir (very low mole fraction, as a higher concentration of SO_2 or H_2S is in the reservoir due to preferential dissolution of SO_2 (or H_2S) gas in the formation water. Thus, the brittleness index of the shale caprock is largely dependent on the reaction of CO_2 with the rock minerals. Hence, the brittleness index of the shale caprock for all the injection cases is similar and decreased slightly during the period of CO_2 geosequestration.

In the CO_2 alone and CO_2-H_2S co-injection cases, after the first cycle of fluid injection and withdrawal, the brittleness index of the shale caprock decreased to about 0.1072; while in the CO_2-SO_2 co-injection case, after the first cycle of injection and withdrawal, the brittleness index of the shale caprock decreased to about 0.1071. After seven cycles of injection and withdrawal, the brittleness index of the shale caprock decreased to about 0.1071 for the CO_2 alone and CO_2-H_2S cases and decreased to about 0.1063 for the CO_2-SO_2 case.

In most part of the sandstone reservoir, after the first cycle of fluid injection and withdrawal, the brittleness index of the formation decreased to about 0.5887 for the CO_2 alone and CO_2-H_2S cases, and decreased to about 0.5705 (and exceptionally, decreased to 0.3872 at the lowest

production perforation) for the CO_2-SO_2 case. After seven cycles of fluid injection and withdrawal, the brittleness index of the sandstone reservoir decreased to about 0.5885 for the CO_2 alone and CO_2-H_2S cases and decreased to about 0.5575 for the CO_2-SO_2 case. Thus, the percentage decrease in brittleness index (BI_{bm}) in the sandstone reservoir and shale caprock after seven cycles of injection and withdrawal for the CO_2-SO_2 case is 5.38% and 0.93%, respectively. At the perforations in the sandstone reservoir, for all the geosequestration cases (with or without impurities), BI_{bm} increased. After seven cycles of fluid injection and withdrawal, the brittleness index of the sandstone reservoir at the perforations increased to about 0.5917 for the CO_2 alone and CO_2-H_2S cases and increased to about 0.5933 for the CO_2-SO_2 case due to severe dissolution of minerals at the perforations.

For all the geosequestration cases, in the regions in the sandstone reservoir where it appears that minerals are deposited or precipitated minerals might be unconsolidated (a few layers below the perforation interval and close to the well), BI_{bm} decreased. However, mineralogical brittleness index models might not be accurate at the perforations and regions where minerals deposited or precipitated might be unconsolidated. Therefore, XRD analyses and mechanical tests on the change in the mineralogical and geomechanical properties of sandstone rock samples and their fracture behaviour upon treatment with pure CO_2 or CO_2 mixture would be required to evaluate the correlation between the mineralogical brittleness index and mechanical brittleness index of the rock samples.

Table 4.8: Brittleness index of the formations before and after the first and seventh cycles of CO_2 injection and withdrawal (Strategy 3).

Formation type	**Brittleness index**	**Before sequestration, t=0**			**After cycle 1**			**After cycle 7**		
		CO_2	**CO_2-H_2S**	**CO_2-SO_2**	**CO_2**	**CO_2-H_2S**	**CO_2-SO_2**	**CO_2**	**CO_2-H_2S**	**CO_2-SO_2**
Shale caprock	BI_{bm}	0.1073	0.1073	0.1073	0.1072-0.1073	0.1072-0.1073	0.1071-0.1073	0.1071-0.1073	0.1071-0.1073	0.1063-0.1073
Sandstone Reservoir	BI_{bm}	0.5892	0.5892	0.5892	0.5887-0.5917	0.5887-0.5917	0.3672-0.5919	0.5885-0.5917	0.5885-0.5917	0.5575-0.5933

To quantify the reliable change between the brittleness index of rocks for the CO_2 alone and CO_2-SO_2 co-injection cases, the reliable change index was computed using brittleness index results (assuming all the minerals have the same molar volume and eliminating the molar volume parameter) from the CO_2 alone and CO_2-SO_2 co-injection cases at 87.5 years. The first column contains brittleness index for the CO_2 alone case, while the second column contains the brittleness index of rocks for the CO_2-SO_2 co-injection case (a total of 1120 rows or observations). The Pearson's correlation coefficient (reliability coefficient, r) is 0.999747 (representing excellent

reliability of the brittleness index), and the calculated standard deviation (σ) of the distribution of the brittleness index for the CO_2 alone case is 0.220965. Therefore, the reliable change index (with 95% confidence) is 0.009745. Hence, the absolute change in brittleness index between the CO_2 alone case and the CO_2-SO_2 co-injection case greater than 0.009745 Is considered significant. Therefore, in the present study, the change in the brittleness index of the sandstone reservoir for the CO_2-SO_2 co-injection case is significant.

4.1.7 Selection of suitable reservoir and cap rocks for CO_2 geosequestration

The changes in the properties of the formations are compared for the different CO_2 geosequestration strategies and cases. In Strategy 1, there is a slight increase in porosity and permeability of the pure and impure limestone formations for the CO_2 alone case, and a slight decrease in the porosity and permeability of the formations for the CO_2-SO_2 case. In the shale formation, there is a significant decrease in the porosity and permeability at 100^0C and 137 bar (at a high salinity of 0.21), while the porosity and permeability increased slightly at 40^0C and 100 bar (at a low salinity of 0.06). Furthermore, there is no noticeable change in the brittleness index of the pure and impure limestone formations for the CO_2 alone case, and their brittleness index decreased slightly for the CO_2-SO_2 both temperature and pressure conditions. However, for the CO_2 alone and the CO_2-SO_2 cases, the brittleness index of the shale formation decreased significantly at 100^0C and 137 bar, while the brittleness index of the shale formation only decreased slightly at 40^0C and 100 bar. The significant change in the porosity, permeability, and brittleness index of the shale caprock at 100^0C and 137 bar makes it a suitable caprock during CO_2 geosequestration at that condition compared to the increase in porosity and permeability of the shale caprock and only a slight decrease in the brittleness index at 40^0C and 100 bar. CO_2 geosequestration at high temperature and pressure conditions may promote the self-sealing potential of the shale caprock and enhance its ductility. The summary of the results is shown in Table 4.9.

Table 4.9: Summary of results in the present study (Strategy 1).

Strategies		Strategy 1					
In situ conditions		T= 100^{0}C, P=137 bar			T= 40^{0}C, P=100 bar		
Rock type		Pure limestone	Impure limestone	Shale	Pure limestone	Impure limestone	Shale
Initial mineralogical composition	Illite	0	0.01	65.30	0	0.01	65.30
	Kaolinite	0	0.01	1.11	0	0.01	1.11
	Smectite-Ca	0	0.01	6.90	0	0.01	6.90
	Chlorite	0	0.01	6.40	0	0.01	6.40
	Quartz	0	0.01	8.00	0	0.01	8.00
	K-feldspar	0	0.01	2.80	0	0.01	2.80
	Albite	0	0.01	3.20	0	0.01	3.20
	Calcite	100.00	99.91	0.83	100.00	99.91	0.83
	Pyrite	0	0.01	0.40	0	0.01	0.40
	Dolomite	0	0.01	5.00	0	0.01	5.00
	Anhydrite	0	0	0	0	0	0
Percentage change in porosity	CO_2	0.01 – 0.06	0.008 – 0.01	-ve (0.64 - 7.44)	0.12 - 0.16	0.10 - 0.11	0.63 - 0.89
	CO_2-H_2S	-	-	-	0.12 - 0.17	0.11 - 0.12	0.63 - 0.91
	CO_2-SO_2	-ve (0.63 - 1.27)	-ve (0.04 – 0.33)	-ve (0.64 - 7.44)	-ve (0.35 - 0.50)	-ve (0.48 - 0.58)	0.63 - 1.21
Percentage change in permeability	CO_2	0.05 – 0.22	0.03 – 0.05	-ve (2.02 - 21.58)	0.48 - 0.66	0.36 - 0.39	1.97 - 2.81
	CO_2-H_2S	-	-	-	0.49 - 0.69	0.36 - 0.40	2.01 - 2.93
	CO_2-SO_2	-ve (2.33 - 4.60)	-ve (0.14 – 1.21)	-ve (2.02 - 21.60)	-ve (1.42 – 2.00)	-ve (1.67 - 2.01)	2.01 - 3.86
Percentage change in brittleness index	CO_2	0.00	0.00	-ve (6.17 -15.84)	0.00	0.00	-ve (0.15 – 0.38)
	CO_2-H_2S	-	-	-	0.00	0.00	-ve (0.15 – 0.38)
	CO_2-SO_2	-2.63-0.00	-0.73-0.00	-ve (6.24 -15.84)	-2.02 – 0.00	-1.02 – 0.00	-ve (0.15 – 0.38)

At the same temperature and pressure conditions of 40^{0}C and 100 bar, the changes in the properties of the formations in Strategy 1 and Strategy 2 are compared. The porosity and permeability of the carbonate formations (pure and impure limestone) in Strategy 1 increased slightly for the CO_2 alone and CO_2-H_2S case, and decreased slightly for the CO_2-SO_2 case. In Strategy 2, the porosity and permeability of the carbonate formation increased slightly, but higher than the increase in the carbonate formations in Strategy 1. In contrast to Strategy 1, the porosity and permeability of the carbonate formation in Strategy 2 increased slightly for the CO_2-SO_2 case due to severe dolomite dissolution in the formation. In Strategy 1, the porosity and permeability of shale formation increased significantly for all the geosequestration cases compared to Strategy 2 where the porosity and permeability of the shale formation only increased slightly. In Strategy 2, the slight decrease in the porosity and permeability of the shale caprock occurred at a layer close to the reservoir rock. The difference in the porosity and permeability of the shale caprock in Strategy 1 and Strategy 2, may be attributed to the mineralogical composition of the formations overlain by the shale caprock, the molecular diffusion coefficient of the gas species, and the initial petrophysical properties of the formations. In Strategy 1, there is no noticeable change in the brittleness index of the carbonate formations for the CO_2 alone and CO_2-H_2S case, while the brittleness index of the formations decreased for the CO_2-SO_2 case due to anhydrite precipitation. In Strategy 2, the brittleness index of the carbonate formation decreased in some part of the reservoir and increased in other parts of the reservoir due to selective dissolution and precipitation

of calcite in the reservoir. Calcite precipitated mainly at the top part of the reservoir, and dissolved in the lower part of the reservoir close to the injection well. In both Strategy 1 and Strategy 2, the brittleness index of the shale caprock decreased slightly for all the geosequestration cases. The very small change in the porosity, permeability, and brittleness index of the shale caprock in Strategy 2, implies that the integrity of the caprock is more preserved compared to Strategy 1. Also, the increase in porosity and permeability of the carbonate formation in Strategy 2, as well as the slight increase in the brittleness index in some part of the formation, makes the carbonate formation (with initial calcite and dolomite content) a more suitable reservoir compared to the carbonate formations in Strategy 1. The summary of the results is shown in Table 4.10.

Table 4.10: Summary of results in the present study (Strategy 1 and Strategy 2).

Strategies		Strategy 1			Strategy 2	
In situ conditions		T= 40^{0}C, P=100 bar			T= 40^{0}C, P=100 bar	
Rock type		Pure limestone	Impure limestone	Shale	Carbonate	Shale
Initial mineralogical composition	Illite	0	0.01	65.30	0	65.30
	Kaolinite	0	0.01	1.11	0	1.11
	Smectite-Ca	0	0.01	6.90	0	6.96
	Chlorite	0	0.01	6.40	0	6.40
	Quartz	0	0.01	8.00	0	8.00
	K-feldspar	0	0.01	2.80	0	2.80
	Albite	0	0.01	3.20	0	3.20
	Calcite	100.00	99.91	0.83	40.00	0.80
	Pyrite	0	0.01	0.40	0	1.43
	Dolomite	0	0.01	5.00	60.00	0
	Anhydrite	0	0	0	0	4.00
Percentage change in porosity	CO_2	0.12 - 0.16	0.10 - 0.11	0.63 - 0.89	0.21 – 0.76	-0.07 - 0.13
	CO_2-H_2S	0.12 - 0.17	0.11 - 0.12	0.63 - 0.91	0.15 – 1.00	-0.07 – 0.16
	CO_2-SO_2	-ve (0.35 - 0.50)	-ve (0.48 - 0.58)	0.63 - 1.21	0.08 – 1.38	-0.49 – 0.11
Percentage change in permeability	CO_2	0.48 - 0.66	0.36 - 0.39	1.97 - 2.81	0.84 -3.11	-0.20 - 0.39
	CO_2-H_2S	0.49 - 0.69	0.36 - 0.40	2.01 - 2.93	0.59 – 4.10	-0.20 – 0.47
	CO_2-SO_2	-ve (1.42 – 2.00)	-ve (1.67 - 2.01)	2.01 - 3.86	0.32 – 5.68	-1.50 – 0.34
Percentage change in brittleness index	CO_2	0.00	0.00	-ve (0.15 – 0.38)	-0.09 – 0.15	-0.19 – 0.00
	CO_2-H_2S	0.00	0.00	-ve (0.15 – 0.38)	-0.09 – 0.26	-0.19 – 0.00
	CO_2-SO_2	-2.02 – 0.00	-1.02 – 0.00	-ve (0.15 – 0.38)	-0.98 – 0.19	-0.47 – 0.00

At the same temperature and pressure conditions of 40^{0}C and 100 bar, the changes in the properties of the formations in Strategy 2 and Strategy 3 are compared. A non-cyclic approach of CO_2 geosequestration was adopted in Strategy 2, while a cyclic approach of CO_2 geosequestration was adopted in Strategy 3. In Strategy 2, the porosity and permeability of the sandstone reservoir increased slightly for the CO_2 alone and CO_2-H_2S case, and decreased for the CO_2-SO_2 case, mainly due to anhydrite precipitation. In Strategy 3, the porosity and permeability of the sandstone reservoir increased significantly in some parts of the reservoir and decreased significantly in other parts of the reservoir for all the geosequestration cases. The

significant increase in the porosity and permeability of the sandstone reservoir in Strategy 3 occurred at the production perforations close to the well compared to the increase in porosity and permeability in other part of the reservoir. In Strategy 3, the decrease in porosity and permeability occurred in a few layers in the reservoir below the production or withdrawal zone, due to deposition or precipitation of minerals in that region. However, for the CO_2-SO_2 case in Strategy 3, the porosity and permeability of the sandstone reservoir decreased everywhere in the reservoir where SO_2 gas dissolved except at the production perforations in the reservoir. In both Strategy 2 and Strategy 3, the brittleness index of the shale caprock decreased slightly for all the geosequestration cases. However the decrease in the brittleness index of the shale caprock is higher in Strategy 3 compared to Strategy 2, as more SO_2 gas dissolved in the brine in the shale caprock during the cyclic approach of CO_2 geosequestration. Therefore, the shale caprock became more ductile for the CO_2-SO_2 case during the cyclic approach of CO_2 geosequestration. The summary of the results is shown in Table 4.11.

Table 4.11: Summary of results in the present study (Strategy 2 and Strategy 3).

Strategies		Strategy 2		Strategy 3	
In situ conditions		T= 40^{0}C, P=100 bar		T= 40^{0}C, P=100 bar	
Rock type		Sandstone	Shale	Sandstone	Shale
Initial mineralogical composition	Illite	2.80	65.30	2.80	65.30
	Kaolinite	0.90	1.11	0.90	1.11
	Smectite-Ca	0	6.96	0	6.96
	Chlorite	2.70	6.40	2.70	6.40
	Quartz	25.80	8.00	25.80	8.00
	K-feldspar	23.30	2.80	23.30	2.80
	Albite	41.50	3.20	41.50	3.20
	Calcite	3.00	0.80	3.00	0.80
	Pyrite	0	1.43	0	1.43
	Dolomite	0	0	0	0
	Anhydrite	0	4.00	0	4.00
Percentage change in porosity (%)	CO_2	0.07 – 0.27	-0.07 - 0.13	-1.56-5.98	-0.03-0.19
	CO_2-H_2S	0.06 – 0.25	-0.07 – 0.16	-1.54-5.97	-0.03-0.21
	CO_2-SO_2	-ve (0.29 - 0.61)	-0.49 – 0.11	-4.42-7.86	-0.3-0.13
Percentage change in permeability (%)	CO_2	0.28 – 1.09	-0.20 - 0.39	-6.12-26.70	-0.10-0.59
	CO_2-H_2S	0.23 – 1.02	-0.20 – 0.47	-6.06-26.68	-0.10-0.66
	CO_2-SO_2	-ve (1.18 - 2.40)	-1.50 – 0.34	-16.54-36.29	-0.92-0.40
Percentage change in brittleness index (%)	CO_2	-0.02-0.02	-0.19 – 0.00	-0.12 – 0.42	-0.19 – 0.00
	CO_2-H_2S	-0.02-0.00	-0.19 – 0.00	-0.12 – 0.42	-0.19 – 0.00
	CO_2-SO_2	-1.99 – 0.00	-0.47 – 0.00	-5.38 – 0.70	-0.93 – 0.00

4.1.8 Evaluation of the impact of CO_2 geosequestration on the brittleness index of rocks based on mineralogical data from previous studies

The brittleness of rocks can be evaluated by their brittleness index. In the present study, the mechanical brittleness of the Pink Desert limestone was determined using data from the study conducted by AL-Ameri et al. (2016). The mechanical brittleness index was determined by applying different models including the ratio of unconfined compressive strength to the Brazilian tensile strength (BI_2), the ratio of the difference to the sum of the unconfined compressive strength and the Brazilian tensile strength (BI_3), and the ratio of static Young's modulus to static Poisson's ratio of the rock (BI_4). The mechanical brittleness index of the pure limestone formation before and after CO_2 geosequestration, evaluated at temperature and pressure condition of 100^0C and 137 bar (~ 2000 psi), respectively (based on mechanical data from AL-Ameri et al., 2016), is presented in Table 4.12. The percentage increase in brittleness index of the pure limestone using BI_2, BI_3, and BI_4 is 1.71%, 0.28%, and 31.09%, respectively.

Table 4.12: Mechanical brittleness index of pure limestone evaluated at 100^0C and 137 bar.

Brittleness index	Before CO_2 sequestration	After CO_2 sequestration (90 days)	Increase in brittleness index (%)
$BI_2 = \frac{\sigma_c}{\sigma_t}$	12.3816	12.5939	1.71
$BI_3 = \frac{\sigma_c - \sigma_t}{\sigma_c + \sigma_t}$	0.8505	0.8529	0.28
$BI_4 = E/v$	45.8357	60.0858	31.09
BI_{bm} (in the present study)	0.5100	0.5100	0.00

The mineralogical brittleness index mainly corresponds to the mechanical brittleness index (BI_3), as there is no significant increase in the brittleness of the pure limestone before and after CO_2 geosequestration. The slight increase in the brittleness index (BI_3) may be attributed to the presence of trace amount of feldspar mineral in the Pink Desert Limestone (pure limestone) which could not be quantified from XRD analysis. Dissolution of feldspar minerals might have resulted in the precipitation of a more brittle mineral such as quartz, thereby increasing its brittleness index slightly. In the numerical simulation, a small amount of quartz precipitated (as feldspar minerals dissolved in the impure limestone layer) only at the top layers in the pure limestone reservoir, which can be attributed to the zonal interaction between the impure limestone and pure limestone formations. Also, the Pink Desert limestone might have had some amount of dolomite (Eliebid et al., 2018), as dolomite dissolution could result in the precipitation of calcite (which is relatively more brittle than dolomite), thereby increasing the brittleness index of the rock. However, the

increase in the brittleness index of the pure limestone calculated using the mineralogical brittleness index model developed in the present study is negligible. BI_2 and BI_4 models of estimating the mechanical brittleness index of the pure limestone exaggerate their brittleness. The mechanical brittleness index of the pure limestone, evaluated using the ratio of the difference to the sum of the unconfined compressive strength and the Brazilian tensile strength of the rock (BI_3), appears more accurate.

Furthermore, experimental data on the mineral composition of rock samples before and after CO_2 sequestration from previous studies were used to evaluate the mineralogical brittleness index of rocks. Li et al. (2022) conducted an experimental study to investigate the mineralogical changes in carbonate-rich shale rock samples during CO_2-brine-rock interactions. The carbonate-rich rock samples tested include limestone, dolomitic shale, and silty dolomite. The soaking fluid is brine (fully saturated with CO_2), and the CO_2-brine soaking experiment was conducted at 90^0C and 35 MPa for 168 hours. The brittleness index based on the model developed by Kang et al. (2020) is shown in Table 4.13. The brittleness index of the dolomitic shale before the CO_2-brine soaking experiment is 0.6082, while the brittleness index of the limestone and silty dolomite is 0.5054 and 0.4970, respectively. The relatively higher brittleness index of the dolomitic shale is due to the significantly high amount of quartz in the rock sample. After the CO_2-brine-rock soaking experiment, the brittleness index of the dolomitic shale, limestone, and silty dolomite increased by 0.10%, 0.49%, and 1.35%, respectively. The significant increase in the brittleness index of the silty dolomite could be attributed to the severe dissolution of calcite and dolomite, and the precipitation of quartz and feldspar minerals (K-feldspar and albite). Overall, the brittleness index of the carbonate-rich shale increased during the period of CO_2 sequestration. Therefore, the brittleness index of carbonate reservoirs and carbonate-rich shale caprock might increase during CO_2 geosequestration (pure CO_2-brine-rock interactions).

Table 4.13: Brittleness index of carbonate-rich shale rock samples during CO_2 sequestration, based on mineralogical composition data from Li et al. (2022).

Rock type	Mineral	Before soaking	After soaking (168 hours)	Before soaking	After soaking (168 hours)	Percentage increase in BI_{bm}
		Wt.%	Wt.%	BI_{bm}	BI_{bm}	
Limestone	Quartz	5.0	6.9	0.5054	0.5079	0.49
	K-feldspar	0.2	0.4			
	Albite	4.9	5.7			
	Calcite	84.4	80.2			
	Siderite	1.1	1.6			
	Clay	4.4	5.2			
Dolomitic shale	Quartz	35.5	38.6	0.6082	0.6088	0.10
	K-feldspar	3.7	3.3			
	Albite	13.0	15.3			
	Calcite	12.8	7.1			
	Dolomite	24.1	21.7			
	Siderite	5.4	7.2			
	Clay	5.5	6.8			
Silty dolomite	Quartz	14.5	17.6	0.4970	0.5037	1.35
	K-feldspar	1.8	2.1			
	Albite	6.1	7.6			
	Calcite	5.1	3.0			
	Dolomite	65.3	60.2			
	Siderite	1.7	2.6			
	Clay	5.5	6.9			

The change in brittleness index of different sandstone rock samples (Cenomanian Sandstone, ZG and Siltstone lateral seal Aptian Sandstone, ZC) were also evaluated using experimental data obtained from a study conducted by Mavhengere et al. (2022) at CO_2 (with and without SO_2) geosequestration conditions of 17.5 MPa and 346 K for the ZC core samples, and 10 MPa and 316K for the ZG core samples for 2 months (Table 4.14). The initial brittleness index of the ZC rock sample (BI_{bm} = 0.6779) is higher than the initial brittleness index of the ZG rock sample (0.5246), due to the relatively higher amount of quartz in the ZC sandstone rock sample. For pure CO_2, the brittleness index of both ZC and ZG changed slightly but changed significantly with the CO_2-SO_2 mixture. For the ZC rock sample (initial calcite content up to 3.5 wt.%), its brittleness index increased slightly from 0.6779 to 0.6912 for the pure CO_2-brine-rock interactions, while the brittleness index of the ZG rock sample (no initial calcite content) decreased slightly from 0.5246 to 0.5175. In the ZC rock sample, the dissolution of plagioclase (feldspar) might have resulted in the relatively higher precipitation of quartz (a more brittle mineral) compared to the ZG rock sample. For the CO_2-SO_2 mixture, the significant decrease in the brittleness index (from 0.6779 to 0.6311) of the ZC rock sample might be attributed to the significant dissolution of plagioclase and calcite (brittle minerals), and the significant precipitation of smectite (clay mineral); while the significant increase in the brittleness index (from 0.5246 to 0.6015) of the ZG rock sample might

be attributed to the precipitation of plagioclase and brittle secondary minerals (calcite and orthoclase) and the severe dissolution of smectite.

Table 4.14: Brittleness index of ZC and ZG sandstone rock samples during CO_2 sequestration, based on mineralogical composition data from Mavhengere et al. (2022).

Sample	Quartz (wt. %)	Plagioclase (wt. %)	Smectite (wt. %)	Calcite (wt. %)	Pyrite (wt. %)	Stilbite (wt. %)	Diopside (wt. %)	Gypsum (wt. %)	Orthoclase (wt. %)	BI_{bm}
ZC untreated	44.1	44.7	1.0	3.5	0.4	3.6	2.7	0.0	0.0	0.6779
ZC CO_2 treated	47.5	42.5	2.5	1.7	0.4	2.7	2.8	0.0	0.0	0.6912
ZC CO_2-SO_2 treated	49.1	28.6	11.8	0.0	0.8	4.9	2.3	2.5	0.0	0.6311
ZG untreated	21.5	46.0	22.2	0.0	0.0	2.0	0.0	0.0	8.3	0.5246
ZG CO_2 treated	22.3	50.5	16.3	2.9	0.0	4.8	0.0	0.0	3.2	0.5175
ZG CO_2-SO_2 treated	26.1	53.4	12.1	2.3	0.0	0.0	0.0	0.0	6.2	0.6015

Unlike ZC, for ZG rock samples, smectite (clay mineral) and stilbite dissolution was observed, while plagioclase and calcite precipitated, thereby inhibiting the precipitation of gypsum and increasing the brittleness index in the CO_2-SO_2 mixture case. The difference in the chemical reaction in the ZC and ZG sandstones is due to their mineralogical composition. For example, ZG rock sample does not have calcite, pyrite and diopside as primary minerals; whereas those are some of the primary minerals in ZC rock sample. Hence, only gypsum precipitated as secondary mineral in ZC rock sample, while calcite precipitated as secondary minerals in ZG rock sample. Therefore, the impact of contaminants on brittleness index of rocks depends on their (rocks') mineralogical composition. Furthermore, although the samples (sandstone samples from Zululand Basin in South Africa) were held in the reactors in the CO_2 and gas mixture only for 2 months, this analysis confirms that the change in the brittleness index of rocks during the storage of pure CO_2 is negligible compared to how much CO_2-SO_2 mixture alters the brittleness of rocks.

Similarly, the brittleness index of sandstone rock samples (no initial calcite content) was evaluated using experimental data obtained from a study conducted by Hedayati et al. (2018) at CO_2 (with and without SO_2) geosequestration conditions of 60^0C and 14.5 MPa (Table 4.15). The model derived in the present study was applied to evaluate the brittleness index of the rock samples before and after CO_2 sequestration. Both the existing model developed by Kang et al. (2020) and the model derived in the present study (based on the molecular weight, molar volume, and volume fraction of minerals) should give the same results, as the new parameters introduced replace the weight or weight fractions of the minerals. The initial brittleness index of the sandstone rock sample is high at 0.8304, due to the significantly large amount of quartz and K-feldspar. After pure CO_2-brine-rock interactions for 62 days, the brittleness index of the sandstone rock sample decreased to 0.8193 (1.34% decrease in brittleness index); while the brittleness index of the rock sample increased to 0.8636 (4.00% increase in brittleness index) after CO_2-SO_2-brine-rock

interactions for 36 days. The decrease in brittleness index for the pure CO_2 case might be attributed to the significant decrease in dolomite and feldspar (K-feldspar and plagioclase) content, while the significant increase in the brittleness index might be attributed to the significant increase in the quartz content and a smaller decrease in the feldspar mineral content for the CO_2-SO_2 case compared to the pure CO_2 case.

Table 4.15: Brittleness index of sandstone rock samples during CO_2 sequestration, based on mineralogical composition data from Hedayati et al. (2018).

Mineral	Molecular weight (g/mol)	Molar volume (cm^3/mol)	Before treatment	After treatment with pure CO_2 (62 days)	After treatment with CO_2+1.5 mol% SO_2 (36 days)
			Vol. %	Vol. %	Vol. %
Quartz	60.084	22.688	75.05	77.78	81.86
K-feldspar	278.330	108.900	12.94	7.66	8.90
Ankerite	206.480	69.522	6.08	4.08	2.86
Anatase/brookite	79.900	19.980	0.52	0.451	0.32
Pyrite	119.980	23.940	0.26	0.21	0.63
Plagioclase	262.222	100.070	3.34	1.21	2.43
Dolomite	184.401	64.341	1.49	0	0
Halite	58.448	27.020	0	0.74	2.08
Clinochlore	634.648	210.260	0	0	1.40
Calcite	100.087	36.934	0	1.37	0
Siderite	115.856	29.378	0	0.40	0
Muscovite	398.306	140.710	0	2.54	0
Magnetite	231.550	44.530	0	0.10	0
Phlogopite	496.950	149.660	0	1.28	0
Kaolinite	258.159	99.520	0	1.84	0
Brittleness Index (BI_{bm})			**0.8304**	**0.8193**	**0.8636**

Therefore, the change in the brittleness index of rocks depends on their mineralogical composition before CO_2 sequestration and the impurity co-injected with CO_2. In the cases considered in the present study and the data from previous studies analysed, the co-injection of CO_2 with a small amount of SO_2 significantly alters the brittleness index of the rocks compared to the pure CO_2 case.

4.1.9 Prediction of brittleness index of rocks using machine learning approach

To investigate the performance of the ANN model in predicting brittleness of rocks, the data set was divided into training set (63%), validation set (27%), and testing set (10%). The testing set was reserved to avoid data leakage and measure the performance of the model. The computed analysis of the final ANN model is shown in Table 4.16, where the model performance on the training, validation, and testing sets are presented. The R^2 value is over 99.98%, MAPE is less than 0.69%, MAE is 0.001, RMSE is about 0.002, and MSE is about 0.000004. The performance

of the model on all the data sets is similar, indicating that the model is not overfitting. Thus, the model predicts the brittleness index of rocks with high accuracy.

Table 4.16: Performance measurements of the final ANN model.

Data set	Performance measures				
	Brittleness index				
	R^2	MAPE (%)	MAE	RMSE	MSE
Training set (63%)	0.999856	0.660224	0.000982	0.002045	0.000004
Validation set (27%)	0.999840	0.686556	0.001023	0.002162	0.000005
Testing set (10%)	0.999850	0.677038	0.001009	0.002084	0.000004

The actual brittleness index (based on the testing data set) is plotted against the predicted brittleness index (R^2 = 1.0) as shown in Figure 4.41. The brittleness index basically forms two clusters: low (indicating shale rocks) and high (indicating carbonate or sandstone rocks).

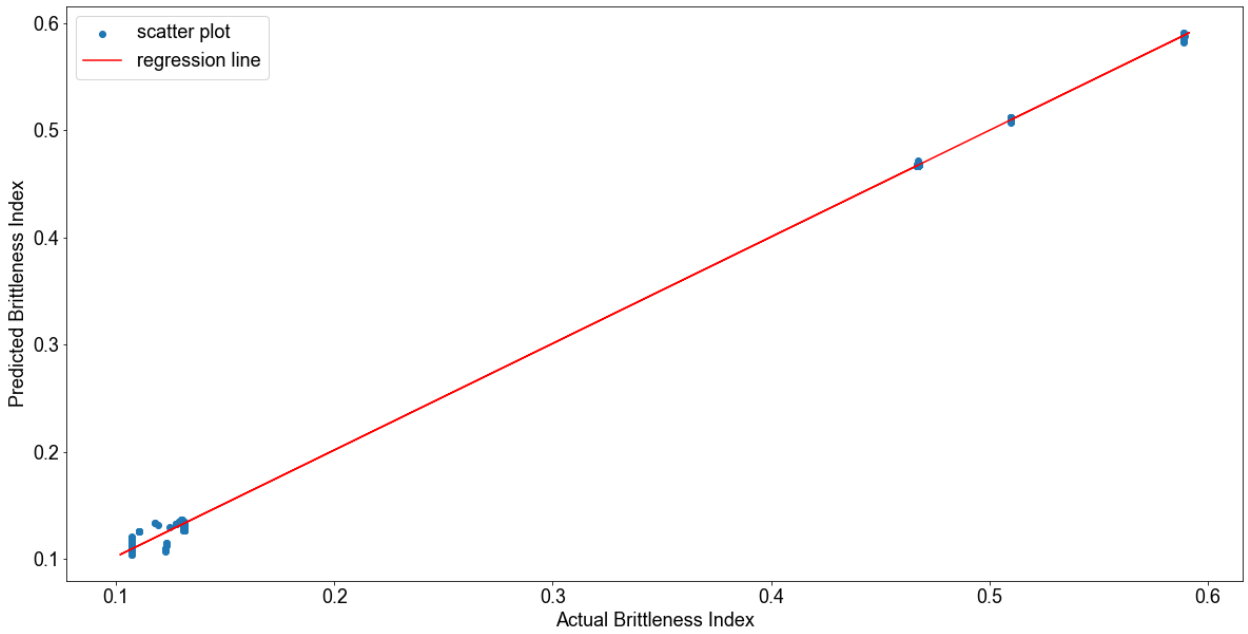

Figure 4.41: A plot of predicted and actual brittleness index from the testing data set.

The final ANN model predicts the brittleness index with high accuracy. The significance of the input features (independent variables) in developing the model, referred to as feature importance, was evaluated based on the sum of the absolute weights of each input feature in the neurons of the first hidden layer (in the final model). The features with higher sum of absolute weights contribute more to the final predictions of the ANN model. The significance of the input features in predicting brittleness index using the final ANN model is shown in Figure 4.42. Based on the ANN model, SiO_2 (aq), formation temperature (T), pH, Mg^{2+}, K^+, and SO_4^{2-} are the most important

factors affecting the brittleness index prediction, while salt saturation least affected the brittleness index.

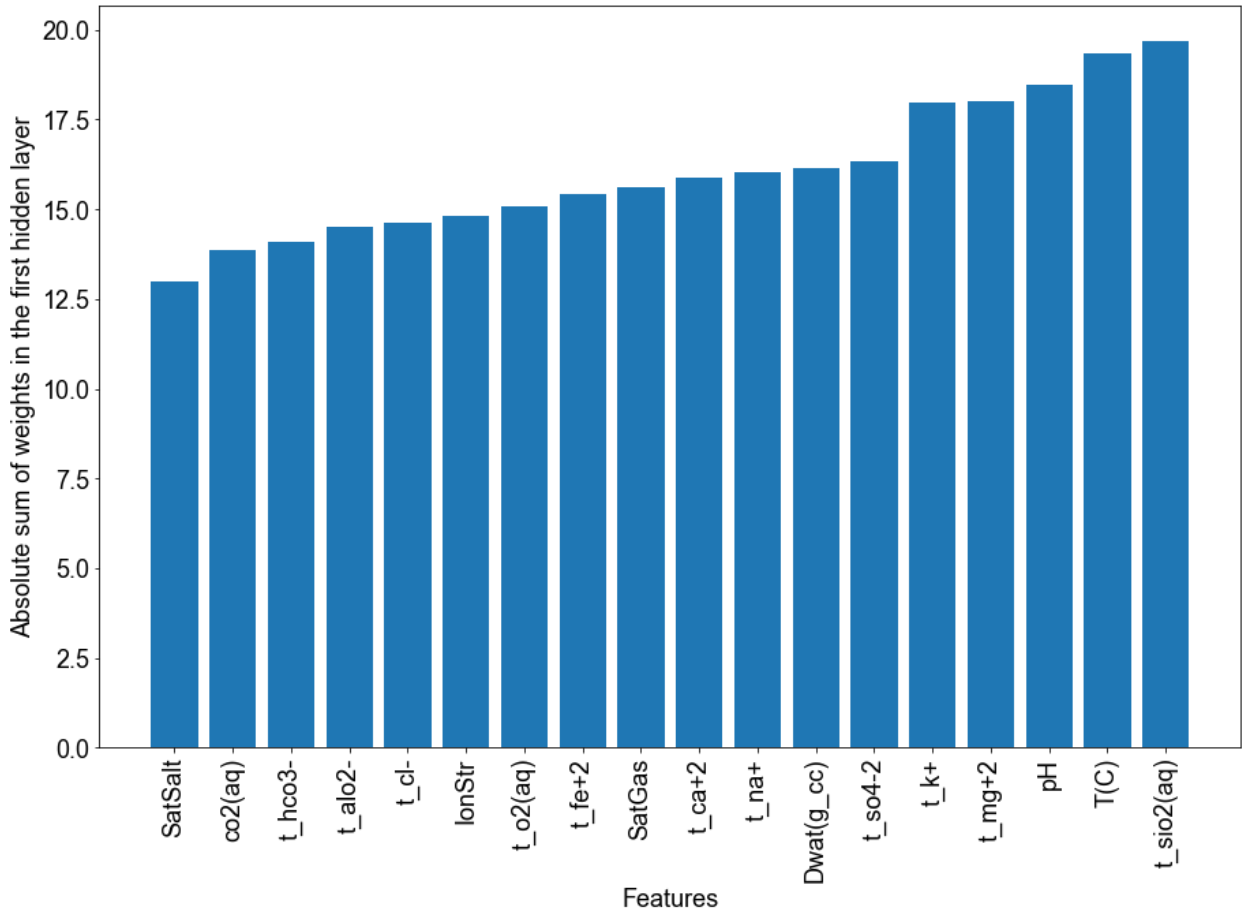

Figure 4.42: Feature importance using the final ANN model.

4.2 Discussion of Key Findings

4.2.1 The impact of CO_2 geosequestration on the geochemical composition of reservoir and cap rocks

The findings of the study revealed that after injection, some mass of CO_2 gas is trapped in the reservoir rocks with higher porosity and permeability, and a certain amount of CO_2 gas begins to dissolve in the formation water; while the mobile CO_2 gas continues to migrate into the shale caprock (with lower porosity and permeability) by buoyancy forces. Meanwhile, the fronts of SO_2 (or H_2S) gas is behind that of CO_2 as these gases preferentially dissolve in formation water compared to CO_2. The preferential dissolution of SO_2 and H_2S in the formation water can be attributed to the closeness of their net dipole moments to that of water compared to CO_2 (López-Rendón and Alejandre, 2008; Miri et al., 2014; Wang et al., 2020). This finding is consistent with

a numerical modelling study conducted by Zhang et al. (2011) on the fate and transport of co-injection of H_2S with CO_2 in deep saline formations. They found that the mass fraction of CO_2 at the advancing gas front was higher than that of the H_2S gas. However, they did not consider SO_2 gas and the migration of injected gas to the low-permeability caprock. The findings of the present study showed that SO_2 gas front is far behind that of H_2S and CO_2 gas fronts, and the mole fractions of the impurities (for the co-injection cases) in CO_2 decrease as the injected gas migrates vertically and horizontally in the formations up to the caprock zone. In fact, at higher temperature and pressure (and salinity up to 0.21) conditions, SO_2 gas completely dissolved in the formation water after 100 years of sequestration (when injection period was only 90 days). In addition, the concentration of total dissolved carbon in the co-injection cases is lower than that in the CO_2 alone case, which is also in line with the findings of Zhang et al. (2011). In the CO_2-SO_2 co-injection case, after 100 years of sequestration, the TDC near the injection well is relatively low compared to the CO_2 alone and CO_2-H_2S co-injection cases. This is due to rapid dissolution of SO_2 gas in formation water. Thus, as soon as SO_2 comes into contact with formation water during injection, it begins to dissolve near the injection well and go into the aqueous phase, inhibiting the dissolution of CO_2 gas in that region. Therefore, H_2S gas is able to migrate more laterally and vertically with the CO_2 gas, as H_2S gas dissolution is less rapid relative to SO_2 gas. However, in the cyclic injection-withdrawal process of CO_2 geosequestration, no notable difference in the total dissolved carbon (TDC) was observed even after seven (7) cycles. This could be attributed to the convective mixing of CO_2 (with or without H_2S/SO_2) with the formation water during the gas (supercritical fluid) withdrawal process, as additional pressure to produce the gas through the perforations in the production zone comes from the formation water. Thus, residually trapped CO_2 might have reconnected with the injected CO_2 in subsequent injection cycles (Lysyy et al., 2023), and water in rock pores containing dissolved H_2S or SO_2 might be flooded with water from different zones in the reservoir, enabling more CO_2 to be dissolved and resulting in a similar TDC for all the injection cases.

Furthermore, dissolution of chlorite, albite, dolomite, and K-feldspar was observed in the shale and impure limestone formations; while quartz, illite, smectite-Ca, and smectite-Na precipitated in those formations (Strategy 1). The mineral reactions are consistent with the findings in the study conducted (up to 5000 years of sequestration) by Ma et al. (2019). However, in the present study, calcite did not dissolve in the shale caprock during the geosequestration period (100 years) for the pure CO_2 case. Anhydrite, and illite dissolved (in the shale caprock) in Strategy 2 of the simulation, to provide enough Ca^{2+} and Mg^{2+} for ankerite precipitation as no dolomite mineral was

initially in the shale caprock (Strategies 2 and 3). At higher temperature (100^0C) and salinity (X_s = 0.21), calcite precipitated in the shale and impure limestone formations (Strategy 1) during CO_2 alone injection case. The precipitation of calcite in the impure limestone formation attenuated the Ca^{2+} concentration, triggering rapid dissolution of dolomite and precipitation of clay minerals (especially, illite and smectite-Na).

The findings of the study revealed that in the CO_2-H_2S co-injection case (Strategy 1), no ankerite and siderite precipitation in the carbonate rocks. Only little amount of ankerite was observed in the shale caprock in the region where dissolved H_2S in the formation water is low in concentration. But, significant amount of ankerite precipitated in the shale caprock in Strategies 2 and 3 of the simulations, due to adequate amount of Ca^{2+} and Mg^{2+} from calcite, anhydrite and illite dissolution. Pyrite precipitation was observed in all the formations considered, in the regions where H_2S dissolved in the formation water. This result is in line with the findings of Zhang et al. (2011), and can be attributed to the fact that precipitation of ankerite and siderite requires Fe^{2+} which can be supplied by the dissolution of iron-bearing minerals such as chlorite. Thus, as CO_2 is co-injected with H_2S, pyrite precipitates (using up most of the Fe^{2+} concentration as H_2S preferentially dissolves in the formation water, delaying CO_2 gas dissolution), inhibiting the precipitation of ankerite and siderite. Furthermore, in the CO_2-SO_2 co-injection case, after 100 years of sequestration, ankerite, magnesite, and pyrite precipitated in the shale caprock; while anhydrite and pyrite mainly precipitated in the carbonate rocks, in the region where SO_2 gas dissolved in formation water. Meanwhile, outside this region, ankerite, siderite, and magnesite precipitation were observed in the shale and impure limestone formations. Therefore, CO_2-SO_2 co-injection creates a better environment for ankerite and siderite precipitation in the formations. Moreover, in the CO_2 alone case, ankerite precipitation was observed in the shale caprock and impure limestone (from the injection well) formations as precipitation and dissolution of pyrite was negligible (without CO_2 co-injection with SO_2 or H_2S). But no ankerite precipitation (mainly pyrite precipitation) in the carbonate and sandstone formations in Strategy 2 of the simulation. This confirms that precipitation of pyrite inhibits ankerite precipitation during CO_2 co-injection with H_2S or SO_2 (Zhang et al., 2011). Dawsonite precipitation was observed in CO_2-SO_2 and CO_2-H_2S co-injection cases in the carbonate formation. This submission is in line with the findings of Li et al. (2016) that the concentrations of Na^+ and K^+ in sandstone formations in the case of CO_2 co-injection with H_2S is greater than CO_2 alone case. However, this effect was observed in the CO_2-SO_2 and CO_2-H_2S cases in carbonate formation (impure limestone) and shale caprock instead, in the present study. Therefore, the increase in Na^+ concentration resulted in the precipitation of more dawsonite in these cases. More dawsonite precipitated in the regions where anhydrite

precipitated, which also represents regions where more SO_2 dissolved. In the sandstone reservoir, dawsonite precipitation was observed only in the cyclic CO_2-SO_2 co-injection case. Therefore, it is possible that SO_2 co-injection with CO_2 yields more dawsonite compared to H_2S co-injection with CO_2. This also confirms that SO_2 dissolves more in formation water in sandstone reservoirs compared to H_2S during CO_2 co-injection cases of geosequestration. Hence, having Fe-bearing minerals in a formation enhances the SO_2 and H_2S dissolution through precipitation of sulphide (for example, pyrite) and sulphate (for example, anhydrite) minerals.

During the 100 years of CO_2 geosequestration, minerals such as quartz and smectite-Na precipitated in some layers of the pure limestone formation (Strategy 1). This is due to the fluid interaction between different formations in the CO_2 gas storage field. A 'fingering' flow pattern exists near the bottom of the CO_2 plume as density of the aqueous-phase increases due to CO_2 dissolution (Xu et al., 2011). Thus, there is advection in the aqueous-phase, enabling fluids in one formation (vertically above) to mix with fluids in another formation (relatively, vertically below). Therefore, fluids in the shale caprock contact fluids in the impure limestone, and fluids in the impure limestone contact fluids in the pure limestone formation during the CO_2 geosequestration. Hence, the petrophysical and geochemical properties of the formations are altered by the fluid-rock interactions, such that these formations exhibit unusual characteristics that could not have been possible if the formations or layers were vertically homogeneous.

4.2.2 The impact of CO_2 geosequestration (non-cyclic) on the porosity, permeability, and brittleness index of rocks

The findings of the study revealed that in Strategy 1, porosity and permeability increase in the shale and carbonate rocks, in the CO_2 alone and CO_2-H_2S co-injections cases; while in the CO_2-SO_2 co-injection case, porosity and permeability increase only in the shale rock, and decrease in the carbonate rocks due to anhydrite precipitation. However, beyond the regions where SO_2 dissolved in the formation water in the carbonate rocks, an increase in porosity and permeability was observed. Meanwhile, in Strategy 2 of the simulation, porosity and permeability increase in the carbonate formation for all the injection cases; while porosity and permeability increase in the sandstone reservoir for the CO_2 only and CO_2-H_2S injection cases, but decreased for the CO_2-SO_2 injection case (in the regions where SO_2 dissolved in the formation water). In Strategy 2, the increase in porosity and permeability of the carbonate rock for the CO_2-SO_2 injection case is due to the severe dolomite dissolution compared to anhydrite and pyrite precipitation. These findings

are consistent with the results in previous studies (Alam et al., 2014, Bolourinejad and Herber, 2014; Pearce et al., 2016; Aminu et al., 2018).

Furthermore, the porosity and permeability of the shale caprock decreased during CO_2 geosequestration (with or without SO_2) at higher temperature (100^0C) and salinity (0.21) in Strategy 1. This finding is in agreement with the results of Ma et al. (2019), as increase in salinity results in increase in the concentration of ions in the caprock and reduce the dissolution effect of the shale caprock. Ma et al. (2019) also found that at a lower salinity, an increase in temperature from 47^0C to 57^0C enhanced dissolution of the caprock (in 5000 years), and mineral dissolution-domination in the mineralization reaction further increases the permeability of the caprock. Therefore, the decrease in porosity and permeability in the present study, when temperature and salinity were up to 100^0C and 0.21, respectively, was mainly impacted by the high salinity of the formation. However, temperature might have had some level of impact on the decrease in the porosity and permeability of the rock (even though not as much as the impact of the formation salinity), as Davila et al. (2017) found that porosity of crushed marl caprock increased more at lower temperature, while porosity reduced as temperature increased.

In Strategy 2, the porosity and permeability of the shale caprock increased especially at the bottom of the caprock (the lowest layer of the shale caprock immediately before the top layer of the sandstone reservoir) when the sandstone reservoir is overlain by the shale caprock during pure CO_2 geosequestration. A similar effect was experienced at the bottom of the caprock in the study conducted by Ma et al. (2019), which is attributed to strong mineral dissolution in that region. However, in the present study, this effect was not experienced at the bottom of the caprock (the lowest layer of the shale caprock immediately before the top layer of the carbonate reservoir) when the carbonate reservoir is overlain by the shale caprock during pure CO_2 geosequestration, instead the porosity and permeability decreased at the bottom of the shale caprock but increased in the other layers of the shale caprock. The contrasting change in the porosity and permeability at the bottom of the shale caprock might be attributed to the mineralogical compositions of the reservoir formations. The sandstone reservoir has Fe-bearing and carbonate minerals, while the carbonate reservoir has only carbonate minerals. Therefore, more CO_2 dissolved in the sandstone formation compared to the carbonate formation. Hence, more CO_2 migrates to the shale caprock from the carbonate reservoir, resulting in significant dissolution of anhydrite and significant precipitation of calcite and ankerite at the bottom of the shale caprock. Hence, the porosity and permeability at the bottom of the shale caprock decreased for the carbonate reservoir-shale caprock system.

The fluid-rock interactions during CO_2 geosequestration, impact the mineralogical composition of the rocks and alter their brittleness. In the present study, the mechanical brittleness index (determined based on ratio of the difference to the sum of unconfined compressive strength and Brazilian tensile strength of the rock) of the pure limestone, analysed based on the experimental data from AL-Ameri et al. (2016) indicates a slight increase in the brittleness index after CO_2 sequestration. The increase in brittleness index might be attributed to small amount of dolomite content in the Pink Desert limestone, which was not detected in the XRD analysis (Eliebid et al., 2018), as dolomite dissolution during CO_2 sequestration could result in the precipitation of calcite (which is relatively more brittle than dolomite), thereby increasing the brittleness index of the rock. As expected, the mineralogical brittleness index of the pure limestone formation remained constant during CO_2 alone sequestration (no significant increase in the brittleness index before and after CO_2 sequestration) at 100^0C and 137 bar (and salinity up to 0.21). This is because no mineral precipitated in the pure limestone formation during the period of geosequestration (0 - 100 years), except in a layer of the pure limestone reservoir at the top (before the impure limestone layer) where quartz (a more brittle mineral) precipitated. Therefore, mechanical brittleness index of rocks evaluated using the simple ratio of unconfined compressive strength to tensile strength and the ratio of Young's modulus to Poisson's ratio tend to overestimate the brittleness or ductility of the rocks. Meng et al. (2015) and Zhang et al. (2016) confirm the failure of these approaches of evaluating mechanical brittleness index of rocks, as the evaluation of brittleness index of rocks based on strength ratio or product, or ratio of elastic modulus to Poisson's ratio cannot properly describe their brittleness. They believe that the brittleness of rocks depends on other factors including bulk modulus, pore pressure, and stress-state of the rock. Thus, the mechanical brittleness index determined based on ratio of the difference to the sum of unconfined compressive strength and Brazilian tensile strength of the rock is more accurate.

The mineralogical brittleness index model derived in the present study are extended to evaluate the impact of impurities on the brittleness of shale and carbonate rocks during CO_2 geosequestration. In Strategy 1, at 100^0C and 137 bar (and salinity of 0.21), after 100 years of geosequestration (in the CO_2 alone case), no notable increase in the brittleness index of the pure and impure limestone formations was observed. But their brittleness index decreased for the CO_2-SO_2 co-injection case. Meanwhile, the brittleness of the shale formation decreased significantly for all the injection cases at 100^0C and 137 bar (and salinity of 0.21). However, the reduction in brittleness of the shale caprock was mainly due to the upward migration of CO_2 by buoyant forces and precipitation of more clay minerals, as SO_2 did not migrate to the shale caprock, due to the preferential dissolution of SO_2 gas in the carbonate formation water. Moreover, during CO_2

geosequestration condition of 40^0C and 100 bar, CO_2 gas reached the shale caprock and some amount of SO_2 (or H_2S) gas. In Strategy 1 of the simulations, the brittleness index of the shale caprock decreased slightly during CO_2 geosequestration (with or without SO_2/H_2S impurities); while the brittleness index of the carbonate (pure and impure limestone) formations remained relatively constant for the CO_2 alone and CO_2-H_2S co-injection cases, but decreased for the CO_2-SO_2 co-injection case.

Meanwhile, in Strategy 2 of the simulations, the brittleness index of the shale caprock and sandstone reservoir decreased slightly during the period of CO_2 geosequestration for all the injection cases; while the brittleness index of the carbonate reservoir increased for the CO_2 only and CO_2-H_2S injection cases, but varies (decreased or increased) vertically (at the same radial distance) for the CO_2-SO_2 injection case. In the CO_2-SO_2 injection case, the upper part of the reservoir is more brittle compared to the lower part of the same carbonate reservoir (Strategy 2). This is because the injected CO_2 (with or without SO_2/H_2S) in shale and sandstone formations result in dissolution of key brittle minerals and precipitation of more non-brittle and clay minerals, while the brittleness index of the carbonate rocks is influenced mainly by calcite precipitation (or dissolution). Significant calcite and dolomite dissolution, corresponds decreased brittleness; while notable calcite precipitation while dolomite dissolves corresponds to increased brittleness index of the carbonate rock in the present study.

4.2.3 The impact of CO_2 geosequestration (cyclic) on the porosity, permeability, and brittleness index of rocks

In Strategy 3, for all the injection cases, the porosity and permeability of the sandstone reservoir at the perforations in the production zone increased due to severe dissolution of calcite and dissolution of some of the primary minerals, creating more flow paths for the gas production. The porosity and permeability of the sandstone reservoir decreased in a few layers (and small lateral distance in the reservoir) directly below the perforation interval in the production zone for all the injection cases. This decrease in porosity and permeability could be attributed to deposition of dissolved (or eroded) minerals (especially calcite) or fines from the production zone in those layers. In other regions in the reservoir, the porosity and permeability increased for the CO_2 alone and CO_2-H_2S co-injection cases, and decreased for the CO_2-SO_2 co-injection case (Strategy 3). This finding is in line with the submission of Saeedi et al. (2011) that rocks susceptible to formation damage (including fines migration) may experience reduced injectivity during cyclic CO_2-brine injection, even though the level of damage would stabilize after several cycles of injection.

In Strategy 3 (gas cyclic injection and withdrawal), the brittleness index of the sandstone reservoir and shale caprock decreased for all the injection cases, except at the production perforations in the sandstone reservoir where the brittleness index increased. The increase in brittleness index at the production perforations may be attributed to the severe dissolution of minerals (resulting in significant increase in porosity) in that region, making the contribution of the brittle minerals (compared to other minerals) to the mineralogical brittleness index more pronounced. In other words, porosity of a formation might impact its brittleness index. For the CO_2 alone and CO_2-H_2S geosequestration cases, the decrease in brittleness index in the sandstone reservoir was higher in the few layers directly below the production perforations interval over a small lateral distance in the reservoir, due to deposition of fines or precipitation of minerals in that region. Overall, a significant change (increase at the production perforations in the sandstone reservoir and decrease in other parts of the reservoir where SO_2 dissolved in the formation water) in brittleness index of the formations was observed for the CO_2-SO_2 co-injection case due to significant amount of anhydrite precipitation.

The decrease in brittleness of the shale caprock is consistent with the results of Lyu et al. (2018). Lyu et al. (2018) adopted the energy-balance method together with the Weibull distribution-based constitutive model to calculate the brittleness values of shale rock samples with or without [CO_2-brine] soaking conditions. They found that the intact shale sample (without soaking with CO_2-brine) has the highest brittleness index value (more brittle), which is in accordance with the high percentage of brittle minerals of the shale sample. They also found that CO_2-brine-shale rock interactions decrease the brittleness values of the shale rock as well as its peak axial strength and Young's modulus. In addition, Lyu et al. (2018) found that CO_2-NaCl-shale interaction has more effect on strength and Young's modulus than brittleness of the shale rock, as the low-clay shale still keeps good fracture performance after CO_2 sequestration. CO_2-brine-rock interactions decrease the unconfined compressive strength and Brazilian tensile strength of carbonate, sandstone, and shale formations (AL-Ameri et al., 2014; Lyu et al., 2018; Heidari et al., 2020). So, even though the strength of the rocks decrease during CO_2 geosequestration, the relative change in their unconfined compressive strength and Brazilian tensile strength impacts their mechanical brittleness index and potential to withstand tensile fracturing. According to Gong and Zhao (2007), a rock mass with low tensile strength is easily subjected to tensile fracture, and a high unconfined compressive strength assists in resisting the closure of natural and induced fractures. Therefore, it is imperative that while the strengths of the caprock decrease during CO_2 geosequestration, the relative decrease in the tensile strength is less than that of the compressive strength, to decrease brittleness of the rock and increase its potential to withstand tensile

fracturing. Furthermore, ductility of caprock would allow it to deform without developing high permeability pathways that can enable CO_2 leakage (Espinoza and Santamarina, 2017). So, instead of developing a higher permeability, the permeability is maintained or decreases to reduce the chance of CO_2 leakage to the earth surface. Thus, the shale caprock at high formation temperature and pressure (and high salinity) conditions may be preferable as its porosity and permeability decreased, as well as its brittleness index during CO_2 geosequestration.

4.2.4 Selection of suitable reservoir and cap rocks for CO_2 geosequestration

Findings of this study and the analyses of mineralogical composition experimental data obtained from the study conducted by Li et al. (2022) show that the brittleness index of carbonate-rich rocks with very low clay content increases during CO_2 geosequestration, while the brittleness index of rocks with very low carbonate content and high clay content decreases during CO_2 geosequestration. Therefore, the brittleness index of a carbonate reservoir or carbonate-rich shale caprock increases during pure CO_2 geosequestration, while the brittleness index of clay-rich shale caprock (like in the present study with very low carbonate content) decreases during pure CO_2 geosequestration. This result of the carbonate-rich formations is in line with the study conducted by Elwegaa et al. (2019) to evaluate the brittleness index of carbonate-rich shale rock samples during cold CO_2 sequestration (cyclic temperature conditions). They found that the brittleness index of the rock samples at injection pressures of 1000 psi, 2000 psi, and 4000 psi increased after CO_2 sequestration. The brittleness index of rocks in the extreme mineralogical compositions (carbonate, carbonate-rich shale, and clay-rich shale) might be different from the intermediate cases, which is common with sandstone rocks. For instance, the analyses of the mineralogical composition data obtained from the study conducted by Mavhengere et al. (2022) using Cenomanian Sandstone (initial mineralogical compositions: 21.5 wt.% quartz, 46.0 wt.% plagioclase, 22.2 wt.% smectite, 8.3 wt.% orthoclase, and 2.0 wt.% stilbite) and Siltstone lateral seal Aptian Sandstone (initial mineralogical compositions: 44.1 wt.% quartz, 44.7 wt.% plagioclase, 3.5 wt.% calcite, 1.0 wt.% smectite, and other minerals) revealed that the brittleness index of sandstone rocks with different initial mineralogical compositions in these intermediate cases is different. The brittleness index of the Cenomanian Sandstone (ZG) decreased during pure CO_2 sequestration, while the brittleness index of the Siltstone lateral seal Aptian Sandstone (ZC) increased during pure CO_2 sequestration. Therefore, the brittleness index of sandstone reservoirs changes (increases or decreases) during pure CO_2 geosequestration based on their initial mineralogical compositions. However, the brittleness index of the carbonate, sandstone, and shale formations change slightly during pure CO_2 (or CO_2-H_2S) geosequestration, compared

to the significant change in the brittleness index of the formations during CO_2 geosequestration with a small amount of SO_2 gas.

The brittleness index of the shale caprock decreased for the CO_2-SO_2 case; while the brittleness index of the carbonate formations and sandstone formations changed (increased or decreased) for the CO_2-SO_2 case, depending on the initial mineralogical compositions of the rocks. In the carbonate formations (with over 90 wt.% calcite content) in Strategy 1, the brittleness index of the formations decreased for the CO_2-SO_2 case; while in the carbonate formation (with 40 wt.% calcite and 60 wt.% dolomite content) in Strategy 2, the brittleness index decreased in the lower part of the reservoir where a higher concentration of SO_2 gas dissolved in the formations water, and increased in the upper part of the reservoir and other parts of the reservoir (few metres laterally away from the well) with lower concentration of dissolved SO_2. The brittleness index of the sandstone formation in Strategy 2 and Strategy 3, decreased for the CO_2-SO_2 case, except at the production perforations in Strategy 3 (due to severe erosion and dissolution of minerals in that part of the reservoir). However, based on the analyses of the mineralogical experimental data obtained from the studies conducted by Hedayati et al. (2018) and Mavhengere et al. (2022), the brittleness index of sandstone formations could increase or decrease for the CO_2-SO_2 case, depending on their initial mineralogical compositions.

The findings of the study suggest that shale formations with high clay content are preferable for cap rocks, as they have low brittleness index and their brittleness index decreases during CO_2 geosequestration for all injection cases and formation conditions considered in the present study. Carbonate or carbonate-rich formations are not suitable cap rocks during CO_2 geosequestration, as they are very brittle and their brittleness index increases or decreases depending on the formation temperature, pressure, salinity, and impurities co-injected with supercritical CO_2. Carbonate rocks composed of more than one carbonate mineral (for instance, calcite and dolomite) may be suitable reservoir rocks for cyclic injection of CO_2 (with or without SO_2/H_2S), as their porosity and permeability increase during CO_2 geosequestration (enabling injectivity) and carbonate formation may become more brittle in the CO_2 production or withdrawal zone (enhancing productivity). During the cyclic injection and withdrawal process, CO_2 would be stored mainly by residual and solubility trapping, as mineral trapping of CO_2 may not be effective in carbonate formations (Zhang et al., 2011). Sandstone formation would be suitable for cyclic injection-withdrawal and long-term storage of CO_2 as the change in porosity and permeability during injection is minimal, but may increase or decrease significantly after several years of storage. In addition, the change in brittleness is negligible; thus, the injected CO_2 would have little

or no impact on the flow pathways (in terms of creating more paths to enhance fluid flow). Also, sandstone formations have been reported to be more favourable for CO_2 mineral trapping than carbonate formations (Zhang et al., 2011). Thus, CO_2 can be stored (long-term) in the sandstone formation by mineral, solubility, and residual trapping mechanisms. Overall, based on the mineralogical compositions of the formations in this study, clay-rich shale formations are preferrable cap rocks to carbonate-rich shale formations for short- and long-term storage of CO_2; carbonate rocks may be suitable reservoirs for non-cyclic and cyclic CO_2 geosequestration, except that mineral trapping of CO_2 in carbonate formations is lower compared to sandstone formations; while sandstone formations are suitable reservoirs for non-cyclic and cyclic injection and withdrawal of CO_2 for sustainable energy development, as well as for long-term underground storage of CO_2.

4.2.5 Prediction of the brittleness index of rocks based on their formation fluid geochemical properties using a machine learning approach

The machine learning model developed in the present study, predicts the brittleness index of the formations with a Mean Absolute Percentage Error (MAPE) of less than 0.7%. Based on the model, the more important features include SiO_2 (aq) concentration, formation temperature, pH, Mg^{2+} concentration, K^+ concentration, SO_4^{2-} concentration, density of the formation fluid, Na^+ concentration, and Ca^{2+} concentration. These features significantly impact the brittleness of rocks as they reflect minerals, in situ, and operating conditions that influence the brittleness index of rocks. For instance, high SO_4^{2-} concentration relates to the volume fraction of anhydrite (Hedayati et al., 2018), which negatively correlated ($r = -0.74$) with the brittleness index; Ca^{2+} concentration relates to calcite and dolomite minerals, while Mg^{2+} concentration relates to dolomite, smectite, illite, and chlorite minerals; SiO_2 (aq) concentration relates to quartz and other silicon oxide-based minerals; K^+ concentration relates to K-feldspar and illite; pH and density of the formation fluid relate to the ionic composition of the formation fluid while temperature relates to in situ and operating condition (low or high temperature). Therefore, the geochemical composition of the formation fluid, and in situ and operating conditions during CO_2 geosequestration impact the prediction of brittleness index of the formation using machine learning model. The dissolution of one mineral might result in the precipitation of another mineral having a common ion. For example, dissolution of dolomite might result in the precipitation of calcite (having Ca^{2+} as a common ion). Proper training of the machine learning model, makes it possible for the model to learn the concentration changes (as well as their rates of change) as some minerals dissolve or precipitate.

CHAPTER FIVE

CONCLUSIONS AND RECOMMENDATIONS

5.1 Conclusions

In this study, a 2-D reactive transport model was developed for geosequestration of CO_2 in reservoir formations overlain by shale caprock. Numerical simulations were performed by adopting three strategies: Strategy 1, Strategy 2, and Strategy 3. Strategies 1 and 2 are non-cyclic approach of CO_2 geosequestration, while Strategy 3 is a model of cyclic injection-withdrawal technology during CO_2 geosequestration. Strategy 1 involves numerical simulations using pure limestone formation (as reservoir), impure limestone formation (to evaluate carbonate rock as a possible caprock), and shale caprock; Strategy 2 involves numerical simulations using sandstone or carbonate rock as a reservoir, and shale caprock; while Strategy 3 involves numerical simulations using sandstone formation as reservoir and shale formation as caprock, to model the process of cyclic injection-withdrawal of CO_2 in the reservoir. Furthermore, mathematical models were derived for evaluating mineralogical brittleness index of the formations before and after CO_2 sequestration (with or without SO_2 or H_2S). The mineralogical brittleness index model that take into consideration the relative level of brittleness of different brittle minerals based on their bulk modulus was applied in the analyses of the brittleness index of the formations, using the volume fraction, molecular weight, and molar volume of the minerals. In addition, a machine learning model was developed to evaluate the brittleness index of reservoir and cap rocks using the geochemical properties of the formation fluid, and in situ and operating conditions of the formations. Based on the key findings in this study, the conclusions from the numerical simulations, mathematical and machine learning models, and analyses of secondary experimental data from previous studies are summarized based on the objectives of the study.

1. Based on the impact of CO_2 impurities on porosity, permeability, and geochemical composition of reservoir and cap rocks during injection, withdrawal, and storage of CO_2 gas stream, the following conclusions are made:
    - Co-injection of CO_2 with H_2S does not result in significant delay in solubility trapping of CO_2 in formations with low amount of Fe^{2+} concentration. In this case, the porosity and permeability of the reservoir increases slightly during CO_2 geosequestration. In a thick reservoir, the amount (mole fraction) of H_2S in the moving [CO_2] gas front is relatively low, and may not alter the brittleness of the caprock should the moving gas front breakthrough or enters the shale caprock formation during injection. This is because CO_2 reduced the

brittleness index of the clay-rich shale caprock, with or without impurities. Therefore, CO_2 co-injection with H_2S in formations with low amount of Fe^{2+} will maintain the porosity and permeability of the reservoir and the integrity of the shale caprock. Similarly, CO_2 co-injection with SO_2 will maintain the integrity of the shale caprock. However, the porosity and permeability of the sandstone rock (relatively few distance from the injection well compared to H_2S co-injection, due to rapid dissolution of SO_2 in formation water) will decrease, reducing the storage capacity of the reservoir. Therefore, CO_2-SO_2 injection should be over a shorter period compared to CO_2-H_2S injection, to reduce the reservoir radial distance contacted by SO_2.

- Formations with high amount of Mg^{2+} concentration will attenuate the inhibitive effect of precipitation of pyrite on ankerite during CO_2 co-injection with H_2S or SO_2. This information would help control the precipitation of pyrite (brittle mineral) as required in the reservoir and caprock formations.
- Geosequestration of CO_2 in a homogeneous reservoir (in terms of mineralogy), will help minimize inadvertent precipitation of minerals that could alter the porosity, permeability, and brittleness of the reservoir. To adopt the cyclic injection and withdrawal of CO_2, proper well control measures should be implemented (such as control of gas production rate) to combat migration of fines from the production zone into the well or tubing string.
- Co-injection of CO_2 with significant amount (up to 0.025 mole fraction) of SO_2 should be avoided to maintain the reservoir porosity and permeability during CO_2 geosequestration, except in carbonate formations with significantly high amount of dolomite.
- Dawsonite precipitation was observed in CO_2-SO_2 and CO_2-H_2S co-injection cases in the carbonate (impure limestone) formation as a result of increase in Na^+ concentration. Therefore, the increase in Na^+ concentration resulted in the precipitation of more dawsonite in these cases. More dawsonite precipitated in the regions where anhydrite precipitated, which also represents regions where more SO_2 dissolved. In the sandstone reservoir, dawsonite precipitation was observed only in the cyclic CO_2-SO_2 co-injection case. Therefore, it is possible that SO_2 co-injection with CO_2 yields more dawsonite compared to H_2S co-injection with CO_2. This also confirms that SO_2 dissolves more in formation water in sandstone reservoirs compared to H_2S during CO_2 co-injection cases of geosequestration. Hence, having Fe-bearing minerals in a formation enhances the SO_2 and H_2S dissolution through precipitation of sulphide (for example, pyrite) and sulphate (for example, anhydrite) minerals.

2. Based on the evaluation of the impact of CO_2 impurities on the brittleness of reservoir and cap rocks during injection and storage of CO_2 gas stream the following conclusions are made:
    - CO_2 geosequestration in high salinity and temperature formations will enhance self-sealing ability of shale caprock, while the carbonate reservoir storage capacity is maintained, as the change in brittleness index of the carbonate formations is negligible during CO_2 geosequestration (except in the CO_2-SO_2 co-injection case).
    - The brittleness index of clay-rich shale formations decreases during pure CO_2 geosequestration, while the brittleness index of carbonate-rich shale formations increases during pure CO_2 geosequestration. In addition, the brittleness index of clay-rich shale formations decreases during CO_2-SO_2 co-injection. Therefore, clay-rich shale formations are preferable cap rocks during CO_2 geosequestration due to their low brittleness index (high ductility), and their brittleness index decreases during CO_2 geosequestration.
    - The change in the brittleness index of sandstone reservoirs depend on their initial mineralogical composition (before CO_2 geosequestration). In some sandstone formations, the brittleness index increases during pure CO_2 geosequestration, while in other sandstone formations the brittleness index decreases during pure CO_2 geosequestration. Similarly, the brittleness index of sandstone reservoirs can increase or decrease during CO_2 co-injection with SO_2, depending on the initial mineralogical composition of the formation.
    - Co-injection of CO_2 with significant amount (up to 0.025 mole fraction) of SO_2 should be avoided to maintain the reservoir brittleness during CO_2 geosequestration. Nevertheless, anhydrite precipitation is negligible in the carbonate reservoir (initially composed of calcite and dolomite) during CO_2 co-injection with SO_2, due to significant dissolution of dolomite and precipitation of calcite. The precipitation of calcite limits anhydrite precipitation. Hence the change in the brittleness index of the formation is negligible. Therefore, carbonate reservoirs with high amount of dolomite might be suitable for the co-injection and storage of CO_2 with some amount of SO_2 gas.
    - Mechanical brittleness index of a rock should be evaluated based on the ratio of the difference to the sum of unconfined compressive strength and Brazilian tensile strength of the rock, which is more accurate (compared to the simple ratio of unconfined compressive strength to Brazilian tensile strength and the ratio of Young's modulus to Poisson's ratio which overestimates brittleness or ductility of the rock).

3. Based on the evaluation of the impact of CO_2 impurities on the brittleness of reservoir and cap rocks during cyclic injection and withdrawal of CO_2 gas stream, the following conclusions are made:
    - In the cyclic injection and withdrawal approach of CO_2 geosequestration, the brittleness index of the sandstone reservoir and shale caprock decreased for all the injection cases, except at the production perforations in the reservoir where severe erosion or dissolution of minerals occurred. The change in the brittleness index of the formations is lower for the CO_2 alone and CO_2-H_2S co-injection cases, compared to the CO_2-SO_2 co-injection case.
4. Based on the changes in the porosity, permeability, geochemical composition, and brittleness of the reservoir rocks during CO_2 geosequestration, conclusions made in the selection of best formations for CO_2 geosequestration are as follows:
    - Clay-rich shale formations are preferable cap rocks, as their brittleness index is low and decreases slightly during CO_2 geosequestration at low or high temperature conditions.
    - Carbonate formations might be suitable reservoirs for cyclic injection and withdrawal of CO_2 due to increased chance of injectivity and productivity at the different zones of the reservoir. Carbonate formations with significant amount of dolomite mineral might be suitable reservoirs for the storage of some amount of SO_2 gas in a CO_2 gas stream, as the change in the brittleness index is negligible in most part of the reservoir except a few metres in the reservoir near the injection well. Also, the porosity and permeability of the carbonate reservoir with such mineralogical composition increase during CO_2-SO_2 storage.
    - Sandstone formations are suitable for long-term storage of CO_2 as they would be more favourable for CO_2 mineral trapping due to availability of Fe-bearing minerals in the sandstone formation. Sandstone formations are also suitable reservoirs for cyclic injection and withdrawal of CO_2, as their porosity and permeability increase at the injection and production zones, and the change in their brittleness index is negligible during the CO_2 geosequestration, except during CO_2-SO_2 co-injection case where porosity, permeability, and brittleness index decrease significantly in most part of the reservoir where SO_2 dissolves in. In some sandstone formations, the brittleness index might increase significantly during CO_2-SO_2 co-injection case, depending on the initial mineralogical composition of the formation.
5. Based on the machine learning model developed to predict the brittleness index of rocks before and during CO_2 geosequestration, the following conclusions are made:

- In terms of feature importance in predicting the brittleness index of rocks, SiO_2 (aq) concentration, formation temperature, pH, Mg^{2+} concentration, K^+ concentration, SO_4^{2-} concentration, density of the formation fluid, Na^+ concentration, and Ca^{2+} concentration have stronger impact on the brittleness of rocks considered in the present study. High SiO_2 concentration could suggest the presence of highly brittle minerals, such as quartz, in the rock. In contrast, higher SO_4^{2-} concentration could suggest lower brittleness. Higher SO_4^{2-} concentration could also signify the presence of non-brittle minerals such as anhydrite or promote the precipitation of such minerals. Besides, oxidation of pyrite in the presence of water can increase SO_4^{2-} concentration. So for formations that have pyrite as one of their primary minerals, it's oxidation will increase SO_4^{2-} concentration.
- Formation fluid geochemical compositions and formation temperature are important parameters in predicting brittleness index of rocks; while the amount of dissolved CO_2 in formation water have little or no effect on the brittleness index of rocks. It appears that what matters in terms of the amount of CO_2 is that CO_2 gas dissolves in the formation water up to the amount required to enable fluid-rock chemical reaction. Other extra amount of dissolved CO_2 subsequently during the period of storage might not impact the brittleness of the rocks over a long time.

5.2 Recommendations for Future Studies

1. Future studies should consider performing experiments to determine changes in the mechanical strengths (compressive and tensile strengths) of rocks and their corresponding changes in the mechanical brittleness index of the rocks during CO_2 co-injection with H_2S or SO_2 gas.
2. Future studies should conduct experiments to investigate the fracture behaviour (stress-strain relationship) of reservoir and caprock samples before and after pure CO_2 injection or CO_2 co-injection with H_2S or SO_2 gas. The corresponding changes in the mineralogical compositions of the rock samples should also be determined through XRD analyses, to validate the mineralogical brittleness index with the fracture behaviour of the rock samples for the different cases (CO_2-brine-rock, CO_2-H_2S-brine-rock, and CO_2-SO_2-brine-rock interactions).
3. Future studies should perform numerical simulations over thousands of years and determine the impact of mineral trapping of CO_2, as well as the solubility and residual trapping mechanisms, on the brittleness of rocks.

4. Future studies should consider developing mathematical models to estimate brittleness of rocks by incorporating formation fluid chemical compositions, formation temperature, and other important parameters that relate to dissolution and precipitation of minerals.

5.3 Contribution to Practice

1. The dual tubing string design for cyclic injection and withdrawal of CO_2 can be adopted in the Carbon Capture, Utilization, and Storage (CCUS) industry to save cost of drilling additional CO_2 production wells and enhance the production of CO_2 with very little chance of producing formation water alongside.
2. The mathematical model for rock brittleness index evaluation derived in this study can be adopted in developing numerical simulation software or codes, as majority of the existing software (or codes) mainly output volume fraction of minerals. Thus, it would be good to implement brittleness index model into the software (or codes) as one of the outputs of the numerical simulation. This would save the software (or codes) users' time in manually computing brittleness index, as the results can be outputted automatically during the coupled numerical simulation of thermal-hydrological-chemical (THC) interactions of rock and fluids in the formations.
3. The machine learning model developed in this study would serve as a guide to other developers in automating the prediction of brittleness index of rocks or similar parameters during fluid injection and storage (CO_2, hydrogen, methane, etc.) in porous media.

REFERENCES

Abedini, A. and Torabi, F. (2014). On the CO_2 storage potential of cyclic CO_2 injection process for enhanced oil recovery. *Fuel,* 124, pp. 14-27.

Ahn, H., Kim, S.-O., Lee, M. and Wang, S. (2020). Migration and residual trapping of immiscible fluids during cyclic injection : Pore-scale observation and quantitative analysis. *Geofluids*, 2020, pp. 1-13. https://doi.org/10.1155/2020/4569208

Alam, M.M., Hjuler, M.L., Christensen, H.F. and Fabricius, I.L. (2014). Petrophysical and rock-mechanics effects of CO_2 injection for enhanced oil recovery: Experimental study on chalk from South Arne field, North Sea. *Journal of Petroleum Science and Engineering*, 122, pp. 468–487.

AL-Ameri, W.A., Abdulraheem, A., Mahmoud, M., Abdullatif, O. and Adebayo, A.R. (2014). Effect of CO_2 Sequestration Period on the Mechanical Properties of Carbonate Aquifers. Paper SPE 171702-MS presented at the Abu Dhabi International Petroleum Exhibition and Conference held in Abu Dhabi, UAE, 10–13 November 2014. https://doi.org/10.2118/171702-MS

AL-Ameri, W.A., Abdulraheem, A. and Mahmoud, M. (2016). Long-term effects of CO_2 sequestration on rock mechanical properties. *Journal of Energy Resources Technology*, 138(1), 012201. https://doi.org/10.1115/1.4032011

Al-Yaseri, A., Yekeen, N., Al-Mukainah, H.S., Kakati, A., Alfarge, D. and Myers, M. (2022). Rock-Wettability Impact on CO_2-Carbonate Rock Interaction and the Attendant Effects on CO_2 Storage in Carbonate Reservoirs. *Journal of Natural Gas Science and Engineering*, 104, 104664. https://doi.org/10.1016/j.jngse.2022.104664

Aminu, M.D., Nabavi, S.A. and Manovic, V. (2018) CO_2-brine-rock interactions: The effect of impurities on grain size distribution and reservoir permeability. *International Journal of Greenhouse Gas Control, 7*8, pp. 168-176.

Bachu, S. (2002). Sequestration of CO_2 in geological media in response to climate change: road map for site selection using the transform of the geological space into the CO_2 phase space. *Energy Conversion and Management,* 43, pp. 87-102.

Badrouchi, N., Pu, H., Smith, S., Yu, Y. and Badrouchi, F. (2022). Experimental investigation of CO_2 injection side effects on reservoir properties in ultra tight formations. *Journal of Petroleum Science and Engineering,* 215, 110605. https://doi.org/10.1016/j.petrol.2022.110605

Bérubé, C. L., Olivo, G.R., Chouteau, M., Perrouty, S., Shamsipour, P., Enkin, R.J., Morris, W. A., Feltrin, L. and Thiémonge, R. (2018) Predicting rock type and detecting hydrothermal alteration using machine learning and petrophysical properties of the Canadian Malartic ore and host rocks, Pontiac Subprovince, Quebec, Canada. *Ore Geology Reviews,* 96, pp. 130-145.

Blampied, N.M. (2016). Reliable change & the reliable change index in the context of evidence-based practice: A tutorial review. Paper presented at the NZPsS Conference, Wellington, 2-4 September 2016.

Bolourinejad, P. and Herber, R. (2014). Experimental and modelling study of storage of CO_2 and impurities in a depleted gas field in northeast Netherlands. *Energy Procedia,* 63, pp. 2811-2820.

Cao, C., Liao, J., Hou, Z., Wang, G., Feng, W. and Fang, Y. (2020). Parametric uncertainty analysis for CO_2 sequestration based on distance correlation and support vector regression. *Journal of Natural Gas Science and Engineering,* 77, 103237. https://doi.org/10.1016/j.jngse.2020.103237

Chen, B., Harp, D.R., Lin, Y., Keating, E.H. and Pawar, R.J. (2018). Geologic CO_2 sequestration monitoring design: A machine learning and uncertainty quantification based approach. *Applied Energy,* 225, pp. 332-345.

Chicco, D., Warrens, M.J. and Jurman, G. (2021). The coefficient of determination R-squared is more informative than SMAPE, MAE, MAPE, MSE and RMSE in regression analysis evaluation. PeerJ Computer Science, 7, 623. https://doi.org/10.7717/peerj-cs.623

Choi, C.-S., Kim, J. and Song, J.-J. (2021). Analysis of shale property changes after geochemical interaction under CO_2 sequestration conditions. *Energy*, 214, 118933. https://doi.org/10.1016/j.energy.2020.118933

Dávila, G., Cama, J., Luquot, L., Soler, J.M. and Ayora, C. (2017). Experimental and modeling study of the interaction between a crushed marl caprock and CO_2-rich solutions under different pressure and temperature conditions. *Chemical Geology*, 448, 26-42.

Deer, D.A., Howie, R.A. and Zussman, J. (1966). *An introduction to the rock forming minerals.* Essex: Longman Scientific & Technical.

Du, H. and Radonjic, M. (2019). The Mechanism of Fracture Initiation in Shale Rocks: Pottsville cap-rock-shale vs. Marcellus unconventional reservoir-shale. In: *53rd U.S. Rock Mechanics/Geomechanics Symposium, New York City, New York, June 2019.* New York: American Rock Mechanics Association.

Edlmann, K., Hinchliffe, S., Heinemann, N., Johnson, G., Ennis-King, J. and McDermott, C.I. (2019). Cyclic CO_2-H_2O injection and residual trapping: Implications for CO_2 injection efficiency and storage security. *International Journal of Greenhouse Gas Control,* 80, pp. 1-9.

Edlmann, K., Haszeldine, S. and McDermott, C.I. (2013). Experimental investigation into the sealing capability of naturally fractured shale caprocks to supercritical carbon dioxide flow. *Environ Earth Sci*, 70, pp. 3393–3409.

Eliebid, M., Mahmoud, M., Shawabkeh, R., Elkatatny, S. and Hussein, I.A. (2018). Effect of CO_2 adsorption on enhanced natural gas recovery and sequestration in carbonate reservoirs. *Journal oof Natural Gas Science and Engineering,* 55, pp. 575-584.

Elwegaa, K., Emadi, H., Soliman, M., Gamadi, T. and Elsharafi, M. (2019). Improving oil recovery from shale oil reservoirs using cyclic cold carbon dioxide injection – An experimental study. *Fuel,* 254, 115586. https://doi.org/10.1016/j.fuel.2019.05.169

Espinoza, D.N. and Santamarina, J.C. (2017). CO_2 breakthrough – Caprock sealing efficiency and integrity for carbon geological storage. *International Journal of Greenhouse Gas Control,* 66, pp. 218-219.

Ezema, I.C., Edelugo, S.O., Menon, A.R.R. and Omah, A.D. (2015). A Comparative Prediction of the Tensile Properties of Sisal Fiber Reinforced Epoxy Composite Using Volume Fraction and

Mass Fraction Models. *Journal of Metallurgical and Materials Engineering Research*, 1(2), pp. 9-18.

Fatah, A., Mahmud, H.B., Bennour, Z., Gholami, R. and Hossain, M. (2022). Geochemical modelling of CO_2 interactions with shale: Kinetics of mineral dissolution and precipitation on geological time scales. *Chemical Geology*, 592, 120742. https://doi.org/10.1016/j.chemgeo.2022.120742

Fatima, S., Khan, H.M.M., Tariq, Z., Abdalla, M. and Mahmoud, M. (2021). An Experimental and Simulation Study of CO_2 Sequestration in Underground Formations: Impact on Geomechanical and Petrophysical Properties. Paper (SPE-204726-MS) presented at the SPE Middle East Oil & Gas Show and Conference, November 28–December 1, 2021. https://doi.org/10.2118/204726-MS

Fjaer, E., Holt, R.M., Horsrud, P., Raaen, A.M. and Risnes, R. (2008). *Petroleum Related Rock Mechanics*. Developments in Petroleum Science. Vol 53. 2nd ed. Amsterdam: Elsevier.

Gheibi, S., Holt, R.M. and Vilarrasa, V. (2016). Stress path evolution during fluid injection into geological formations. In: *50th U.S. Rock Mechanics/Geomechanics Symposium, Houston, Texas, June 2016.* Texas: American Rock Mechanics Association.

Gong, Q.M. and Zhao, J. (2007). Influence of rock brittleness on TBM penetration rate in Singapore granite. *Tunn. Undergr. Space Technol*, 22 (3), pp. 317–324.

Gou, Y., Hou, Z., Li, M., Feng, W. and Liu, H. (2016). Coupled thermo-hydro-mechanical simulation of CO_2 enhanced gas recovery with an extended equation of state module for TOUGH2MPFLAC3D. *Journal of Rock Mechanics and Geotechnical Engineering*, 8, pp. 904-920.

Guo, L., Jiang, Z. and Liang, C. (2016). Mineralogy and Shale Gas Potential of Lower Silurian Organic-Rich Shale at the Southeastern Margin of Sichuan Basin, South China. *Oil Shale*, 33(1), pp. 1–17.

He, K., Zhang, X., Ren, S. and Sun, J. (2015). Delving deep into rectifiers: Surpassing human-level performance on imagenet classification. Paper presented at IEEE International Conference on Computer Vision held in Santiago, Chile, 7-13 December 2015, pp. 1026-1034. https://doi.org/10.1109/ICCV.2015.123

He, Y., Zhou, Y., Wen, T., Zhang, S., Huang, F., Zou, X., Ma, X. and Zhu, Y.Q. (2022). A review of machine learning in geochemistry and cosmochemistry: Method improvements and applications. *Applied Geochemistry,* 140, pp. 1-13. https://doi.org/10.1016/j.apgeochem.2022.105273

Hedayati, M., Wigston, A., Wolf, J.L., Rebscher, D. and Niemi, A. (2018). Impacts of SO_2 gas impurity within a CO_2 stream on reservoir rock of a CCS pilot site: experimental and modelling approach. *International Journal of Greenhouse Gas Control*, 70, pp. 32–44. https://doi.org/10.1016/j.ijggc.2018.01.003

Heidari, M., Ajalloeian, R., Ghazifard, A. and Isfahanian, M.H. (2020). Evaluation of P and S Wave Velocities and Their Return Energy of Rock Specimen at Various Lateral and Axial Stresses. Geotech Geol Eng, 38, pp. 3253–3270.

Herring, A.L., Anderson, L. and Wildenschild, D. (2016). Enhancing residual trapping of supercritical CO_2 via cyclic injections. *Geophysical Research Letters*, 43(18), pp. 9677-9685.

Hou, B., Zeng, Y., Fan, M. and Li, D. (2018). Brittleness Evaluation of Shale Based on the Brazilian Splitting Test. *Geofluids,* 2018, 3602852. https://doi.org/10.1155/2018/3602852

Huang, Y.-H., Yang, S.-Q., Hall, M.R. and Zhang, Y.-C. (2018). The Effects of NaCl Concentration and Confining Pressure on Mechanical and Acoustic Behaviors of Brine-Saturated Sandstone. *Energies*, 11(2), 385. https://doi.org/10.3390/en11020385

Huang, Y.-H., Yang, S.-Q., Li, W.-P. and Hall, M.R. (2020). Influence of Super-Critical CO_2 on the Strength and Fracture Behavior of Brine-Saturated Sandstone Specimens. *Rock Mechanics and Rock Engineering,* 53, pp. 653–670.

Hucka, V. and Das, B. (1974). Brittleness Determination of Rocks by Different Methods. *Int. J. Rock Mech. Min. Sci. & Geomech*, 11, pp. 389-392.

Ibrahim, A.F. (2022). Prediction of coal wettability using machine learning for the application of CO_2 sequestration. *International Journal of Greenhouse Gas Control*, 118, 103670. https://doi.org/10.1016/j.ijggc.2022.103670

Jijo, B.T. and Abdulazeez, A. M. (2021). Classification Based on Decision Tree Algorithm for Machine Learning. *Journal of Applied Science and Technology Trends,* 2(1), pp. 20-28.

Jin, X., Shah, S.N., Roegiers, J.-C. and Zhang, B. (2015). An Integrated Petrophysics and Geomechanics Approach for Fracability Evaluation in Shale Reservoirs. *SPE Journal,* 20 (3), pp. 518-526.

Kang, Y., Shang, C., Zhou, H., Huang, Y., Zhao, Q. Deng, Z., Wang, H. and Ma, Y.Z. (2020). Mineralogical brittleness index as a function of weighting brittle minerals—from laboratory tests to case study. *Journal of Natural Gas Science and Engineering,* 77, 103278. https://doi.org/10.1016/j.jngse.2020.103278

Kannaiah, P.V.D. and Maurya, N.K. (2023). Machine learning approaches for formation matrix volume prediction from well logs: Insights and lessons learned. *Geoenergy Science and Engineering*, 229, 212086. https://doi.org/10.1016/j.geoen.2023.212086

Ke, Q., Li, C., Yao, W., Fan, Y., Zhan, H., Li., B. and Zhang, X. (2023). Comparative characterization of sandstone microstructure affected by cyclic wetting-drying process. *International Journal of Rock Mechanics & Mining Sciences*, 170, 105486. https://doi.org/10.1016/j.ijrmms.2023.105486

Khan, M.Y. and Mandal, A. (2020). Analytical model for gravity segregation in WAG displacement recovery of inclined stratified reservoirs. *Journal of Petroleum Science and Engineering,* 186, 106722. https://doi.org/10.1016/j.petrol.2019.106722

Kim, C., Kim, J., Joo, S., Bu, Y., Liu, M., Cho, J. and Kim, G. (2018). Efficient CO_2 utilization via a hybrid Na-CO_2 system based on CO_2 dissolution. *iScience, 9, pp. 278 – 285.*

Klokov, A., Treviño, R.H. and Meckel, T.A. (2017) Diffraction imaging for seal evaluation using ultra high resolution 3D seismic data. *Marine and Petroleum Geology*, 82, pp. 85-96.

Kolawole, O., Assaad, R.H., Adams, M.P., Ngoma, M.C., Anya, A. and Assaf, G. (2023). Coupled experimental assessment and machine learning prediction of mechanical integrity of MICP and

cement paste as underground plugging materials. *Biogeotechnics*, 1(2), 100020. https://doi.org/10.1016/j.bgtech.2023.100020

Koomson, S., Park, S., Kim, W., No, C., Lee, C., Choi, H. and Lee, C.-G. (2023). Electrochemical hydrogen production using captured CO_2 in alkaline solution. *International Journal of Electrochemical Science,* 18(6), 100175. https://doi.org/10.1016/j.ijoes.2023.100175

Lasaga, A.C., Soler, J.M., Ganor, J., Burch, T.E. and Nagy, K.L. (1994). Chemical weathering rate laws and global geochemical cycles. *Geochimica et Cosmochimica Acta*, 58, pp. 2361-2386.

Li, B., Wong, R.C.K. and Heidari, S. (2018). A modified Kozeny-Carman model for estimating anisotropic permeability of soft mudrocks. *Marine and Petroleum Geology*, 98, pp. 356–368.

Li, C., Zhang, F., Lyu, C., Hao, J., Song, J. and Zhang, S. (2016). Effects of H_2S injection on the CO_2-brine-sandstone interaction under 21 MPa and 70 °C. *Marine Pollution Bulletin,* 106, pp. 17–24.

Li, D., Saraji, S., Jiao, Z. and Zhang, Y. (2021). CO_2 injection Strategies for enhanced oil recovery and geological sequestration in a tight reservoir: An experimental study. *Fuel,* 284(15), 119013. https://doi.org/10.1016/j.fuel.2020.119013

Li, G. (2016). Numerical investigation of CO_2 storage in hydrocarbon field using a geomechanical-fluid coupling model. *Petroleum*, 2, pp. 252-257.

Li, G., Jin, Z., Li, X., Liu, K., Yang, W., Qiao, M., Zhou, T. and Sun, X. (2023). Experimental study on mechanical properties and fracture characteristics of shale layered samples with different mineral components under cyclic loading. *Marine and Petroleum Geology,* 150, 106114. https://doi.org/10.1016/j.marpetgeo.2023.106114

Li, H. (2022). Research progress on evaluation methods and factors influencing shale brittleness: A review. *Energy Reports*, 8, pp. 4344–4358.

Li, S., Zhang, S., Xing, H. and Zou, Y. (2022). CO_2-brine-rock interactions altering the mineralogical, physical, and mechanical properties of carbonate-rich shale oil reservoirs. *Energy*, 256, 124608. https://doi.org/10.1016/j.energy.2022.124608

Liu, M., Bai, B. and Li, X. (2014). Experimental studies on the short term effect of CO_2 on the tensile failure of sandstone. *Energy Procedia*, 63, pp. 3357 – 3363.

Liu, E. and Martinez, A. (2014). *Seismic Fracture Characterization*. EAGE Publications.

Liu, Y., Ma, T., Wu, H. and Chen, P. (2020). Investigation on mechanical behaviors of shale cap rock for geological energy storage by linking macroscopic to mesoscopic failures. *Journal of Energy Storage*, 29, 101326. https://doi.org/10.1016/j.est.2020.101326

Liu, Y. and Dai, F. (2021). A review of experimental and theoretical research on the deformation and failure behavior of rocks subjected to cyclic loading. *Journal of Rock Mechanics and Geotechnical Engineering,* 13, pp. 1203-1230.

López-Rendón, R. and Alejandre, J. (2008). Molecular dynamics simulations of the solubility of H_2S and CO_2 in water. *J. Mex. Chem. Soc*., 52(1), pp. 88-92.

Lu, J., Mickler, P.J., Nicot, J.-P., Yang, C. and Darvari, R. (2016). Geochemical impact of O_2 impurity in CO_2 stream on carbonate carbon-storage reservoirs on siliciclastic carbon storage reservoirs. *International Journal of Greenhouse Gas Control*, 47, pp. 159–175.

Lu, J., Mickler, P.J., Nicot, J.-P., Yang, C. and Romanak, K.D. (2014). Geochemical impact of oxygen on siliciclastic carbon storage reservoirs. *International Journal of Greenhouse Gas Control*, 21, pp. 214–231.

Luan, X., Di, B., Wei, J., Li, X., Qian, K., Xie, J. and Ding, P. (2014). Laboratory Measurements of Brittleness Anisotropy in Synthetic Shale with Different Cementation. Presented at the SEG Denver 2014 Annual Meeting.

Lysyy, M., Liu, N., Solstad, C.M., Fernø, M.A. and Ersland, G. (2023). Microfluidic hydrogen storage capacity and residual trapping during cyclic injections: Implications for underground storage. *International Journal of Hydrogen Energy*, 48(80), pp. 31294-31304. https://doi.org/10.1016/j.ijhydene.2023.04.253

Lyu, Q., Long, X., Ranjith, P.G., Tan, J., Kang, Y. and Luo, W. (2018). A Damage Constitutive Model for the Effects of CO_2-Brine-Rock Interactions on the Brittleness of a Low-Clay Shale. *Geofluids*, 2018, 7321961. https://doi.org/10.1155/2018/7321961

Ma, X., Yang, G., Li, X., Yu, Y. and Dong, J. (2019). Geochemical modeling of changes in caprock permeability caused by CO_2–brine–rock interactions under the diffusion mechanism. *Oil & Gas Science and Technology - Rev. IFP Energies Nouvelles*, 74, 83. https://doi.org/10.2516/ogst/2019055

Mahmud, H.B., Leong, V.H. and Lestariono, Y. (2020). Sand production: A smart control framework for risk mitigation. *Petroleum*, 6(1), pp. 1-13.

Marini, L. ed. (2007). "The Product Solid Phases" in Geological Sequestration of Carbon Dioxide: Thermodynamics, Kinetics, and Reaction Path Modeling. *Developments in Geochemistry*, 11, pp. 79-167. https://doi.org/10.1016/S0921-3198(06)80025-6

Masoudi, R., Jalil, M.A.A., Press, D.J., Lee, K.-H., Tan, C.P., Anis, L., Darman, N.B. and Othman, M. (2011). An Integrated Reservoir Simulation-Geomechanical Study on Feasibility of CO_2 Storage in M4 Carbonate Reservoir, Malaysia. Paper IPTC 15029 presented at the International Petroleum Technology Conference held in Bangkok, Thailand, 15-17 November 2011.

Mavhengere, P., Wagner, N. and Malumbazo, N. (2022). Influences of SO_2 contamination in long term supercritical CO_2 treatment on the physical and structural characteristics of the Zululand Basin caprock and reservoir core samples. *Journal of Petroleum Science and Engineering*, 215, 110554. https://doi.org/10.1016/j.petrol.2022.110554

McNaughton, B.A.P. (2019). Two-Dimensional Ising Spin Model and Machine Learning. https://doi.org/10.13140/RG.2.2.33154.43201

Meng, F., Zhou, H., Zhang, C., Xu, R. and Lu, J. (2015). Evaluation Methodology of Brittleness of Rock Based on Post-Peak Stress–Strain Curves. *Rock Mech Rock Eng*, 48, pp. 1787–1805.

Minardi, A., Stavropoulou, E., Kim, T., Ferrari, A. and Laloui, L. (2021). Experimental assessment of the hydro-mechanical behaviour of a shale caprock during CO_2 injection. *Internation Journal of Greenhouse Gas Control,* 106, 103225. https://doi.org/10.1016/j.ijggc.2020.103225

Miri, R., Aagaard, P. and Hellevang, H. (2014). Examination of CO_2-SO_2 solubility in water by SAFT1: Implications for CO_2 transport and storage. *J. Phys. Chem. B*, 118, pp. 10214-10223.

Narasimhan, T. N. and Whiterspoon, P. A. (1976). An integrated finite difference method for analyzing fluid flow in porous media. *Water Resour. Res.*, 12(1), pp. 57-64. https://doi.org/10.1029/WR012i001p00057

Nooraiepour, M., Mondol, N.H., Hellevang, H. and Bjørlykke, K. (2017). Experimental mechanical compaction of reconstituted shale and mudstone aggregates: Investigation of petrophysical and acoustic properties of SW Barents Sea cap rock sequences. *Marine and Petroleum Geology*, 80, pp. 265-292.

Nyakilla, E.E., Jun, G., Kasimu, N.A., Robert, E.F., Innocent, N., Mohamedy, T., Shaame, M., Ngata, M.R. and Mabeyo, P.E. (2022). Application of machine learning in the prediction of compressive and shear strengths from the experimental data in oil well cement at 80^0C: Ensemble trees boosting approach. *Construction and Building* Materials, 317(4), 125778. https://doi.org/10.1016/j.conbuildmat.2021.125778

Okamoto, I., Li, X. and Ohsumi, T. (2005). Effect of supercritical CO_2 as the organic solvent on cap rock sealing performance for underground storage. *Energy*, 30(11-12), pp. 2344–2351.

Palandri, J.L. and Kharaka, Y.K. (2004). A Compilation of Rate Parameters of Water-Mineral Interaction Kinetics for Application to Geochemical Modeling (No. Open File Report 2004-1068). US Geological Survey.

Panfilov, M. (2016). 'Underground and pipeline hydrogen storage', In B. Ram et al. (eds) Compendium of Hydrogen Energy. Woodhead Publishing, 2, pp. 91-115. https://doi.org/10.1016/B978-1-78242-362-1.00004-3

Parmentier, M., Renard, S., Corvisier, J., Parra, T., Gaucher, E., Azaroual, M. and Sterpenich, J. (2013). Experimental and numerical study of sulphur dioxide reactivity on calcite. Paper presented at Le Studium Conference "Geochemical reactivity in CO_2 geological storage sites" held in Orléans, France, 25-26 February 2013.

Pearce, J.K., Dawson, G.K.W, Law, A.C.K., Biddle, D. and Golding, S.D. (2016). Reactivity of micas and cap-rock in wet supercritical CO_2 with SO_2 and O_2 at CO_2 storage conditions. *Applied Geochemistry,* 72, pp. 59-76.

Pearce, J.K., Kirste, D.M., Dawson, G.K.W., Rudolph, V. and Golding, S.D. (2019). Geochemical modelling of experimental O_2–SO_2–CO_2 reactions of reservoir, cap-rock, and overlying cores. *Applied Geochemistry,* 109, 104400. https://doi.org/10.1016/j.apgeochem.2019.104400

Pruess, K. (2004). The TOUGH Codes - A family of simulation tools for multiphase flow and transport processes in permeable media. *Vadose Zone Journal*, 3, pp. 738-746.

Rashidi, S., Mohamadian, N., Ghorbani, H., Wood, D.A., Shahbazi, K. and Alvar, M.A. (2020) Shear modulus prediction of embedded pressurized salt layers and pinpointing zones at risk of casing collapse in oil and gas wells. *Journal of Applied Geophysics,* 183, 104205. https://doi.org/10.1016/j.jappgeo.2020.104205

Reeves, S.R. (2001). Geologic sequestration of CO_2 in deep, unmineable coalbeds: an integrated research and commercial-scale field demonstration project. First National Carbon Sequestration Conference, U.S.DOE/NETL, pp. 1-12.

Rickman, R., Mullen, M., Petre, E., Grieser, B and Kundert, D. (2008). A practical use of shale petrophysics for stimulation design optimization: All shale plays are not clones of the Barnett Shale. In: Proceedings of the SPE Annual Technical Conference and Exhibition, Society of Petroleum Engineers.

Robie, R.A., Bethke, P.M. and Beardsley, K.M. (1967). *Selected x-ray crystallographic data molar volumes, and densities of minerals and related substances*. Washington: United States Government Printing Office, pp. 42-72.

Saeedi, A., Rezaee, R., Evans, B. and Clennell, B. (2011). Multiphase flow behaviour during CO_2 geo-sequestration: Emphasis on the effect of cyclic CO_2-brine flooding. *Journal of Petroleum Science and Engineering*, 79 (3-4), pp. 65-85.

Sánchez-Díaz, Á (2017). MefCO_2 – Synthesis of methanol from captured carbon dioxide using surplus electricity (EU-H2020). *Impact,* 2017 (5), pp. 6-8.

Santos, E.C.D., Silva, J.C. and Duarte, H.A. (2016). Pyrite Oxidation Mechanism by Oxygen in Aqueous Medium. *The Journal of Physical Chemistry,* 120, pp. 2760-2768.

Saraji, S., Goual, L., Piri, M. and Plancher, H. (2013). Wettability of Supercritical Carbon Dioxide/Water/Quartz Systems: Simultaneous Measurement of Contact Angle and Interfacial Tension at Reservoir Conditions*. Langmuir,* 29, pp. 6856-6866.

Schifflechner, C., Wieland, C. and Spliethoff, H. (2022). CO_2 plume geothermal (CPG) systems for combined heat and power production: an evaluation of various plant configurations. *Journal of Thermal Science*, 31(5), pp. 1266-1278.

Shafiq, M.U., Mahmud, H.K.B., Wang, L., Abid, K. and Gishkori, S.N. (2022). Comparative elemental, mineral and microscopic investigation of sandstone matrix acidizing at HPHT conditions. *Petroleum Research*, 7, pp. 448-458.

Shen, X., Kolluru, G.K., Yuan, S. and Kevil, C.G. (2015). 'Measurement of H_2S In Vivo and In Vitro by the Monobromobimane Method', in Cadenas, E. and Packer, L. (eds) Methods in Enzymology. Academic Press, 554, pp. 31-45. https://doi.org/10.1016/bs.mie.2014.11.039

Singh, H. (2019). Machine learning for surveillance of fluid leakage from reservoir using only injection rates and bottomhole pressures. *Journal of Natural Gas Science and Engineering,* 69, 102933. https://doi.org/10.1016/j.jngse.2019.102933

Smith, S.A., McLellan, P., Hawkes, C., Steadman, E. and Harju, J. (2009). Geomechanical testing and modeling of reservoir and cap rock integrity in an acid gas EOR/sequestration project, Zama, Alberta, Canada. *Energy Procedia*, 1, pp. 2169–2176.

SNC-Lavalin Inc. (2004). Impact of Impurities on CO_2 Capture, Transport and Storage. IEA Greenhouse Gas R&D Programme Report (No. PH4/32). Available at: https://ieaghg.org/docs/General_Docs/Reports/Ph4-32%20Impurities.pdf (Accessed: 20 March 2022).

Sollai, S., Porcu, A., Tola, V., Ferrara, F. and Pettinau, A. (2023). Renewable methanol production from green hydrogen and captured CO_2: A techno-economic assessment. *Journal of CO_2 Utilization,* 68, 102345. https://doi.org/10.1016/j.jcou.2022.102345

Spycher, N.F., Llanos, E.M., Vu, H.P. and Haese, R.R. (2019). Reservoir scale reactive-transport modeling of a buoyancy-controlled CO_2 plume with impurities (SO_2, NO_2, O_2). *International Journal of Greenhouse Gas Control*, 89, pp. 40-51.

Su, E., Liang, Y. and Zou, Q. (2021). Structures and fractal characteristics of pores in long-flame coal after cyclical supercritical CO_2 treatment. *Fuel,* 286(1), 119305. https://doi.org/10.1016/j.fuel.2020.119305

Su, E., Liang, Y., Chang, X., Zou, Q., Xu, M. and Sasmito, A.P. (2020). Effects of cyclic saturation of supercritical CO_2 on the pore structures and mechanical properties of bituminous coal: An experimental study. *Journal of CO_2 Utilization,* 40, 101208. https://doi.org/10.1016/j.jcou.2020.101208

Sun, Y., Li, Q., Yang, D. and Liu, X. (2016). Laboratory core flooding experimental systems for CO_2 geosequestration: An updated review over the past decade. Journal of Rock Mechanics and Geotechnical Engineering, 8, pp. 113-126.

Tariq, Z., Abdulraheem, A., Elkatatny, S., Mahmoud, M., Muqtadir, A. and Murtaza, M. (2018). Geomechanical Studies on CO_2 Sequestrated Rocks in an Aqueous Saline Environment. Paper SPE 192242-MS presented at the Annual Technical Symposium & Exhibition held in Dammam, Saudi Arabia, 23–25 April 2018.

Thanh, H.V., Yasin, Q., Al-Mudhafar, W.J. and Lee, K.-K. (2022). Knowledge-based machine learning techniques for accurate prediction of CO_2 storage performance in underground saline aquifers. *Applied Energy*, 314, 118985. https://doi.org/10.1016/j.apenergy.2022.118985

Torsæter, M., Todorovic, J., Lavrov, A., Gawel, K., Lund, H., Roy, P. and Carroll, S. (2017). Avoiding damage of CO_2 injection wells caused by temperature variations. *Energy Procedia*, 114, pp. 5275 – 5286.

Totten, M.W., Hanan, M.A., Knight, D. and Borges, J. (2002). Characteristics of mixed-layer smectite/illite density separates during burial diagenesis. *American Mineralogist,* 87, pp. 1571-1579.

Turšič, J., Grgić, I. and Podkrajšek, B. (2003). Influence of ionic strength on aqueous oxidation of SO_2 catalyzed by manganese. *Atmospheric Environment*, 37(19), pp. 2589–2595.

Vincent, O.N., Abiola, S.O., Felix, O.O. and Ajienka, J.A. (2012). Sanding in oil well reservoir completions. Paper SPE-163010-MS presented at the Nigeria Annual International Conference and Exhibition, Lagos, Nigeria, August 2012. https://doi.org/10.2118/163010-MS

Wang, D., Li, J., Meng, W., Liao, Z., Yang, S., Hong, X., Zhou, H., Yang, Y. and Li, G. (2023). A near-zero carbon emission methanol production through CO_2 hydrogenation integrated with renewable hydrogen: Process analysis, modification and evaluation. *Journal of Cleaner Production,* 412, 137388. https://doi.org/10.1016/j.jclepro.2023.137388

Wang, H., Zhang, L., Lei, H., Wang, Y., Liu, H., Li, X. and Su, X. (2021). Potential for uranium release under geologic CO_2 storage conditions: The impact of Fe(III). *International Journal of Greenhouse Gas Control,* 107, 103266. https://doi.org/10.1016/j.ijggc.2021.103266

Wang, J., Zhao, Y., An, Z. and Shabani, A. (2022). CO_2 storage in carbonate rocks: An experimental and geochemical modeling study. *Journal of Geochemical Exploration,* 234, 106942. https://doi.org/10.1016/j.gexplo.2021.106942

Wang, L., Zhang, Y., Liu, Y., Xie, H., Xu, Y. and Wei, J. (2020). SO_2 absorption in pure ionic liquids: Solubility and functionalization. *Journal of Hazardous Materials*, 392, 122504. https://doi.org/10.1016/j.jhazmat.2020.122504

Wang, Y., Zhang, X. and Liu, X. (2021). Machine learning approaches to rock fracture mechanics problems: Mode-I fracture toughness determination. *Engineering Fracture Mechanics,* 253, 107890. https://doi.org/10.1016/j.engfracmech.2021.107890

Wei, X.C., Li, Q., Li, X.-Y., Sun, Y.-K. and Liu, X.H. (2015) Uncertainty analysis of impact indicators for the integrity of combined caprock during CO_2 geosequestration. *Engineering Geology*, 196, pp. 37–46.

Wolfgang, M., Weißensteiner, M., Clarke, P., Hsiao, W.-K. and Khinast, J.G. (2020). Deep convolutional neural networks: Outperforming established algorithms in the evaluation of industrial optical coherence tomography (OCT) images of pharmaceutical coatings. *International Journal of Pharmaceutics: X*, 2, 100058. https://doi.org/10.1016/j.ijpx.2020.100058

Wu, H., Lubbers, N., Viswanathan, H.S. and Pollyea, R.M. (2021). A multi-dimensional parametric study of variability in multi-phase flow dynamics during geologic CO_2 sequestration accelerated with machine learning. *Applied Energy,* 287, 116580. https://doi.org/10.1016/j.apenergy.2021.116580

Wu, J., Fan, T., Gomez-Rivas, E., Gao, Z., Yao, S., Li, W., Zhang, C., Sun, Q., Gu, Y. and Xiang, M. (2019). Impact of pore structure and fractal characteristics on the sealing capacity of Ordovician carbonate cap rock in the Tarim Basin, China. *Marine and Petroleum Geology*, 102, pp. 557–579.

Xu, J., Zhai, C., Ranjith, P.G., Sang, S., Yu, X., Sun, Y., Cong, Y., Zheng, Y. and Tang, W. (2022). Mechanical responses of coals under the effects of cyclical liquid CO_2 during coalbed methane recovery process. *Fuel,* 308, 121890. https://doi.org/10.1016/j.fuel.2021.121890

Xu, J., Zhai, C., Ranjith, P.G., Sun, Y., Cong, Y., Zheng, Y., Tang, W. and Yang, W. (2021). Investigation of non-isothermal effect of cyclic carbon dioxide on the petrography of coals for coal mine methane recovery. *Fuel,* 290, 120085. https://doi.org/10.1016/j.fuel.2020.120085

Xu, T., Sonnenthal, E., Spycher, N. and Zheng, L. (2014). TOUGHREACT V3.0-OMP Reference Manual: A Parallel Simulation Program for Non-Isothermal Multiphase Geochemical Reactive Transport.

Xu, T., Spycher, N., Sonnenthal, E., Zhang, G., Zheng, L. and Pruess, K. (2011). TOUGHREACT Version 2.0: A simulator for subsurface reactive transport under non-isothermal multiphase flow conditions. *Computers & Geosciences*, 37, pp. 763-774.

Xu, T., Sonnenthal, E., Spycher, N. and Pruess, K. (2006). TOUGHREACT: A simulation program for non-isothermal multiphase reactive geochemical transport in variably saturated geologic media. *Computer & Geosciences,* 32, pp. 145-165. https://doi.org/10.1016/j.cageo.2005.06.014

Yao, P., Yu, Z., Zhang, Y. and Xu, T. (2023). Application of machine learning in carbon capture and storage: An in-depth insight from the perspective of geoscience. *Fuel*, 333(1), 126296. https://doi.org/10.1016/j.fuel.2022.126296

Yeh, G.T. and Tripathi, V.S. (1991). A model for simulating transport of reactive multispecies components: model development and demonstration. *Water Resour. Res.*, 27, pp. 3075-3094.

Yu, H., Wang, Z., Rezaee, R., Zhang, Y., Nwidee, L.N., Liu, X., Verrall, M. and Iglauer, S. (2020). Formation water geochemistry for carbonate reservoirs in Ordos basin, China: Implications for hydrocarbon preservation by machine learning. *Journal of Petroleum Science and Engineering*, 185, 106673. https://doi.org/10.1016/j.petrol.2019.106673

Zhang, D., Ranjith, P.G. and Perera, M.S.A. (2016). The brittleness indices used in rock mechanics and their application in shale hydraulic fracturing: A review. *Journal of Petroleum Science and Engineering,* 143, pp. 158–170.

Zhang, W., Xu, T. and Li, Y. (2011). Modeling of fate and transport of coinjection of H_2S with CO_2 in deep saline formations. *Journal of Geophysical Research*, 116, B02202. https://doi.org/10.1029/2010JB007652

Zheng, L., Apps, J.A., Zhang, Y., Xu, T. and Birkholzer, J.T. (2009). On mobilization of lead and arsenic in groundwater in response to CO_2 leakage from deep geological storage. *Chemical Geology*, 268(3-4), pp. 281-297.

Zhou, Y., Hatzignatiou, D.G. and Helland, J. O. (2017). On the estimation of CO_2 capillary entry pressure: Implications on geological CO_2 storage. *International Journal of Greenhouse Gas Control,* 63, pp. 26-36.

APPENDICES

A1. Cyclic CO_2 Injection-Withdrawal Strategy

INJECT (10 years) –> SHUT-IN (3 months) -> PRODUCE (2 years) -> SHUT-IN (3 months)

Time in seconds.

CYCLE 1:			
0	315360000	323244000	386316000
(beginning of cycle 1)			
CYCLE 2:			
394200000	709560000	717444000	780516000
(end of cycle 1 & beginning of cycle 2)			
CYCLE 3:			
788400000	1103760000	1111644000	1174716000
(end of cycle 2 & beginning of cycle 3)			
CYCLE 4:			
1182600000	1497960000	1505844000	1568916000
(end of cycle 3 & beginning of cycle 4)			
CYCLE 5:			
1576800000	1892160000	1900044000	1963116000
(end of cycle 4 & beginning of cycle 5)			
CYCLE 6:			
1971000000	2286360000	2294244000	2357316000
(end of cycle 5 & beginning of cycle 6)			
CYCLE 7:			
2365200000	2680560000	2688444000	2751516000
(end of cycle 6 & beginning of cycle 7)			

END OF CYCLE 7:
2759400000 (87.5 years)
(end of cycle 7)

A2. Dissolution and precipitation of minerals in the formations (Strategy 1) for the CO_2 alone case at 100^0C and 137 bar